“Piezoelectric and Triboelectric Nanogenerators: A Multifunctional Approach for Biomechanical Energy Conversion and Motion Sensing”

Thesis submitted to

Jadavpur University

By

Md. Minarul Saikh

In partial fulfilment of the requirements for the degree of

Doctor of Philosophy (PhD)

In Science

Department of Physics

Jadavpur University

Kolkata-700032

August 2024

যাদবপুর বিশ্ববিদ্যালয়
কলকাতা-৭০০০৩২, ভারত

JADAVPUR UNIVERSITY
KOLKATA-700032, INDIA

FACULTY OF SCIENCE : DEPARTMENT OF PHYSICS

Certificate from the Supervisor

This is to certify that the thesis entitled **"Piezoelectric and Triboelectric Nanogenerators: A Multifunctional Approach for Biomechanical Energy Conversion and Motion Sensing"** submitted by **Mr. Md. Minarul Saikh** who got his name registered on 14/03/2022 (Registration Index No: 92/22/Phys./27) for the award of Ph.D. (Science) degree of **Jadavpur University**, is absolutely based upon his own work under the supervision of Prof. Sukhen Das and that neither this thesis nor any part of it. has been submitted for either any degree/diploma or any other academic award anywhere before.

30/08/2024

Prof. Sukhen Das
Professor
Department of Physics
Jadavpur University
Kolkata-700032

Prof. Sukhen Das
Department of Physics,
Jadavpur University
Kolkata - 700 032

যাদবপুর বিশ্ববিদ্যালয়
কলকাতা-৭০০০৩২, ভারত

JADAVPUR UNIVERSITY
KOLKATA-700032, INDIA

FACULTY OF SCIENCE : DEPARTMENT OF PHYSICS

CERTIFICATE OF SIMILARITY CHECK

This is to certify that the plagiarism checking for this thesis entitled **"Piezoelectric and Triboelectric Nanogenerators: A Multifunctional Approach for Biomechanical Energy Conversion and Motion Sensing"** authored by **Mr. Md. Minarul Saikh** has been performed using professional plagiarism prevention software iThenticate. According to the report generated after plagiarism checking there is an 7% similarity in this thesis, which is in the category "Level 0" (minor similarities) as per the "Promotion of Academic Integrity and Prevention of Plagiarism in Higher Education Institutions Regulations, 2018" of the University Grand Commission (UGC) of India. The common knowledge or coincidental terms up to 10 (ten) consecutive words (as prescribed in the above said UGC Regulation up to 14 (fourteen) terms for such common knowledge or coincidental terms can be excluded) and own works of the candidate published in various peer-reviewed journals (those are attached in the thesis) are excluded from the similarity checking. It is certified that the present thesis submitted by **Mr. Md. Minarul Saikh** is plagiarism-free and has followed standard norms of academic integrity and scientific ethics.

30/09/2024

Prof. Sukhen Das
Professor
Department of Physics
Jadavpur University
Kolkata-700032

Prof. Sukhen Das
Department of Physics,
Jadavpur University
Kolkata-700 032

* Established on and from 24th December, 1955 vide Notification No.10986-Edn/IU-42/55 dated 6th December, 1955 under Jadavpur University Act, 1955 (West Bengal Act XXXIII of 1955) followed by Jadavpur University Act, 1981 (West Bengal Act XXIV of 1981)

ফোন : +৯১-৩৩-২৪১৩-৮৯১৭
ফ্যাক্স : +৯১-৩৩ ২৪১৩-৮৯১৭

Website : www.jadavpur.edu

Phone : + 91-33-2413-8917
Fax : + 91-33-2413-8917

Index No.: 92/22/Phys./27

ABSTRACT

THESIS TITLE: "Piezoelectric and Triboelectric Nanogenerators: A Multifunctional Approach for Biomechanical Energy Conversion and Motion Sensing"

Submitted by: Md. Minarul Saikh

Emerging energy harvesting technologies leverage biomechanical sources to generate electricity, offering promising prospects for sustainable energy solutions. Notably, Piezoelectric Nanogenerators (PENGs) and Triboelectric Nanogenerators (TENGs) stand out for their potential to integrate with wearable devices, facilitating electric energy harvesting and health monitoring applications. PENGs convert mechanical vibrations into electrical energy through the piezoelectric effect, exploiting materials' ability to generate electric fields under mechanical stress. TENGs, on the other hand, harness the triboelectrification phenomenon, where contact and separation of different surface charge layers result in electrical charging.

Polymer nanocomposites, particularly polyvinylidene fluoride (PVDF) due to its exceptional electroactive properties, offer a platform for tailored material design. By incorporating nanoparticles (e.g., ZrO_2, Er/ZrO_2, WO_3, Cus, NiO) and natural nanofibers, the potential of PVDF for energy harvesting and health monitoring applications can be further enhanced.

This proposal aims to develop TENGs for healthcare applications, focusing on Single Electrode TENGs (STENGs) based on polymer thin films with varied surface charges. Employing highly elastic and flexible polymers such as PDMS and Ecoflex, with polyamide or mica sheets for positive charges, enhances device performance. Incorporating nanoparticles into the polymer matrix improves electron transportation, thereby enhancing output performance.

Synthesis of nanoparticles will be conducted using methods like sol-gel and hydrothermal processes, while polymer nanocomposite thin films will be fabricated using drop-casting and

spin coating techniques. A variety of techniques will be employed to characterize the synthesized nanoparticles and fabricated polymer nanocomposite thin films. These techniques include sol-gel and hydrothermal synthesis for nanoparticle production, followed by drop-casting and spin-coating methods for thin film fabrication. The structural, morphological, and optical properties of the nanocomposites will be investigated using UV-visible spectroscopy, photoluminescence spectroscopy, micro-Raman spectroscopy, Fourier transform infrared spectroscopy, piezoresponse force microscopy (PFM), X-ray diffraction (XRD), electron microscopy (SEM, TEM), differential scanning calorimetry (DSC), differential thermal analysis (DTA), and LCR meter measurements. Furthermore, the optical properties (photocurrent, photovoltage, photoconductivity, photocatalytic effect) and electrical properties (capacitance, dielectric constant, dielectric loss, AC conductivity, resistivity, I-V characteristics, DC electrical conductivity, piezoelectricity, and polarization loops) of the nanocomposites will be comprehensively studied.

The flexible PENGs and STENGs, owing to their flexible and deformable nature, can be strategically placed on the human skin to monitor various physiological activities such as joint bending, extension, and body rotation. This project holds significant promise for advancing sustainable and safe biomechanical energy harvesting technologies with applications in real-time health monitoring systems. The ultimate goal is to develop a comprehensive health monitoring system that integrates a PENG and TENG-based self-powered device with wireless communication capabilities to not only monitor health parameters but also trigger alerts for potential health emergencies.

30/08/2024

Prof. Sukhen Das
Department of Physics,
Jadavpur University
Kolkata - 700 032

Dedicated to

My Parents

Acknowledgements

Reflecting on my journey, I am deeply grateful to my advisor, Professor Sukhen Das. His encouragement, guidance, and constant support were extremely helpful to me throughout my research work. The wealth of knowledge and experience he shared with me was invaluable, and his consistent backing ensured my research was completed successfully. Professor Das inspired me to be an independent thinker, providing the necessary guidance and support throughout the challenges of this journey. I consider myself extremely lucky to have had such a distinguished mentor in my academic life.

I would like to express my sincere gratitude to Prof. Papiya Nandy, Dr. Ruma Basu, Dr. Alakananda Bhattacharya and Dr. Soumyaditya Sutradhar for their insightful advice and friendly behaviour. Their advice has been invaluable throughout my research journey.

I want to convey my special thanks to my lab senior (but junior brother according to age), Dr. Nur Amin Hoque, who has been an exceptional mentor and guide throughout my Ph.D. journey. His guidance, support, and mentorship have not only enhanced my research skills but have also provided me with constant encouragement and insight. I wholeheartedly thank him for being such a remarkable source of support and inspiration. His contributions have greatly enriched my academic experience, and I am truly grateful for all that he has done.

I express deep appreciation for my lab seniors and lab mates, with whom I experienced many moments of pure enjoyment throughout my research work. Their valuable suggestions and continuous support over the years have been crucial in ensuring the smooth progress of my research. I want to extend my sincere gratitude to, Dr. Biswajoy Bagchi, Dr. Pradip Thakur, Dr. Arpan Kool, Dr. Niranjan Bala, Dr. Swagata Roy, Dr. Biplab Kumar Paul, Dr. Farha Khatun, Dr. Somtirtha Kool Banerjee, Dr. Navonil Bose, Dr. Madhuchhanda Sarkar, Dr. Dheeraj Mondal, Dr. Bidisha Ghosh, Dr. Souravi Bardhan, Dr. Subham Roy, Dr. Santanu Das, Dr. Tanumoy Debnath, Dr. Debopriya Bhattacharyya, Dr. Debbithi Bera, Dr. Anandalal Gayen, Mr. Somen Biswas, Miss Satarupa Bhattacharya.

I would like to extend my heartfelt appreciation to my dear friend and school classmate Dr. Wahida Rahman, whose support and guidance have been invaluable throughout every phase of my life. Her continuous help and encouragement have been a foundation of my academic journey.

I am extremely thankful to my junior brother, Mr. Debmalya Sarkar and junior sister Miss Namrata Das, for their invaluable support throughout this journey. Their teamwork, enthusiasm, and commitment to excellence have greatly contributed to the success of this journey. I am deeply grateful to both of them for their hard work and unwavering support. I couldn't have accomplished this without them.

I am undeniably thankful to my junior brother, Mr. Prosenjit Biswas, who has been extremely helpful in every aspect in my journey. I am grateful to him for being such an incredible source of encouragement and support.

I would like to extend my gratitude to my lab senior brother Mr. Puskar Naskar, whose kindness and support have been crucial to my Ph.D. journey. His kindness in offering me shelter in his apartment has provided me with a comfortable and supportive environment throughout my research. I am grateful to him for being such a remarkable source of support and inspiration.

I would also like to express my appreciation to my lab seniors and juniors: Manisha, Sanghita, Souvik, Shriparna, Saheli, Dhananjoy, Jhilik, Tanmoy, Piyali, Indrajit, Anuja, Anwesha, Monisha (Chhoto), Suman, Sumana, Anwesha (Chhoto), Aliva, Shubojit, Jaba, Solanky, Neelanjana, Shireen, Ayan, Amartya, Sucheta, Trishita, Biswarup and Swati. Their support in various aspects of laboratory work has been invaluable.

I wish to convey my sincere thanks to Professor Nabin Baran Manik, Head of Physics Department, Jadavpur University, for his invaluable support in ensuring the smooth handling of all official work throughout my time in the department. His efficient management, clear communication, and dedication to resolving any administrative challenges have greatly facilitated my academic tenure.

I would like to express my sincere gratitude to all the faculty members and office staffs of the Jadavpur University Physics Department. Their combined knowledge, support, and constant dedication in fostering a vibrant scholarly atmosphere have significantly contributed to my growth as a researcher.

My sincere appreciation is extended to my research scholar friends, seniors, and juniors: Dr. Nayim Sepay, Dr. Rajkumar Jana, Dr. Rituparna Mandal, Dr. Subhrajyoti Dey, Dr. Tanmoy Mondal, Dr. Ayesha Sultana. I'm deeply thankful for their support in my work, their compassionate care, our inspiring conversations, and their unwavering love and kindness.

I wish to express my deepest appreciation to my intelligent and kind brothers, Dr. Sayan Patra, Dr. Souradeep Sasmal, Dr. Rafikul Ali Sah, Mr. Supradip Bose, Mr. Arnabnil Jana. I am deeply grateful to their parents for their heartfelt wishes, blessings, unwavering care, and unconditional love.

Furthermore, I would like to express my gratitude to Miss Shubhraja Chowdhury and Miss Anashmita Ghosh for their unexpected contributions in finalizing my thesis writing.

I also express my gratitude to Dr. Swapnadip Jalal, Mr. Surajit Majumdar, Mr. Nawaz Sarif, Mr. Subhankar Pradhan, Mr. Biswajit Das, Mr. Rashidul Hassan, Mr. Mebar Hossain, Mr. Jubair Saikh, Mr. Gokul Sarkar and Mr. Ratan Ray. I've shared countless joyful moments with them.

A heartfelt token of gratitude is expressed to my childhood friends: Dr. Rakesh Kr. Mandal, Sirajuddin Sarkar, Dr. Mehebub Alam, Bulbul Saikh, Dr. Majibur Rahman, Prosenjit Sinha and Mehebub Mandal. I am thankful for their steady presence and warm companionship.

Thanks to my all classmates and school friends for their enduring support and good wishes. Their love and trust have been pillars of strength for me.

I would like to express my deepest appreciation to my friends, seniors, and sisters: Mrs Priyanka Banerjee, Joydeep Banerjee, Mr. Samrat Sarkar, Mr. Raktim Sasmal, Miss Rina Paul, Mrs. Minakshi Sarkar, Miss Pushpita Padhi, Miss Oindrila Bhattacharjee, Miss Hasina Khatun, Mr. Sahanuz Paik, Mr Ratan Manna, Mrs. Rupali Murmu, Mrs Monika Hansda for their constant encouragement and support.

I would like to express my deep appreciation to our esteemed Officer-in-Charge of Govt. General Degree College at Pedong, Mr. Navin Poudyal, for giving me the incredible support and opportunity to pursue my Ph.D. work. His understanding and encouragement, along with the flexibility provided through on-duty leave, have been crucial in allowing me to balance my professional responsibilities with my academic pursuits. This achievement would not have been possible without his constant belief in my potential.

I want to share my sincere appreciation to my colleagues at Govt. General Degree College at Pedong: Dr. Samiran Mandal, Dr. Koustav Chatterjee, Dr. Yusuf Ali, Dr. Subhashis Kumar, Mrs. Eeesha Moktan, Mrs. Prativa Pradhan, Dr. Uden Bhutia, Dr. Varun Adhikary, Dr. Dipti Tamang, Dr. Ambika Thami, Mrs. Shikha Tamang, Mr. Babul Pramanik, Mr. Laxuman Sherpa, Mr. Dipesh Lama, Mr. Bapon

Chandra Saha, Dr. Ikbal Hossein Sarkar, Dr. Subhadeep Saha, Dr. Sajad Ali, Mr. Himanish Roy, for their invaluable support and encouragement throughout my research journey. Their insights and companionship have greatly enriched my work.

My sincere appreciation goes to the college office staff and security personnel of Govt. General Degree College at Pedong: Mr. Tej Kumar Dulal, Mr. Ramesh Bhandari, Miss Sadhna Sewa, Mr. Sanjeev Subba, Miss Nima Ongmu Bhutia, Mr. Safiar Ali, Mr. Palzor Bhutia, Mr. Pema Bhutia, Mr. Lalgen Tamang, Mr. Kiren Pradhan, and Mr. Narbi Rai for being a part of this journey. I am extremely thankful to all of them for their constant support and encouragement, which have played a significant role in the successful completion of my Ph.D. work.

I also want to thank my colleagues of Govt. General Degree College at Pedong, who have transferred to other Colleges and Universities, Dr. Puja Gurung, Mr. John Kapil Chhetri, Mrs. Rippandi Lepcha, Dr. Golum Masud, Dr. Ashis Biswas, Mr. Koushik Saha, Dr. Prafullya Kumar Mudi, and Dr. Habibur Rahman. Their collaboration, insights, and companion were helpful in shaping my academic experience. I extend my heartfelt gratitude to them for their invaluable contributions and for being such a vital part of my journey.

Finally, I would like to express my deepest gratitude to my mother Momina Bewa, whose unwavering love, encouragement, and sacrifices have been the cornerstone of my success. Her belief in me, even during the most challenging times, has been my greatest source of strength. My deepest, heartfelt gratitude to her for being a constant presence in my life, offering her sage wisdom, guidance, and unwavering support every step of the way. Her selfless love and encouragement have made a profound impact on my journey.

To my father, late Md. Matiur Saikh, I dedicate this work to your memory. His values, hard work, and the lessons imparted by him have been a constant source of inspiration. Though he is no longer with us, I feel his presence in every achievement, and I know he would have been proud of this milestone.

I extend my deep gratitude to my elder brother Abutaher Saikh and elder sister-in-law Sarifa Bibi, who have been my pillars of strength. Their unconditional support, sacrifices, and shared precious moments have been the foundation of my journey. They were always big believers in me, and they gave me the strength to confront all obstacles with courage. Their endless love has been a constant source of motivation.

I wanted to share my warmest thanks to my two dear nieces, Susmita Khatun (Soma) and Sumi Sarmin. Their innocent smiles, boundless energy, and pure joy have been a constant source of happiness and motivation throughout this journey.
I'm deeply grateful to my extended family, which includes numerous younger brothers and sisters: Mukadder Saikh, Sekendar Saikh, Babor Ali, Rahema Bibi, Priyanka Bibi, Mazarul Saikh, Mahasen Saikh, Ahasen Saikh, Mafijul Saikh, Raseda Bibi, Sabina Bibi, Afrida Bibi, Beauty Bibi, Rejina Bibi, Nasima Bibi, Ruma Bibi, Asikul Islam and Mainul Saikh for their constant encouragement, love, and friendship.
I extend my sincerest thanks to my wonderful nieces and nephews: Rahul Saikh, Rohit Ali, Neha khatun, Tania Khatun, Kishan Saikh, Disha Khatun, Sandhiya Khatun, Bishal Saikh, Sagor, Khusbu, Kasmira, Imtiaz, Asik, Payel for being a constant source of happiness and encouragement during my Ph.D. journey.
In the end, this journey would have been incomplete without the love and support of my all-beloved family and friends. To each one of them, I extend my deepest gratitude. I'm grateful to have them all by my side throughout this incredible journey.
Thank you all.

Md. Minarul Saikh
Research Scholar
Department of Physics
Jadavpur University
Kolkata-700032
And
Assistant Professor
Department of Physics
Govt. General Degree College at Pedong

List of Publications

1. Elevating the performance of nanoporous bismuth selenide incorporated arch-shaped triboelectric nanogenerator by implementing piezo-tribo coupling effect: harvesting biomechanical energy and low scale energy sensing applications.
Debmalya Sarkar, Namrata Das, **Md. Minarul Saikh,** Shubham Roy, Sumana Paul, Nur Amin Hoque, Ruma Basu, Sukhen Das.
Advanced Composites and Hybrid Materials (2023) 6:232

2. High β-crystallinity comprising nitrogenous carbon dot/PVDF nanocomposite decorated self-powered and flexible piezoelectric nanogenerator for harvesting human movement mediated energy and sensing weights
Debmalya Sarkar, Namrata Das, **Md Minarul Saikh,** Prosenjit Biswas, Shubham Roy, Sumana Paul, Nur Amin Hoque, Ruma Basu, Sukhen Das.
Ceramics International, 2022

3. Piezoelectric activity assessment of size-dependent naturally acquired mud volcano clay nanoparticles assisted highly pressure sensitive nanogenerator for green mechanical energy harvesting and body motion sensing.
Namrata Das, Debmalya Sarkar, **Md. Minarul Saikh,** Prosenjit Biswas, Sukhen Das, Nur Amin Hoque, Partha Pratim Ray. ***Nano Energy,*** Volume 102, 2022, 107628

4. Development of a Sustainable and Biodegradable *Sonchus asper* Cotton Pappus Based Piezoelectric Nanogenerator for Instrument Vibration and Human Body Motion Sensing with Mechanical Energy Harvesting Applications
Debmalya Sarkar, Namrata Das, **Md. Minarul Saikh,** Prosenjit Biswas, Solanky Das, Sukhen Das, Nur Amin Hoque, Ruma Basu**.** ***ACS Omega*** 2021, 6, 43, 28710–28717

5. Self-Polarized ZrO_2/PVDF-HFP Nanocomposite based Piezoelectric Nanogenerator and Single Electrode Triboelectric Nanogenerator for Sustainable Energy Harvesting from Human Movement
Md. Minarul Saikh, Nur Amin Hoque, Prosenjit Biswas, Wahida Rahaman, Namrata Das, Sukhen Das, Pradip Thakur
Physica Status Solidi (A) Applications and Materials **,** 2021, 218(9)

6. Portable Self-Powered Piezoelectric Nanogenerator and Self-Charging Photo-Power Pack Using In Situ Formed Multifunctional Calcium Phosphate Nanorod-Doped PVDF Films
Prosenjit Biswas, Nur Amin Hoque, Pradip Thakur, **Md. Minarul Saikh**, Swagata Roy, Farha Khatun, Biswajoy Bagchi, Sukhen Das**.**
Langmuir, 2019, 35, 52, 17016–17026

7. Highly Efficient and Durable Piezoelectric Nanogenerator and Photo-power cell Based on CTAB Modified Montmorillonite Incorporated PVDF Film
Prosenjit Biswas, Nur Amin Hoque, Pradip Thakur, **Md. Minarul Saikh,** Swagata Roy, Farha Khatun, Biswajoy Bagchi, Sukhen Das**.**
ACS Sustainable Chem. Eng. 2019, 7, 5.

8. Bio-Waste Crab Shell extracted Chitin Nanofiber Based Superior Piezoelectric Nanogenerator.
Nur Amin Hoque, Pradip Thakur, Prosenjit Biswas, **Md Minarul Saikh,** Swagata Roy, BIswajoy Bagchi, Sukhen Das, Partha Pratim Ray
Journal of Materials Chemistry A, **2018**,6(28), 13848-13858.

9. Er^{3+}/Fe^{3+} Stimulated Electroactive, Visible Light Emitting, and High Dielectric Flexible PVDF Film Based Piezoelectric Nanogenerators: A Simple and Superior Self-Powered Energy Harvester with Remarkable Power Density.
Nur Amin Hoque, Pradip Thakur, Swagata Roy, Arpan Kool, Biswajoy Bagchi, Prosenjit Biswas, **Md. Minarul Saikh**, Farha Khatun, Sukhen Das, Partha Pratim Ray
ACS applied materials & interfaces**, 2017**, 9(27), 23048-23059.

List of Conferences Attended

1. Participating in "**ACS Publication Summit**" at "**nano tech 2024 International Nanotechnology Exhibition & conference**" on February 02, 2024.

2. Presenting a poster entitled **"Piezoelectric Nanogenerator Mediated Energy Harvesting"** in National Seminar on **"New Direction in Physical Sciences 2020 (NDPS 2020)"** organised by Department of Physics, Jadavpur University in association with Indian Photobiology Society, on February 25, 2020.

3. Presenting a paper entitled **"Piezoelectric Nanogenerator and its Applications"** in DST-SERB Sponsored **"One Day Workshop on Material Synthesis & Characterization Techniques"** organised by Department of Physics, Jadavpur University in association with Indian Photobiology Society, on February 29, 2020.

4. Participating in the Workshop on **"Nanolithography and Nanofabrication"** organised by Raith India in Cooperation with S.N. Bose National Centre for Basic Science, Kolkata, on July 9, 2019.

5. Participating in two-day seminar on **"Twists and Turns in Physics Research: Special Emphasis on Condensed Matter and Biophysics (TTPR-2017)"** organised by Department of Physics, Jadavpur University, Kolkata, Supported by UGC-DSA- I Programme, on 21-22 February, 2017.

6. Presenting a poster in "**ONE DAY NATIONAL SYMPOSIUM ON NANOTECHNOLOGY: FROM MATERIALS TO MADEICINE AND THEIR SOCIAL IMPACT**" on March, 2017 at Birla Industrial and Technological Museum, Kolkata.

7. Participating in International Workshop on **"Advanced Hybrid Techniques in Industrial Wastewater Management"** Sponcered by UGC, under Indo-Norwegian Collaboration program (INCP-2014), organised by Chemical Engineering Department, Jadavpur University in association with CHEMBridge, on December 8-9, 2017.

8. Participating in TEQIP-II Sponsored one day National Workshop on **"REVISITING INTELECTUAL PROPERTY RIGHTS IN THE CONTEXT OF RECENT DEVLOPMENTS IN SCIENCE & TECHNOLOGY"** organised by Faculty of Engineering and Technology, Jadavpur University, on October 20, 2016.

9. Participating in one day Seminar on **"RECENT TREND IN COMPOSITE MATERIAL"** Sponsored by Technical Education Quality Improvement Programme-II (TEQIP), in Mechanical Engineering Department, Jadavpur University, on August 8, 2016.

10. Participating in one day National Webinar on **"Advancement of Plasma Physics and Nano Science"** organised by Department of Physics, Kharagpur College, on June 30, 2020.

11. Participating in Two-day Webinar on **"Advanced Nanotechnology, Versatile Molecule & Spectrocopy"** organised by Department of Chemistry, Sikkim Manipal Institute of Technology in collaboration of with Association of Chemistry Teachers (ACT) C/O Homi Bhabha Centre for Science Education, Mumbai, on July 3-4, 2020.

12. Participating in five-day Faculty Development Programme on "**Recent Advances in Material Science**" organised by Amity Institute of Applied Science (Department of Chemistry), Amity University, Kolkata, on July 8-12, 2020.

13. Participating in International Webinar on **"NANOMATERIALS & ITS TOOLS"** organized by PG and Research Department of Physics, Idhaya College for Women, Kumbakonam, Thanjavur-612001, on July 22, 2020

14. Participating in International Webinar on **"New Ideas and Innovation in the Technology and Use of IoT, Nigeria"** organised by Raj Kumar Goel Institute of Technology, Gaziabad, Uttar Pradesh, India, on July 23, 2020.

15. Participating in International e-Conference on **"RECENT TRENDS ON ADVACED MATERIALS & ENVIRONMENT (RTAME) 2020"** organised by Department of Chemistry, IQAC and Research & Development Cell of DLS College, Chhattisgarh, on August 05, 2020.

16. Participating in International Webinar on **"Next Generation High Power Laser Technology"** delivered by **"Dr. Rajeev, Professor** Participating in International Webinar on **Ruttherford Appleton Lboratory, United Kingdom"** organised by Raj Kumar Goel Institute of Technology, Gaziabad, Uttar Pradesh, India, on August 7, 2020.

17. Participating in National Webinar on **"Recent Advances in Nanotechnology"** organized by Department of Chemistry, Shri. Shivaji Science and arts College, Chikhli, on August 8, 2020.

18. Participating in International Webinar on **"ADVACED FUNCTIONAL MATERIALS VIA VAPOR DEPOSITION: PROCESS DEVELOPMENT AND APPLICATION"** organized by Department of Physics, Sri Bhuvanendra College, Karkala, Udipi-574104, Karnataka, India, on August 11, 2020.

19. Participating in International Webinar on "**Photonics Revolution**" organised by Department of Applied Science and Humanities, Raj Kumar Goel Institute of Technology, Gaziabad, Uttar Pradesh, India, on August 12, 2020.

20. Participating in Two-day National Webinar on "**Emerging Trends in Modern Chemistry**" organized by Department of Chemistry, Faculty of Humanities and Science, Adaylampattu Phase-II campus, Dr.M.G.R. Educational and Research Institute, on September 14-15, 2020.

21. Participating in Three Day International Webinar on "**Synthesis and Characterization of Nano-materials and their Novel Applications**" organized by Department of Physics, R.K.Valley, Rajiv Gandhi University of Knowledge Technology, A.P(RGUKT-AP), on August 17-19, 2020.

22.Participating in One Day International Webinar on "**Material Science and Importance of Developing Composite Materials**" organised by Department of Science and Humanities, Sreenivasa Institute of Technology and Manegement Studies, Chittor, AP, India, on August 21, 2020.

23. Participating in One Day International Webinar on "**Remote Sensing and Its Apllication in Disaster Management**" organized jointly by Mazbat College, Udalguri, Assam and Khoribari College, Udalguri, Assam, India, on August 24, 2020.

24. Participating in One Day International Webinar on "**Physics & Life at Nano Scale of Length**" organized by Department of Physics, P.R. Thakur Government College, on August 26, 2020.

25. Participating in One Day National Level Webinar on **"Introduction to Nanoscience and Nanotechnology"** organized by the Department of Chemistry, Faculty of Humanities and Science, Adayalampattu Phase - II campus on 28th August 2020.

26. Participating in the One Day National Level Webinar on **"Ceramic Materials in Biomedical Field: A Prospective View"** organized by the Department of Physics, Faculty of Humanities and Science, Adayalampattu Phase - II campus on 1st September 2020.

Table of Contents

Abbreviations

PENGs	Piezoelectric nanogenerators
TENGs	Triboelectric nanogenerators
PVDF	Poly(vinylidene fluoride)
EAPs	Electroactive Polymers
VF_2 or VDF	Vinylidene Fluoride
α, β, γ	PVDF Crystal Structure (Phase)
TTTT	All trans
P(VDF-HFP)	Poly(vinylidene fluoride-co-hexafluoropropene)
PVDF-TrFE	Poly (vinylidene fluoride-Trifluoroethylene
P(VDF-CTFE)	Poly(vinylidene fluoride-chloride trifluoride ethylene)
P(VDF-TrFECFE)	Poly(vinylidene fluoride-trifluoroethylenechlorofluoroethylene)
P(VDF-TrFE-CTFE)	Poly(vinylidene fluoride-Trifluoroethylene-chloride trifluoride ethylene)
DMSO	Dimethyl sulfoxide
DMF	Dimethyl formamide
NPs	Nanoparticles
CNT	Carbon nanotube
DNA	Deoxyribonucleic Acid
PDMS	Polydimethylsiloxane
FPENGs	Flexible Piezoelectric nanogenerators
XRD	X-Ray Diffraction
FTIR	Fourier transform infrared spectroscopy
FESEM	Field emission scanning electron microscopy
UV	Ultraviolet
TGA	Thermal Gravimetric Analysis
DSC	Differential Scanning Calorimetry
UTM	Universal Tensile Machine
ac	Alternating current
V_{oc}	Open-circuit voltage

Isc	Short-circuit current
STENGs	Single Electrode Triboelectric Nanogenerators
TGTG’	T-trans, G-gauche+, G’ -gauche
ZrO_2	Zirconium oxide
wt%	Weight Percent
NCs	Nanocomposites
f	Frequency
DSO	Digital storage oscilloscope
σ_{ac}	AC conductivity
d_{33}	Piezoelectric constant
μA	Micro-Ampere
Hz	Hertz
μ	Micro
mV	mili-Volt
nA	nano-Ampere
pA	pico-Ampere
CNF	Chitin nanofibers
Cp	Capacitance
CPENG	CuS nanoroses-based Piezoelectric nanogenerator
CTFE	Chloride trifluoride ethylene
A	area
χ_c	Degree of crystallinity
ε	Dielectric constant
C	Capacitance
ε_0	Permittivity of free space
tan δ	tangent loss
ΔH_m	Melting enthalpy
$\Delta H_{100\%}$	Melting enthalpy of 100% Crystalline

F(β)	Fraction of β-phase
LEDs	Light Emitting Diodes
MWS	Maxwell-Wagner-Sillars
HFP	Hexafluropropylene
PL	Photoluminescence

List of Figures

List of Tables

Chapter 1

Introduction

1.1. Motivation:

Piezoelectric nanogenerators (PENGs) and triboelectric nanogenerators (TENGs) have demonstrated remarkable efficacy in seamlessly integrating with wearable low-power devices, resulting them highly suitable for supplying power to portable electronics and facilitating uninterrupted health monitoring. Nanogenerators possess the capacity to convert even minor mechanical motions, such as walking, jogging, or the periodic pulses of blood flow, into usable electrical energy. The aforementioned capability not only reduces dependency on conventional power sources but also presents prospects for self-regulating health monitoring gadgets capable of operating independently. The objective of this study is to examine the advancement and improvement of Proton Exchange Nanogenerators (PENGs) and triboelectric nanogenerators (TENGs) in order to create energy harvesting systems that exhibit higher efficiency, durability, and flexibility. By leveraging these technologies, our aim is to make a significant contribution towards the overarching purpose of sustainable energy solutions, while simultaneously enhancing the performance and dependability of wearable health monitoring devices.

1.2. Biomechanical Energy Harvesting Devices:

The pressing issues of modern society, including climate change and energy scarcity [1-4], have prompted the scientific community to develop sustainable solutions [5-7]. One promising approach is biomechanical energy harvesting, which involves converting human movement and other biological sources into electrical energy. This technology has the potential to power portable devices such as wearable sensors, prosthetics, and implantable devices [8-19]. To address this challenge, researchers have focused on designing efficient energy harvesting systems using advanced materials like poly (vinylidene fluoride) (PVDF) and its copolymers [20-26]. These materials offer exceptional properties, including ferroelectricity, high dielectric constants, flexibility, and mechanical strength [21,22, 27-34]. In this thesis, a novel biomechanical energy harvesting device is presented, leveraging electroactive PVDF composite thin films to convert human movement into electrical energy. This innovative technology has far-reaching implications for developing self-powered, wearable devices that can improve human health and quality of life [35-37].

This thesis aims to develop innovative Piezoelectric Nanogenerators (PENGs) and Triboelectric Nanogenerators (TENGs) based on polymer nanocomposites for biomechanical energy harvesting and healthcare applications, with a focus on designing flexible, wearable devices for real-time physiological activity monitoring and wireless health monitoring systems [38-40].

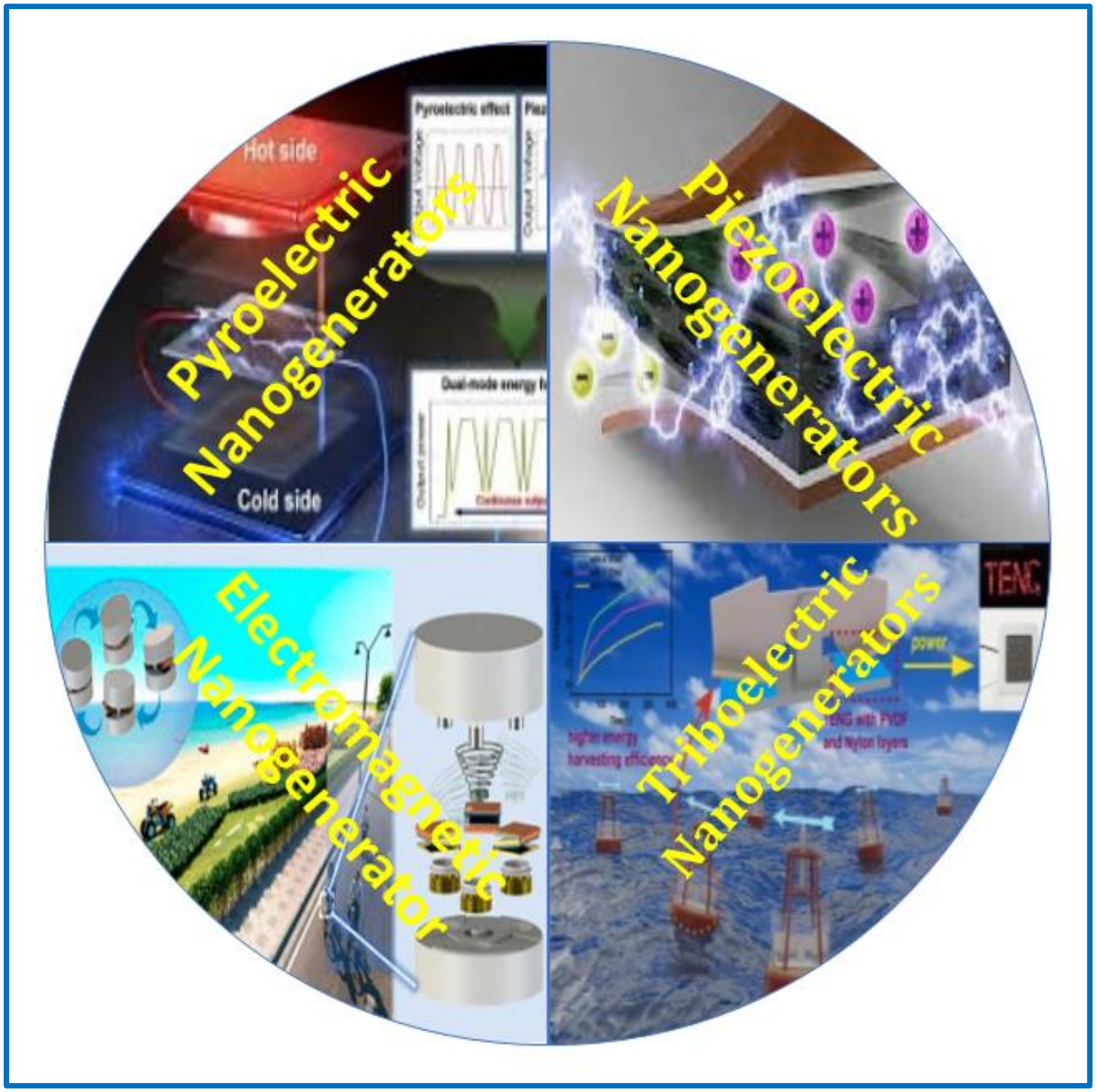

Figure1.1: Different type Mechanical and Biomechanical Energy Harvester's.

1.2.1. Piezoelectric Nanogenerators:

Piezoelectric nanogenerators (PENGs) harness periodic mechanical energy resources and convert it into electrical energy through piezoelectric materials [41-43]. The piezoelectric materials generate an electric charge in response to mechanical stress, such as stretching, compressing, or vibrating [44-50], schematic representation of piezoelectric energy harvesting process shown in figure 1.2. When subjected to mechanical deformation, the piezoelectric material's internal electric dipoles align in a direction, creating an electric potential difference across the material [51-57]. This potential difference drives an electric current and generating a voltage output.

PENGs have numerous applications, including:

i. Energy harvesting from environmental biomechanical sources (e.g., vibrations, wind, or water flow) [58-63]

ii. Powering small-scale devices (e.g., sensors, wearable technology, or IoT devices) [64-68].

iii. Self-sustaining systems for remote or hard-to-reach locations [70-71].

iv. Wearable sensor for health monitoring.

Advantages of PENGs include:

i. High efficiency, ii. Low cost, iii. Small size, iv. Flexibility, v. Durability

PENGs hold promise for sustainable energy solutions and innovative device powering [72-77].

1.2.1. (a) Piezoelectric Effect:

The piezoelectric effect refers to the capacity of specific materials to exhibit a change in polarization when subjected to mechanical stress. This phenomenon is derived from the Greek term "Piezein," meaning "pressure-induced electricity." French physicists Jacques and Pierre Curie discovered piezoelectricity in 1880, with Hankel proposing the term a year prior [54, 78-79]. When mechanical stress is applied to these materials, a polarization is generated across the material, known as the direct piezoelectric effect {Figure 1.2: (a)}. Notably, this process exhibit reversibility. In contrast, the application of an electric field induce the deformation in the material deforms, illustrating the inverse piezoelectric effect {Figure 1.2: (b)}. The piezoelectric properties of these materials are influenced by their microscopic charge distribution. In the absence of stress, the molecules appear neutral, with coinciding centers of charge for positive and negative charges {Figure 1.2: (c)}. However, upon applying mechanical force, molecular deformation occurs, resulting in the separation of the centers of gravity and creating small dipoles {Figure 1.2: (c)}. This polarization generates an electric field, enabling the conversion of mechanical energy into electrical energy.

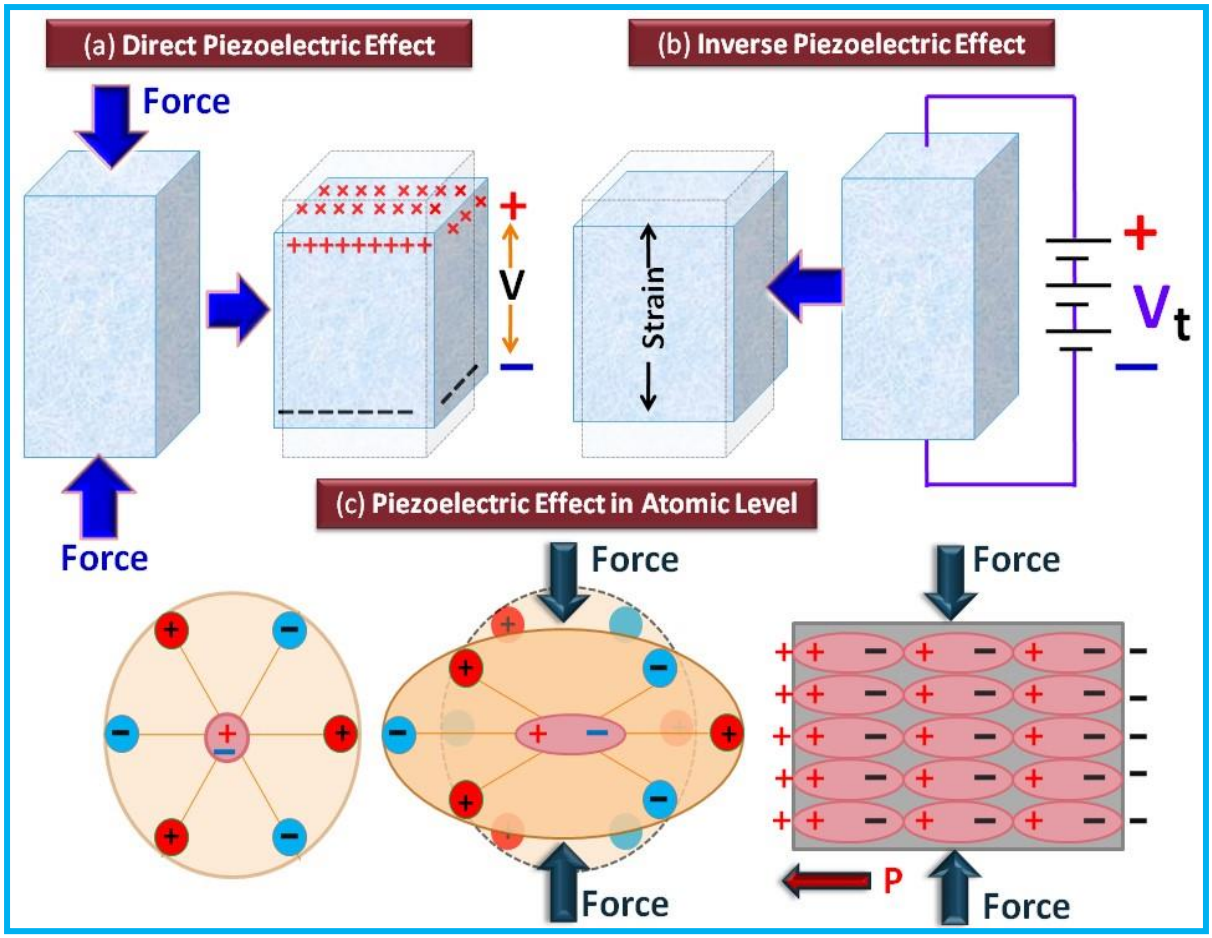

Figure1.2: (a) Direct piezoelectric effect; (b) Inverse piezoelectric effect and (c) piezoelectric effect in atomic level.

1.2.1. (b) Piezoelectric Materials:

As of now, more than 200 piezoelectric materials have been found as capable of turning mechanical energy into electrical energy. Natural materials such as Rochelle salt, quartz, and biological tissues were initially employed [80-83]. Later, developed materials such as zinc oxide [84-90], lead zirconate titanate [91-94], and barium titanate [94-96] were introduced. Recently, polymers like poly (vinylidene fluoride) (PVDF) and its copolymers have emerged as promising piezoelectric materials due to their flexibility, light weight, and excellent thermal stability [20, 22, 23]. These polymers exhibit good piezoelectric coefficients, ferroelectric properties, and chemical resistance, making them ideal for developing efficient piezoelectric nanogenerators [97-110]. Research has focused on enhancing the piezoelectricity and dielectric properties of PVDF for practical applications. The relationships of ferroelectric, pyroelectric, piezoelectric and dielectric materials are shown in figure 1.3.

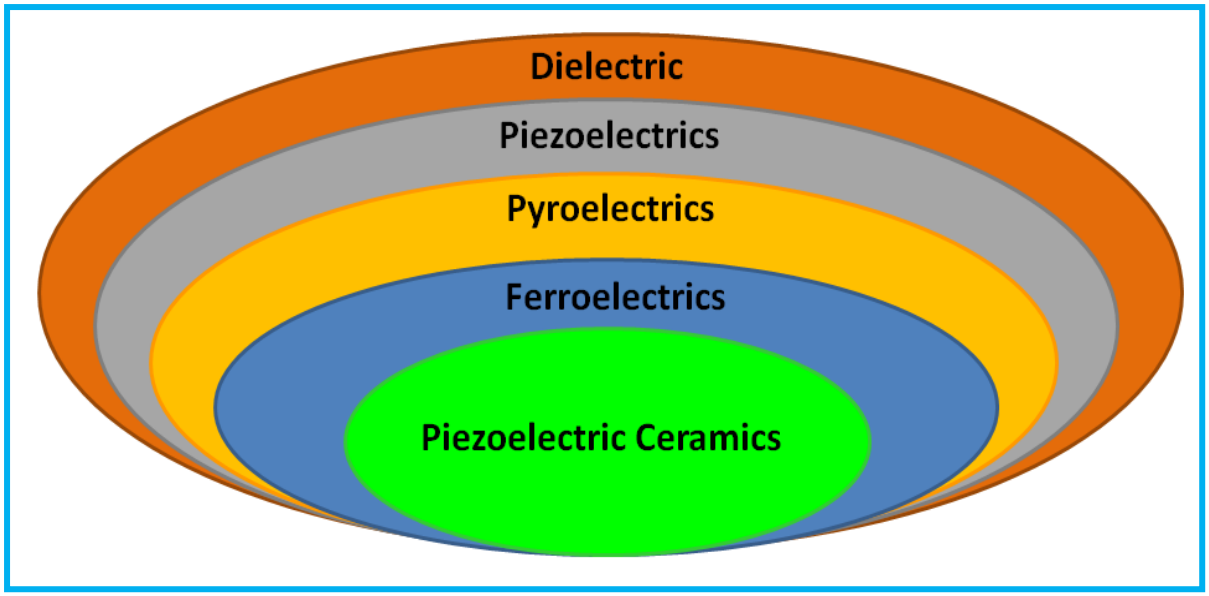

Figure 1.3: The relationships of ferroelectric, pyroelectric, piezoelectric and dielectric materials.

1.2.1. (c) Piezoelectric nanogenerators: a literature review:

Piezoelectric nanogenerators (PENGs) are innovative devices that harness mechanical energy and convert it into electrical energy through the piezoelectric effect. This technology has gained significant attention in recent years due to its potential to serve as a power source for small-scale devices, such as wearable electronics and sensors. The first PENG was successfully demonstrated by Wang et al. in 2006, using zinc oxide (ZnO) nanowires [111]. Since then, various materials, including lead zirconate titanate (PZT) [91-94], barium titanate (BTO) [94-96], and polyvinylidene fluoride (PVDF) [97-110], have been explored for PENG applications. Various procedures have been employed to generate piezoelectric nanomaterials and composite thin films for PENGs, including hydrothermal synthesis [112-114], sol-gel processing [74, 115-119], electrospinning, drop-casting, and spin coating [120-124]. These techniques enable the development of nanostructured materials featuring enlarged surface areas, hence boosting the piezoelectric capabilities. Several studies have focused on improving the efficiency of PENGs. For example, Chen et al. reported a PENG with a high output voltage of 1.26 V using a PZT nanofiber array [125]. Similarly, Lee et al. demonstrated a PENG with a high-power density of 1.14 μW/cm² using a BTO nanoparticle-based device [126]. In addition to material and structural optimization, researchers have also explored various applications for PENGs [20, 117, 73, 127-129]. For instance, PENGs have been integrated into wearable devices, such as shoes and textiles, to harvest energy from human motion [109, 130-132]. They have also been used to power sensors and small-scale electronics [64, 111, 133-135]. Despite the progress made in PENG research, challenges remain, such as improving the long-term stability and

durability of these devices [20, 101, 136-138]. Further research is needed to address these issues and fully realize the potential of PENGs.

1.2.2. Triboelectric Nanogenerators (TENGs):

Triboelectric nanogenerators harness the power of electron transfer between charged surfaces. When two materials interact with friction, they become electrically charged, triggering electron transfer. Separating the surfaces creates an imbalance, driving electrons to flow between positive and negative poles, generating an electrical response [139-145].

TENGs operate through four primary contact modes:

i. Lateral Sliding mode: In lateral sliding mode, two parallel triboelectric layers are placed close to each other {Figure 1.4: (a)}. When these triboelectric layers slide against each other laterally, friction causes a transfer of charges between them [146-149, 151]. The contact and separation during lateral sliding led to the buildup of opposite charges on each layer. This charge separation induces an electric field between the two triboelectric layers. As the two layers continue to slide frequently, the generated electric field drives the flow of electrons through an external circuit, producing an electrical current [151, 153-155]. This is useful in applications where relative motion between two surfaces can be maintained, such as in wearable devices or flexible electronics.

ii. Vertical Contact-Separation: In vertical contact-separation mode, two triboelectric layers with different triboelectric charges come into contact with each other {Figure 1.4: (b)}. This contact causes charge transfer between the two layers, creating an electric potential difference. Following the separation of the films, the charges that had been accumulated on the surfaces persist. This potential difference creates an electric field between the two surfaces. The electric field drives electrons to move through an external circuit, generating an electric current as the films periodically separate and contact [146, 152]. This technique is usually used in TENGs that it promotes periodic contact and separation, a crucial aspect for the extraction of mechanical energy from vibrations or motion [152].

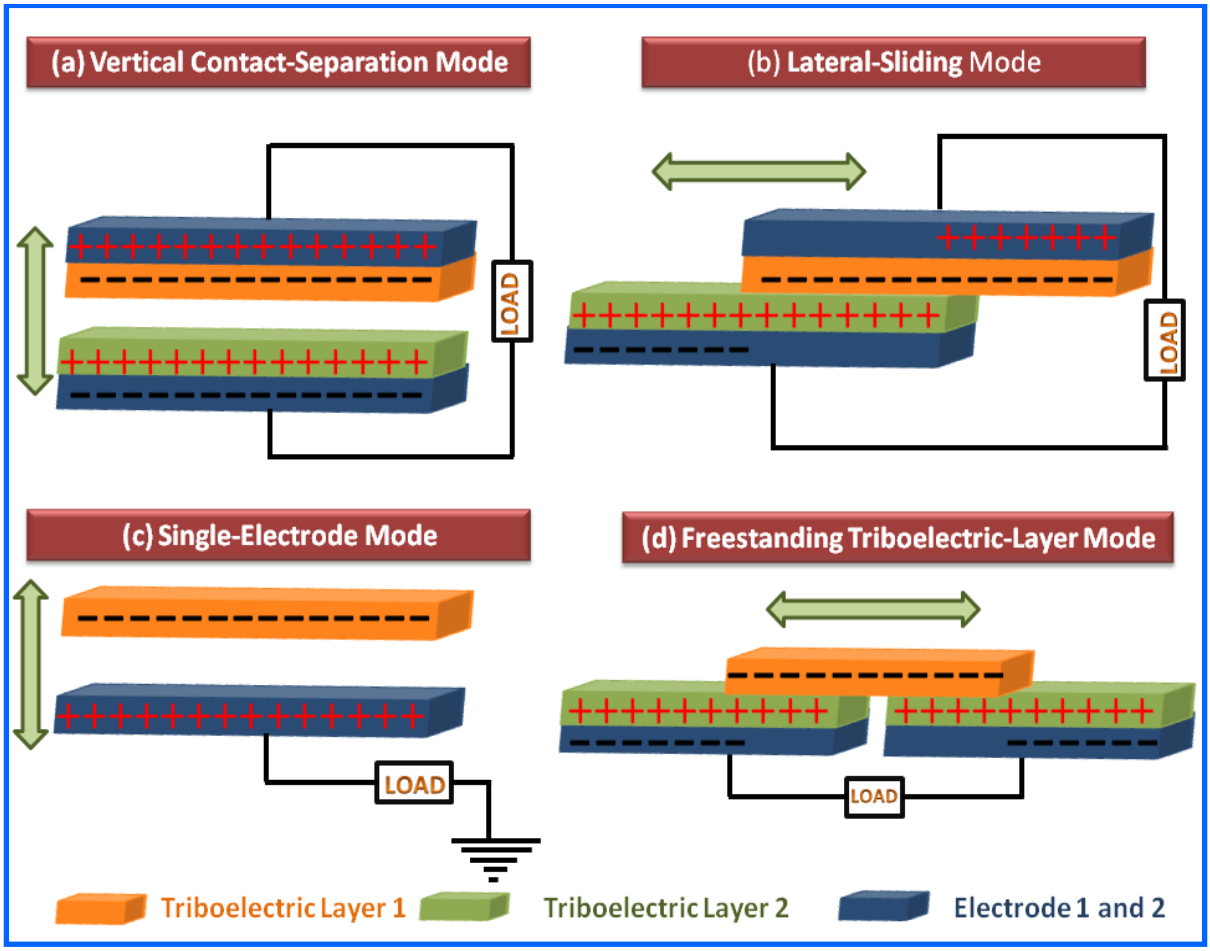

Figure1.4: Four triboelectric nanogenerator (TENG) operational modes: the (a) vertical contact-separation mode, (b) lateral sliding mode, (c) single-electrode mode, and (d) freestanding triboelectric-layer modes.

iii. Single-Electrode: In single-electrode mode, one electrode is exposed to the surrounding while the other is isolated. The triboelectric layer is separated from the ground, and electrostatic induction occurs due to the presence of an external electric field. When the dielectric triboelectric layer is moved or deformed, it changes the local electric field and induces charge accumulation on the triboelectric layer {Figure 1.4: (c)}. This change in potential allows for electron exchange between the triboelectric layer and the external environment [146, 150, 151]. As the triboelectric layers moves, it induces electron flow through an external circuit to balance the charge distribution. It is suitable for use in low-power electronics, wearable and self-powered sensors, where the TENG is not directly connected to the ground [150-151].

iv. Freestanding Triboelectric-Layer: In this mode, a freestanding triboelectric layer is placed between two electrodes. The layer can move or vibrate independently, making contact

with the electrodes during its movement. As the freestanding layer moves or vibrates, it generates triboelectric charges through contact with the electrodes {Figure 1.4: (d)}. The movement leads to continuous charge transfer and accumulation on the electrodes. The movement of the freestanding layer generates an alternating electric field between the electrodes, which is harvested to produce electrical energy [146, 148]. Suitable for applications where a freely moving or vibrating layer can be integrated, such as in flexible or wearable energy harvesters and self-powered electronic devices [148].

1.2.2. (a) Triboelectric Effect:

The phenomenon known as the triboelectric effect arises when two materials with different surface charge make contact and subsequently undergo separation, resulting in the transfer of electrons. This phenomenon results in the creation of a positive charge by one material, compared to the other material accumulates a negative charge[156-158]. Influenced by material properties, contact force, and separation speed, this effect has various applications, including triboelectric nanogenerators (TENGs) for energy harvesting, electrostatic charging and discharging, surface modification, and particle manipulation [143, 159-161]. With its potential to enable innovative technologies, such as self-powered devices and wearable technology, the triboelectric effect is a promising area of research and development [162-168].

1.2.2. (b) Triboelectric series and layers.

The triboelectric series is a classification system that categorizes materials according to their tendency to induce electron gain or loss upon interaction with other materials. Materials at the top of the series, such as fur and glass, tend to lose electrons and become positively charged, while materials at the bottom, like gold and copper, tend to gain electrons and become negatively charged [157, 168-172].

Triboelectric layers refer to the arrangement of materials in a specific order to maximize the triboelectric effect shown in figure1.5. Typically, a triboelectric layer consists of:

1. A top layer: a material with high electron affinity (e.g., Teflon or silicone)
2. A middle layer: a dielectric material (e.g., polymer or ceramic)
3. A bottom layer: a material with low electron affinity (e.g., metal or carbon)

By carefully selecting and arranging these layers, the triboelectric effect can be enhanced, leading to increased energy harvesting capabilities in triboelectric nanogenerators (TENGs) and other applications.

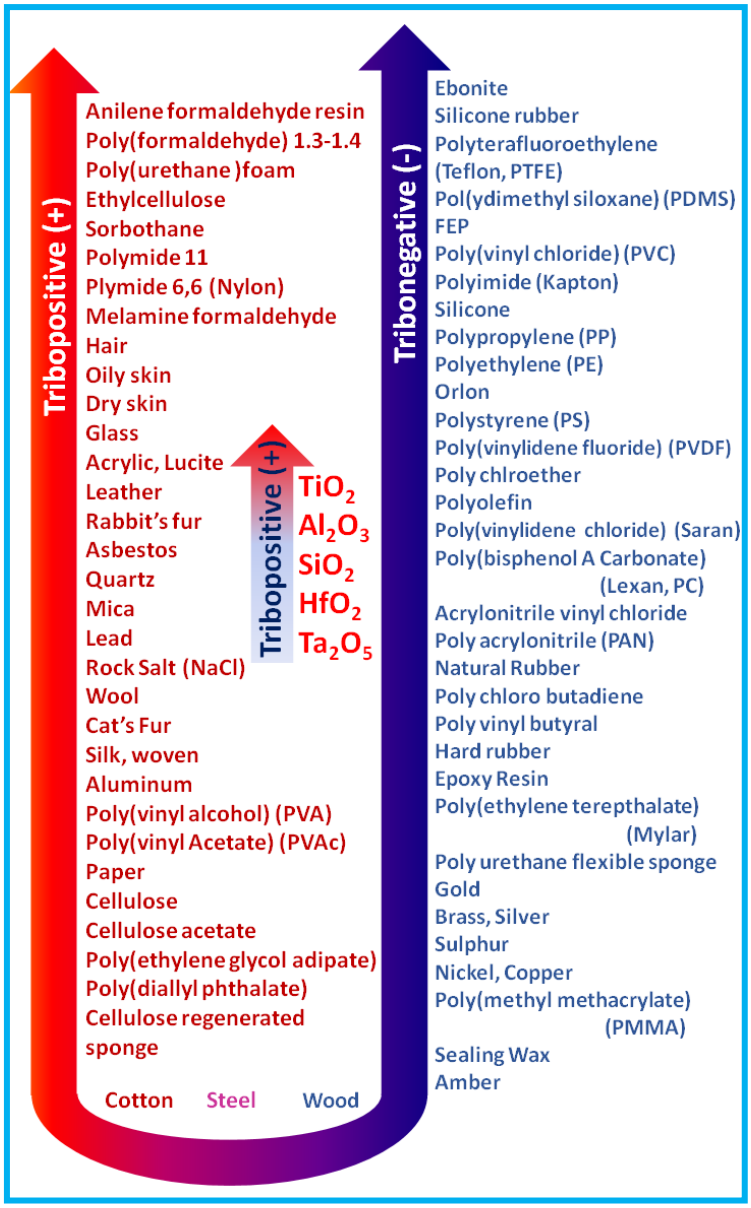

Figure 1.5: Triboelectric series.

1.2.2.(c) Triboelectric nanogenerators: a literature review:

Triboelectric nanogenerators (TENGs) are innovative devices that harness mechanical energy and convert it into electrical energy through the triboelectric effect [156-158]. This technology has gained significant attention in recent years due to its potential to power small-scale devices, such as wearable electronics and sensors [162-168]. The first TENG was demonstrated by Wang et al. in 2012, using a contact-separation mode to generate electricity from mechanical motion [173]. Since then, various modes, including sliding, rotating, and vibrating, have been explored to enhance the performance of TENGs [174-179]. TENGs have been fabricated using different materials, such as polymers, metals, and nanomaterials [157, 168-172]. The choice of materials plays a crucial role in determining the triboelectric properties and output performance

of TENGs. Several studies have focused on improving the efficiency of TENGs. For example, Zhou et al. reported a TENG with a high output voltage of 1.3 kV using a sliding-mode operation [180]. Similarly, Chen et al. demonstrated a TENG with a high-power density of 100 mW/cm^3 using a rotating-mode operation [181]. In addition to material and structural optimization, researchers have also explored various applications for TENGs. For instance, TENGs have been integrated into wearable devices, such as shoes and textiles, to harvest energy from human motion. They have also been used to power sensors and small-scale electronics [162-168]. Recent advancements in TENG research include the development of hybrid nanogenerators, which combine triboelectric and piezoelectric effects to enhance energy harvesting capabilities [182-188]. Despite the progress made in TENG research, challenges remain, such as improving the long-term stability and durability of these devices. Further research is needed to address these issues and fully realize the potential of TENGs.

1.3. Electroactive polymers:

Electroactive Polymers (EAPs) are cutting-edge materials that alter their shape and size in response to external electrical stimuli, boasting exceptional responsiveness, large deformation potential, lightweight, low density, and affordability [189-194]. With vast applications in sensors, actuators, soft robotics, artificial muscles, biomedical devices, energy harvesting, piezoelectric nanogenerators, EMI shielding, and stimuli-responsive biomaterials, EAPs are revolutionizing various fields [195-203]. Their adaptability and unique properties, such as dielectric elastomers, make them an exciting area of research and development, with diverse activation modes paving the way for innovative technologies.

1.3.1. Properties of Polyvinlydine Fluoride (PVDF):

Polyvinylidene fluoride (PVDF) is a synthetic polymer composed of repeated units of 1,1-difluoroethene, also known as vinylidene fluoride (VF_2 or VDF) [204]. This semi-crystalline fluoro-polymer boasts exceptional properties, including high chemical resistance, low weight, and pure thermoplastic behavior [205]. PVDF's molecular structure comprises 59.4% fluorine and 3% hydrogen, distinguishing it from other fluoropolymers. Its low cost and density (1.78 g/cm^3) make it an attractive material for various applications [206]. The piezoelectric properties of PVDF were first discovered by Dr. Heiji Kawai at the Kobayashi Institute of Physical Research Laboratory in Tokyo in 1969[207]. Since then, extensive research has been conducted on the piezoelectric phases of PVDF, leading to significant advancements in the field.

1.3.2. PVDF: Crystal Structure and Phases:

Extensive research has been conducted on the various phases of PVDF, a semi-crystalline polymer composed of repeated units of $(CH_2\text{-}CF_2)_n$. The polymer's crystalline structure is characterized by five distinct phases - α, β, γ, δ, and ε - which are determined by the orientation of the $-CF_2$ and $-CH_2$ chains. Figure 1.6 illustrates the chain orientation of these different phases. Among these, the β-phase has garnered significant attention due to its exceptional piezoelectricity, strength, and ferroelectricity. As a result, the nucleation of the β-phase has become a topic of great interest. The non-polar α-phase, with its TGTG′ conformation, exhibits high thermodynamic stability. In contrast, the polar γ-phase, with its TTTGTTTG′ configuration, displays moderate piezoelectricity. Notably, the all-trans (TTTT) structure of the polar β-crystalline phase yields maximum piezoelectric, ferroelectric, pyroelectric, and dielectric properties, making it a promising material for practical applications [208-213].

PVDF has been modified into various copolymers to enhance its properties and suit different technological requirements (figure 1.7). One such copolymer is poly (vinylidene fluoride-Trifluoroethylene) (PVDF-TrFE), shown in Figure 1.7: (c), which exhibits improved electroactive β crystallinity compared to pure PVDF [49, 210, 214]. The addition of TrFE monomer induces an all-trans conformation, resulting in a ferroelectric β-phase with high remnant polarization (~110 mCm^{-2}) and attractive piezoelectric properties. PVDF-TrFE also demonstrates thermal stability up to 100 °C higher than PVDF [49, 210, 214]. Another cost-effective copolymer is poly (vinylidene fluoride-co-hexafluoropropene) (PVDF-HFP), formed by incorporating amorphous hexafluoropropylene (HFP) into PVDF {Figure 1.7 (b)}. Although the degree of crystallinity is lower due to bulky CF3 groups, PVDF-HFP shows high piezoelectric properties, with a piezoelectric coefficient (d33) of ~30 pC N^{-1}, making it suitable for piezoelectric and ferroelectric applications [21, 215-216].

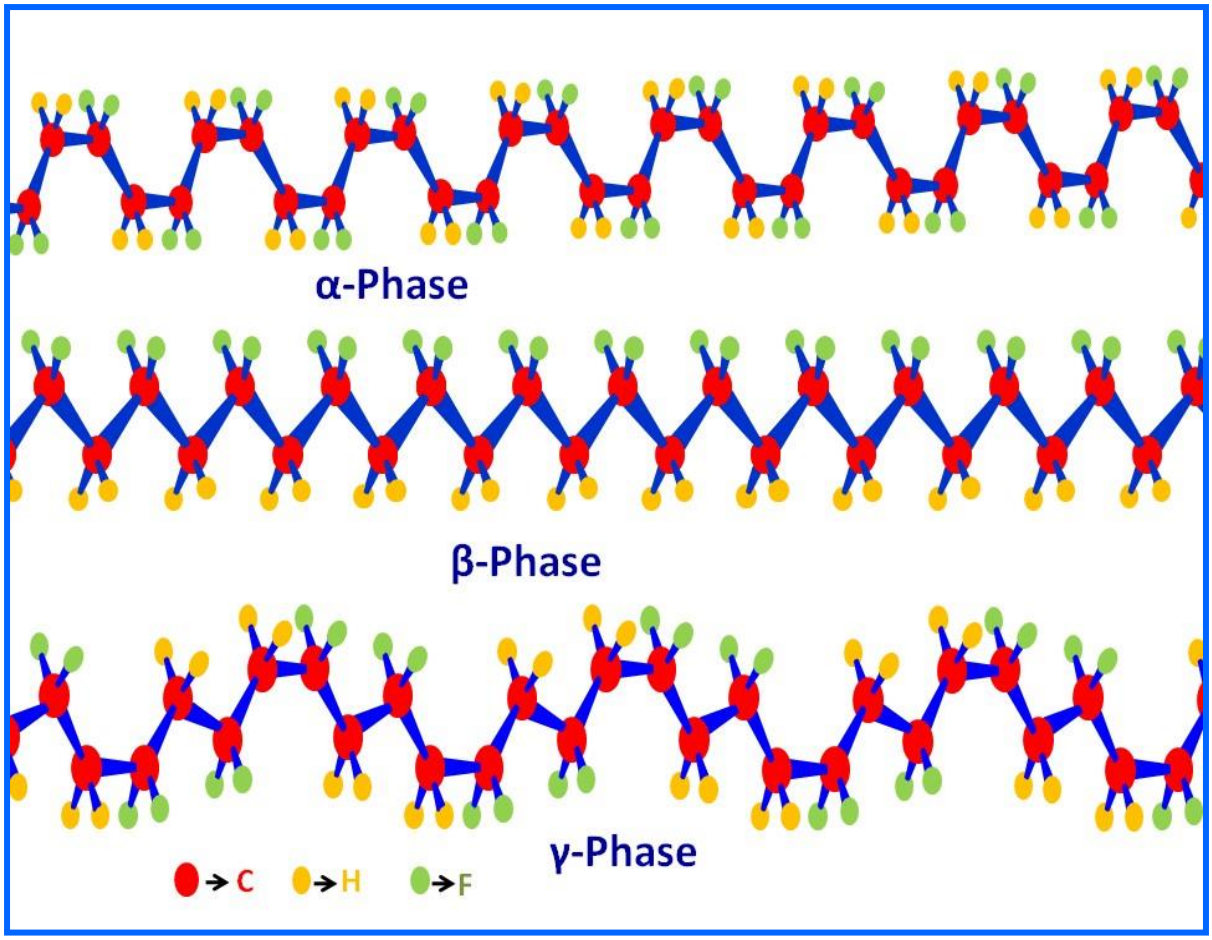

Figure 1.6: Schematic diagram of different phases of PVDF (α, β and γ).

Additionally, PVDF-HFP is used as a solid electrolyte in lithium-ion battery preparation. Other notable ferroelectric copolymers include poly (vinylidene fluoride-chloride trifluoride ethylene) (PVDF-CTFE) [217-219] and poly (vinylidene fluoride-Trifluoroethylene-chloride trifluoride ethylene) (PVDF-TrFE-CTFE) [220-221], synthesized by introducing CTFE into PVDF and PVDF-TrFE matrices, respectively {Figure 1.7 (e) and (d)}. These copolymers exhibit good electrostrictive strain response, high dielectric values, and enhanced piezoelectric properties compared to pure PVDF. The piezoelectric and dielectric constants of pure PVDF and its copolymers are summarized in Table 1 [99, 100, 210, 222-228].

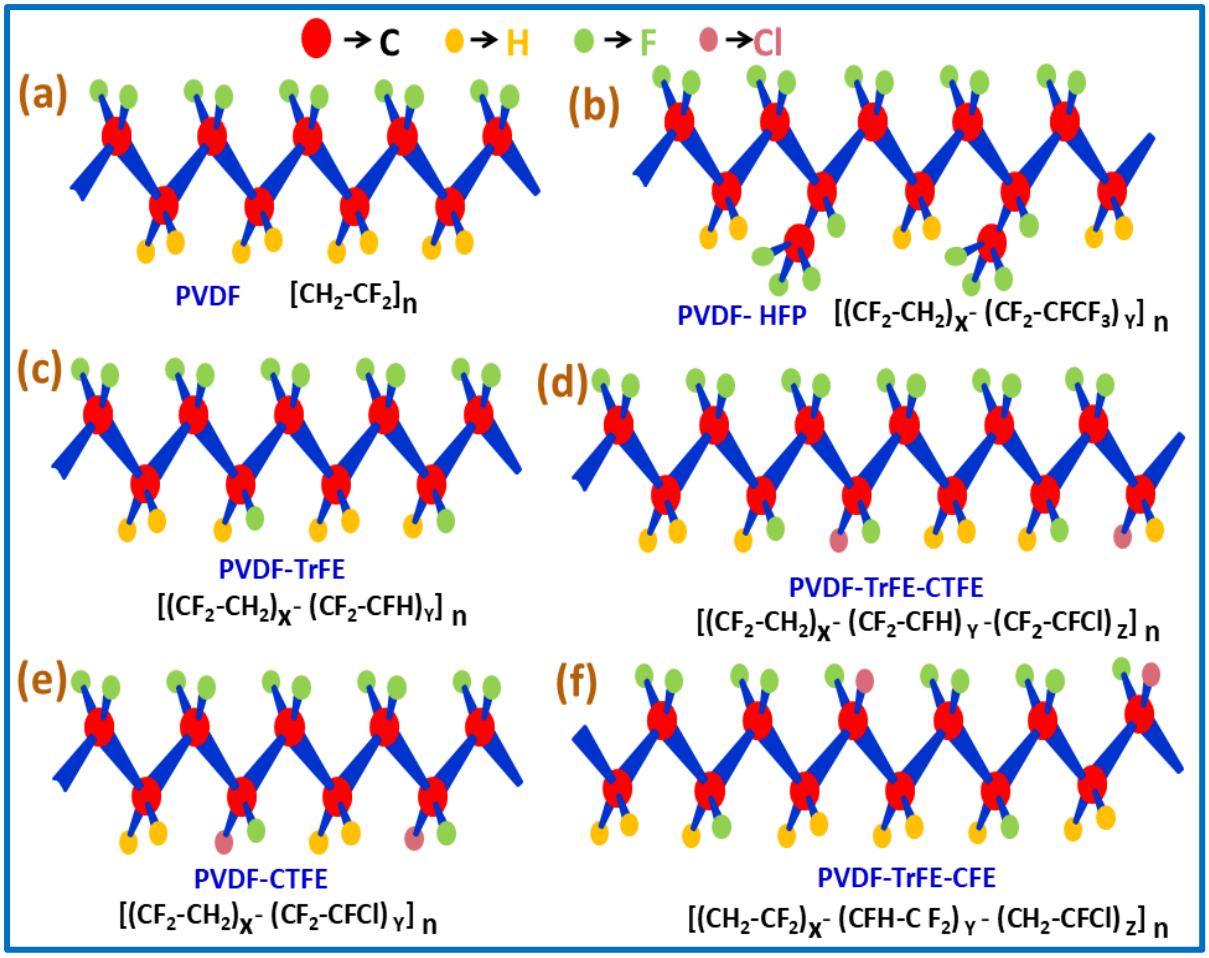

Figure 1.7: Schematic diagram of copolymers with repeated unit: (a) PVDF (b) PVDF-HFP, (c) PVDF-TrFE, (d) PVDF-TrFE-CTFE (e) PVDF-CTFE and (f) PVDF-TrFE-CFE

Table 1.1: The comparison of piezoelectric coefficient (d_{33}) and dielectric constant of PVDF and its copolymers:

	Pure PVDF	PVDF-HFP	PVDF-TrFE	PVDF-CTFE
Piezoelectric Coefficient (d_{33}) (pC/N)	-24 to -34 [210, 222, 223]	-24 [210, 227]	-38 [210, 226]	-140 [210, 228]
Dielectric constant	6-12 [210, 223]	11 [210, 224]	18 [210, 100]	13 [210, 99]

1.3.3. Energy storage:

Energy storage refers to the capture and retention of energy for later use, reducing the gap between energy supply and demand. Common energy storage methods include:

1. Batteries (chemical energy)

2. Supercapacitors (electrostatic double-layer capacitance)
3. Fuel cells (chemical energy)
4. Pumped hydro storage (mechanical energy)
5. Compressed air energy storage (mechanical energy)
6. Thermal energy storage (sensible heat or latent heat)

Energy storage systems enable:

1. Renewable energy integration (smoothing out intermittent sources like solar and wind)
2. Grid stability and reliability
3. Peak demand management
4. Electric vehicle range extension
5. Backup power during outages

Advancements in energy storage technologies aim to improve efficiency, cost-effectiveness, and scalability, driving innovation in various industries and contributing to a more sustainable energy future.

1.3.4. Electroactive Phase Nucleation Process:

Electroactive phase nucleation is a process where an external electric field induces the formation of a new phase or structure within a material, enhancing its properties [229-230] (Figure 1.8). The electric field creates nucleation sites, allowing the new phase to grow and stabilize, persisting even after the field is removed. This process can lead to improved ferroelectric, piezoelectric, and pyroelectric properties, as well as enhanced dielectric, optical, and electrochemical properties. With applications in energy storage and conversion devices, sensors, actuators, memory devices, and biomedical devices, electroactive phase nucleation enables the creation of innovative technologies by tailoring material properties through controlled phase formation.

Various techniques have been used to fabricate the electroactive β-phase of PVDF.

These methods include:

i. Applying strong external fields and high pressure
ii. Mechanical quenching and stretching of α-PVDF
ii. Ultra-fast cooling
iv. Electrospinning
v. Chemical vapor deposition

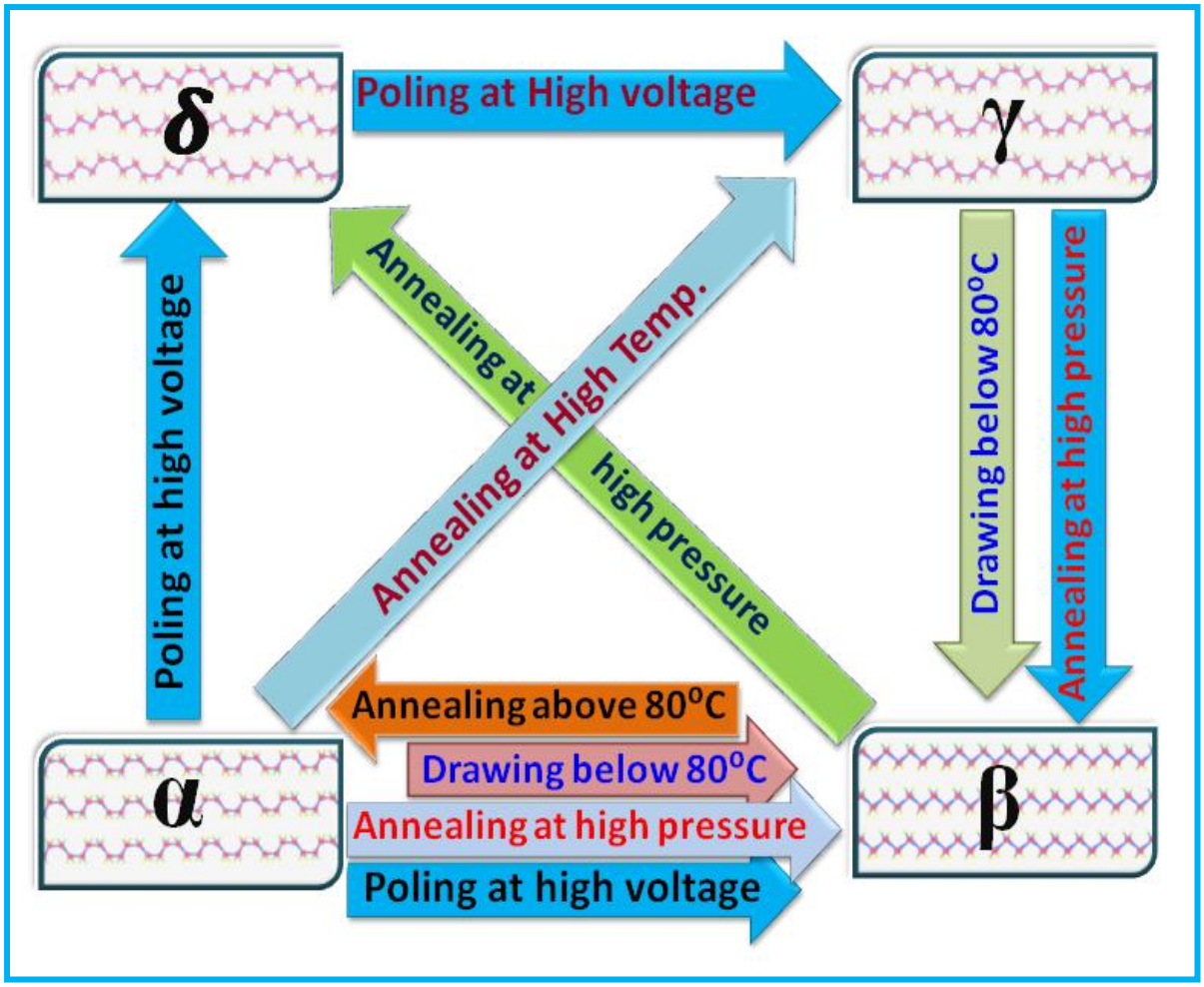

Figure 1.8: Phase transformation of the PVDF.

Additionally, the PVDF polymer matrix has been doped with a range of fillers such as: Metal and metal oxide nanoparticles; Organically and inorganically modified clays; Graphene; ferrites; ceramics; inorganic salts; gold, and palladium etc.

In this thesis, the focus is on enhancing PVDF-based composite thin films using the well-known solution casting technique.

1.3.4. (a) Solution Casting:

The solution casting process is a straightforward and widely used method for fabricating polymer nanocomposite thin films. This technique is suitable when both the polymer and inorganic powder can be dissolved and dispersed. In this approach, the base material, typically a polymer (PVDF or its copolymer), is dispersed in a suitable solvent (such as DMSO or DMF) using mechanical forces like magnetic stirring, ultra-sonication, or electric force stirring. Although particle agglomeration remains a challenge, this method allows for acceptable surface modification of the thin films compared to other techniques. The composite solution,

containing the dopant and casting solution, is then cast onto a solid surface, typically glass, and the solvent is evaporated in a dust-free oven to produce contaminant-free polymer composite thin films, as illustrated in figure 1.9 [231].

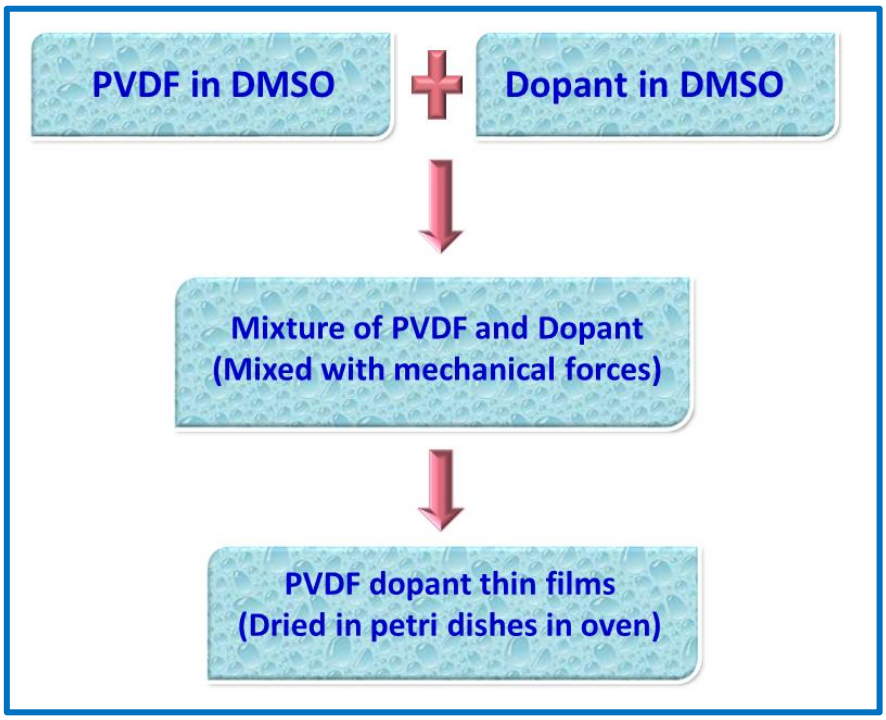

Figure 1.9: Synthesis procedure of nanocomposite polymer thin films via solution casting method.

1.3.4. (b) *In situ* process followed by solution casting

In situ process for synthesizing polymer nanocomposite thin films, stands out for its simplicity and effectiveness. Essentially, it allows for the one-step synthesis of thin films, with the desired precursors and nanoparticles (NPs) being synthesized directly within the polymer matrix. In this method the nanoparticles is integrated directly into the polymer chain during synthesis. This approach has significant advantages, notably in preventing the agglomeration of nanoparticles and ensuring a well-distributed nanocomposite thin film. The typical synthesis procedure using this in situ technique is detailed in figure 1.10.

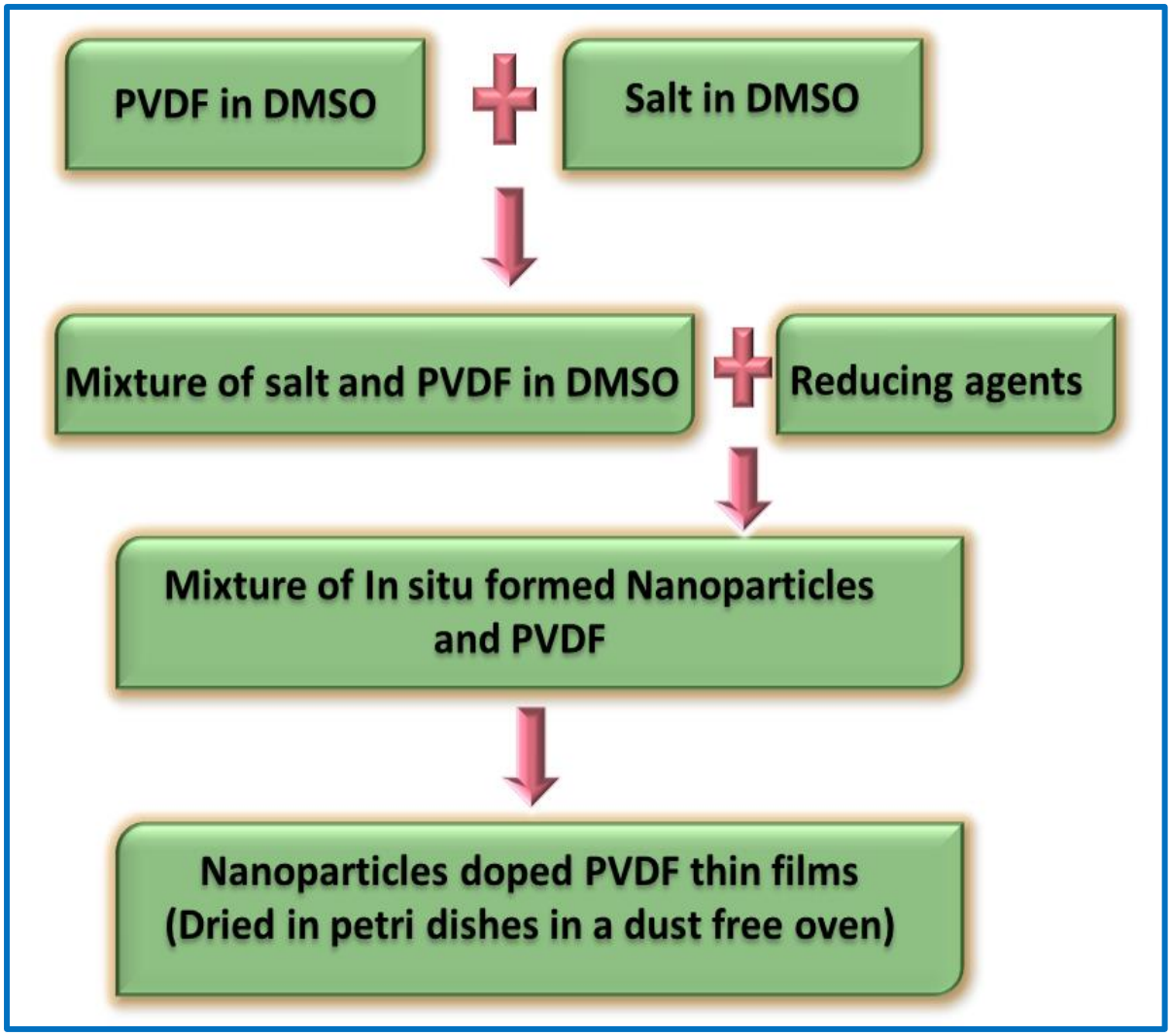

Figure 1.10: Schematic representation of the *In situ* process of polymer nanocomposite thin films synthesis.

1.3.4. (c): Electrospinning technique:

Electrospinning technique is interesting due to its ability to produce nanofiber mats with a high degree of uniformity and control over the film's thickness and morphology.

Electrospinning involves using an electric field to draw a polymer solution into fine fibers, which are then deposited onto a collector to form a thin film. For PVDF, the process starts by preparing a polymer solution in a suitable solvent. The solution is then loaded into a syringe, and a high voltage is applied between the syringe's needle and the collector. The electric field causes the polymer solution to be ejected from the needle as a fine jet, which solidifies into nanofibers as it travels through the air and lands on the collector shown in figure 1.11. the needle and collector. This results in PVDF thin films with desired properties for specific applications.

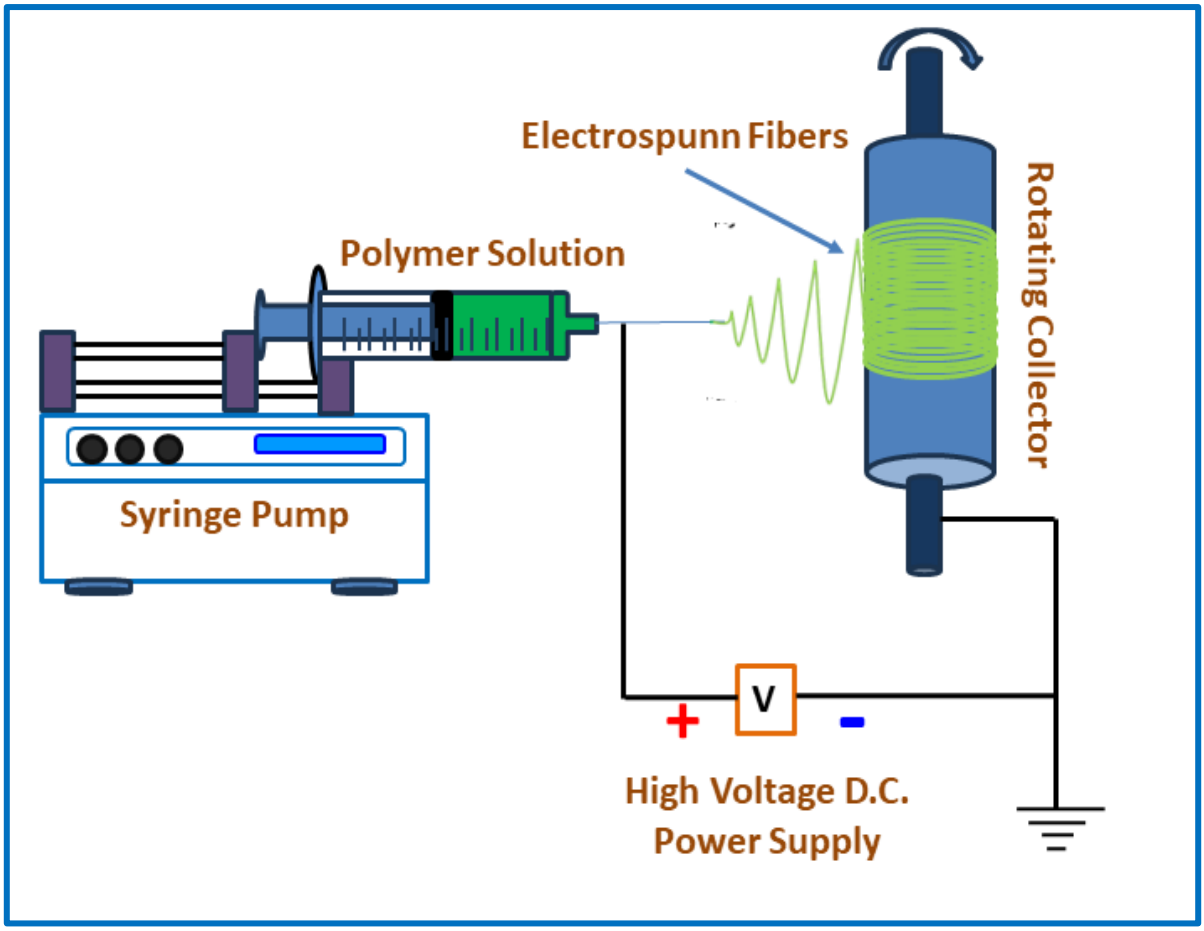

Figure 1.11: Schematic representation of the electrospinning process of polymer nanocomposite thin films synthesis.

1.3.4. (d) Literature Review of PVDF and Applications on Energy Harvestings:

The electroactive β-phase of Polyvinylidene Fluoride (PVDF) is a crucial aspect of its piezoelectric, ferroelectric, dielectric, and pyroelectric properties, making it a highly sought-after material for various technological applications [20-26]. To nucleate this phase, researchers have employed a range of techniques, including mechanical stretching, solvent casting, and the incorporation of micro-fillers or nanoparticles.

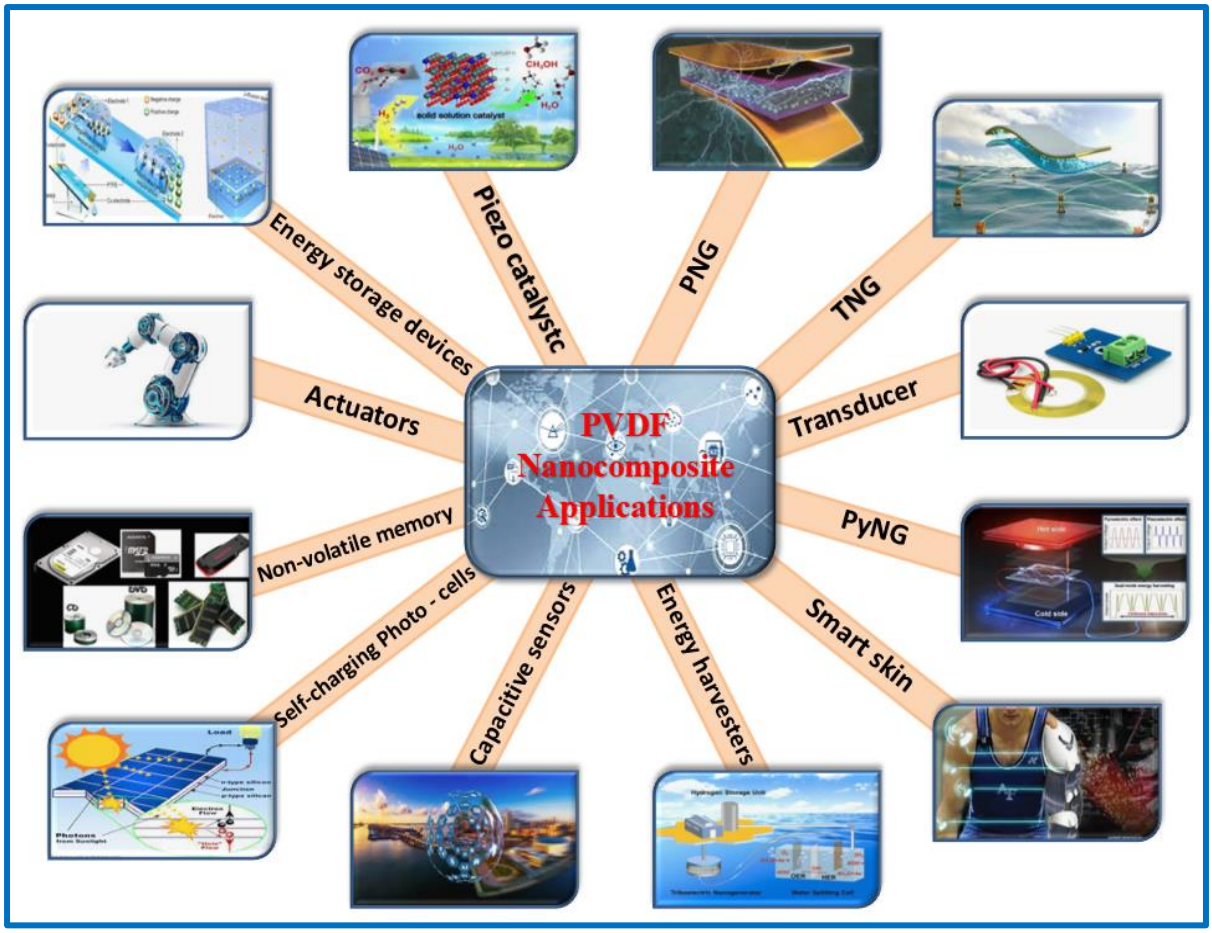

Figure 1.12: Flow chart representation of the applications of PVDF nanocomposite thin films.

Numerous studies, such as those conducted by Hassen et al [232-234]., Thakur et al [211, 235-236]., Roy et al [237-238]., and Lopes et al [210, 239-240]., have investigated the incorporation of diverse materials to nucleate the β-phase and enhance dielectric properties. These materials include metal oxides (e.g., SiO2, Al2O3, ZnO), metal nanoparticles (e.g., Au, Pd, Pt), clay minerals (e.g., Cloisite, montmorillonite), and carbon nanotubes (CNTs). The results of these studies have shown significant enhancements in piezoelectricity, dielectric constants, and energy harvesting capabilities.

Recent research by Fu et al [241-242]., Tamang et al [343]., Xie et al [244]., and Issa et al [245]. has also explored the use of bio-organic materials, such as cellulose nanocrystals, DNA [243], chitin, and cellulose particles [23], to induce β-phase crystallization and improve PVDF's properties. These innovative approaches have opened up new avenues for the development of PVDF nanocomposite thin films with enhanced performance.

The advancements in PVDF research have paved the way for its use in various applications, including piezoelectric nanogenerators, supercapacitors, actuators, and biomedical devices. By optimizing PVDF's properties and designing innovative materials, researchers can unlock its

full potential for cutting-edge technological applications, leading to breakthroughs in fields such as energy harvesting, sensing, and biomedicine.

1.4. Nanogenerator (PENG) Fabrication:

To construct our flexible piezoelectric nanogenerators (FPENGs), we began by preparing two flexible composite thin films of the desired dimensions. Next, 40 µm thick aluminium electrodes were affixed to both sides of the films using conductive ink, and two wires were extended from each film for performance measurement. The films, now equipped with electrodes and connecting wires, were then encased in polydimethylsiloxane (PDMS) (Sylgard 184, Dow Corning, ratio 1:10) by immersion in PDMS gel. The assembly was subsequently dried for 15 minutes under vacuum, followed by a 1-hour drying period at 60 °C to eliminate bubbles from the PDMS solution and yield flexible FPENGs (figure 1.13).

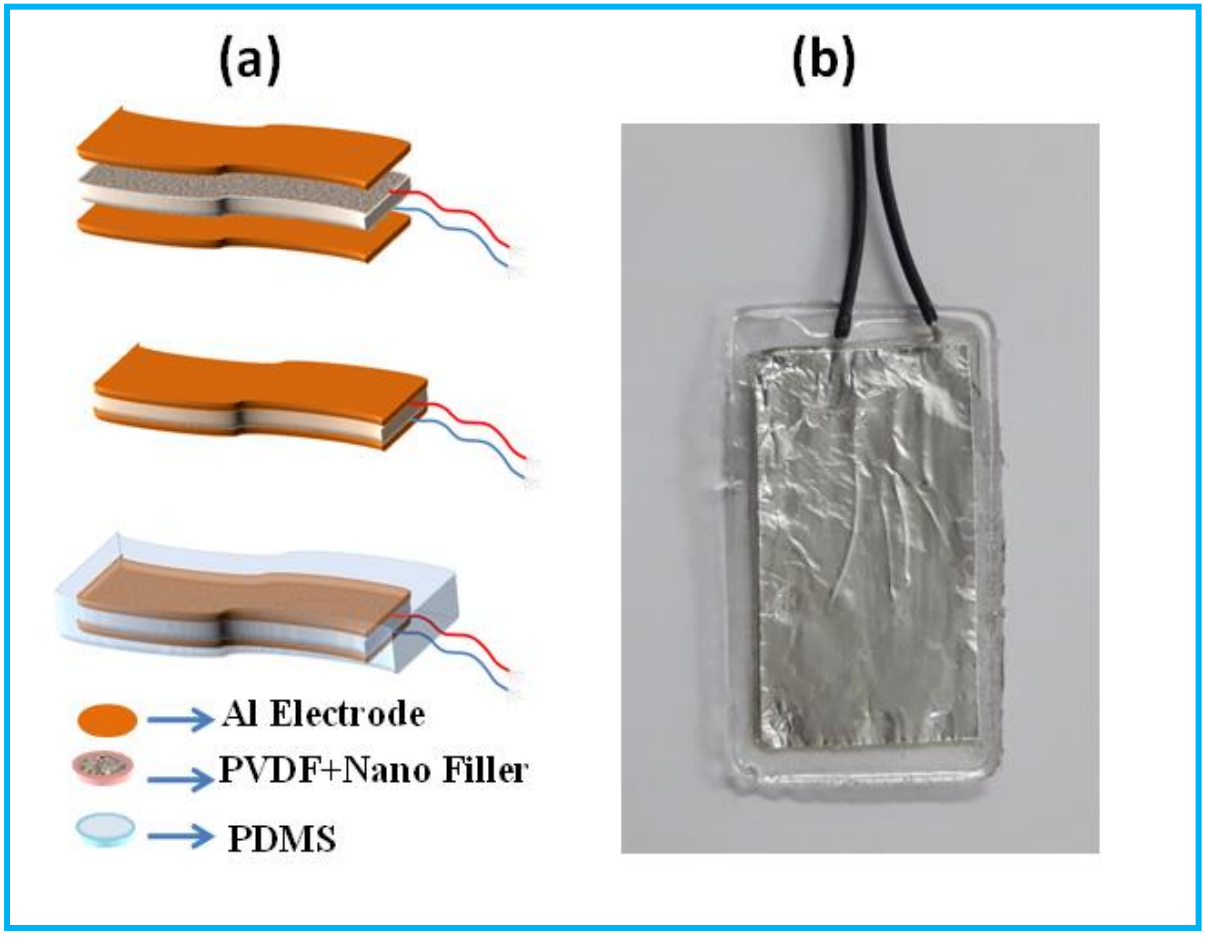

Figure 1.13: (a) Schematic of nanogenerator fabrication and (b) Digital Photograph of fabricated PENG.

1.5. Characterizations and Methodology:

1.5.1. X-ray diffraction (XRD)

X-Ray Diffraction (XRD) is a technique that utilizes electromagnetic radiation with photon energies between 100 eV and 100 keV to probe the structural arrangement of atoms and molecules in materials. Hard X-rays with short wavelengths (1-0.1 Å) are used to penetrate the material's structure. The X-ray beam, generated by an X-ray tube or synchrotron radiation, is directed at the material, causing elastic scattering (Thompson Scattering) of X-ray photons. The scattered X-rays provide information about the crystal structure, which is decoded by characterizing the scattered X-rays. In my research, a Bruker X-ray diffractometer (D8, AXS, Advance) with a Germanium (022) monochromator and Cu Kα (1.5406 Å) X-ray radiation is used. The diffraction pattern is recorded in θ-2θ mode, and the lattice spacing is calculated using Bragg's equation 1.1.

Mathematically, Bragg's law is expressed as:

$$\mathbf{2\, d_{hkl} sin\theta = n\lambda} \qquad \textbf{(1.1)}$$

Where n is the order of reflection, λ is the wavelength of incident X-ray, d_{hkl} is the distance between the (*hkl)* Bragg planes in the crystal, and θ is the angle between the incident x-ray beam and the Bragg plane

Peak shifting and broadening indicate changes in lattice constant and crystallite size, respectively. The average crystallite size is estimated using Scherrer's formula 1.2.

According to the Scherrer equation, the size of the particle is

$$\boldsymbol{D = \frac{k\lambda}{\beta cos\theta}} \qquad \textbf{(1.2)}$$

where K is the Scherrer constant, λ is the X-ray beam's wavelength, β is the peak's full width at half maximum (FWHM), and θ is the Bragg angle.

Figure 1.14 shows the Bruker-D8 X-ray diffractometer and a schematic diagram of X-ray interaction with the material.

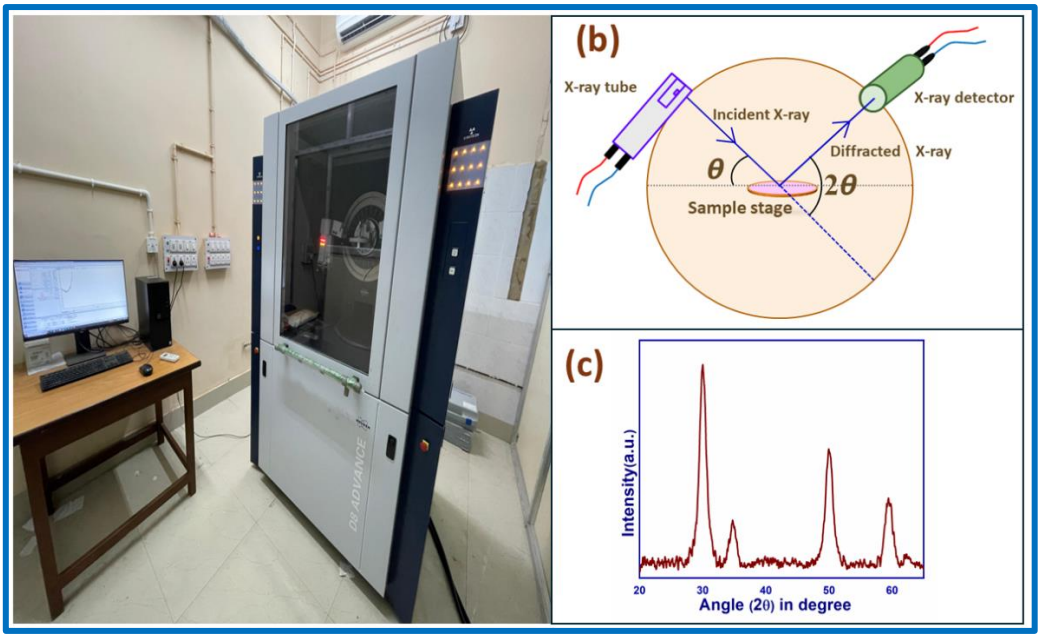

Figure 1.14: (a) Digital Photograph of XRD-Instrument, (b) Schematic diagram of X-ray diffractometer and (c) a typical XRD spectra pattern of crystalline material.

1.5.2. Fourier transform infrared spectroscopy (FTIR)

Fourier Transform Infrared Spectroscopy (FTIR) is a powerful technique for analysing the infrared absorption, emission, or transmission spectrum of solids, liquids, or gases. By measuring the frequencies of absorbed energy, FTIR identifies chemical bonding in molecular assemblies. The FTIR setup uses infrared light as the radiation source, covering a wide spectral range. The IR spectrum is divided into three subcategories: near-IR (14000-4000 cm^{-1}), mid-IR (4000-400 cm^{-1}), and far-IR (400-20 cm^{-1}). The FTIR spectrometer employs an interferometer to collect sample signals, which are then transformed into the actual spectrum via Fourier Transformation. The absorption intensity is proportional to the number of molecules involved in IR interactions, characterized using the Beer-Lambert principle. Modern FTIR systems utilize Michelson Interferometers for enhanced optical characterization. FTIR enables sample identification, consistency determination, and component analysis. Figure 1.15 shows the FTIR instrument and FTIR spectra. In this thesis, all FTIR spectra were obtained using the FTIR-8400S Shimadzu instrument.

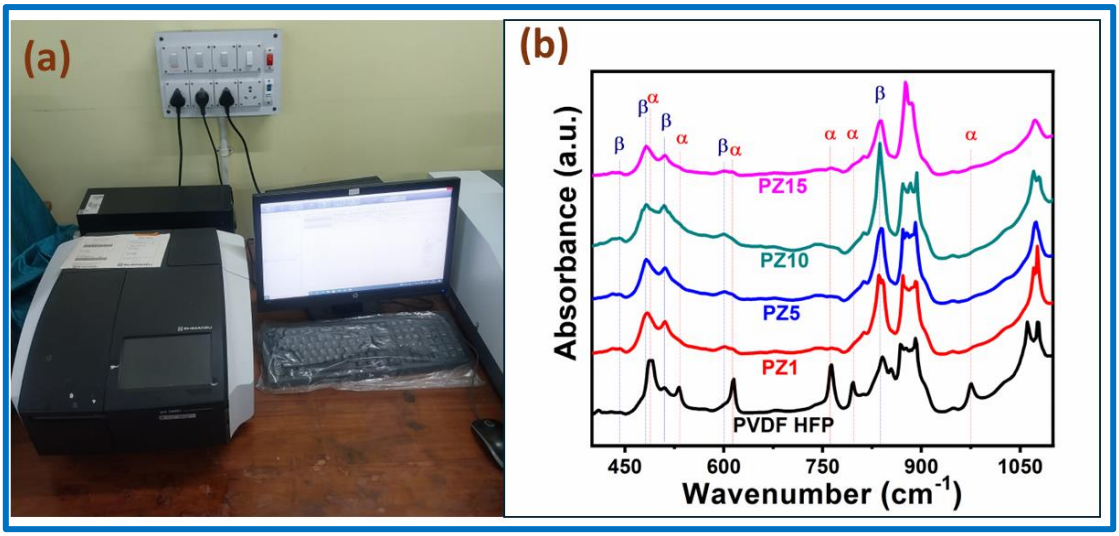

Figure 1.15 : (a) Digital Photograph of FTIR-Instrument and (b) a typical FTIR spectra.

1.5.3. Field emission scanning electron microscopy (FESEM)

Field Emission Scanning Electron Microscopy (FESEM) is a widely used technique for imaging the surface morphology of nano/micro-sized materials. It employs a field-emitted electron source, typically made of Lanthanum hexaboride or tungsten, and a system of electromagnetic lenses to focus electrons on the sample. The interaction between high-energy electrons and the sample releases secondary and backscattered electrons, which are detected and converted into electronic signals, generating an imaging view. FESEM is suitable for well-conducting surfaces, but insulating samples require a conductive coating, such as gold or platinum, to prevent charging and ensure high-quality images. In this thesis, FESEM images were obtained using the FESEM, INSPECT, F50 (Netherlands). Figure 1.16 shows the FESEM instrument and some FE-SEM image of PVDF nano composite sheet, nanoparticle surface and nanofibers obtained by this instrument.

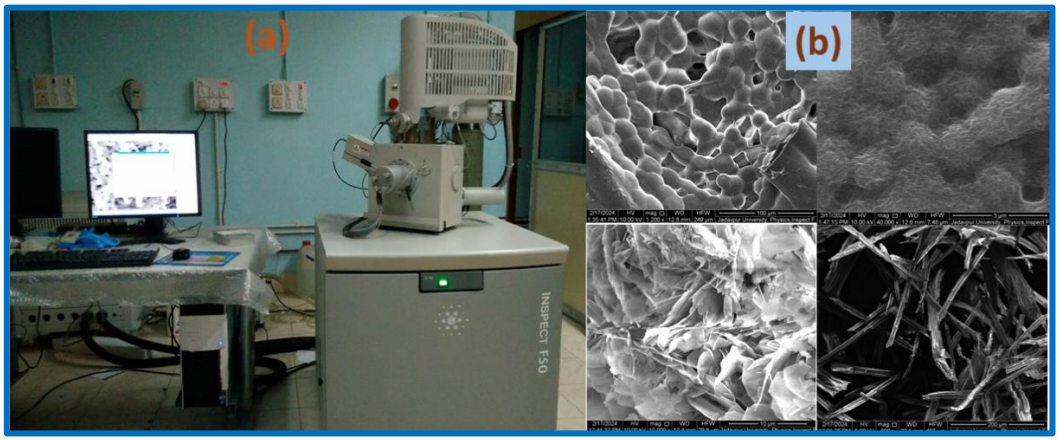

Figure 1.16: (a) Digital Photograph of FESEM-Instrument and (b) FE-SEM micrograph of PVDF nano composite sheet, nanoparticle surface morphology and nanofibers.

1.5.4. UV-Visible spectroscopy

UV-vis spectroscopy is a crucial characterization tool for investigating synthesized materials, applicable to a wide range of particle sizes. This technique examines optical properties like absorption, transmission, or reflection spectra, enabling the estimation of band-gap energy using Kubelka-Monk's function or Tauc plot. The nature of the band-gap (direct or indirect) can also be determined. In UV-vis spectroscopy, photons with selective energies interact with the sample. Photons with energy above the band-gap energy are absorbed, while those below are transmitted. The spectrophotometer uses visible, near-UV, and near-infrared light, inducing electronic transitions in the molecules. Absorbance is calculated using the Beer-Lambert law: $A = \log_{10} (I_o/I) = \varepsilon cl$. The spectrophotometer employs two prisms: one for dispersing emitted light and another for splitting monochromatic light into two beams, which pass through sample and reference solutions. The resulting signals are amplified and visualized on a monitor screen. In this thesis, UV-vis absorption spectra were obtained using a Lambda 365 UV-Vis spectrophotometer.

1.5.5. TGA analysis:

Thermal Gravimetric Analysis (TGA) is a technique that measures the temperature-dependent mass change of a material, providing insights into its thermal stability, decomposition, moisture content, and oxidation. Using a Mettler Toledo SDTA machine {figure 1.17: (a)}, TGA involves heating or cooling a material in a controlled atmosphere while measuring its mass change with a sensitive balance. The resulting TGA curve reveals valuable information, including mass loss or gain, temperature range of stability, decomposition temperature, and rate of mass change, making TGA an essential tool in materials science research to understand a material's thermal behaviour and properties.

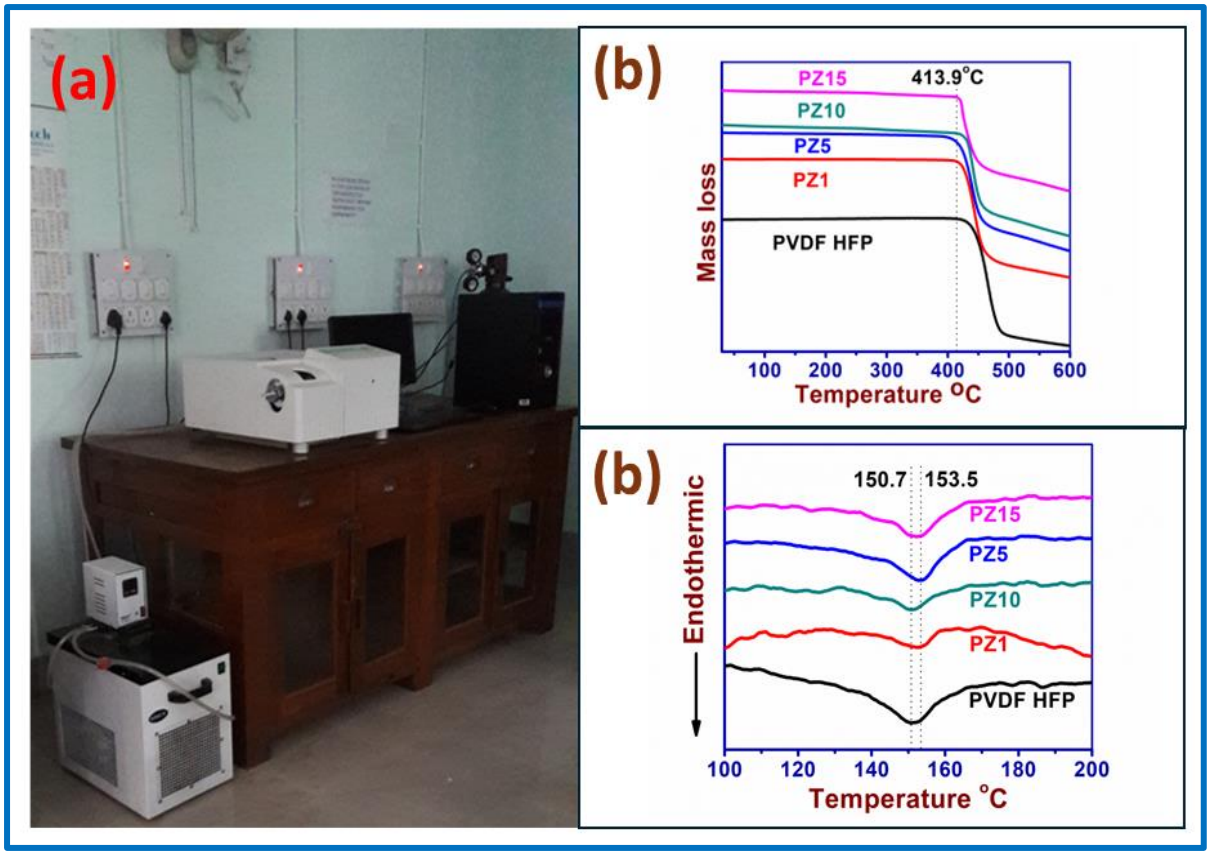

Figure 1.17: (a) Digital Photograph of SDTA-Instrument, (b) TGA-Curve and (c) DSC thermograph.

1.5.6. DSC Analysis:

The thermal properties of PVDF composite films or nanoparticles, specifically phase crystallization and melting behavior, were examined using differential scanning calorimetry (DSC-60, Shimadzu). Samples were heated to 100°C at a rate of 10°C/min under a nitrogen atmosphere. Differential Scanning Calorimetry (DSC) is a thermal analysis technique used to study the thermal properties of materials, including melting, crystallization, glass transitions, and oxidation. It measures the difference in heat flow between a sample and a reference material as they are heated or cooled at a controlled rate. The resulting DSC curves allowed for the calculation of melting enthalpies (ΔHm) or enthalpies of fusion, which were then used to determine the degree of crystallinity (Xc) of the samples. This was achieved through the equation:

$$\chi_c = \frac{\Delta H_m}{\Delta H_{100\%}} \times 100\% \qquad (1.3)$$

where ΔHm represents the heat of melting or enthalpy of fusion, and ΔH100% is the melting enthalpy of 100% crystalline PVDF, with a value of 104.6 J/g. This calculation enabled the evaluation of the crystalline structure and thermal stability of the PVDF composites.

1.5.7. Surface charge analysis (Zeta Potential)

The surface charge of the nanoparticles (NPs) was characterized using zeta potential measurements, performed on a Zeta-sizer-5000 (Malvern Instruments, UK). This technique employs laser Doppler electrophoresis to determine the electrophoretic mobility of the particles, which is then converted to zeta potential values. The zeta potential is a critical parameter that indicates the surface charge of the NPs, providing insight into their stability, aggregation behavior, and potential interactions with other molecules or surfaces. The zeta potential measurement is based on the principle that particles in a solution will move in response to an applied electric field, with the velocity of this movement being proportional to the surface charge. By measuring the velocity of the particles, the zeta potential can be calculated, typically expressed in millivolts (mV) (figure 1.18).

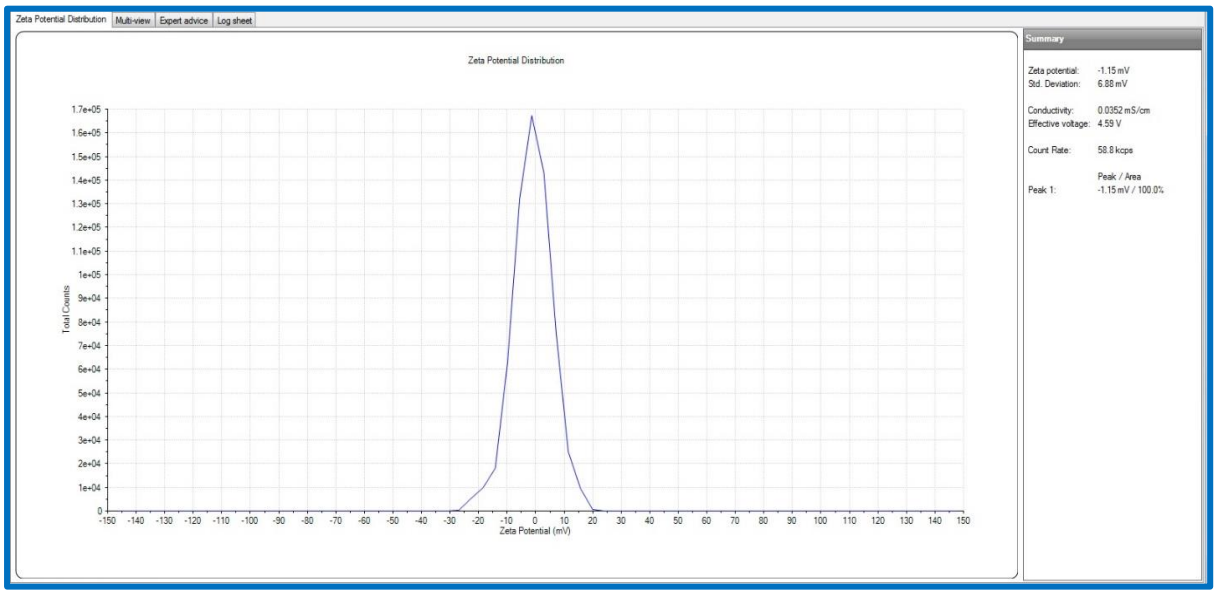

Figure 1.18: Zeta Potential Curve.

1.5.8. The stress–strain measurement:

The mechanical properties of PVDF-based composite thin films were thoroughly evaluated using a Universal Tensile Machine (UTM). The testing protocol involved a cross-head speed of 2 mm/min, ensuring a controlled and precise application of force. A constant load cell of 10N was employed to measure the tensile strength and elongation at break of the composite films. The specimens were carefully prepared with dimensions of 1 cm in breadth and 5 cm in length, adhering to standard testing procedures. The UTM tests provided valuable insights into the mechanical behavior of the PVDF composite films, including their tensile strength, which represents the maximum stress they can withstand before failure. Additionally, the elongation

at break was measured, indicating the films' flexibility and ability to deform without rupturing. These critical parameters are essential for understanding the suitability of the PVDF composites for various applications, particularly in energy harvesting devices where mechanical robustness is crucial. By conducting these mechanical tests, researchers can optimize the composition and fabrication processes of the PVDF composites to achieve enhanced tensile strength, elongation at break, and overall durability. This, in turn, can lead to the development of more efficient and reliable energy harvesting systems.

1.5.9. Dielectric and Tangent Loss Measurements:

The dielectric properties of the samples were investigated using a digital LCR meter (Agilent, E4980A) at room temperature, with capacitance (C) and tangent loss (tan δ) measurements collected over a frequency range of 40 Hz to 10 MHz A 1 V ac voltage was applied across the two opposite surfaces of the samples. The dielectric constant (ε_r) and tangent loss were derived through the following relationships:

$$\varepsilon_r = \frac{Cd}{A\varepsilon_0} \quad \textbf{(1.4)}$$

$$tan\delta = \frac{\varepsilon_i}{\varepsilon_r} \quad \textbf{(1.5)}$$

where ε_r represents the real part of the dielectric permittivity, indicating the material's polarizing capacity, ε_i denotes the imaginary part corresponding to the loss factor or energy dissipation, C is the capacitance, d is the film thickness, A is the membrane area, and ε_0, is the permittivity of free space (8.85×10^{-12} F/m). The digital LCR meter used in this study offers high accuracy and precision, allowing for reliable measurements of the dielectric properties. The frequency range of 40 Hz to 10 MHz covers a broad spectrum, enabling the investigation of the material's behavior under various frequency conditions. By analysing the dielectric constant and ac conductivity, researchers can gain a deeper understanding of the material's electrical properties, which is crucial for applications in electronics, energy storage, and other fields.

1.5.10. Open circuit voltage Measurements:

The open-circuit voltage (V_{oc}) is a critical parameter that represents the equilibrium voltage between two electrodes when no current is flowing. In this study, Voc was measured by applying pressure directly to the sample and detecting the resulting voltage using a digital storage oscilloscope (Keysight, Oscilloscope DSO-X 3012A) (Figure 1.19). This technique allows for the precise determination of Voc, which is essential for understanding the electrical

properties of materials. The digital storage oscilloscope used in this study offers high-resolution and high-sensitivity measurements, enabling the accurate detection of even slight changes in voltage. By measuring Voc, researchers can gain insights into the material's electrical behavior, including its potential for energy harvesting and sensing applications. The measurement of Voc involves creating an open circuit, where the electrodes are not connected to an external circuit, allowing the voltage to stabilize. The resulting Voc value represents the maximum voltage that can be generated by the material, making it a crucial parameter for evaluating its performance.

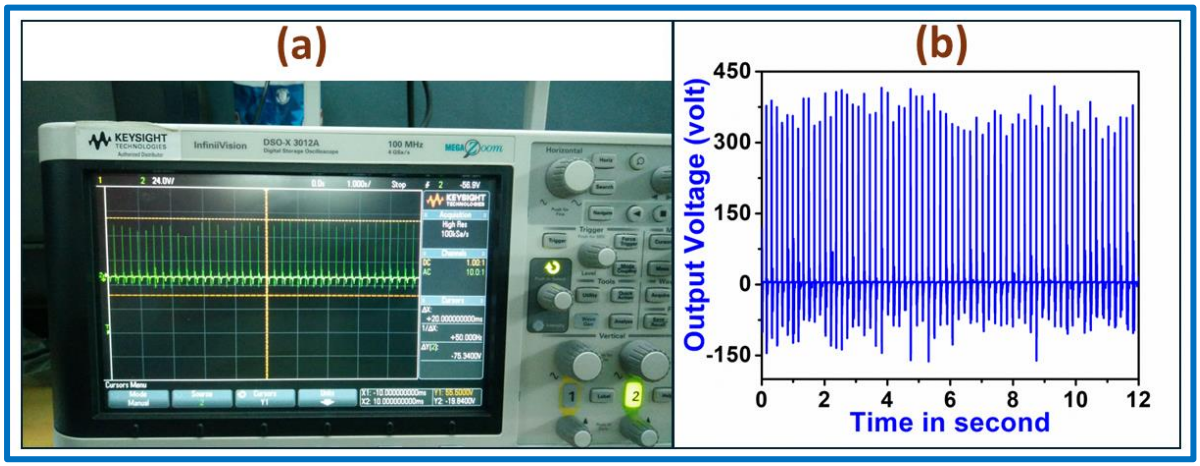

Figure 1.19 : (a) Digital Photograph of DSO-Instrument and (b) Open circuit voltage pattern.

1.5.11. Short circuit current Measurements:

The short-circuit current (Isc) of a Piezoelectric Energy Harvesting (PENG) device was measured using a Keysight Electrometer B2985A. This parameter represents the maximum current output when the device is connected to a circuit with zero external load. To simulate real-world operating conditions, a periodic mechanical force was applied to the PENG device while the Isc was measured. This experiment aimed to evaluate the device's ability to generate electricity from mechanical stress.

1.6. Objectives:

The primary objectives of this thesis are:

1. To develop Single Electrode Triboelectric Nanogenerators (STENGs) based on polymer thin films with varied surface charges for healthcare applications.
2. To enhance the performance of STENGs by incorporating nanoparticles into the polymer matrix and optimizing the device design.
3. To investigate the structural, morphological, and optical properties of the synthesized nanoparticles and fabricated polymer nanocomposite thin films.

4. To comprehensively study the optical and electrical properties of the nanocomposites.

5. To develop flexible PENGs and STENGs that can be strategically placed on the human skin to monitor various physiological activities.

6. To integrate the developed PENG and TENG-based self-powered device with wireless communication capabilities to create a comprehensive health monitoring system.

By achieving these objectives, this thesis aims to advance sustainable and safe biomechanical energy harvesting technologies and contribute to the development of real-time health monitoring systems.

******

References:

[1]. Jonsson, F.A., Brewer, J., Fromer, N. and Trentmann, F., 2019. *Scarcity in the modern world: History, politics, society and sustainability, 1800–2075*. Bloomsbury Academic.
[2]. Brown, M.A. and Sovacool, B.K., 2011. *Climate change and global energy security: technology and policy options*. MIT Press.
[3]. Owusu, P.A. and Asumadu-Sarkodie, S., 2016. A review of renewable energy sources, sustainability issues and climate change mitigation. *Cogent Engineering*, *3*(1), p.1167990.
[4]. Yáñez-Arancibia, A., Day, J.W., Hall, C.A.S. and Reyes, E., 2013. Diminished resources, energy scarcity and climate change: unsustainable future development. *WIT Transactions on State-of-the-art in Science and Engineering*, *64*.
[5]. Kozar, R., Galang, E., Alip, A., Sedhain, J., Subramanian, S. and Saito, O., 2019. Multi-level networks for sustainability solutions: the case of the International Partnership for the Satoyama Initiative. *Current Opinion in Environmental Sustainability*, *39*, pp.123-134.
[6]. Lafortezza, R. and Sanesi, G., 2019. Nature-based solutions: Settling the issue of sustainable urbanization. *Environmental research*, *172*, pp.394-398.
[7]. Bansard, J.S., Hickmann, T. and Kern, K., 2019. Pathways to urban sustainability: How science can contribute to sustainable development in cities. *GAIA-ecological perspectives for science and society*, *28*(2), pp.112-118.
[8]. Sobianin, I., Psoma, S.D. and Tourlidakis, A., 2022. Recent advances in energy harvesting from the human body for biomedical applications. *Energies*, *15*(21), p.7959.
[9]. Zou, Y., Bo, L. and Li, Z., 2021. Recent progress in human body energy harvesting for smart bioelectronic system. *Fundamental Research*, *1*(3), pp.364-382.
[10]. Afroz, A.S., Romano, D., Inglese, F. and Stefanini, C., 2021. Towards bio-hybrid energy harvesting in the real-world: pushing the boundaries of technologies and strategies using bio-electrochemical and bio-mechanical processes. *Applied Sciences*, *11*(5), p.2220.
[11]. Dong, L., Closson, A.B., Jin, C., Trase, I., Chen, Z. and Zhang, J.X., 2019. Vibration-energy-harvesting system: transduction mechanisms, frequency tuning techniques, and biomechanical applications. *Advanced materials technologies*, *4*(10), p.1900177.
[12]. Zou, H., Li, M., Zhao, L., Liao, X., Gao, Q., Yan, G., Du, R., Wei, K. and Zhang, W., 2022. Cooperative compliant traction mechanism for human-friendly biomechanical energy harvesting. *Energy Conversion and Management*, *258*, p.115523.
[13]. Khalid, S., Raouf, I., Khan, A., Kim, N. and Kim, H.S., 2019. A review of human-powered energy harvesting for smart electronics: recent progress and challenges. *International Journal of Precision Engineering and Manufacturing-Green Technology*, *6*, pp.821-851.
[14]. Zheng, Q., Shi, B., Li, Z. and Wang, Z.L., 2017. Recent progress on piezoelectric and triboelectric energy harvesters in biomedical systems. *Advanced Science*, *4*(7), p.1700029.
[15]. Qi, Y. and McAlpine, M.C., 2010. Nanotechnology-enabled flexible and biocompatible energy harvesting. *Energy & Environmental Science*, *3*(9), pp.1275-1285.
[16]. Panda, S., Hajra, S., Mistewicz, K., In-na, P., Sahu, M., Rajaitha, P.M. and Kim, H.J., 2022. Piezoelectric energy harvesting systems for biomedical applications. *Nano Energy*, *100*, p.107514.
[17]. M. Zhu, Q. Shi, T. He, Z. Yi, Y. Ma, B. Yang, T. Chen, C. Lee, Self-powered and self-functional cotton sock using piezoelectric and triboelectric hybrid mechanism for healthcare and sports monitoring, ACS Nano 13(2019)1940-1952.
[18]. Shi, B., Li, Z. and Fan, Y., 2018. Implantable energy-harvesting devices. *Advanced Materials*, *30*(44), p.1801511.
[19]. Niu, L., Miao, X., Jiang, G., Wan, A., Li, Y. and Liu, Q., 2020. Biomechanical energy harvest based on textiles used in self-powering clothing. *Journal of Engineered Fibers and Fabrics*, *15*, p.1558925020967352.

[20]. Yan, J., Liu, M., Jeong, Y.G., Kang, W., Li, L., Zhao, Y., Deng, N., Cheng, B. and Yang, G., 2019. Performance enhancements in poly (vinylidene fluoride)-based piezoelectric nanogenerators for efficient energy harvesting. *Nano energy*, *56*, pp.662-692.
[21]. Sukumaran, S., Chatbouri, S., Rouxel, D., Tisserand, E., Thiebaud, F. and Ben Zineb, T., 2021. Recent advances in flexible PVDF based piezoelectric polymer devices for energy harvesting applications. *Journal of Intelligent Material Systems and Structures*, *32*(7), pp.746-780.
[22]. Mohammadpourfazeli, S., Arash, S., Ansari, A., Yang, S., Mallick, K. and Bagherzadeh, R., 2023. Future prospects and recent developments of polyvinylidene fluoride (PVDF) piezoelectric polymer; fabrication methods, structure, and electro-mechanical properties. *RSC advances*, *13*(1), pp.370-387.
[23]. Feng, Z., Zhao, Z., Liu, Y., Liu, Y., Cao, X., Yu, D.G. and Wang, K., 2023. Piezoelectric effect polyvinylidene fluoride (PVDF): from energy harvester to smart skin and electronic textiles. *Advanced Materials Technologies*, *8*(14), p.2300021.
[24]. Mishra, S., Unnikrishnan, L., Nayak, S.K. and Mohanty, S., 2019. Advances in piezoelectric polymer composites for energy harvesting applications: a systematic review. *Macromolecular Materials and Engineering*, *304*(1), p.1800463.
[25]. Costa, C.M., Cardoso, V.F., Brito-Pereira, R., Martins, P., Correia, D.M., Correia, V., Ribeiro, C., Martins, P.M. and Lanceros-Méndez, S., 2020. Electroactive poly (vinylidene fluoride)-based materials: Recent progress, challenges, and opportunities. *Fascinating Fluoropolymers and Their Applications*, pp.1-43.
[26]. Sharma, S., Mishra, S.S., Kumar, R. and Yadav, R.M., 2022. Recent progress on polyvinylidene difluoride-based nanocomposites: applications in energy harvesting and sensing. *New Journal of Chemistry*, *46*(39), pp.18613-18646.
[27]. Saxena, P. and Shukla, P., 2021. A comprehensive review on fundamental properties and applications of poly (vinylidene fluoride)(PVDF). *Advanced Composites and Hybrid Materials*, *4*, pp.8-26.
[28]. Lu, L., Ding, W., Liu, J. and Yang, B., 2020. Flexible PVDF based piezoelectric nanogenerators. *Nano Energy*, *78*, p.105251.
[29]. Sui, Y., Chen, W.T., Ma, J.J., Hu, R.H. and Liu, D.S., 2016. Enhanced dielectric and ferroelectric properties in PVDF composite flexible films through doping with diisopropylammonium bromide. *RSC advances*, *6*(9), pp.7364-7369.
[30]. Xie, L., Wang, G., Jiang, C., Yu, F. and Zhao, X., 2021. Properties and applications of flexible poly (vinylidene fluoride)-based piezoelectric materials. *Crystals*, *11*(6), p.644.
[31]. Xia, W. and Zhang, Z., 2018. PVDF-based dielectric polymers and their applications in electronic materials. *Iet Nanodielectrics*, *1*(1), pp.17-31.
[32]. Mohammadpourfazeli, S., Arash, S., Ansari, A., Yang, S., Mallick, K. and Bagherzadeh, R., 2023. Future prospects and recent developments of polyvinylidene fluoride (PVDF) piezoelectric polymer; fabrication methods, structure, and electro-mechanical properties. *RSC advances*, *13*(1), pp.370-387.*Materials*, *33*(38), p.2301302.
[33]. Liu, X., Luo, H., Yan, C., Liu, Y., Luo, H., Zhang, D. and Chen, S., 2022. Achieving synergistic improvement in dielectric constant and energy storage properties of all-organic liquid crystal molecule/PVDF composites. *Journal of Materials Chemistry C*, *10*(46), pp.17757-17767.
[34]. Laudari, A., Barron, J., Pickett, A. and Guha, S., 2020. Tuning charge transport in PVDF-based organic ferroelectric transistors: status and outlook. *ACS applied materials & interfaces*, *12*(24), pp.26757-26775.
[35]. Yang, H., Fan, F.R., Xi, Y. and Wu, W., 2020. Bio-derived natural materials based Triboelectric devices for self-powered ubiquitous wearable and implantable intelligent devices. *Advanced Sustainable Systems*, *4*(9), p.2000108.

[36]. Shao, Y., Shen, M., Zhou, Y., Cui, X., Li, L. and Zhang, Y., 2021. Nanogenerator-based self-powered sensors for data collection. *Beilstein Journal of Nanotechnology*, *12*(1), pp.680-693.
[37]. Wang, W., Yu, A., Zhai, J. and Wang, Z.L., 2021. Recent progress of functional fiber and textile triboelectric nanogenerators: towards electricity power generation and intelligent sensing. *Advanced Fiber Materials*, *3*(6), pp.394-412.
[38]. Zou, Y., Raveendran, V. and Chen, J., 2020. Wearable triboelectric nanogenerators for biomechanical energy harvesting. *Nano Energy*, *77*, p.105303.
[39]. Solanki, S., Gupta, A.K., Saha, U., Krasnoslobodtsev, A.V., Gupta, R.K. and Malhotra, B.D., 2023. Triboelectric Nanogenerator-based smart biomedical sensors for healthcare. *Sustainable Energy Technologies and Assessments*, *57*, p.103233.
[40]. Zheng, Q., Shi, B., Li, Z. and Wang, Z.L., 2017. Recent progress on piezoelectric and triboelectric energy harvesters in biomedical systems. *Advanced Science*, *4*(7), p.1700029.
[41]. Tat, T., Libanori, A., Au, C., Yau, A. and Chen, J., 2021. Advances in triboelectric nanogenerators for biomedical sensing. *Biosensors and Bioelectronics*, *171*, p.112714.
[42]. Sapkal, S., Kandasubramanian, B. and Panda, H.S., 2022. A review of piezoelectric materials for nanogenerator applications. *Journal of Materials Science: Materials in Electronics*, *33*(36), pp.26633-26677.
[43]. Sripadmanabhan Indira, S., Aravind Vaithilingam, C., Oruganti, K.S.P., Mohd, F. and Rahman, S., 2019. Nanogenerators as a sustainable power source: state of art, applications, and challenges. *Nanomaterials*, *9*(5), p.773.
[44]. Mariello, M., 2022. Recent Advances on hybrid piezo-triboelectric bio-nanogenerators: Materials, architectures and circuitry. *Nanoenergy Advances*, *2*(1), pp.64-109.
[45]. Raj, N.P.M.J., Alluri, N.R., Khandelwal, G. and Kim, S.J., 2019. Lead-free piezoelectric nanogenerator using lightweight composite films for harnessing biomechanical energy. *Composites Part B: Engineering*, *161*, pp.608-616.
[46]. Parida, K. and Bendi, R., 2021. Piezoelectric Energy Harvesting and Piezocatalysis. In *Nano-catalysts for Energy Applications* (pp. 171-189). CRC Press.
[47]. Bera, B. and Sarkar, M.D., 2017. Piezoelectricity in PVDF and PVDF based piezoelectric nanogenerator: a concept. *IOSR J. Appl. Phys*, *9*(3), pp.95-99.
[48]. Pusty, M. and Shirage, P.M., 2022. Insights and perspectives on graphene-PVDF based nanocomposite materials for harvesting mechanical energy. *Journal of Alloys and Compounds*, *904*, p.164060.
[49]. Wu, L., Jin, Z., Liu, Y., Ning, H., Liu, X., Alamusi and Hu, N., 2022. Recent advances in the preparation of PVDF-based piezoelectric materials. *Nanotechnology Reviews*, *11*(1), pp.1386-1407.
[50]. Mrlík, M., Osička, J., Cvek, M., Ilčíková, M., Srnec, P., Gorgol, D. and Tofel, P., 2021. Comparative study of PVDF sheets and their sensitivity to mechanical vibrations: The role of dimensions, molecular weight, stretching and poling. *nanomaterials*, *11*(7), p.1637.
[51]. Vijaya, M.S., 2012. *Piezoelectric materials and devices: applications in engineering and medical sciences*. CRC press.
[52]. Uchino, K., 2017. The development of piezoelectric materials and the new perspective. In *Advanced Piezoelectric Materials* (pp. 1-92). Woodhead Publishing.
[53]. Bowen, C.R., Kim, H.A., Weaver, P.M. and Dunn, S., 2014. Piezoelectric and ferroelectric materials and structures for energy harvesting applications. *Energy & Environmental Science*, *7*(1), pp.25-44.
[54]. Behera, A. and Behera, A., 2022. Piezoelectric materials. *Advanced Materials: An Introduction to Modern Materials Science*, pp.43-76.
[55]. Qian, W., Yang, W., Zhang, Y., Bowen, C.R. and Yang, Y., 2020. Piezoelectric materials for controlling electro-chemical processes. *Nano-Micro Letters*, *12*, pp.1-39.

[56]. Rajabi, A.H., Jaffe, M. and Arinzeh, T.L., 2015. Piezoelectric materials for tissue regeneration: A review. *Acta biomaterialia*, *24*, pp.12-23.
[57]. Mahapatra, S.D., Mohapatra, P.C., Aria, A.I., Christie, G., Mishra, Y.K., Hofmann, S. and Thakur, V.K., 2021. Piezoelectric materials for energy harvesting and sensing applications: roadmap for future smart materials. *Advanced Science*, *8*(17), p.2100864.
[58]. Hamlehdar, M., Kasaeian, A. and Safaei, M.R., 2019. Energy harvesting from fluid flow using piezoelectrics: A critical review. *Renewable Energy*, *143*, pp.1826-1838.
[59]. Egbe, K.J.I., Nazar, A.M., Jiao, P., Yang, Y., Ye, X. and Wang, H., 2021. Vibrational turbine piezoelectric nanogenerators for energy harvesting in multiphase flow fields. *Energy Reports*, *7*, pp.6384-6393.
[60]. Chen, X., Wang, J., Wang, Z., Xu, H., Liu, C., Huo, B., Meng, F., Wang, Y. and Sun, C., 2023. Low-frequency mechanical energy in the environment for energy production and piezocatalytic degradation of organic pollutants in water: a review. *Journal of Water Process Engineering*, *56*, p.104312.
[61]. Li, X., Zhou, Y., Li, Z., Guo, H., Gong, Y., Zhang, D., Zhang, D., Zhang, Q., Wang, B. and Peng, Y., 2023. Vortex-induced vibration triboelectric nanogenerator for energy harvesting from low-frequency water flow. *Energy Conversion and Management*, *292*, p.117383.
[62]. Gong, Y., Yang, Z., Shan, X., Sun, Y., Xie, T. and Zi, Y., 2019. Capturing flow energy from ocean and wind. *Energies*, *12*(11), p.2184.
[63]. Lu, C., Jiang, X., Li, L., Zhou, H., Yang, A., Xin, M., Fu, G. and Wang, X., 2022. Wind energy harvester using piezoelectric materials. *Review of Scientific Instruments*, *93*(3).
[64]. Pu, X., Hu, W. and Wang, Z.L., 2018. Toward wearable self-charging power systems: the integration of energy-harvesting and storage devices. *Small*, *14*(1), p.1702817.
[65]. Chandrasekaran, S., Bowen, C., Roscow, J., Zhang, Y., Dang, D.K., Kim, E.J., Misra, R.D.K., Deng, L., Chung, J.S. and Hur, S.H., 2019. Micro-scale to nano-scale generators for energy harvesting: Self powered piezoelectric, triboelectric and hybrid devices. *Physics Reports*, *792*, pp.1-33.
[66]. Liu, L., Guo, X., Liu, W. and Lee, C., 2021. Recent progress in the energy harvesting technology—from self-powered sensors to self-sustained IoT, and new applications. *Nanomaterials*, *11*(11), p.2975.
[67]. Calautit, K., Nasir, D.S. and Hughes, B.R., 2021. Low power energy harvesting systems: State of the art and future challenges. *Renewable and Sustainable Energy Reviews*, *147*, p.111230.
[68]. Ramasubramanian, B., Sundarrajan, S., Rao, R.P., Reddy, M.V., Chellappan, V. and Ramakrishna, S., 2022. Novel low-carbon energy solutions for powering emerging wearables, smart textiles, and medical devices. *Energy & Environmental Science*, *15*(12), pp.4928-4981.
[69]. Bhatnagar, V. and Owende, P., 2015. Energy harvesting for assistive and mobile applications. *Energy Science & Engineering*, *3*(3), pp.153-173.
[70]. Chandrasekhar, A., Basith, S.A., Vivekananthan, V., Khandelwal, G., Raj, N.P.M.J., Purusothaman, Y. and Kim, S.J., 2024. Smart maracas: An innovative triboelectric nanogenerator for earthquake detection and energy harvesting. *Nano Energy*, *123*, p.109379.
[71]. Alam, S.N., Ghosh, A., Shrivastava, P., Shukla, U., Garg, K., Edara, A.C. and Sahoo, N., 2023. An introduction to triboelectric nanogenerators. *Nano-Structures & Nano-Objects*, *34*, p.100980.
[72]. Sripadmanabhan Indira, S., Aravind Vaithilingam, C., Oruganti, K.S.P., Mohd, F. and Rahman, S., 2019. Nanogenerators as a sustainable power source: state of art, applications, and challenges. *Nanomaterials*, *9*(5), p.773.
[73]. Wang, A.C., Wu, C., Pisignano, D., Wang, Z.L. and Persano, L., 2018. Polymer nanogenerators: opportunities and challenges for large-scale applications. *Journal of Applied Polymer Science*, *135*(24), p.45674.

[74]. Raj, N.P.M.J., Alluri, N.R., Vivekananthan, V., Chandrasekhar, A., Khandelwal, G. and Kim, S.J., 2018. Sustainable yarn type-piezoelectric energy harvester as an eco-friendly, cost-effective battery-free breath sensor. *Applied Energy*, *228*, pp.1767-1776.
[75]. Karan, S.K., Maiti, S., Lee, J.H., Mishra, Y.K., Khatua, B.B. and Kim, J.K., 2020. Recent advances in self-powered tribo-/piezoelectric energy harvesters: all-in-one package for future smart technologies. *Advanced Functional Materials*, *30*(48), p.2004446.
[76]. Mariello, M., 2022. Recent Advances on hybrid piezo-triboelectric bio-nanogenerators: Materials, architectures and circuitry. *Nanoenergy Advances*, *2*(1), pp.64-109.
[77]. Chang, N.L., Ho-Baillie, A.W.Y., Vak, D., Gao, M., Green, M.A. and Egan, R.J., 2018. Manufacturing cost and market potential analysis of demonstrated roll-to-roll perovskite photovoltaic cell processes. *Solar Energy Materials and Solar Cells*, *174*, pp.314-324.
[78]. Schneider, G.A., 2007. Influence of electric field and mechanical stresses on the fracture of ferroelectrics. *Annu. Rev. Mater. Res.*, *37*(1), pp.491-538.
[79]. Yudin, Peter V., and Alexander K. Tagantsev. "Fundamentals of flexoelectricity in solids." *Nanotechnology* 24, no. 43 (2013): 432001.
[80]. Manbachi, A. and Cobbold, R.S., 2011. Development and application of piezoelectric materials for ultrasound generation and detection. *Ultrasound*, *19*(4), pp.187-196.
[81]. Tandon, B., Blaker, J.J. and Cartmell, S.H., 2018. Piezoelectric materials as stimulatory biomedical materials and scaffolds for bone repair. *Acta biomaterialia*, *73*, pp.1-20.
[82]. Lay, R., Deijs, G.S. and Malmström, J., 2021. The intrinsic piezoelectric properties of materials–a review with a focus on biological materials. *RSC advances*, *11*(49), pp.30657-30673.
[83]. Uchino, K., 2017. The development of piezoelectric materials and the new perspective. In *Advanced Piezoelectric Materials* (pp. 1-92). Woodhead Publishing.
[84]. AlAhzm, A.M., Alejli, M.O., Ponnamma, D., Elgawady, Y. and Al-Maadeed, M.A.A., 2021. Piezoelectric properties of zinc oxide/iron oxide filled polyvinylidene fluoride nanocomposite fibers. *Journal of Materials Science: Materials in Electronics*, *32*(11), pp.14610-14622.
[85]. Zhao, M.H., Wang, Z.L. and Mao, S.X., 2004. Piezoelectric characterization of individual zinc oxide nanobelt probed by piezoresponse force microscope. *Nano Letters*, *4*(4), pp.587-590.
[86]. Wang, Z.L., 2004. Nanostructures of zinc oxide. *Materials today*, *7*(6), pp.26-33.
[87]. Khan, A., Ali Abbasi, M., Hussain, M., Hussain Ibupoto, Z., Wissting, J., Nur, O. and Willander, M., 2012. Piezoelectric nanogenerator based on zinc oxide nanorods grown on textile cotton fabric. *Applied Physics Letters*, *101*(19).
[88]. Gao, P.X. and Wang, Z.L., 2005. Nanoarchitectures of semiconducting and piezoelectric zinc oxide. *Journal of Applied Physics*, *97*(4).
[89]. Agrawal, R. and Espinosa, H.D., 2011. Giant piezoelectric size effects in zinc oxide and gallium nitride nanowires. A first principles investigation. *Nano letters*, *11*(2), pp.786-790.
[90]. Kaur, J. and Singh, H., 2020. Fabrication and analysis of piezoelectricity in 0D, 1D and 2D Zinc Oxide nanostructures. *Ceramics International*, *46*(11), pp.19401-19407.
[91]. Weston, T.B., Webster, A.H. and McNamara, V.M., 1969. Lead zirconate-lead titanate piezoelectric ceramics with iron oxide additions. *Journal of the American Ceramic Society*, *52*(5), pp.253-257.
[92]. Yamada, T., Ueda, T. and Kitayama, T., 1982. Piezoelectricity of a high-content lead zirconate titanate/polymer composite. *Journal of Applied Physics*, *53*(6), pp.4328-4332.
[93]. Sekhar, M.C., Veena, E., Kumar, N.S., Naidu, K.C.B., Mallikarjuna, A. and Basha, D.B., 2023. A review on piezoelectric materials and their applications. *Crystal Research and Technology*, *58*(2), p.2200130.

[94]. Ibn-Mohammed, T., Koh, S.C.L., Reaney, I.M., Acquaye, A., Wang, D., Taylor, S. and Genovese, A., 2016. Integrated hybrid life cycle assessment and supply chain environmental profile evaluations of lead-based (lead zirconate titanate) versus lead-free (potassium sodium niobate) piezoelectric ceramics. *Energy & Environmental Science*, *9*(11), pp.3495-3520.
[95]. Butt, Z., Rahman, S.U., Pasha, R.A., Mehmood, S., Abbas, S. and Elahi, H., 2017. Characterizing barium titanate piezoelectric material using the finite element method. *Transactions on Electrical and Electronic materials*, *18*(3), pp.163-168.
[96]. Vijatović, M.M., Bobić, J.D. and Stojanović, B.D., 2008. History and challenges of barium titanate: Part II. *Science of Sintering*, *40*(3), pp.235-244.
[97]. Nath, A. K., and Nirmali Medhi. "Piezoelectric properties of environmental friendly bismuth doped barium titanate ceramics." *Materials Letters* 73 (2012): 75-77.
[98]. Saxena, P. and Shukla, P., 2021. A comprehensive review on fundamental properties and applications of poly (vinylidene fluoride)(PVDF). *Advanced Composites and Hybrid Materials*, *4*, pp.8-26.
[99]. Ameduri, B., 2009. From vinylidene fluoride (VDF) to the applications of VDF-containing polymers and copolymers: recent developments and future trends. *Chemical reviews*, *109*(12), pp.6632-6686.
[100]. Saxena, P. and Shukla, P., 2022. A comparative analysis of the basic properties and applications of poly (vinylidene fluoride)(PVDF) and poly (methyl methacrylate)(PMMA). *Polymer Bulletin*, *79*(8), pp.5635-5665.
[101]. Wu, Y., Ma, Y., Zheng, H. and Ramakrishna, S., 2021. Piezoelectric materials for flexible and wearable electronics: A review. *Materials & Design*, *211*, p.110164.
[102]. Nivedhitha, D.M., Jeyanthi, S., Venkatraman, P., Viswapriyan, A.S., Nishaanth, S.G. and Manoranjith, S., 2023. Polyvinylidene Fluoride as an advanced polymer for multifunctional applications-a review. *Materials Today: Proceedings*.
[103]. Shepelin, N.A., Glushenkov, A.M., Lussini, V.C., Fox, P.J., Dicinoski, G.W., Shapter, J.G. and Ellis, A.V., 2019. New developments in composites, copolymer technologies and processing techniques for flexible fluoropolymer piezoelectric generators for efficient energy harvesting. *Energy & Environmental Science*, *12*(4), pp.1143-1176.
[104]. Bae, J.H. and Chang, S.H., 2019. PVDF-based ferroelectric polymers and dielectric elastomers for sensor and actuator applications: a review. *Functional Composites and Structures*, *1*(1), p.012003.
[105]. Koroglu, L., Ayas, E. and Ay, N., 2021. 3D printing of polyvinylidene fluoride based piezoelectric nanocomposites: an overview. *Macromolecular Materials and Engineering*, *306*(10), p.2100277.
[106]. Stadlober, B., Zirkl, M. and Irimia-Vladu, M., 2019. Route towards sustainable smart sensors: ferroelectric polyvinylidene fluoride-based materials and their integration in flexible electronics. *Chemical Society Reviews*, *48*(6), pp.1787-1825.
[107]. Ramadan, K.S., Sameoto, D. and Evoy, S., 2014. A review of piezoelectric polymers as functional materials for electromechanical transducers. *Smart Materials and Structures*, *23*(3), p.033001.
[108]. Ruan, L., Yao, X., Chang, Y., Zhou, L., Qin, G. and Zhang, X., 2018. Properties and applications of the β phase poly (vinylidene fluoride). *Polymers*, *10*(3), p.228.
[109]. Surmenev, R.A., Orlova, T., Chernozem, R.V., Ivanova, A.A., Bartasyte, A., Mathur, S. and Surmeneva, M.A., 2019. Hybrid lead-free polymer-based nanocomposites with improved piezoelectric response for biomedical energy-harvesting applications: A review. *Nano Energy*, *62*, pp.475-506.
[110]. Rajeevan, S., John, S. and George, S.C., 2021. Polyvinylidene fluoride: A multifunctional polymer in supercapacitor applications. *Journal of Power Sources*, *504*, p.230037.

[111]. Wang, Z.L. and Song, J., 2006. Piezoelectric nanogenerators based on zinc oxide nanowire arrays. *Science*, *312*(5771), pp.242-246.
[112] Jiang, B., Iocozzia, J., Zhao, L., Zhang, H., Harn, Y.W., Chen, Y. and Lin, Z., 2019. Barium titanate at the nanoscale: controlled synthesis and dielectric and ferroelectric properties. *Chemical Society Reviews*, *48*(4), pp.1194-1228.
[113]. Liu, P., Sun, H., Liu, X., Sui, H., Zhang, Y., Zhou, D., Guo, Q. and Ruan, Y., 2017. Enhanced photocatalytic performance of Bi2Fe4O9/graphene via modifying graphene composite. *Journal of the American Ceramic Society*, *100*(8), pp.3540-3549.
[114]. Sun, H., Liu, Y., Zhang, Y., Lv, L., Zhou, J. and Chen, W., 2014. Synthesis of Bi 2 Fe 4 O 9/reduced graphene oxide composite by one-step hydrothermal method and its high photocatalytic performance. *Journal of Materials Science: Materials in Electronics*, *25*, pp.4212-4218.
[115]. Ren, X., Fan, H., Zhao, Y. and Liu, Z., 2016. Flexible lead-free BiFeO3/PDMS-based nanogenerator as piezoelectric energy harvester. *ACS applied materials & interfaces*, *8*(39), pp.26190-26197.
[116]. Zhang, Y., Kim, H., Wang, Q., Jo, W., Kingon, A.I., Kim, S.H. and Jeong, C.K., 2020. Progress in lead-free piezoelectric nanofiller materials and related composite nanogenerator devices. *Nanoscale Advances*, *2*(8), pp.3131-3149.
[117]. Abbasipour, M., Khajavi, R. and Akbarzadeh, A.H., 2022. A comprehensive review on piezoelectric polymeric and ceramic nanogenerators. *Advanced Engineering Materials*, *24*(6), p.2101312.
[118]. Sengupta, P., Sadhukhan, P., Saha, S., Das, S. and Ray, R., 2023. Improved energy harvesting ability of C3H7NH3PbI3 decorated PVDF nanofiber based flexible nanogenerator. *Nano Energy*, *109*, p.108277.
[119]. Bai, Y., Liu, Y., Lv, H., Shi, H., Zhou, W., Liu, Y. and Yu, D.G., 2022. Processes of electrospun polyvinylidene fluoride-based nanofibers, their piezoelectric properties, and several fantastic applications. *Polymers*, *14*(20), p.4311.
[120]. Li, J., Chen, S., Liu, W., Fu, R., Tu, S., Zhao, Y., Dong, L., Yan, B. and Gu, Y., 2019. High performance piezoelectric nanogenerators based on electrospun ZnO nanorods/poly (vinylidene fluoride) composite membranes. *The Journal of Physical Chemistry C*, *123*(18), pp.11378-11387.
[121]. Schaub, N.J., Johnson, C.D., Cooper, B. and Gilbert, R.J., 2016. Electrospun fibers for spinal cord injury research and regeneration. *Journal of neurotrauma*, *33*(15), pp.1405-1415.
[122]. Li, Y., Xu, M.H., Xia, Y.S., Wu, J.M., Sun, X.K., Wang, S., Hu, G.H. and Xiong, C.X., 2020. Multilayer assembly of electrospun/electrosprayed PVDF-based nanofibers and beads with enhanced piezoelectricity and high sensitivity. *Chemical Engineering Journal*, *388*, p.124205.
[123]. Maity, K. and Mandal, D., 2018. All-organic high-performance piezoelectric nanogenerator with multilayer assembled electrospun nanofiber mats for self-powered multifunctional sensors. *ACS applied materials & interfaces*, *10*(21), pp.18257-18269.
[124]. Mandal, D., Henkel, K. and Schmeißer, D., 2014. Improved performance of a polymer nanogenerator based on silver nanoparticles doped electrospun P (VDF–HFP) nanofibers. *Physical Chemistry Chemical Physics*, *16*(22), pp.10403-10407.
[125]. Chen, X., Xu, S., Yao, N. and Shi, Y., 2010. 1.6 V nanogenerator for mechanical energy harvesting using PZT nanofibers. *Nano letters*, *10*(6), pp.2133-2137.
[126]. Park, K.I., Lee, M., Liu, Y., Moon, S., Hwang, G.T., Zhu, G., Kim, J.E., Kim, S.O., Kim, D.K., Wang, Z.L. and Lee, K.J., 2012. Flexible nanocomposite generator made of BaTiO3 nanoparticles and graphitic carbons. *Advanced materials*, *24*(22), pp.2999-3004.

[127]. Zhang, X., Xia, W., Liu, J., Zhao, M., Li, M. and Xing, J., 2022. PVDF-based and its copolymer-based piezoelectric composites: Preparation methods and applications. *Journal of Electronic Materials*, *51*(10), pp.5528-5549.
[128]. Surmenev, R.A., Orlova, T., Chernozem, R.V., Ivanova, A.A., Bartasyte, A., Mathur, S. and Surmeneva, M.A., 2019. Hybrid lead-free polymer-based nanocomposites with improved piezoelectric response for biomedical energy-harvesting applications: A review. *Nano Energy*, *62*, pp.475-506.
[129]. Chowdhury, A.R., Jaksik, J., Hussain, I., Longoria III, R., Faruque, O., Cesano, F., Scarano, D., Parsons, J. and Uddin, M.J., 2019. Multicomponent nanostructured materials and interfaces for efficient piezoelectricity. *Nano-Structures & Nano-Objects*, *17*, pp.148-1.
[130]. Zhu, D., Tudor, M.J. and Beeby, S.P., 2009. Strategies for increasing the operating frequency range of vibration energy harvesters: a review. *Measurement Science and Technology*, *21*(2), p.022001.
[131]. J. Chen, G. Zhu, W. Yang, Q. Jing, P. Bai, Y. Yang, T. C. Hou, Z. L. Wang, Adv. Mater. 2013, 25, 6094.
[132]. Wu, W. and Haick, H., 2018. Materials and wearable devices for autonomous monitoring of physiological markers. *Advanced Materials*, *30*(41), p.1705024.
[133]. Shin, S.H., Kim, Y.H., Lee, M.H., Jung, J.Y., Seol, J.H. and Nah, J., 2014. Lithium-doped zinc oxide nanowires–polymer composite for high performance flexible piezoelectric nanogenerator. *ACS nano*, *8*(10), pp.10844-10850.
[134]. Wang, L., Fu, X., He, J., Shi, X., Chen, T., Chen, P., Wang, B. and Peng, H., 2020. Application challenges in fiber and textile electronics. *Advanced Materials*, *32*(5), p.1901971.
[135]. Pan, S., Ren, J., Fang, X. and Peng, H., 2016. Integration: an effective strategy to develop multifunctional energy storage devices. *Advanced Energy Materials*, *6*(4), p.1501867.
[136]. Zhang, C., Fan, W., Wang, S., Wang, Q., Zhang, Y. and Dong, K., 2021. Recent progress of wearable piezoelectric nanogenerators. *ACS Applied Electronic Materials*, *3*(6), pp.2449-2467.
[137]. Cao, X., Xiong, Y., Sun, J., Zhu, X., Sun, Q. and Wang, Z.L., 2021. Piezoelectric nanogenerators derived self-powered sensors for multifunctional applications and artificial intelligence. *Advanced Functional Materials*, *31*(33), p.2102983.
[138]. Parvez Mahmud, M.A., Huda, N., Farjana, S.H., Asadnia, M. and Lang, C., 2018. Recent advances in nanogenerator-driven self-powered implantable biomedical devices. *Advanced Energy Materials*, *8*(2), p.1701210.
[139]. Liu, Y., Mo, J., Fu, Q., Lu, Y., Zhang, N., Wang, S. and Nie, S., 2020. Enhancement of triboelectric charge density by chemical functionalization. *Advanced Functional Materials*, *30*(50), p.2004714.
[140]. Liu, D., Zhou, L., Gao, Y., Liu, D., Qiao, W., Shi, J., Liu, X., Zhao, Z., Wang, Z.L. and Wang, J., Interface Charge Regulation Enhancing Output and Durability of Triboelectric Nanogenerator for Efficient Wastewater Treatment. *Advanced Energy Materials*, p.2401958.
[141]. Wu, H., Wang, S., Wang, Z. and Zi, Y., 2021. Achieving ultrahigh instantaneous power density of 10 MW/m2 by leveraging the opposite-charge-enhanced transistor-like triboelectric nanogenerator (OCT-TENG). *Nature communications*, *12*(1), p.5470.
[142]. Luo, J. and Wang, Z.L., 2020. Recent progress of triboelectric nanogenerators: From fundamental theory to practical applications. *EcoMat*, *2*(4), p.e12059.
[143]. Lone, S.A., Lim, K.C., Kaswan, K., Chatterjee, S., Fan, K.P., Choi, D., Lee, S., Zhang, H., Cheng, J. and Lin, Z.H., 2022. Recent advancements for improving the performance of triboelectric nanogenerator devices. *Nano Energy*, *99*, p.107318.
[144] Li, H.Y., Su, L., Kuang, S.Y., Pan, C.F., Zhu, G. and Wang, Z.L., 2015. Significant enhancement of triboelectric charge density by fluorinated surface modification in nanoscale for converting mechanical energy. *Advanced Functional Materials*, *25*(35), pp.5691-5697.

[145]. Zhang, J., Coote, M.L. and Ciampi, S., 2021. Electrostatics and electrochemistry: mechanism and scope of charge-transfer reactions on the surface of tribocharged insulators. *Journal of the American Chemical Society*, *143*(8), pp.3019-3032.
[146]. Niu, S. and Wang, Z.L., 2015. Theoretical systems of triboelectric nanogenerators. *Nano Energy*, *14*, pp.161-192.
[147]. Wang, Z.L., Lin, L., Chen, J., Niu, S., Zi, Y., Wang, Z.L., Lin, L., Chen, J., Niu, S. and Zi, Y., 2016. Triboelectric nanogenerator: Lateral sliding mode. *Triboelectric nanogenerators*, pp.49-90.
[148]. Wang, Z.L., Lin, L., Chen, J., Niu, S., Zi, Y., Wang, Z.L., Lin, L., Chen, J., Niu, S. and Zi, Y., 2016. Triboelectric nanogenerator: Freestanding triboelectric-layer mode. *Triboelectric Nanogenerators*, pp.109-153.
[149]. Wang, S., Lin, L., Xie, Y., Jing, Q., Niu, S. and Wang, Z.L., 2013. Sliding-triboelectric nanogenerators based on in-plane charge-separation mechanism. *Nano letters*, *13*(5), pp.2226-2233.
[150]. Wang, Zhong Lin, Long Lin, Jun Chen, Simiao Niu, Yunlong Zi, Zhong Lin Wang, Long Lin, Jun Chen, Simiao Niu, and Yunlong Zi. *Triboelectric nanogenerator: single-electrode mode*. Springer International Publishing, 2016.
[151]. Wang, Z.L., Lin, L., Chen, J., Niu, S., Zi, Y., Wang, Z.L., Lin, L., Chen, J., Niu, S. and Zi, Y., 2016. *Triboelectric nanogenerator: single-electrode mode* (pp. 91-107). Springer International Publishing.
[152]. Wang, Z.L., Lin, L., Chen, J., Niu, S., Zi, Y., Wang, Z.L., Lin, L., Chen, J., Niu, S. and Zi, Y., 2016. Triboelectric nanogenerator: Vertical contact-separation mode. *Triboelectric nanogenerators*, pp.23-47.
[153]. Hasan, S., Kouzani, A.Z., Adams, S., Long, J. and Mahmud, M.P., 2022. Comparative study on the contact-separation mode triboelectric nanogenerator. *Journal of electrostatics*, *116*, p.103685.
[154]. Lee, Y., Kang, S.G. and Jeong, J., 2021. Sliding triboelectric nanogenerator with staggered electrodes. *Nano Energy*, *86*, p.106062.
[155]. Long, L., Liu, W., Wang, Z., He, W., Li, G., Tang, Q., Guo, H., Pu, X., Liu, Y. and Hu, C., 2021. High performance floating self-excited sliding triboelectric nanogenerator for micro mechanical energy harvesting. *Nature communications*, *12*(1), p.4689.
[156]. Lungu, M., 2004. Electrical separation of plastic materials using the triboelectric effect. *Minerals Engineering*, *17*(1), pp.69-75.
[157]. Wang, Z.L., 2021. From contact electrification to triboelectricnanogenerators. *Reports on Progress in Physics*, *84*(9), p.096502.
[158]. Kim, W.G., Kim, D.W., Tcho, I.W., Kim, J.K., Kim, M.S. and Choi, Y.K., 2021. Triboelectric nanogenerator: Structure, mechanism, and applications. *ACS nano*, *15*(1), pp.258-287.
[159]. Nie, J., Chen, X. and Wang, Z.L., 2019. Electrically responsive materials and devices directly driven by the high voltage of triboelectric nanogenerators. *Advanced Functional Materials*, *29*(41), p.1806351.
[160]. Ibrahim, M., Jiang, J., Wen, Z. and Sun, X., 2021. Surface engineering for enhanced triboelectric nanogenerator. *Nanoenergy Advances*, *1*(1), pp.58-80.
[161]. Wang, N., Liu, Y., Ye, E., Li, Z. and Wang, D., 2022. Control methods and applications of interface contact electrification of triboelectric nanogenerators: a review. *Materials Research Letters*, *10*(3), pp.97-123.
[162]. Kwak, S.S., Yoon, H.J. and Kim, S.W., 2019. Textile-based triboelectric nanogenerators for self-powered wearable electronics. *Advanced Functional Materials*, *29*(2), p.1804533.
[163]. Liu, Z., Li, H., Shi, B., Fan, Y., Wang, Z.L. and Li, Z., 2019. Wearable and implantable triboelectric nanogenerators. *Advanced Functional Materials*, *29*(20), p.1808820.

[163]. Karan, S.K., Maiti, S., Lee, J.H., Mishra, Y.K., Khatua, B.B. and Kim, J.K., 2020. Recent advances in self-powered tribo-/piezoelectric energy harvesters: all-in-one package for future smart technologies. *Advanced Functional Materials*, *30*(48), p.2004446.
[165]. Li, Z., Zheng, Q., Wang, Z.L. and Li, Z., 2020. Nanogenerator-based self-powered sensors for wearable and implantable electronics. *Research*.
[166]. Ha, M., Park, J., Lee, Y. and Ko, H., 2015. Triboelectric generators and sensors for self-powered wearable electronics. *Acs Nano*, *9*(4), pp.3421-3427.
[167]. Lei, H., Chen, Y., Gao, Z., Wen, Z. and Sun, X., 2021. Advances in self-powered triboelectric pressure sensors. *Journal of Materials Chemistry A*, *9*(36), pp.20100-20130.
[168]. Dassanayaka, D.G., Alves, T.M., Wanasekara, N.D., Dharmasena, I.G. and Ventura, J., 2022. Recent progresses in wearable triboelectric nanogenerators. *Advanced Functional Materials*, *32*(44), p.2205438.
[169]. Zou, H., Guo, L., Xue, H., Zhang, Y., Shen, X., Liu, X., Wang, P., He, X., Dai, G., Jiang, P. and Zheng, H., 2020. Quantifying and understanding the triboelectric series of inorganic non-metallic materials. *Nature communications*, *11*(1), p.2093.
[170]. Zou, H., Zhang, Y., Guo, L., Wang, P., He, X., Dai, G., Zheng, H., Chen, C., Wang, A.C., Xu, C. and Wang, Z.L., 2019. Quantifying the triboelectric series. *Nature communications*, *10*(1), p.1427.
[171]. Jiang, W., Li, H., Liu, Z., Li, Z., Tian, J., Shi, B., Zou, Y., Ouyang, H., Zhao, C., Zhao, L. and Sun, R., 2018. Fully bioabsorbable natural-materials-based triboelectric nanogenerators. *Advanced Materials*, *30*(32), p.1801895.
[172]. Zhang, R. and Olin, H., 2020. Material choices for triboelectric nanogenerators: A critical review. *EcoMat*, *2*(4), p.e12062.
[173]. Wang, S., Lin, L. and Wang, Z.L., 2012. Nanoscale triboelectric-effect-enabled energy conversion for sustainably powering portable electronics. *Nano letters*, *12*(12), pp.6339-6346.
[174]. Long, L., Liu, W., Wang, Z., He, W., Li, G., Tang, Q., Guo, H., Pu, X., Liu, Y. and Hu, C., 2021. High performance floating self-excited sliding triboelectric nanogenerator for micro mechanical energy harvesting. *Nature communications*, *12*(1), p.4689.
[175]. Wang, S., Lin, L. and Wang, Z.L., 2015. Triboelectric nanogenerators as self-powered active sensors. *Nano Energy*, *11*, pp.436-462.
[176]. Wang, Zhong Lin. "Triboelectric nanogenerators as new energy technology for self-powered systems and as active mechanical and chemical sensors." *ACS nano* 7, no. 11 (2013): 9533-9557.
[178]. Jiang, T., Chen, X., Yang, K., Han, C., Tang, W. and Wang, Z.L., 2016. Theoretical study on rotary-sliding disk triboelectric nanogenerators in contact and non-contact modes. *Nano Research*, *9*, pp.1057-1070.
[180]. Zhou, L., Liu, D., Zhao, Z., Li, S., Liu, Y., Liu, L., Gao, Y., Wang, Z.L. and Wang, J., 2020. Simultaneously enhancing power density and durability of sliding-mode triboelectric nanogenerator via interface liquid lubrication. *Advanced Energy Materials*, *10*(45), p.2002920.
[181]. Jie, Y., Ma, J., Chen, Y., Cao, X., Wang, N. and Wang, Z.L., 2018. Efficient delivery of power generated by a rotating triboelectric nanogenerator by conjunction of wired and wireless transmissions using maxwell's displacement currents. *Advanced Energy Materials*, *8*(31), p.1802084.
[182]. Pang, Y., Cao, Y., Derakhshani, M., Fang, Y., Wang, Z.L. and Cao, C., 2021. Hybrid energy-harvesting systems based on triboelectric nanogenerators. *Matter*, *4*(1), pp.116-143.
[183]. Sriphan, S. and Vittayakorn, N., 2022. Hybrid piezoelectric-triboelectric nanogenerators for flexible electronics: Recent advances and perspectives. *Journal of Science: Advanced Materials and Devices*, *7*(3), p.100461.

[184]. Zhang, J., He, Y., Boyer, C., Kalantar-Zadeh, K., Peng, S., Chu, D. and Wang, C.H., 2021. Recent developments of hybrid piezo–triboelectric nanogenerators for flexible sensors and energy harvesters. *Nanoscale Advances*, *3*(19), pp.5465-5486.
[185]. Chandrasekaran, S., Bowen, C., Roscow, J., Zhang, Y., Dang, D.K., Kim, E.J., Misra, R.D.K., Deng, L., Chung, J.S. and Hur, S.H., 2019. Micro-scale to nano-scale generators for energy harvesting: Self powered piezoelectric, triboelectric and hybrid devices. *Physics Reports*, *792*, pp.1-33.
[186]. Zhao, C., Zhang, Q., Zhang, W., Du, X., Zhang, Y., Gong, S., Ren, K., Sun, Q. and Wang, Z.L., 2019. Hybrid piezo/triboelectric nanogenerator for highly efficient and stable rotation energy harvesting. *Nano Energy*, *57*, pp.440-449.
[187]. Li, Z., Saadatnia, Z., Yang, Z. and Naguib, H., 2018. A hybrid piezoelectric-triboelectric generator for low-frequency and broad-bandwidth energy harvesting. *Energy conversion and management*, *174*, pp.188-197.
[188]. Song, Y., Shi, Z., Hu, G.H., Xiong, C., Isogai, A. and Yang, Q., 2021. Recent advances in cellulose-based piezoelectric and triboelectric nanogenerators for energy harvesting: a review. *Journal of Materials Chemistry A*, *9*(4), pp.1910-1937.
[189]. Bar-Cohen, Y., 2002, July. Electroactive polymers: current capabilities and challenges. In *Smart Structures and Materials 2002: Electroactive Polymer Actuators and Devices (EAPAD)* (Vol. 4695, pp. 1-7). SPIE.
[190]. Bar-Cohen, Y. and Anderson, I.A., 2019. Electroactive polymer (EAP) actuators—background review. *Mechanics of Soft Materials*, *1*(1), p.5.
[191]. Wang, T., Farajollahi, M., Choi, Y.S., Lin, I.T., Marshall, J.E., Thompson, N.M., Kar-Narayan, S., Madden, J.D. and Smoukov, S.K., 2016. Electroactive polymers for sensing. *Interface focus*, *6*(4), p.20160026.
[192]. Bar-Cohen, Y. and Zhang, Q., 2008. Electroactive polymer actuators and sensors. *MRS bulletin*, *33*(3), pp.173-181.
[193]. Kim, K.J. and Tadokoro, S., 2007. Electroactive polymers for robotic applications. *Artificial Muscles and Sensors*, *23*, p.291.
[194]. Bar-Cohen, Yoseph, and Qiming Zhang. "Electroactive polymer actuators and sensors." *MRS bulletin* 33, no. 3 (2008): 173-181.
[195]. Mutlu, R., Alici, G. and Li, W., 2013, July. Electroactive polymers as soft robotic actuators: Electromechanical modeling and identification. In *2013 IEEE/ASME International Conference on Advanced Intelligent Mechatronics* (pp. 1096-1101). IEEE.
[196]. Bar-Cohen, Y., 2002. Electroactive polymers as artificial muscles: a review. *Journal of Spacecraft and Rockets*, *39*(6), pp.822-827.
[197]. Maksimkin, A.V., Dayyoub, T., Telyshev, D.V. and Gerasimenko, A.Y., 2022. Electroactive polymer-based composites for artificial muscle-like actuators: a review. *Nanomaterials*, *12*(13), p.2272.
[198]. Carpi, F. and De Rossi, D., 2005. Electroactive polymer-based devices for e-textiles in biomedicine. *IEEE transactions on Information Technology in biomedicine*, *9*(3), pp.295-318.
[199]. Carpi, F. and Smela, E. eds., 2009. *Biomedical applications of electroactive polymer actuators*. John Wiley & Sons.
[200]. Jean-Mistral, C., Basrour, S. and Chaillout, J.J., 2010. Comparison of electroactive polymers for energy scavenging applications. *Smart Materials and Structures*, *19*(8), p.085012.
[201]. Dhawan, S.K., Ohlan, A. and Singh, K., 2011. Designing of nano composites of conducting polymers for EMI shielding. *Advances in Nanocomposites-Synthesis, Characterization and Industrial Applications*, p.429.

[202]. Zhang, L., Du, W., Nautiyal, A., Liu, Z. and Zhang, X., 2018. Recent progress on nanostructured conducting polymers and composites: synthesis, application and future aspects. *Sci. China Mater*, *61*(3), pp.303-352.
[203]. Guarino, V., Zuppolini, S., Borriello, A. and Ambrosio, L., 2016. Electro-active polymers (EAPs): a promising route to design bio-organic/bioinspired platforms with on demand functionalities. *Polymers*, *8*(5), p.185.
[204]. Dohany, Julius E. "Fluorine-containing polymers, poly (vinylidene fluoride)." *Kirk-Othmer Encyclopedia of Chemical Technology* (2000).
[205]. Sanyal, A. and Sinha-Ray, S., 2021. Ultrafine PVDF nanofibers for filtration of air-borne particulate matters: A comprehensive review. *Polymers*, *13*(11), p.1864.
[206]. Dani, S.S., Sundaray, B., kumar Nayak, S. and Mohanty, S., 2023. Electrospun PVDF and composite nanofiber: current status and future prescription towards hybrid Piezoelectric nanogenerators. *Materials Today Communications*, p.107661.
[207]. Kawai, H., 1969. The piezoelectricity of poly (vinylidene fluoride). *Japanese journal of applied physics*, *8*(7), p.975.
[208]. Adhikary, P. and Mandal, D., 2017. Enhanced electro-active phase in a luminescent P (VDF–HFP)/Zn 2+ flexible composite film for piezoelectric based energy harvesting applications and self-powered UV light detection. *Physical Chemistry Chemical Physics*, *19*(27), pp.17789-17798.
[209]. Thakur, P., Kool, A., Bagchi, B., Hoque, N.A., Das, S. and Nandy, P., 2015. In situ synthesis of Ni (OH) 2 nanobelt modified electroactive poly (vinylidene fluoride) thin films: remarkable improvement in dielectric properties. *Physical Chemistry Chemical Physics*, *17*(19), pp.13082-13091.
[210]. Martins, P., Lopes, A.C. and Lanceros-Mendez, S., 2014. Electroactive phases of poly (vinylidene fluoride): Determination, processing and applications. *Progress in polymer science*, *39*(4), pp.683-706.
[211]. Thakur, P., Kool, A., Hoque, N.A., Bagchi, B., Khatun, F., Biswas, P., Brahma, D., Roy, S., Banerjee, S. and Das, S., 2018. Superior performances of in situ synthesized ZnO/PVDF thin film based self-poled piezoelectric nanogenerator and self-charged photo-power bank with high durability. *Nano Energy*, *44*, pp.456-467.
[212]. Martins, P., Nunes, J.S., Hungerford, G., Miranda, D., Ferreira, A., Sencadas, V. and Lanceros-Méndez, S., 2009. Local variation of the dielectric properties of poly (vinylidene fluoride) during the α-to β-phase transformation. *Physics Letters A*, *373*(2), pp.177-180.
[213]. Ruan, L., Yao, X., Chang, Y., Zhou, L., Qin, G. and Zhang, X., 2018. Properties and applications of the β phase poly (vinylidene fluoride). *Polymers*, *10*(3), p.228.
[214]. Meng, N., Zhu, X., Mao, R., Reece, M.J. and Bilotti, E., 2017. Nanoscale interfacial electroactivity in PVDF/PVDF-TrFE blended films with enhanced dielectric and ferroelectric properties. *Journal of Materials Chemistry C*, *5*(13), pp.3296-3305.
[215]. Wang, F., Xia, Z., Qiu, X., Shen, J., Zhang, X. and An, Z., 2006. Piezoelectric properties and charge dynamics in poly (vinylidene fluoride-hexafluoropropylene) copolymer films with different content of HEP. *IEEE transactions on dielectrics and electrical insulation*, *13*(5), pp.1132-1139.
[216]. Sousa, R.E., Nunes-Pereira, J., Ferreira, J.C.C., Costa, C.M., Machado, A.V., Silva, M.M. and Lanceros-Mendez, S., 2014. Microstructural variations of poly (vinylidene fluoride co-hexafluoropropylene) and their influence on the thermal, dielectric and piezoelectric properties. *Polymer testing*, *40*, pp.245-255.
[217]. Wang, J., Zheng, L., Wu, Z., Zhang, Y. and Zhang, X., 2016. Fabrication of hydrophobic flat sheet and hollow fiber membranes from PVDF and PVDF-CTFE for membrane distillation. *Journal of Membrane Science*, *497*, pp.183-193.

[218]. Zheng, L., Wang, J., Li, J., Zhang, Y., Li, K. and Wei, Y., 2017. Preparation, evaluation and modification of PVDF-CTFE hydrophobic membrane for MD desalination application. *Desalination*, *402*, pp.162-172.
[219]. Zheng, L., Wu, Z., Wei, Y., Zhang, Y., Yuan, Y. and Wang, J., 2016. Preparation of PVDF-CTFE hydrophobic membranes for MD application: Effect of LiCl-based mixed additives. *Journal of membrane science*, *506*, pp.71-85.
[220]. Chaipo, S. and Putson, C., 2021. Preparation and enhanced electrical breakdown strength of PVDF-TrFE-CTFE/PVDF-HFP film composites. In *Journal of Physics: Conference Series* (Vol. 1719, No. 1, p. 012065). IOP Publishing.
[221]. Xu, H., Cheng, Z.Y., Olson, D., Mai, T., Zhang, Q.M. and Kavarnos, G., 2001. Ferroelectric and electromechanical properties of poly (vinylidene-fluoride–trifluoroethylene–chlorotrifluoroethylene) terpolymer. *Applied Physics Letters*, *78*(16), pp.2360-2362.
[222]. Gomes, J., Nunes, J.S., Sencadas, V. and Lanceros-Méndez, S., 2010. Influence of the β-phase content and degree of crystallinity on the piezo-and ferroelectric properties of poly (vinylidene fluoride). *Smart Materials and Structures*, *19*(6), p.065010.
[223]. Aldas, M., Boiteux, G., Seytre, G. and Ghallabi, Z., 2010, July. Dielectric behaviour of BaTiO 3/P (VDF-HFP) composite thin films prepared by solvent evaporation method. In *2010 10th IEEE International Conference on Solid Dielectrics* (pp. 1-4). IEEE.
[224]. Lutkenhaus, J.L., McEnnis, K., Serghei, A. and Russell, T.P., 2010. Confinement effects on crystallization and curie transitions of poly (vinylidene fluoride-co trifluoroethylene). *Macromolecules*, *43*(8), pp.3844-3850.
[226]. Huan, Y., Liu, Y. and Yang, Y., 2007. Simultaneous stretching and static electric field poling of poly (vinylidene fluoride-hexafluoropropylene) copolymer films. *Polymer Engineering & Science*, *47*(10), pp.1630-1633.
[227]. Li, Z., Wang, Y. and Cheng, Z.Y., 2006. Electromechanical properties of poly (vinylidene-fluoride-chlorotrifluoroethylene) copolymer. *Applied physics letters*, *88*(6).
[228]. Li, C., Wu, P.M., Lee, S., Gorton, A., Schulz, M.J. and Ahn, C.H., 2008. Flexible dome and bump shape piezoelectric tactile sensors using PVDF-TrFE copolymer. *Journal of Microelectromechanical Systems*, *17*(2), pp.334-341.
[229]. Ribeiro, C., Costa, C.M., Correia, D.M., Nunes-Pereira, J., Oliveira, J., Martins, P., Gonçalves, R., Cardoso, V.F. and Lanceros-Mendez, S., 2018. Electroactive poly (vinylidene fluoride)-based structures for advanced applications. *Nature protocols*, *13*(4), pp.681-704.
[230]. Gebrekrstos, A., Muzata, T.S. and Ray, S.S., 2022. Nanoparticle-enhanced β-phase formation in electroactive PVDF composites: a review of systems for applications in energy harvesting, EMI shielding, and membrane technology. *ACS Applied Nano Materials*, *5*(6), pp.7632-7651.
[231]. Madaeni, S.S. and Taheri, A.H., 2011. Effect of casting solution on morphology and performance of PVDF microfiltration membranes. *Chemical engineering & technology*, *34*(8), pp.1328-1334.
[232]. Issa, A.A., Al-Maadeed, M., Luyt, A.S., Mrlik, M. and Hassan, M.K., 2016. Investigation of the physico-mechanical properties of electrospun PVDF/cellulose (nano) fibers. *Journal of Applied Polymer Science*, *133*(26).
[233]. Issa, A.A., Al-Maadeed, M.A., Luyt, A.S., Ponnamma, D. and Hassan, M.K., 2017. Physico-mechanical, dielectric, and piezoelectric properties of PVDF electrospun mats containing silver nanoparticles. *C*, *3*(4), p.30.
[234]. Al-Saygh, A., Ponnamma, D., AlMaadeed, M.A., Vijayan P, P., Karim, A. and Hassan, M.K., 2017. Flexible pressure sensor based on PVDF nanocomposites containing reduced graphene oxide-titania hybrid nanolayers. *Polymers*, *9*(2), p.33.

[235]. Thakur, A., Mandeep, J., Dam, S., Shekar, N.C., Amarendra, G., Hussain, S., Rajesh, P.V. and Saha, A., 2021. Enhancing the electroactive phases in freestanding flexible films of MoS2/PVDF. *Polymer Crystallization*, *4*(2), p.e10164.
[236]. Thakur, P., Kool, A., Bagchi, B., Das, S. and Nandy, P., 2015. Effect of in situ synthesized Fe 2 O 3 and Co 3 O 4 nanoparticles on electroactive β phase crystallization and dielectric properties of poly (vinylidene fluoride) thin films. *Physical Chemistry Chemical Physics*, *17*(2), pp.1368-1378.
[237]. Roy, S., Thakur, P., Hoque, N.A., Bagchi, B. and Das, S., 2016. Enhanced electroactive β-phase nucleation and dielectric properties of PVdF-HFP thin films influenced by montmorillonite and Ni (OH) 2 nanoparticle modified montmorillonite. *RSC advances*, *6*(26), pp.21881-21894.
[238]. Roy, J., Chikkonda, R., Kishor, G., Thankamani Sathyanathan, A.R., Raju, K.J. and Gangineni, R.B., 2022. Structural, microstructural, and ferroelectric studies of polyvinylidene fluoride-hexafluoropropylene (PVDF-HFP) thin films in Ag/Cu/PVDF-HFP/Cu capacitor structures. *Journal of Applied Polymer Science*, *139*(21), p.52187.
[239]. Lopes Pereira, E.C., Soares, B.G., Silva, A.A. and Barra, G.M., 2021. Master batch approach for developing PVDF/EVA/CNT nanocomposites with co-continuous morphology and improved electrical conductivity. *Journal of Applied Polymer Science*, *138*(39), p.51164.
[240]. Lopes, A.C., Ferreira, J.C., Costa, C.M. and Lanceros-Méndez, S., 2013. Crystallization kinetics of montmorillonite/poly (vinylidene fluoride) composites and its correlation with the crystalline polymer phase formation. *Thermochimica Acta*, *574*, pp.19-25.
[241]. Fu, J., Hou, Y., Zheng, M., Wei, Q., Zhu, M. and Yan, H., 2015. Improving dielectric properties of PVDF composites by employing surface modified strong polarized BaTiO3 particles derived by molten salt method. *ACS applied materials & interfaces*, *7*(44), pp.24480-24491.
[242]. Fu, J., Hou, Y., Gao, X., Zheng, M. and Zhu, M., 2018. Highly durable piezoelectric energy harvester based on a PVDF flexible nanocomposite filled with oriented BaTi2O5 nanorods with high power density. *Nano Energy*, *52*, pp.391-401.
[243]. Tamang, A., Ghosh, S.K., Garain, S., Alam, M.M., Haeberle, J., Henkel, K., Schmeisser, D. and Mandal, D., 2015. DNA-assisted β-phase nucleation and alignment of molecular dipoles in PVDF film: a realization of self-poled bioinspired flexible polymer nanogenerator for portable electronic devices. *ACS applied materials & interfaces*, *7*(30), pp.16143-16147.
[244]. Xie, Y., Jiang, W., Fu, T., Liu, J., Zhang, Z. and Wang, S., 2018. Achieving high energy density and low loss in PVDF/BST nanodielectrics with enhanced structural homogeneity. *ACS applied materials & interfaces*, *10*(34), pp.29038-29047.
[245]. Issa, A.A., Al-Maadeed, M., Luyt, A.S., Mrlik, M. and Hassan, M.K., 2016. Investigation of the physico-mechanical properties of electrospun PVDF/cellulose (nano) fibers. *Journal of Applied Polymer Science*, *133*(26).

Chapter 2

Self-Polarized ZrO_2/Poly(vinylidene fluoride-co-hexafluoropropylene) Nanocomposite-Based Piezoelectric Nanogenerator and Single-Electrode Triboelectric Nanogenerator for Sustainable Energy Harvesting from Human Movements

2.1. Introduction

The pursuit of wearable, portable, flexible, and sustainable self-powered nanodevices, spanning sensors, mobile phones, roll-up displays, wearable electronics, calculators, actuators, wristwatches, implantable medical devices, and speakers, has catalysed extensive exploration of pollution-free green energy sources [1–5]. In the drive towards sustainable development for modern civilizations, the significance of alternative energy resources has surpassed that of finite and environmentally detrimental fossil fuels, such as coal, petroleum, and gas [6–8]. Piezoelectric nanogenerators (PENGs) emerge as a promising solution for harvesting energy from the surrounding environment, propelling the swift evolution of low-power electronic devices [6]. Recent advancements emphasize the development of environmentally friendly, biocompatible, lightweight, durable, flexible, and thin self-powered nanogenerators capable of harnessing energy from readily available natural resources and our living environment [9–11].

Various renewable energy sources, including sea-water wave, solar energy, geothermal energy, rainfall, biomass energies, nuclear energy, thermal energy, transportation, and mechanical resources such as human body movement (touching, walking, talking, breathing, finger imparting, pushing, pumping, jogging, stretching, bending, twisting, etc.), have been identified [11–13]. These modern trends have prompted the development of green energy-harvesting devices. Nanogenerators utilizing triboelectric [3,6,8–13], piezoelectric [1,3–5,7], and pyroelectric effects [14–16] have emerged as viable options for energy harvesting. Among these, triboelectric nanogenerators (TENGs) and piezoelectric nanogenerators (PENGs) are particularly suitable for harvesting energy from mechanical and biomechanical motions. Recent studies have explored the hybridization of piezoelectric and triboelectric effects in the same unit [17,18]. While TENGs demonstrate large output and excellent conversion efficiency, they are often plagued by drawbacks such as low durability and susceptibility to humidity [17,18]. Most TENGs employ two layers of differently polarized triboelectric materials to induce electric induction and form a closed circuit for electron flow [19]. Single-electrode TENGs (STENGs) are favoured for wearable electronics due to their ease of development on flexible substrates and high efficiency for moving bodies [19–22]. In pursuit of highly sensitive, long-lasting, low-power-consuming, self-powered systems and devices with high energy conversion coefficients, PENGs have emerged as promising green techniques for harvesting electrical energy from mechanical energy resources via the piezoelectric effect [23–25]. Common piezoelectric materials or ceramics, such as ZnO [1],

$BaTiO_3$ [26], PMN-PT [27,28], PZT [29], and (Na, K) NbO [5], have been studied for the construction of prototype flexible self-powered PENGs.

In recent years, poly(vinylidene fluoride) (PVDF) and its copolymers, including poly(vinylidene fluoride-co-hexafluoropropene) (PVDF-HFP), poly(vinylidene fluoride-trifluoroethylene) (PVDF-TrFE), poly(vinylidene fluoride-chloride trifluoride ethylene) (PVDF-CTFE), poly(vinylidene fluoride-trifluoro ethylene-chlorofluoroethylene) (PVDF-TrFECFE), and poly(vinylidene fluoride-trifluoroethylene-chloride trifluoride ethylene) (PVDF-TrFE-CTFE), have emerged as promising candidates for sophisticated piezoelectric nanogenerators (PENGs) [30–36]. These materials offer desirable piezoelectric properties such as lightweight, flexibility, and environmental compatibility.

Semicrystalline PVDF exhibits five distinct crystalline polymorphs: α, β, γ, δ, and ε. Among these, the nonpolar α phase is the most common and stable, characterized by a monoclinic unit cell with TGTG' (T-trans, G-gauche+, G' -gauche) dihedral conformation. The polar polymorphs β phase and γ phase feature orthorhombic unit cells with all-trans (TTTT) and TTTGTTG' conformations, respectively [38–42]. The β phase, in particular, demonstrates attractive piezoelectric properties, boasting the highest polarization per unit cell (8×10^{-30} cm) and a lower melting point compared to the γ phase [39,42]. Therefore, the electroactive β and γ phases play a crucial role in the development of PVDF-based PENGs.

Recent studies have focused on using nanofillers to enhance the functionality of PVDF by stabilizing its crucial β-polymorph, thereby improving the piezoelectric energy-harvesting properties of PVDF-based nanocomposites [40–42]. Researchers have explored various methods to achieve this enhancement, including the addition of nano- or microfillers, stretching, melt quenching, blending with polymers containing carbonyl groups, applying high pressure, solution growth, electrospinning, adding metal salts, and polarization via an applied field [38–43]. In our study, we utilize zirconium oxide (ZrO_2) nanoparticles (NPs) as nanofillers to enhance the nucleation of the polar and electroactive β phase in PVDF-HFP polymer [43]. ZrO_2 is widely used in industrial ceramics due to its unique properties, including high oxygen ion conductivity, low thermal conductivity, high strength, high fracture toughness, high coefficient of thermal expansion, thermal stability, and thermal shock resistance [44–46]. It finds applications in various engineering fields, such as cutting tools, thermal barrier coatings, automobile engine parts, refractory materials, wire-drawing dies, jewellery, abrasion-resistant materials, sands, and refractory ceramics, owing to its high refractive index, toughness, and wear resistance [47–50]. Furthermore, ZrO_2 NPs are utilized in optically transparent devices, oxygen sensors, and fuel cells due to their high refractive

index and oxygen-ion conductivity [51–54]. Additionally, ZrO_2 nanoparticles are a component of lead zirconate titanate (PZT), a well-known piezoelectric material [27]. In our study, ZrO_2 NPs serve as effective nucleating agents to enhance the piezoelectric properties of PVDF-HFP polymer [43].

This chapter presents the synthesis of electroactive β-polymorph ZrO_2 NPs/PVDF-HFP composite thin films using the solution-casting method. The incorporation of ZrO_2 NPs enhances the electroactive β-polymorph phase in PVDF-HFP, leading to an increase in the dielectric constant. Subsequently, a highly flexible ZrO_2 NPs/PVDF-HFP composite thin film-based piezoelectric nanogenerator (PENG) is developed to harvest electrical energy from mechanical sources. The fabricated PENG exhibits high output performance and long-term durability. Additionally, a single-layer triboelectric nanogenerator (STENG) is fabricated using the same composite film cast onto an ITO-coated PET surface. Due to the inherent triboelectric properties of the epidermis layer, only one triboelectric layer is utilized. The flexible, lightweight, and easily fabricated STENG demonstrates high output voltage upon finger contact, demonstrating its potential as an energy collector, supplier, and pressure sensor.

2.2. Experimental Section

2.2.1. Materials

- Zirconium (IV) oxychloride octahydrate ($ZrOCl_2.8H_2O$).
- PVDF-HFP pellets (Aldrich, Germany).
- Hydrazine hydrate (>99% purity) (N_2H_4) from Merck, India.
- Dimethyl sulfoxide (DMSO) from Merck, India.

2.2.2. ZrO_2 Nanoparticle synthesis

To synthesize ZrO_2 nanoparticles, 4.834 g of $ZrOCl_2.8H_2O$ solid salt was dissolved in 150 mL of deionized water to prepare a 0.1 M aqueous solution. After constant magnetic stirring at room temperature for 2 hours, 6 mL of hydrazine hydrate (N_2H_4) was slowly added dropwise. The solution was then stirred for an additional 4 hours at the same temperature. Another 6 mL of hydrazine hydrate was added to complete the reaction. The solution was transferred to an autoclave and heated in an electric oven at 160℃ for 24 hours for the hydrothermal reaction. The resulting white ZrO_2 nanoparticles precipitate was collected

through repeated centrifugation and washed with deionized water to remove any unreacted components. Finally, the ZrO_2 nanoparticles were dried at 80℃ in a hot air oven.

2.2.3. Synthesis of PVDF-HFP ZrO_2 Nanocomposite films

Commencing with the dissolution of 0.25 g of PVDF-HFP in 5 mL of DMSO, the mixture was stirred at 60℃ until a clear solution formed. Following this, the desired quantity of ZrO_2 NPs (1–15 mass%) was added to the PVDF-HFP solution and stirred for 12 hours at 60℃ to achieve a homogeneous blend. The resulting mixture was then cast onto clean petri dishes and placed in a hot air oven at 80℃ for 12 hours to produce a nanocomposite thin film. The thicknesses of the PVDF/ZrO_2 nanocomposite thin films were determined using field emission scanning electron microscope (FESEM) micrograph images, revealing a thickness range of 50–60 µm, as depicted in figure 2.1. Similarly, a pure PVDF-HFP film was drop-cast into a petri dish. All synthesized thin films were stored in a vacuum desiccator for subsequent characterizations. Sample designations are presented in Table 2.1.

Table 2. 1. Designation of the Sample and different amount of ZrO_2 NPs added in PVDF HFP matrix.

Sample Designation	Amount of PVDF HFP (g)	Percentage of ZrO_2 NPs (mass %)	Amount of ZrO_2 NPs (g)
PZ0 (Pure PVDF HFP)	0.25	00	0.0000
PZ1	0.25	01	0.0005
PZ5	0.25	05	0.0125
PZ10	0.25	10	0.0250
PZ15	0.25	15	0.0375

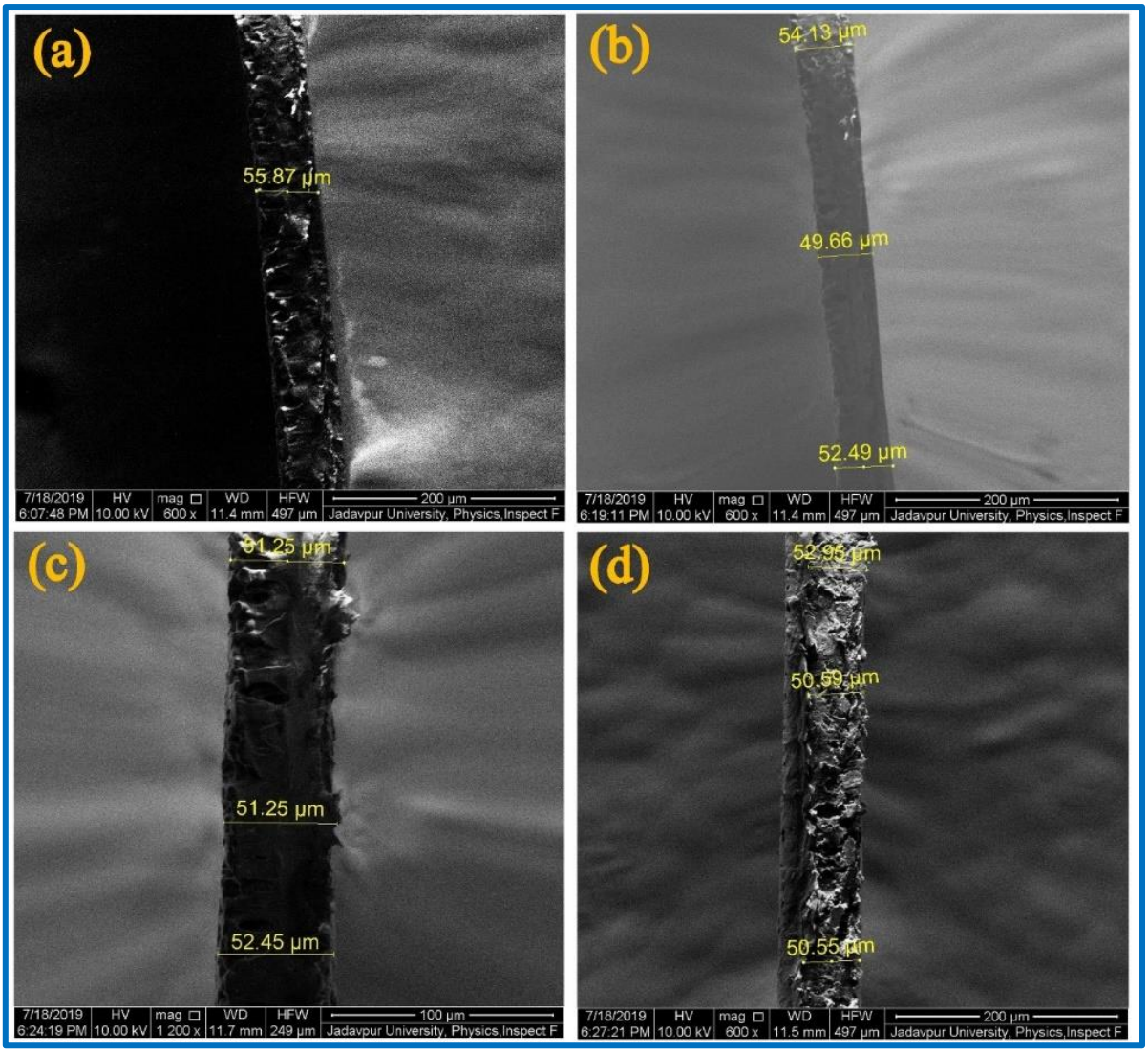

Figure 2.1: Cross section FESEM micrograph of PZ1, PZ2, PZ3 and PZ4 (a to d respectively).

2.2.4. Fabrication of PENG

Initially, a standardized PVDF-HFP/ZrO_2 film (PZ10) measuring (2.5 cm × 2.6 cm × 54 µm) was prepared. Subsequently, two aluminum electrodes, slightly smaller in area (2.4 cm × 2.5 cm), were affixed to both sides of the film, with two wires connected to the electrodes. Following this, the film and electrodes underwent encapsulation with polydimethyl siloxane (PDMS) ($[Si(CH_3)_2O]_n$) (Sylgard 184, Dow Corning, in a 1:10 ratio) and were then dried at 60℃ for 45 minutes in a dust-free hot air oven. Ultimately, the resulting PENG was obtained with dimensions of 5 cm × 3 cm × 0.3 cm.

2.2.5. Fabrication of STENG

To fabricate the STENG, we deposited 750 µL of PZ10 sample onto an ITO-coated PET substrate (1.5 × 2 cm^2) and cured it at 80℃ until completely dry. A copper wire was then attached to the ITO-coated PET surface for subsequent output characterizations.

2.3. Characterization techniques

The surface morphological microstructure of both the pure PVDF-HFP and PVDF-HFP/ZrO_2 nanocomposite thin films underwent examination via FESEM (INSPECT F50, the Netherlands). Crystallographic structural patterns of the samples were obtained using X-ray diffraction (XRD) (Model-D8, Bruker AXS Inc., Madison, WI) and Fourier transform infrared spectroscopy (FTIR) (FTIR-8400S, Shimadzu). The total crystallinity and thermal stability of the PVDF-HFP/ZrO_2 composite thin films were assessed using differential scanning calorimetry (DSC) (DSC-60, Shimadzu, Singapore). The degree of crystallinity (X_c) was derived by calculating the ratio of the enthalpy of fusion (ΔH_m) to the melting enthalpy $\Delta H_{100\%}$ of 100% crystalline PVDF, with a value of 104.6 Jg^{-1}. Additionally, the dielectric constant, tangent loss, and AC conductivity of the samples were measured using a digital LCR meter (Agilent, E4980A).

2.4. Results & discussions

2.4.1. Morphology analysis

In Figure 2.1, the FESEM micrograph illustrates a range of samples including ZrO_2 NPs, the pure PVDF-HFP film (PZ0), and films labelled PZ1, PZ5, PZ10, and PZ15. Specifically, the FESEM image of ZrO_2 depicts the formation of consistently sized ZrO_2 NPs, measuring around 50–60 nm in diameter. Conversely, the pure PVDF-HFP film displays larger spherulites with a diameter of approximately 40 µm, suggesting the dominance of the nonpolar α phase [38]. Subsequent images {Figures 2.2:(c)–(f)} reveal the dispersion and distribution of NPs within the PVDF-HFP matrix. These composite films exhibit smaller spherulites, ranging from 4–6 µm in diameter, with a uniform distribution of NPs, indicating the initiation of the electroactive β phase [31,35]. Further elucidation of the detailed structure and β phase formation was achieved through analysis of FTIR spectra, XRD patterns, and DSC results.

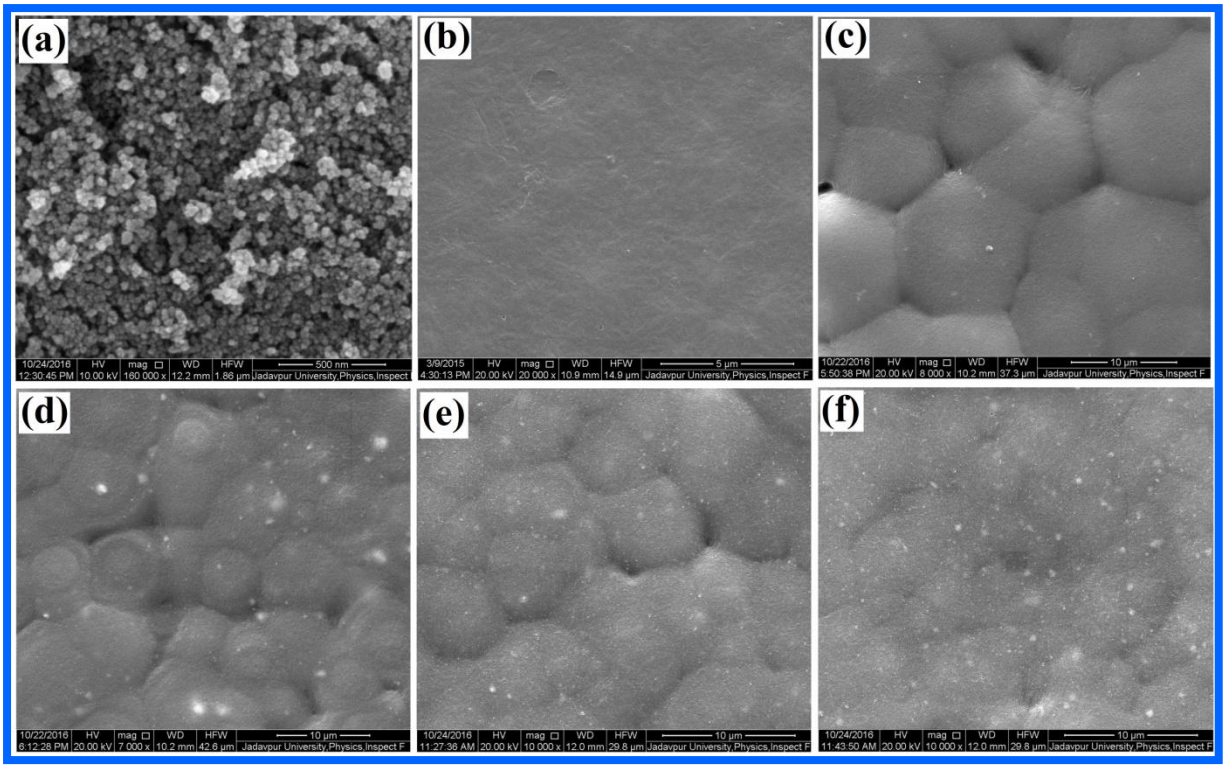

Figure 2.2: FESEM images of a) Pure ZrO_2 NPs; b) Pure PVDF-HFP thin film; c) PZ1; d) PZ5; e) PZ10; and f) PZ15.

2.4.2. Structural analysis

Figure 2.3:(a) illustrates the XRD patterns of both pure PVDF-HFP and ZrO_2 NPs/PVDF-HFP nanocomposite films. In the pure PVDF-HFP films, diffraction peaks at 2θ values of 17.7°, 18.4°, 19.9°, and 26.4° correspond to the (100), (020), (110), and (021) reflections, respectively, indicative of the α-crystalline phase. These peaks match those of standard α-PVDF. Upon addition of ZrO_2 NPs to the PVDF-HFP matrix, the intensity of all diffraction peaks associated with α and γ phases decreases. However, the peak at 2θ = 20.4°, corresponding to the (110) and (200) planes, becomes prominent, suggesting the presence of the polar β phase in the nanocomposite. Specifically, the nanocomposite film with 10% ZrO_2 NPs (PZ10) exhibits the highest intensity of the main β-crystalline diffraction peak.

Quantitative measurement of the nucleation of the β phase is achieved through the ratio ($I_{20.5}/I_{18.2}$), where $I_{20.5}$ and $I_{18.2}$ represent the intensities of the peaks at 20.5° (200) and 18.2° (020), respectively. In pure PVDF-HFP, this ratio is approximately 0.499 {Figure 2.3:(c)}. Interestingly, the value of this ratio varies with the loading wt% of ZrO_2 NPs, with the highest value of 2.92 observed for the PZ10 sample.

The following equations compute the total degree of total crystallinity for ($\boldsymbol{\chi_{ct}}$), α($\boldsymbol{\chi_{c\alpha}}$), β($\boldsymbol{\chi_{c\beta}}$) and $\boldsymbol{\gamma}$($\boldsymbol{\chi_{c\gamma}}$) crystallinities.

$$\chi_{ct} = \frac{\sum A_{crys}}{\sum A_{crys} + \sum A_{ap}} \times 100\% \quad (2.1)$$

$$\chi_{c\alpha} = \chi_{ct} \times \frac{\sum A_{\alpha}}{\sum A_{\alpha} + \sum A_{\beta} + \sum A_{\gamma}} \% \quad (2.2)$$

$$\chi_{c\beta} = \chi_{ct} \times \frac{\sum A_{\beta}}{\sum A_{\alpha} + \sum A_{\beta} + \sum A_{\gamma}} \% \quad (2.3)$$

$$\chi_{c\gamma} = \chi_{ct} \times \frac{\sum A_{\gamma}}{\sum A_{\alpha} + \sum A_{\beta} + \sum A_{\gamma}} \% \quad (2.4)$$

where the integral area of all crysalline phases and amorphous peaks are summated as $\sum A_{crys}$ and $\sum A_{ap}$, respectively. The total integral area obtained from the peaks of the α, β, and γ crystalline phases is represented by A_{α}, A_{β} and A_{γ} respectively.

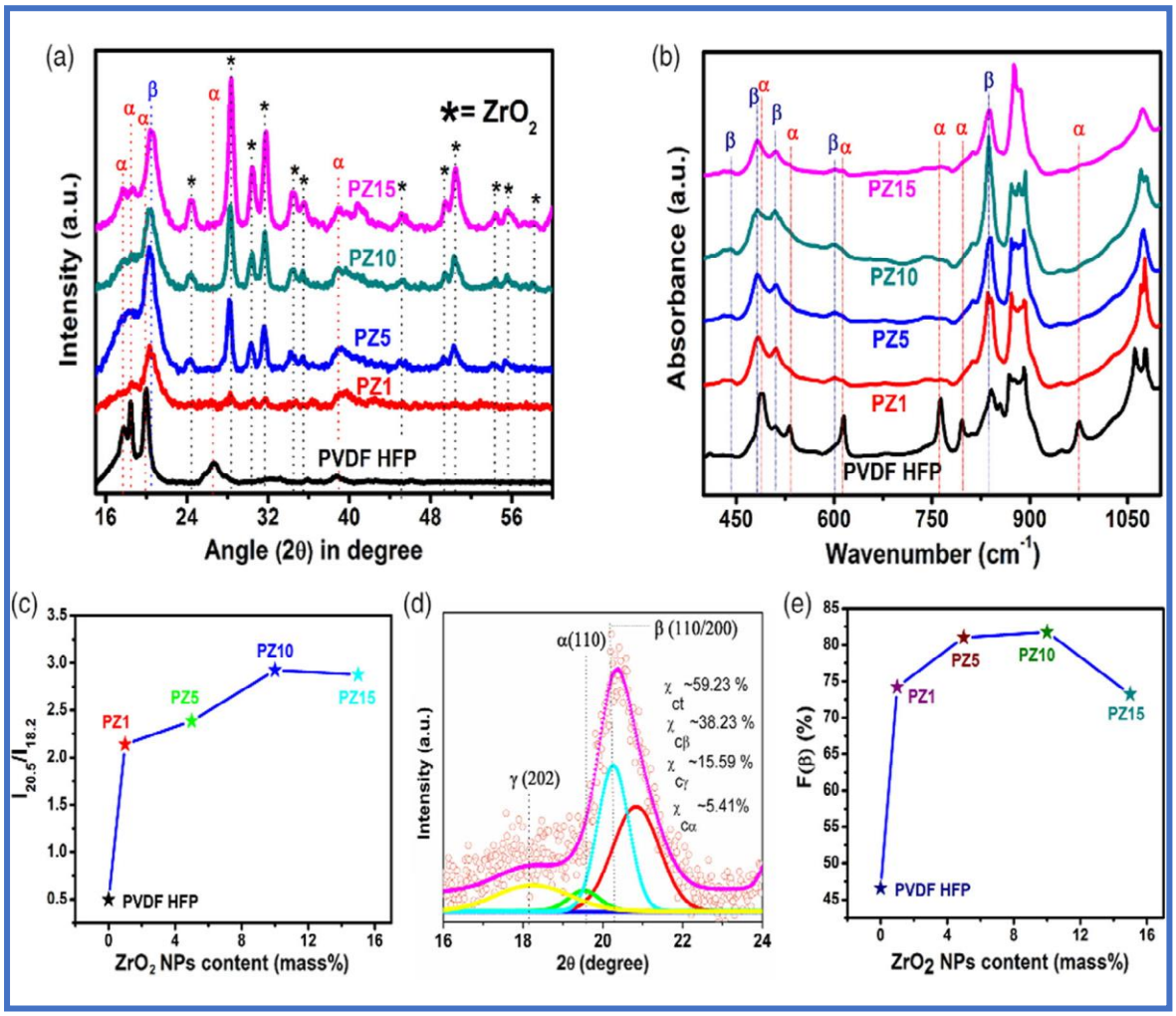

Figure 2.3: (a) XRD pattern of pure PVDF-HFP and ZrO_2 NPs-doped PVDF-HFP thin films (PZ1, PZ5, PZ5, PZ10, and P15). (b) FTIR spectra of pure PVDF-HFP and ZrO_2/PVDF-HFP composite thin films (PZ1, PZ5, PZ5, PZ10, and P15). (c) Ratio of $I_{20.5}$ and $I_{18.2}$ of the samples. (d) Deconvolution of XRD (e) Evaluation of β-phase content of the samples.

Figure 2.3:(b) displays the FTIR spectra of both pure PVDF-HFP and ZrO_2 NPs/PVDF-HFP composite thin films. For the nonpolar α phase of pure PVDF-HFP, absorbance bands are observed at 488 cm^{-1} (CF_2 wagging), 532 cm^{-1} (CF_2 bending), 615 and 764 cm^{-1} (CF_2 bending and skeletal bending), and 796 and 976 cm^{-1} (CH_2 rocking). The characteristic absorbance bands at 840 cm^{-1} (CH_2 rocking, CF_2 stretching, and skeletal C═C stretching) and 813 cm^{-1} (CF_2 asymmetric stretching) indicate the presence of polar β and γ configurations, respectively. These bands suggest that the pure PVDF-HFP contains primarily the nonpolar α phase with a minimal amount of polar β and γ phases. In contrast, the electroactive β phase of the ZrO_2 NPs/PVDF-HFP composite thin films exhibits prominent absorbance bands at 445 cm^{-1} (CF_2 rocking and CH_2 rocking), 479 cm^{-1} (CF_2 deformation), 510 cm^{-1} (CF_2 stretching), 600 cm^{-1} (CF_2 wagging), and 840 cm^{-1} (CF_2 rocking, CF_2 stretching, and skeletal C═C stretching). The absence of absorbance bands corresponding to the α phase and the appearance of bands indicative of the β phase suggest enhanced polar β-phase crystallization in the PVDF-HFP matrix due to the nucleating effect of ZrO_2 NPs. Notably, the PZ10 sample exhibits the highest intensity of the main characteristic band for the β phase, aligning with the XRD results.

The enhancement of the electroactive β phase can be quantified by measuring its fraction, denoted as F(β). This fraction was determined from FTIR spectra using the Lambert–Beer law, as described in Equation (2.5).

$$\mathbf{F(\beta)} = \frac{\mathbf{A_\beta}}{\left(\frac{\mathbf{K_\beta}}{\mathbf{K_\alpha}}\right)\mathbf{A_\alpha + A_\beta}} \times \mathbf{100\%} \qquad \mathbf{(2.5)}$$

where, A_α represents the absorbance at 764 cm^{-1}, A_β is the absorbance at 840 cm^{-1}, K_β and K_α are the absorption coefficients at 840 cm^{-1} and 764 cm^{-1}, respectively. The values for K_α and K_β are 6.1 x 10^4 cm^2 mol^{-1} and 7.7 x 10^4 cm^2 mol^{-1} respectively [32].

The fluctuation of the β phase fraction (F(β)) with the ZrO_2 NPs concentration (vol%) is depicted in Figure 2d. It has been determined that the pure PVDF-HFP composite matrix has a F(β) value of 46.58%. This F(β) value rises as NPs are loaded up to 10% mass% of ZrO_2 NPs content, after which it falls. The maximum amount that F(β) for the PZ10 sample is 82%. This result is also excellent correlated with the results of XRD. Strong electrostatic coupling between the negatively charged and the polymer chains results in the TTTT conformation alignment, or the electroactive β phase nucleation in composite materials. Figure 2.4 provides a schematic representation of the potential interaction and self-polarization of the polymer matrix in the presence of ZrO_2 NPs.

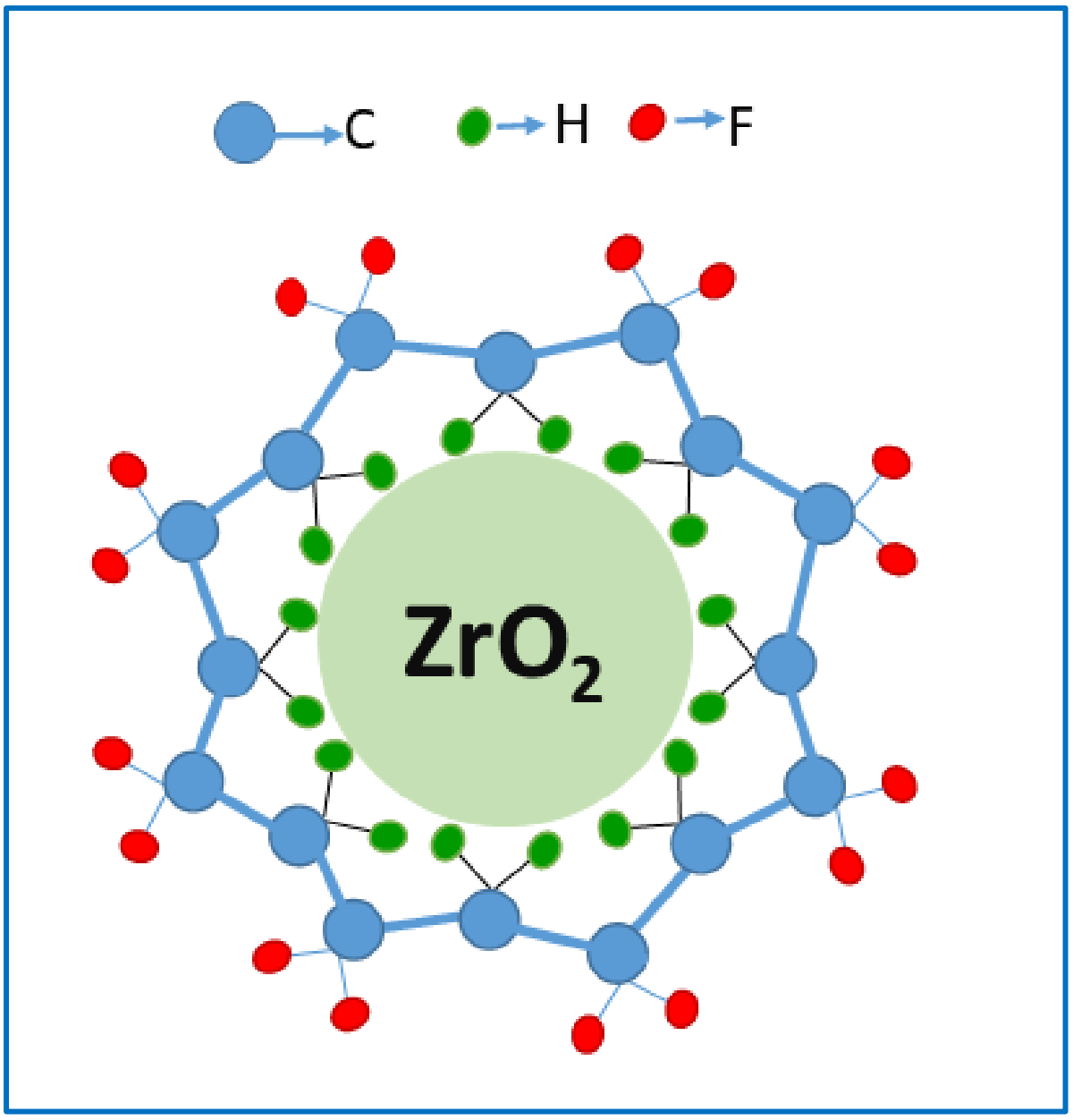

Figure 2.4: Schematic presentation of self-polarization and interaction between ZrO_2 NPs and Polymer matrix.

2.4.3. Thermal property analysis

Figure 2.5:(a) shows the DSC thermographs of both pure PVDF-HFP and PVDF-HFP composites with ZrO_2 nanoparticles. The thermograph for pure PVDF-HFP has a melting peak at 164.5℃, corresponding to the nonpolar α polymorph, as noted in previous studies [28]. When ZrO_2 nanoparticles are added to the polymer matrix, the melting peak shifts to a higher temperature, indicating a morphological change in the crystallinity of PVDF-HFP. Specifically, this shift suggests a transition from the nonpolar α crystal form (TGTG conformation) to the β crystal form (TTTT conformation), consistent with XRD results.

Consequently, the melting temperature (Tc) increases from 150.8℃ to 153.5℃ with the inclusion of ZrO_2 nanoparticles, implying that these nanoparticles act as nucleating agents for PVDF-HFP. The degree of crystallinity (χ_c) was quantitatively measured using Equation (2.5) [40].

$$\chi_c = \frac{\Delta H_m}{\Delta H_{100\%}} \times 100\% \quad \textbf{(2.6)}$$

ΔH_m denotes the melting enthalpy or enthalpy of fusion, while $\Delta H_{100\%}$ corresponds to the melting enthalpy of 100% crystalline PVDF, valued at 104.6 J/g. Figures 3b and 3c depict the enthalpy of fusion (ΔH_m) and the crystallinity degree (χ_c) for both the pure PVDF-HFP and its composites. As illustrated in Figure 3c, both the enthalpy of fusion and the crystallinity degree (χ_c)) increase with ZrO_2 nanoparticles loading up to 10 masses % in the PVDF-HFP matrix, after which they decline with additional ZrO_2 NP loading. The peak crystallinity degree (χ_c) achieved was 67% at 10 mass% ZrO_2 nanoparticle loading (PZ10).

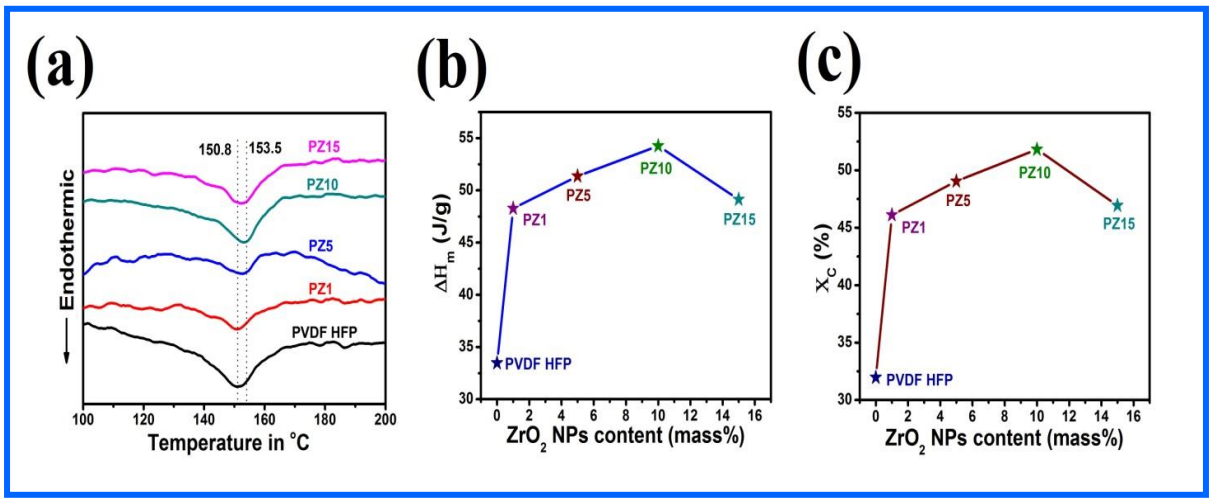

Figure 2.5. (a) DSC thermographs of pure PVDF-HFP and ZrO_2 NPs/PVDF-HFP composite thin films. (b) Evaluation of enthalpy of fusion and (c) degree of crystallinity of pure PVDF-HFP and ZrO_2 NP-loaded PVDF-HFP thin films.

2.4.4. Electrical property analysis

Capacitance (C) and tangent loss (tan δ) were measured using an Agilent E4980A digital LCR meter over a frequency range of 20 Hz to 2 MHz at an AC voltage of 1 V applied between two electrodes. The dielectric constant (ε_r) and AC conductivity (σ_{ac}) were calculated using the following equations:

$$\varepsilon_r = \frac{C \times d}{\varepsilon_0 A} \quad \textbf{(2.7)}$$

$$\sigma_{ac} = 2\pi f \varepsilon_r \varepsilon_0 \tan\delta \quad \textbf{(2.8)}$$

Here, A is the area of the film, d is the thickness, f is the frequency in Hz, and ε_0 is the permittivity of free space (8.854×10^{-12} F/m) [41].

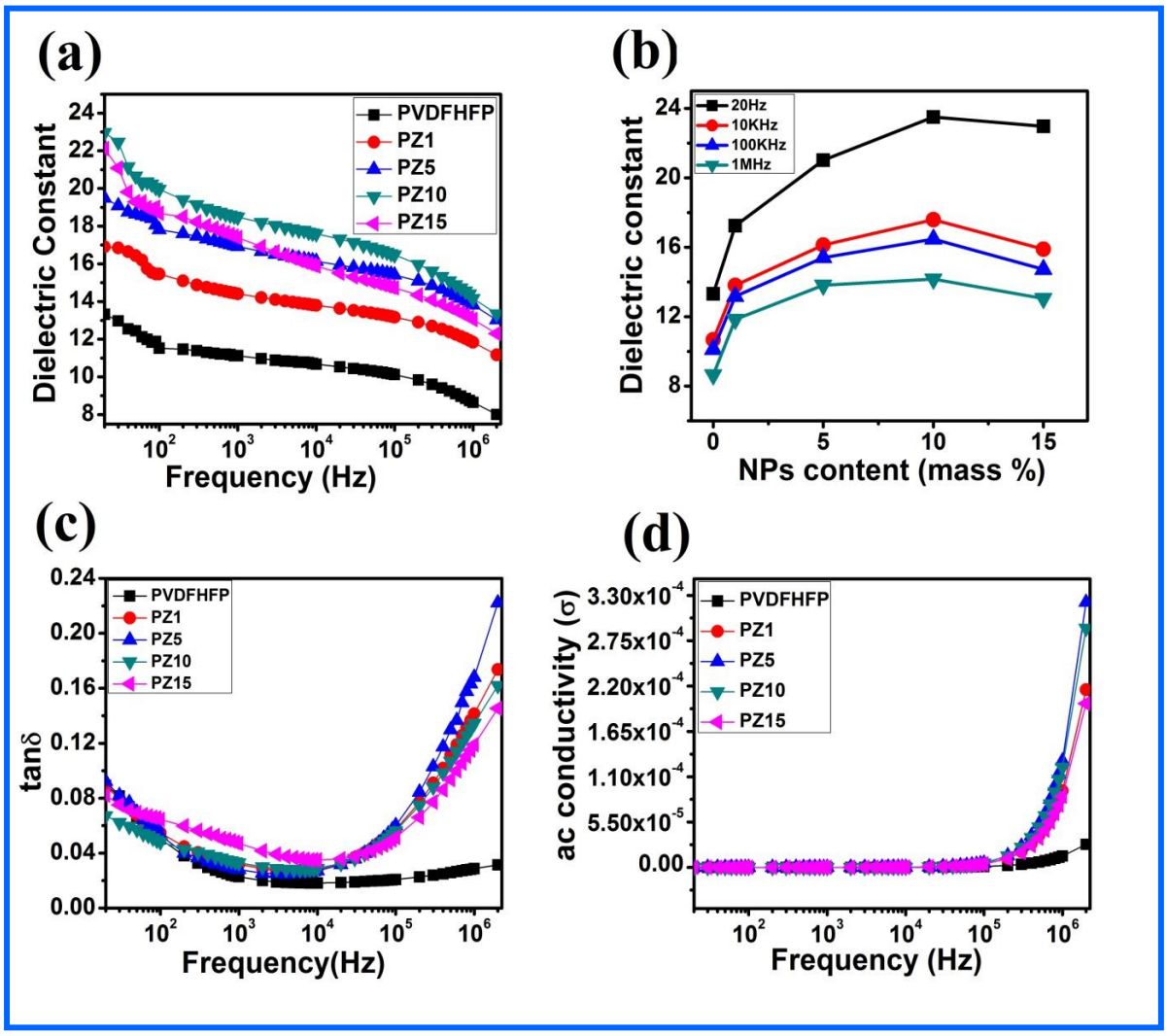

Figure 2.6: Frequency dependence of dielectric properties of pure PVDF-HFP and ZrO_2/PVDF-HFP nanocomposite thin films; (a) and (b) dielectric constant, (c) tangent loss, and (d) AC conductivity.

As shown in Figure 2.6:(a), the dielectric constant of the ZrO_2 NP /PVDF-HFP nanocomposite film increases with ZrO_2 NP concentration up to 10 masses % and then decreases with further doping. Additionally, the dielectric constant decreases as frequency increases. This is explained by Maxwell-Wagner-Sillars (MWS) interfacial polarization, where at low frequencies, electric dipoles can follow the applied AC field and align toward the electrode over a longer period. At higher frequencies, however, the dipoles cannot keep up with the AC field, resulting in a lower dielectric constant. The highest dielectric constant is achieved at a 10 mass% ZrO_2 NP loading due to the formation of the maximum

electroactive β phase of PVDF-HFP {Figure 2.6:(b)}. Similarly, tan δ decreases with increasing frequency {Figure 2.6:(b)}. The highest recorded dielectric constant was about 23 for the PZ10 sample at 20 Hz. Figure 2.6:(d) shows the frequency dependence of AC conductivity (σ_{ac}) for pure PVDF-HFP and ZrO_2 NP-modified PVDF-HFP samples. The MWS effect at the interface between ZrO_2 NPs and the PVDF-HFP polymer chain results in an increase in AC conductivity (σ_{ac}) with frequency [26].

2.4.5. Performance of the PENG

The procedures for device fabrication are detailed in the Experimental Section. Figure 2.7:(a) displays the transparencies of ZrO_2/PVDF-HFP composite thin films with varying concentrations, while figure 2.7:(b) provides a schematic illustration of the fabricated device. Among the composite films, PZ10 demonstrates the highest electroactive β phase and an improved dielectric constant. Additionally, the PZ10 sample exhibits a notable piezoelectric coefficient (d_{33}) of approximately 72.5 pC/N at 50 Hz under a constant applied force of 0.5 N, as measured by a Piezotest PM300. Based on these results, the PZ10 film was selected for fabricating a piezoelectric nanogenerator (PENG) and further characterized for its piezoelectric response and sensitivity. Figure 2.7:(c) represents the flexibility of the fabricated PENG.

Figure 2.7:(d) depicts the open-circuit output voltage response of the PENG when subjected to continuous finger tapping at a frequency of approximately 6 Hz, as recorded by a digital storage oscilloscope (DSO) (Keysight, Oscilloscope DSO-X 3012 A). A close-up of the open-circuit voltage is shown in Figure 2.7:(e), where a small secondary voltage peak is observed. This secondary peak may result from the damping force within the PENG after the finger is released and the subsequent vibration of the device. The short-circuit current output performance and its magnified view are recorded using a Keysight Electrometer B2985 and are illustrated in figures 2.7:(g) and 2.7:(h), respectively. Under periodic finger tapping, the fabricated PENG generates a positive open-circuit voltage (V_{oc}) of approximately 120 V and a short-circuit current (I_{sc}) of about 1.95 μA at an imparting frequency of approximately 6 Hz, corresponding to an instantaneous power density of approximately 7091 μW/cm³.

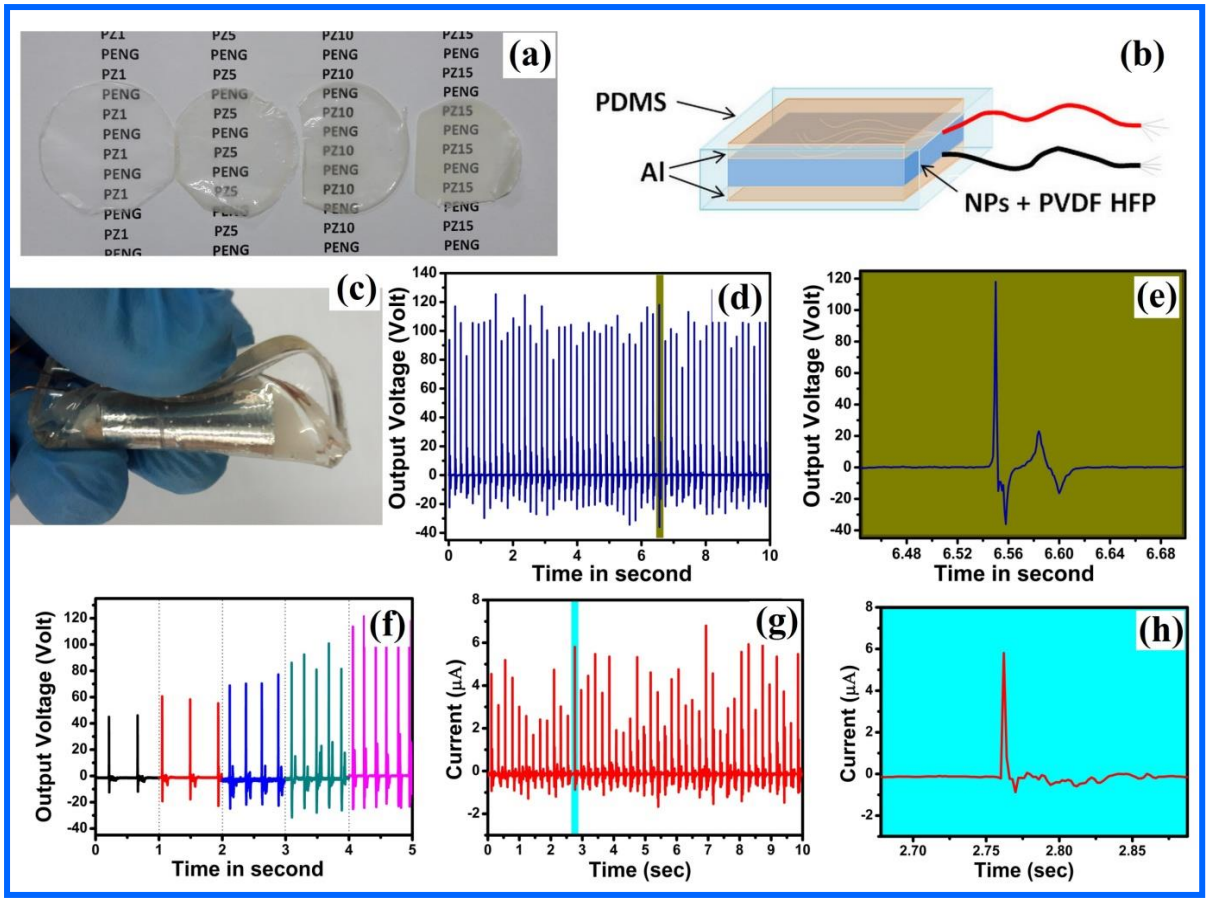

Figure 2.7:(a) Transparency nature of ZrO_2/PVDF-HFP nanocomposite thin films; (b) schematic diagram of the fabricated; (c) Photograph of fabricated PENG. (d) Open-circuit output voltage (Voc); (e) Magnified view of open-circuit output voltage (Voc); (f) Frequency-dependent output voltage (Voc); (g) Short-circuit output current (Isc) of PENG under the finger impetrating and (h) Magnified view of short-circuit output current (Isc).

The fabricated PENG achieves a maximum instantaneous power density that surpasses the values reported for PVDF/AlO-rGO composite PENGs by Karan et al. and various other studies, as detailed in Table 2.2 [26, 40, 55, 62–79]. The frequency-dependent output voltage performance of the PENGs was examined over a range from 1 to 6 Hz using finger tapping with an imparting force of approximately 28 N, as shown in figure 2.7:(f). The highest output voltage was recorded at 6 Hz. The underlying mechanism for this frequency-dependent performance is discussed in the energy-harvesting mechanism section. The stability of the fabricated devices was tested over a period of 18 months, during which the output voltage remained consistent, with a V_{oc} of approximately 120 V, demonstrating the high stability of the devices. Additionally, the piezoelectric output was evaluated in bending mode and by connecting the device in reverse mode to assess the triboelectric effect. The output in bending

mode was found to be minimal, around 70 mV (peak-to-peak voltage), indicating that the triboelectric contribution to the piezoelectric output is negligible in this study.

Table 2.2: Comparison of output characteristics of our PENG with other PENG reported earlier.

Piezoelectric Nanogenerator	**Current (I_{sc})**	**Output voltage (V_{oc})**	**Power density (P)**
$BaTiO_3$ nanotubes [40]	350 nA	5.5 V	64 μW cm^{-3}
$BaTiO_3$-PVDF [62]	600 nA	35 V	------
$BaTiO_3$-PDMS [63]	350 nA	5.5 V	-----
$FAPbBr_3$-PDMS [64]	3.8 μA/cm^2	8.5 V	32.3 μW cm^{-2}
$BaTiO_3$/PDMS/C [65]	-------	7.43V	7.92 μW
ZnO NWs/Paper [66]	400-520 pA	17 mV	5×10^{-3}μW cm^{-2}
$NaNbO_3$-PDMS [67]	16 nA/cm^2	3.2 V	51.2 nWcm^{-2}
PVDF/DNA [68]	0.184μA	20 V	11 μW cm^{-2}
Cellulose-ZnO [69]	1.25 μA	80 mV	50 nW cm^{-3}
Cellulose/PDMS/MWCNT [70]	500 nA	30 V	9 μW cm^{-3}
ZnO NWs/PVDF [71]	10 nA cm^{-2}	0.1 V	2 μW cm^{-3}
$KNbO_3$ Nanorods [72]	67.5 nA	3.2 V	11.9 μW cm^{-3}
PDMS/$ZnSnO_3$/MWCNT [73]	0.4μA	40 V	10.8 μW cm^{-3}
γ-PVDF/ZnO [74]	450 nA	28 V	Not measured
$NaNbO_3$/PVDF [75]	2.6 μA	18 V	-------
$FAPbBr_3$-PVDF [76]	6.2 μA/cm^2	30 V	186 μW cm^{-2}
$ZnTiO_3$/γ-PVDF [77]	1.2 μA	25.7 V	8.22 μW cm^{-2}
Nano ZnO/PVDF (0.2M ZnO loading) [78]	Not measured	4 V	N.A.
$KNbO_3$ nanowires [79]	1.3 μA	10.5 V	42 μW cm^{-3}
PVDF/AlO-rGO [55]	0.8 μA	36 V	27.97 μW cm^{-3}
Present work	**1.95 μA**	**120 V**	**7091 μWcm^{-3}**

The energy-harvesting mechanism by which PENGs convert mechanical energy into electrical signals is depicted in figure 2.8:(a). This mechanism highlights the synergistic effects of molecular dipoles in PVDF-HFP. ZrO_2 nanoparticles enhance the electroactive β phase and improve the piezoelectric properties of PVDF-HFP through strong electrostatic interactions with the polymer's dipoles. When subjected to mechanical stress from finger tapping, a secondary potential is induced in the ZrO_2 molecules, aligning the PVDF-HFP dipoles in the direction of the applied force. This nanoparticle-loaded PVDF-HFP exhibits self-polarization due to the mechanical stress and interfacial surface charge polarization. A positive piezoelectric potential is generated at the top electrode under compressional stress, while a negative potential forms at the bottom electrode upon stress release, due to the deformation of the PVDF-HFP crystalline structure. This self-polarization facilitates the movement of electrons between the two electrodes when connected through an external load resistor. Upon releasing the compressive stress, the piezoelectric potential decreases rapidly, causing the accumulated electrons at the bottom electrode to flow back through the external circuit to the other electrode, producing an opposite electrical output [55, 61]. Consequently, the fabricated PENGs generate a periodic output voltage during repeated compression and relaxation cycles.

To assess the practical application of the fabricated PENG, its ability to charge a 1 μF capacitor was tested, resulting in a charging time of just 13 seconds to reach 3.4 V, as depicted in figure 2.8:(c). Furthermore, the PENG demonstrated its capability to illuminate 55 different types of commercially available blue light emitting diodes (LEDs) connected in series, as illustrated in figure 2.8:(d).

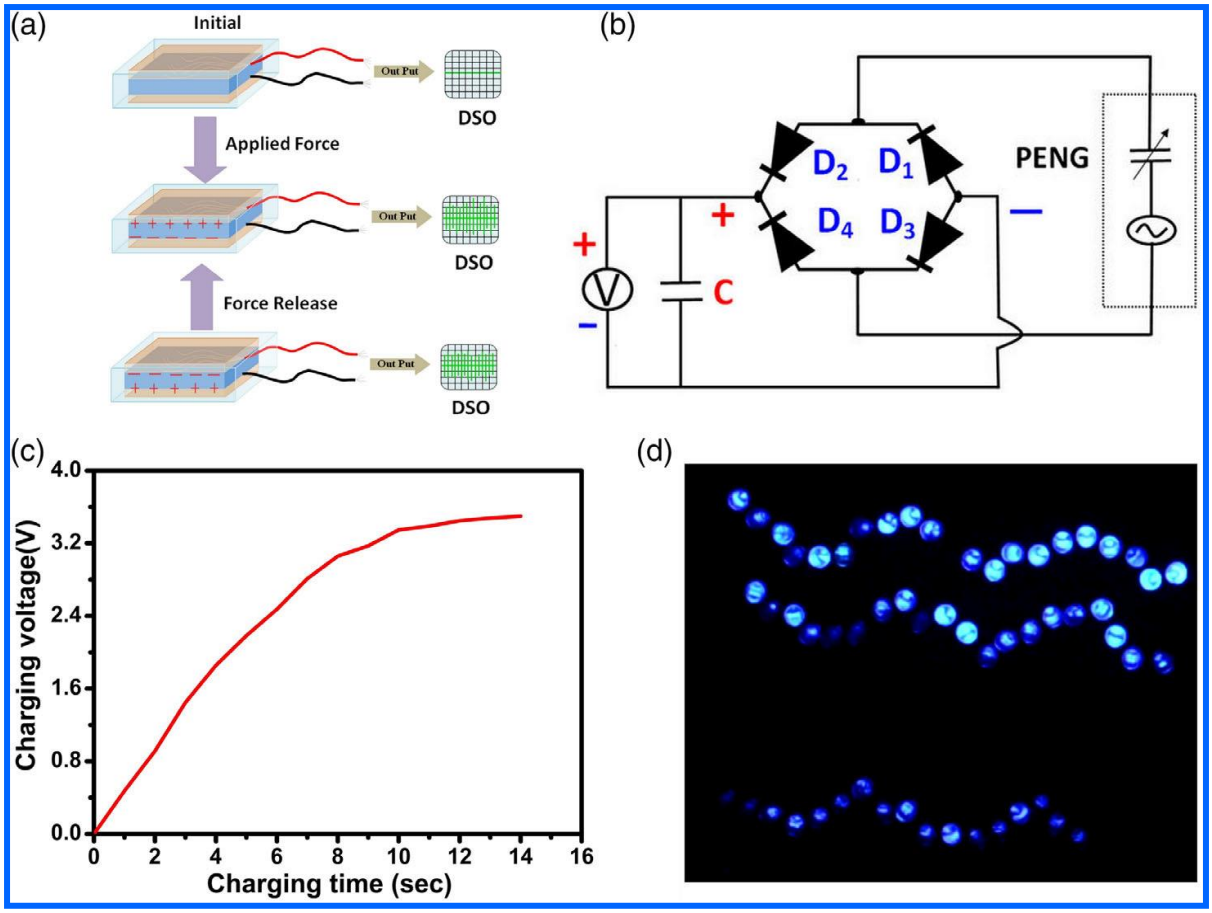

Figure 2.8:(a) Working mechanism of the PENG; (b) Circuit diagram of the charging capacitor; (c) Capacitor charging (voltage vs time) graph by PENG and (d) Photograph of glowing of LEDs by PENG.

2.4.6. Performance of the STENG

A digital photograph of a single-electrode triboelectric nanogenerator (STENG) is presented in figure 2.9(b). In this setup, the upper surface of the STENG and the epidermis are utilized as the two triboelectric layers. The epidermis, being highly prone to losing electric charge to the PVDF/ZrO_2 thin film according to the triboelectric series, was chosen as an ideal triboelectric layer for generating electric charge, as it is readily available on the human body. The output performance of the fabricated STENG was assessed using a digital storage oscilloscope (DSO) (Keysight, Oscilloscope DSO-X 3012A). The STENG was attached to the forearm, and data were collected while the arm was in motion. The maximum output voltage recorded was approximately 7 V, as shown in figure 2.9:(c). The potential electrical output generation mechanism is schematically illustrated in Figure 6a. Before contact between the PVDF/ ZrO_2 thin film and the epidermis (human finger), no charge transfer occurs, and there is no potential difference. However, upon contact, charges are induced on

the PVDF/ ZrO_2 thin film and transferred to the human body, resulting in equivalent negative and positive electric charges on the two surfaces. When the finger is removed from the composite film surface, the accumulated electrons on the film surface are transferred to the aluminium electrode from the ground electrode due to their differing potentials. This electron transfer ceases once electrostatic equilibrium is reached as the distance between the two surfaces increases. As the finger moves toward the composite surface again, electrons flow from the aluminium electrode to the ground until full contact is established between the two surfaces, generating a reversed output signal.

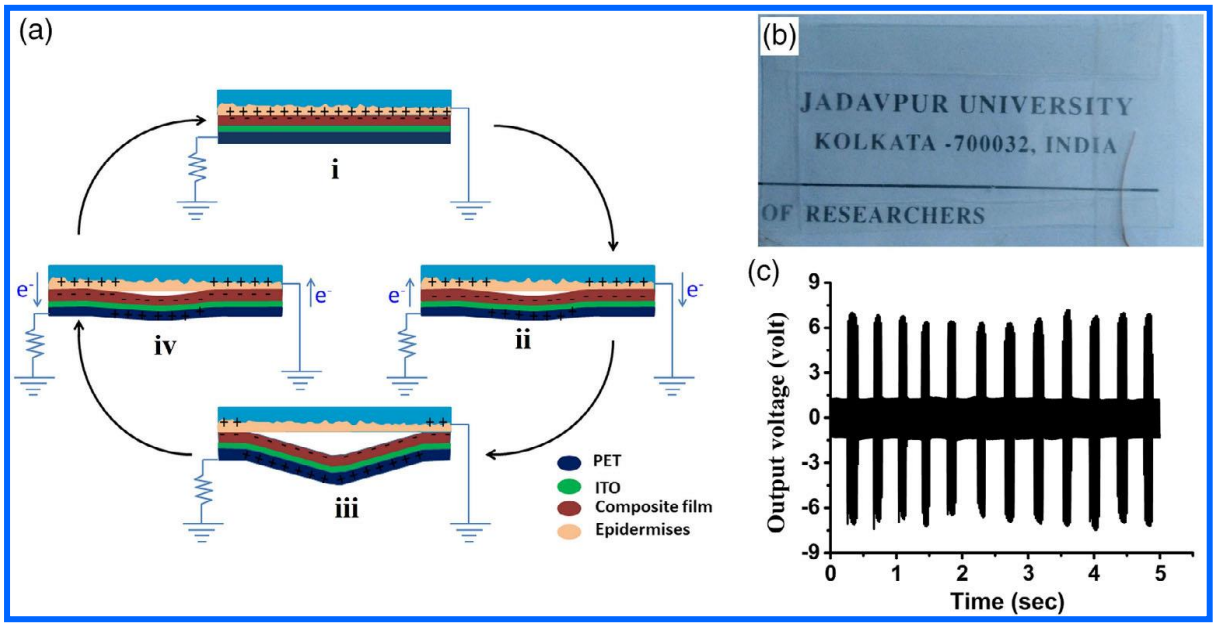

Figure 2.9:(a) Working mechanism of STENG; (b) digital photograph of transparent STENG and (c) output voltage performance of STENG.

2.5. Conclusions

To summarize, we have developed a high-performance Piezoelectric Nanogenerator (PENG) using ZrO_2/PVDF-HFP composite thin film to harvest mechanical energy from the surrounding environment. The incorporation of ZrO_2 nanoparticles (NPs) into the PVDF-HFP matrix leads to significant enhancements in both the β phase and output signals of the PENG. This enhancement is attributed to the nucleation of the electroactive β phase and the promotion of large interfacial polarization. As a result, the developed PENG achieves impressive performance metrics, including a substantial open-circuit voltage (V_{oc}) of 120 V, a short-circuit current (I_{sc}) of 1.95 μA, and a power density of 7091 μW cm^{-3} during periodic finger tapping. Utilizing a bridge rectifier, this PENG can readily illuminate a multitude of LEDs and charge a capacitor. Furthermore, a Single-Electrode Triboelectric Nanogenerator

(STENG) based on ZrO_2/PVDF-HFP composite also exhibits remarkable output performance, generating approximately 7 V with a simple finger touch. This innovative approach offers a scalable solution for powering systems, effectively converting small mechanical energy from human activities into usable electrical energy. The STENG holds promise for applications in touch sensor technologies and as a power source for low-energy-consuming portable devices.

*****

References:

[1] Wang, Z.L. and Song, J., 2006. Piezoelectric nanogenerators based on zinc oxide nanowire arrays. Science, 312(5771), pp.242-246.

[2] Martins, P., Costa, C.M., Benelmekki, M., Botelho, G. and Lanceros-Mendez, S., 2012. On the origin of the electroactive poly (vinylidene fluoride) β-phase nucleation by ferrite nanoparticles via surface electrostatic interactions. CrystEngComm, 14(8), pp.2807-2811.

[3] Fan, F.R., Tang, W. and Wang, Z.L., 2016. Flexible nanogenerators for energy harvesting and self-powered electronics. Advanced Materials, 28(22), pp.4283-4305.

[4] Shin, S.H., Kim, Y.H., Lee, M.H., Jung, J.Y., Seol, J.H. and Nah, J., 2014. Lithium-doped zinc oxide nanowires–polymer composite for high performance flexible piezoelectric nanogenerator. ACS nano, 8(10), pp.10844-10850.

[5] Kang, H.B., Chang, J., Koh, K., Lin, L. and Cho, Y.S., 2014. High quality Mn-doped (Na, K) NbO3 nanofibers for flexible piezoelectric nanogenerators. ACS applied materials & interfaces, 6(13), pp.10576-10582.

[6] Chen, J., Yang, J., Guo, H., Li, Z., Zheng, L., Su, Y., Wen, Z., Fan, X. and Wang, Z.L., 2015. Automatic mode transition enabled robust triboelectric nanogenerators. ACS nano, 9(12), pp.12334-12343.

[7] Gu, L., Cui, N., Cheng, L., Xu, Q., Bai, S., Yuan, M., Wu, W., Liu, J., Zhao, Y., Ma, F. and Qin, Y., 2013. Flexible fiber nanogenerator with 209 V output voltage directly powers a light-emitting diode. Nano letters, 13(1), pp.91-94.

[8] Liu, J., Cui, N., Gu, L., Chen, X., Bai, S., Zheng, Y., Hu, C. and Qin, Y., 2016. A three-dimensional integrated nanogenerator for effectively harvesting sound energy from the environment. Nanoscale, 8(9), pp.4938-4944.

[9] Yang, W., Chen, J., Zhu, G., Yang, J., Bai, P., Su, Y., Jing, Q., Cao, X. and Wang, Z.L., 2013. Harvesting energy from the natural vibration of human walking. ACS nano, 7(12), pp.11317-11324.

[10] Yang, J., Chen, J., Liu, Y., Yang, W., Su, Y. and Wang, Z.L., 2014. Triboelectrification-based organic film nanogenerator for acoustic energy harvesting and self-powered active acoustic sensing. ACS nano, 8(3), pp.2649-2657.

[11] Zhu, D., Tudor, M.J. and Beeby, S.P., 2009. Strategies for increasing the operating frequency range of vibration energy harvesters: a review. Measurement Science and Technology, 21(2), p.022001.
[12] Chen, J., Zhu, G., Yang, W., Jing, Q., Bai, P., Yang, Y., Hou, T.C. and Wang, Z.L., 2013. Harmonic-resonator-based triboelectric nanogenerator as a sustainable power source and a self-powered active vibration sensor. Advanced materials, 25(42), pp.6094-6099.
[13] Surmenev, R.A., Orlova, T., Chernozem, R.V., Ivanova, A.A., Bartasyte, A., Mathur, S. and Surmeneva, M.A., 2019. Hybrid lead-free polymer-based nanocomposites with improved piezoelectric response for biomedical energy-harvesting applications: A review. Nano Energy, 62, pp.475-506.
[14] Yang, Y., Guo, W., Pradel, K.C., Zhu, G., Zhou, Y., Zhang, Y., Hu, Y., Lin, L. and Wang, Z.L., 2012. Pyroelectric nanogenerators for harvesting thermoelectric energy. Nano letters, 12(6), pp.2833-2838.
[15] Wang, X., Dai, Y., Liu, R., He, X., Li, S. and Wang, Z.L., 2017. Light-triggered pyroelectric nanogenerator based on a pn-junction for self-powered near-infrared photosensing. ACS nano, 11(8), pp.8339-8345.
[16] Sultana, A., Ghosh, S.K., Alam, M.M., Sadhukhan, P., Roy, K., Xie, M., Bowen, C.R., Sarkar, S., Das, S., Middya, T.R. and Mandal, D., 2019. Methylammonium lead iodide incorporated poly (vinylidene fluoride) nanofibers for flexible piezoelectric–pyroelectric nanogenerator. ACS applied materials & interfaces, 11(30), pp.27279-27287.
[17] Lin, L., Xie, Y., Niu, S., Wang, S., Yang, P.K. and Wang, Z.L., 2015. Robust triboelectric nanogenerator based on rolling electrification and electrostatic induction at an instantaneous energy conversion efficiency of~ 55%. ACS nano, 9(1), pp.922-930.
[18] Seol, M.L., Woo, J.H., Lee, D.I., Im, H., Hur, J. and Choi, Y.K., 2014. Nature-replicated nano-in-micro structures for triboelectric energy harvesting. Small, 10(19), pp.3887-3894.
[19] Guo, H., Li, T., Cao, X., Xiong, J., Jie, Y., Willander, M., Cao, X., Wang, N. and Wang, Z.L., 2017. Self-sterilized flexible single-electrode triboelectric nanogenerator for energy harvesting and dynamic force sensing. ACS nano, 11(1), pp.856-864.
[20] Yang, Y., Zhang, H., Lin, Z.H., Zhou, Y.S., Jing, Q., Su, Y., Yang, J., Chen, J., Hu, C. and Wang, Z.L., 2013. Human skin based triboelectric nanogenerators for harvesting biomechanical energy and as self-powered active tactile sensor system. ACS nano, 7(10), pp.9213-9222.
[21] Yang, Y., Zhang, H., Chen, J., Jing, Q., Zhou, Y.S., Wen, X. and Wang, Z.L., 2013. Single-electrode-based sliding triboelectric nanogenerator for self-powered displacement vector sensor system. Acs Nano, 7(8), pp.7342-7351.
[22] Yang, Y., Zhou, Y.S., Zhang, H., Liu, Y., Lee, S. and Wang, Z.L., 2013. A single-electrode based triboelectric nanogenerator as self-powered tracking system. Advanced Materials (Deerfield Beach, Fla.), 25(45), pp.6594-6601.
[23] Wang, S.J., Wang, H., Du, K., Zhang, W., Sui, M.L. and Mao, S.X., 2014. Deformation-induced structural transition in body-centred cubic molybdenum. Nature communications, 5(1), p.3433.

[24] Zi, Y., Lin, L., Wang, J., Wang, S., Chen, J., Fan, X., Yang, P.K., Yi, F. and Wang, Z.L., 2015. Triboelectric–pyroelectric–piezoelectric hybrid cell for high-efficiency energy-harvesting and self-powered sensing. Advanced Materials, 27(14), pp.2340-2347.
[25] Yang, W., Chen, J., Jing, Q., Yang, J., Wen, X., Su, Y., Zhu, G., Bai, P. and Wang, Z.L., 2014. 3D stack integrated triboelectric nanogenerator for harvesting vibration energy. Advanced Functional Materials, 24(26), pp.4090-4096.
[26] Lin, Z.H., Yang, Y., Wu, J.M., Liu, Y., Zhang, F. and Wang, Z.L., 2012. $BaTiO_3$ nanotubes-based flexible and transparent nanogenerators. The journal of physical chemistry letters, 3(23), pp.3599-3604.
[27] Li, C., Luo, W., Liu, X., Xu, D. and He, K., 2016. PMN-PT/PVDF nanocomposite for high output nanogenerator applications. Nanomaterials, 6(4), p.67.
[28] Hoque, N.A., Thakur, P., Biswas, P., Saikh, M.M., Roy, S., Bagchi, B., Das, S. and Ray, P.P., 2018. Biowaste crab shell-extracted chitin nanofiber-based superior piezoelectric nanogenerator. Journal of Materials Chemistry A, 6(28), pp.13848-13858.
[29] Wang, Y., Furlan, R., Ramos, I. and Santiago-Avilés, J.J., 2004. Synthesis and characterization of micro/nanoscopic Pb (Zr 0.52 Ti 0.48) O_3 fibers by electrospinning. Applied Physics A, 78, pp.1043-1047.
[30] Thakur, P., Kool, A., Bagchi, B., Das, S. and Nandy, P., 2015. Effect of in situ synthesized Fe_2O_3 and Co_3O_4 nanoparticles on electroactive β phase crystallization and dielectric properties of poly (vinylidene fluoride) thin films. Physical Chemistry Chemical Physics, 17(2), pp.1368-1378.
[31] Martins, P.M., Miranda, R., Marques, J., Tavares, C.J., Botelho, G. and Lanceros-Mendez, S., 2016. Comparative efficiency of TiO_2 nanoparticles in suspension vs. immobilization into P(VDF–TrFE) porous membranes. RSC advances, 6(15), pp.12708-12716.
[32] Thakur, P., Kool, A., Bagchi, B., Das, S. and Nandy, P., 2014. Enhancement of β phase crystallization and dielectric behavior of kaolinite/halloysite modified poly (vinylidene fluoride) thin films. Applied Clay Science, 99, pp.149-159.
[33] Singh, H.H. and Khare, N., 2019. Improved performance of ferroelectric nanocomposite flexible film based triboelectric nanogenerator by controlling surface morphology, polarizability, and hydrophobicity. Energy, 178, pp.765-771.
[34] Feng, Y., Li, W.L., Hou, Y.F., Yu, Y., Cao, W.P., Zhang, T.D. and Fei, W.D., 2015. Enhanced dielectric properties of PVDF-HFP/$BaTiO_3$-nanowire composites induced by interfacial polarization and wire-shape. Journal of materials chemistry C, 3(6), pp.1250-1260.
[35] Biswas, P., Hoque, N.A., Thakur, P., Saikh, M.M., Roy, S., Khatun, F., Bagchi, B. and Das, S., 2019. Highly efficient and durable piezoelectric nanogenerator and photo-power cell based on CTAB modified montmorillonite incorporated PVDF film. ACS Sustainable Chemistry & Engineering, 7(5), pp.4801-4813.
[36] Ince-Gunduz, B.S., Alpern, R., Amare, D., Crawford, J., Dolan, B., Jones, S., Kobylarz, R., Reveley, M. and Cebe, P., 2010. Impact of nanosilicates on poly (vinylidene fluoride) crystal polymorphism: Part 1. Melt-crystallization at high supercooling. Polymer, 51(6), pp.1485-1493.

[37] Chang, C., Tran, V.H., Wang, J., Fuh, Y.K. and Lin, L., 2010. Direct-write piezoelectric polymeric nanogenerator with high energy conversion efficiency. Nano letters, 10(2), pp.726-731.

[38] Thakur, P., Kool, A., Bagchi, B., Hoque, N.A., Das, S. and Nandy, P., 2015. The role of cerium (iii)/yttrium (iii) nitrate hexahydrate salts on electroactive β phase nucleation and dielectric properties of poly (vinylidene fluoride) thin films. Rsc Advances, 5(36), pp.28487-28496.

[39] Adhikary, P. and Mandal, D., 2017. Enhanced electro-active phase in a luminescent P (VDF–HFP)/Zn^{2+} flexible composite film for piezoelectric based energy harvesting applications and self-powered UV light detection. Physical Chemistry Chemical Physics, 19(27), pp.17789-17798.

[40] Thakur, P., Kool, A., Hoque, N.A., Bagchi, B., Khatun, F., Biswas, P., Brahma, D., Roy, S., Banerjee, S. and Das, S., 2018. Superior performances of in situ synthesized ZnO/PVDF thin film based self-poled piezoelectric nanogenerator and self-charged photo-power bank with high durability. Nano Energy, 44, pp.456-467.

[41] Thakur, P., Kool, A., Bagchi, B., Hoque, N.A., Das, S. and Nandy, P., 2015. In situ synthesis of $Ni(OH)^2$ nanobelt modified electroactive poly (vinylidene fluoride) thin films: remarkable improvement in dielectric properties. Physical Chemistry Chemical Physics, 17(19), pp.13082-13091.

[42] Martins, P., Lopes, A.C. and Lanceros-Mendez, S., 2014. Electroactive phases of poly (vinylidene fluoride): Determination, processing and applications. Progress in polymer science, 39(4), pp.683-706.

[43] Pal, K., Kang, D.J., Zhang, Z.X. and Kim, J.K., 2010. Synergistic effects of zirconia-coated carbon nanotube on crystalline structure of polyvinylidene fluoride nanocomposites: electrical properties and flame-retardant behavior. Langmuir, 26(5), pp.3609-3614.

[44] Shukla, S. and Seal, S., 2005. Mechanisms of room temperature metastable tetragonal phase stabilisation in zirconia. International materials reviews, 50(1), pp.45-64.

[45] Liang, J., Jiang, X., Liu, G., Deng, Z., Zhuang, J., Li, F. and Li, Y., 2003. Characterization and synthesis of pure ZrO^2 nanopowders via sonochemical method. Materials research bulletin, 38(1), pp.161-168.

[46] Chandra, N., Singh, D.K., Sharma, M., Upadhyay, R.K., Amritphale, S.S. and Sanghi, S.K., 2010. Synthesis and characterization of nano-sized zirconia powder synthesized by single emulsion-assisted direct precipitation. Journal of colloid and interface science, 342(2), pp.327-332.

[47] Mayo, M.J., Seidensticker, J.R., Hague, D.C. and Carim, A.H., 1999. Surface chemistry effects on the processing and superplastic properties of nanocrystalline oxide ceramics. Nanostructured materials, 11(2), pp.271-282.

[48] Song, S.Y., Park, M.S., Lee, D., Lee, J.W. and Yun, J.S., 2019. Optimization and characterization of high-viscosity ZrO^2 ceramic nanocomposite resins for supportless stereolithography. Materials & Design, 180, p.107960.

[49] Mueller, R., Jossen, R., Pratsinis, S.E., Watson, M. and Akhtar, M.K., 2004. Zirconia nanoparticles made in spray flames at high production rates. Journal of the American Ceramic Society, 87(2), pp.197-202.
[50] Gleiter, H., 2000. Nanostructured materials: basic concepts and microstructure. Acta materialia, 48(1), pp.1-29.
[51] Zhu, B., Xia, C., Luo, X. and Niklasson, G., 2001. Transparent two-phase composite oxide thin films with high conductivity. Thin Solid Films, 385(1-2), pp.209-214. [52] N. G. Petrik, D. P. Taylor, T. M. Orlando, J. Appl. Phys. 1999, 85, 6770.
[53] Bastianini, A., Battiston, G.A., Gerbasi, R., Porchia, M. and Daolio, S., 1995. Chemical vapor deposition of ZrO^2 thin films using $Zr(NEt_2)4$ as precursor. Le Journal de Physique IV, 5(C5), pp.C5-525.
[54] Corma, A., 1995. Inorganic solid acids and their use in acid-catalyzed hydrocarbon reactions. Chemical reviews, 95(3), pp.559-614.
[55] Karan, S.K., Bera, R., Paria, S., Das, A.K., Maiti, S., Maitra, A. and Khatua, B.B., 2016. An approach to design highly durable piezoelectric nanogenerator based on self-poled PVDF/AlO-rGO flexible nanocomposite with high power density and energy conversion efficiency. Advanced Energy Materials, 6(20), p.1601016. [56] J. Sun, A. Yang, C. Zhao, F. Liu, Z. Li, Sci. Bull. 2019, 64, 1336.
[56] Sun, J., Yang, A., Zhao, C., Liu, F. and Li, Z., 2019. Recent progress of nanogenerators acting as biomedical sensors in vivo. Science Bulletin, 64(18), pp.1336-1347.
[57] Gaur, A., Tiwari, S., Kumar, C. and Maiti, P., 2019. Retracted Article: A bio-based piezoelectric nanogenerator for mechanical energy harvesting using nanohybrid of poly (vinylidene fluoride). Nanoscale Advances, 1(8), pp.3200-3211. [58] J. Sun, H. Guo, J. Ribera, C. Wu, K. Tu, M. Binelli, G. Panzarasa, F. W. Schwarze, Z. L. Wang, I. Burgert, ACS Nano 2020, 14, 14665.
[58] Sun, J., Tu, K., Büchele, S., Koch, S.M., Ding, Y., Ramakrishna, S.N., Stucki, S., Guo, H., Wu, C., Keplinger, T. and Pérez-Ramírez, J., 2021. Functionalized wood with tunable tribopolarity for efficient triboelectric nanogenerators. Matter, 4(9), pp.3049-3066.
[59] Koç, M., Paralı, L. and Şan, O., 2020. Fabrication and vibrational energy harvesting characterization of flexible piezoelectric nanogenerator (PEN) based on PVDF/PZT. Polymer Testing, 90, p.106695.
[60] Wang, Z.L., 2017. On Maxwell's displacement current for energy and sensors: the origin of nanogenerators. Materials today, 20(2), pp.74-82.
[61] Lee, J.H., Kim, J., Kim, T.Y., Al Hossain, M.S., Kim, S.W. and Kim, J.H., 2016. All-in-one energy harvesting and storage devices. Journal of Materials Chemistry A, 4(21), pp.7983-7999.
[62] Zhao, Y., Liao, Q., Zhang, G., Zhang, Z., Liang, Q., Liao, X. and Zhang, Y., 2015. High output piezoelectric nanocomposite generators composed of oriented $BaTiO_3$ NPs@ PVDF. Nano Energy, 11, pp.719-727.
[63] Park, K.I., Lee, M., Liu, Y., Moon, S., Hwang, G.T., Zhu, G., Kim, J.E., Kim, S.O., Kim, D.K., Wang, Z.L. and Lee, K.J., 2012. Flexible nanocomposite generator made of $BaTiO_3$ nanoparticles and graphitic carbons. Advanced materials, 24(22), pp.2999-3004.

[64] Ding, R., Liu, H., Zhang, X., Xiao, J., Kishor, R., Sun, H., Zhu, B., Chen, G., Gao, F., Feng, X. and Chen, J., 2016. Flexible piezoelectric nanocomposite generators based on formamidinium lead halide perovskite nanoparticles. Advanced Functional Materials, 26(42), pp.7708-7716.
[65] Luo, C., Hu, S., Xia, M., Li, P., Hu, J., Li, G., Jiang, H. and Zhang, W., 2018. A flexible lead-free $BaTiO_3$/PDMS/C composite nanogenerator as a piezoelectric energy harvester. Energy Technology, 6(5), pp.922-927.
[66] Liao, Q., Zhang, Z., Zhang, X., Mohr, M., Zhang, Y. and Fecht, H.J., 2014. Flexible piezoelectric nanogenerators based on a fiber/ZnO nanowires/paper hybrid structure for energy harvesting. Nano Research, 7, pp.917-928.
[67] Jung, J.H., Lee, M., Hong, J.I., Ding, Y., Chen, C.Y., Chou, L.J. and Wang, Z.L., 2011. Lead-free NaNbO3 nanowires for a high output piezoelectric nanogenerator. ACS nano, 5(12), pp.10041-10046.
[68] Tamang, A., Ghosh, S.K., Garain, S., Alam, M.M., Haeberle, J., Henkel, K., Schmeisser, D. and Mandal, D., 2015. DNA-assisted β-phase nucleation and alignment of molecular dipoles in PVDF film: a realization of self-poled bioinspired flexible polymer nanogenerator for portable electronic devices. ACS applied materials & interfaces, 7(30), pp.16143-16147.

[69] Alam, M.M. and Mandal, D., 2016. Native cellulose microfiber-based hybrid piezoelectric generator for mechanical energy harvesting utility. ACS applied materials & interfaces, 8(3), pp.1555-1558.
[70] Kumar, A., Gullapalli, H., Balakrishnan, K., Botello-Mendez, A., Vajtai, R., Terrones, M. and Ajayan, P.M., 2011. Flexible ZnO–cellulose nanocomposite for multisource energy conversion. Small, 7(15), pp.2173-2178.
[71] Lee, M.; Chen, C. Y.; Wang, S.; Cha, S. N.; Park, Y. J.; Kim, J. M.; Chou, L. J.; Wang, Z. L. A hybrid piezoelectric structure for wearable nanogenerators. Advanced Materials **2012**, 24, 1759-1764.
[72] Jung, J.H., Chen, C.Y., Yun, B.K., Lee, N., Zhou, Y., Jo, W., Chou, L.J. and Wang, Z.L., 2012. Lead-free $KNbO_3$ ferroelectric nanorod based flexible nanogenerators and capacitors. Nanotechnology, 23(37), p.375401.
[73] Alam, M.M., Ghosh, S.K., Sultana, A. and Mandal, D., 2015. Lead-free $ZnSnO_3$/MWCNTs-based self-poled flexible hybrid nanogenerator for piezoelectric power generation. Nanotechnology, 26(16), p.165403.
[74] Jana, S., Garain, S., Ghosh, S.K., Sen, S. and Mandal, D., 2016. The preparation of γ-crystalline non-electrically poled photoluminescant ZnO–PVDF nanocomposite film for wearable nanogenerators. Nanotechnology, 27(44), p.445403.
[75] Zhang, C., Fan, Y., Li, H., Li, Y., Zhang, L., Cao, S., Kuang, S., Zhao, Y., Chen, A., Zhu, G. and Wang, Z.L., 2018. Fully rollable lead-free poly (vinylidene fluoride)-niobate-based nanogenerator with ultra-flexible nano-network electrodes. ACS nano, 12(5), pp.4803-4811.
[76] Ding, R., Zhang, X., Chen, G., Wang, H., Kishor, R., Xiao, J., Gao, F., Zeng, K., Chen, X., Sun, X.W. and Zheng, Y., 2017. High-performance piezoelectric nanogenerators

composed of formamidinium lead halide perovskite nanoparticles and poly (vinylidene fluoride). Nano Energy, 37, pp.126-135.

[77] Si, S.K., Karan, S.K., Paria, S., Maitra, A., Das, A.K., Bera, R., Bera, A., Halder, L. and Khatua, B.B., 2018. A strategy to develop an efficient piezoelectric nanogenerator through ZTO assisted γ-phase nucleation of PVDF in ZTO/PVDF nanocomposite for harvesting bio-mechanical energy and energy storage application. Materials Chemistry and Physics, 213, pp.525-537.

[78] Bhunia, R., Das, S., Dalui, S., Hussain, S., Paul, R., Bhar, R. and Pal, A.K., 2016. Flexible nano-ZnO/polyvinylidene difluoride piezoelectric composite films as energy harvester. Applied Physics A, 122, pp.1-13.

[79] Joung, M.R., Xu, H., Seo, I.T., Kim, D.H., Hur, J., Nahm, S., Kang, C.Y., Yoon, S.J. and Park, H.M., 2014. Piezoelectric nanogenerators synthesized using $KNbO_3$ nanowires with various crystal structures. Journal of Materials Chemistry A, 2(43), pp.18547-18553.

Chapter 3

Nanorose like structure CuS tailored electroactive PVDF composite thin film based piezoelectric energy nanogenerator for wireless gait monitoring.

3.1. Introduction

Due to a growing range of applications in biomedical support, human-computer interaction, and real-time health monitoring, all of which are supported by a significant of research, wearable devices have attracted a lot of interest [1-7]. However, piezoelectric nanogenerators (PENGs) have emerged as a promising solution, capable of converting environmental mechanical energy into electrical energy. PENGs leverage piezoelectric materials' ability to generate electricity in response to various mechanical stimuli, enabling self-powered sensors that detect human body movements with exceptional sensitivity [8-12].

The need for external power sources to maintain these devices' performance, however, shows an inherent challenge. Piezoelectric nanogenerators (PENGs) have emerged as a viable solution to this energy supply issue. PENGs may efficiently convert mechanical energy from the surroundings into electrical energy, making them a reliable source of power for recharging wearable technology [8–12]. The development of self-powered PENG sensors has been made possible by the notable characteristic that piezoelectric materials exhibit: the capacity to generate varying amounts of energy in response to diverse mechanical stimuli [13–15]. In fact, self-powered PENG sensors have been shown to be reliable tools for highly sensitive human body movement detection. These sensors have the ability to detect minute movements, like diaphragmatic breathing, joint articulation, and cardiac pulsations, demonstrating their potential utility in a range of applications pertaining to human physiology and health monitoring [16–19]. Gait monitoring is a useful tool in healthcare with various applications, including assessing the risk of falls, evaluating recovery progress, and tracking the movements of individuals with illnesses such as Parkinson's disease [20,21]. Furthermore, researchers have shown the effectiveness of gait tracking devices in sports training, improving the performance of athletes in sports like golf, jogging, and baseball [22–24]. Gait monitoring, a crucial application in healthcare and sports training, has been extensively explored using diverse strategies and operational mechanisms [25-27]. Camera-based approaches excel in observing gait patterns but are limited by spatial and temporal constraints [28]. Force-plate instrumented treadmills provide valuable insights but are costly and confined to laboratory settings. Accelerometers and gyroscopes offer a portable solution but often fall short in delivering quantitative results [29]. Thus, innovative technologies combining wearability, ease of use, affordability, and accurate recognition remain a significant challenge.

To address this, various fabrication techniques have been developed to create PENG sensors, including drop-casting, spin coating, spray coating, and electrospinning [30,31]. Drop-casting

has emerged as a promising technology for crafting PENG sensors utilizing highly flexible nanofibrous membranes [32]. To enhance operational longevity and stability, PENG sensors have been enveloped with protective plastic sealing coatings like polydimethylsiloxane (PDMS), rubber, and ethylene-vinyl acetate [33-35].

Piezoelectric materials, such as semi-crystalline polymer PVDF (poly (vinylidene fluoride)), exhibit excellent piezoelectric, pyroelectric, and ferroelectric properties. The electroactive β-phase, with a TTTT conformation, displays maximum piezoelectricity, making it a focal point for researchers [36-38]. Various techniques, including polling and self-polling, have been employed to improve electroactive β-phase conformation and dielectric properties in PVDF [39-41]. Self-polling involves mixing nanoparticles, or nanofillers, into the PVDF polymer matrix. Metal nanoparticles (NPs), metal oxide NPs, metal salts, organic compounds, carbon nanotubes, ceramic NPs, and clays are often utilized as nanofillers [42–50].

In this study, a self-powered and autonomous piezoelectric nanogenerator (CPENG) based on a PVDF thin film incorporated with CuS nanoroses is presented. The electroactive β phase of the PVDF nano-composite thin film exhibits commendable piezoelectric properties. The CuS nanoroses were synthesized via a straightforward hydrothermal method. The resulting CPENG demonstrates impressive output performance, boasting a power density of approximately 2640.6 μW/cm³ under periodic finger-induced mechanical stress.

The CPENG exhibits an enormous open-circuit voltage (V_{oc}) of ~130V and short-circuit current (I_{sc}) of ~1.25 μA under periodic finger imparting. It efficiently charges a 1μF capacitor to a voltage level of 2.4 V in mere 14 seconds during periodic finger-induced mechanical stress. Furthermore, the CPENG can power 26 commercially available blue light-emitting diodes (LEDs) when connected in parallel or 85 LEDs when connected in series.

This study incorporates a theoretical analysis of piezoelectric voltage generation, exploring its dependence on various factors, including polarization, surface charge, strain frequency, thin film thickness, and surface area of the piezoelectric thin films. The CPENG also possesses the capability to sense various bodily motions, including finger movements and blood flow, and generates distinct waveforms, offering a convenient means for recognizing walking patterns and tracking individual movements in surveillance applications.

3.2. Experimental Section

3.2.1. Materials:

- Copper (II) sulphate ($CuSO_4.H_2O$) from Merck, India

- Citric acid ($C_6H_8O_7$) from Merck, India
- Thiourea ($SC(NH_2)_2$) from Merck, India
- PVDF (Mw: 180,000 GPC, Mn: 71,000) from Aldrich, Germany

3.2.2. Synthesis of CuS nanoroses:

Initially, a solution was prepared by dissolving 2 mmol of $CuSO_4.H_2O$ and 1.2 g of citric acid in 240 ml of deionized water, followed by continuous stirring for 50 minutes. Then, 2 mmol of thiourea was added, and within 10 minutes, a vibrant green hue appeared, indicating a reaction. The mixture was transferred to three Teflon-lined stainless-steel autoclaves (80 ml each) and subjected to hydrothermal reaction conditions at 160°C for 1 hour, followed by cooling to room temperature. This resulted in the precipitation of CuS nanoparticles, which were recovered through centrifugation, washed with deionized water to remove residual H_2S, and dried at 80°C for 24 hours. The obtained CuS powder was prepared using an Agate mortar and pestle and stored under vacuum conditions for characterization. The synthesis process is schematically represented in figure 3.1:(a).

3.2.3. Synthesis of PVDF CuS Nanocomposite Thin Films

To prepare PVDF-CuS nanocomposite thin films, 0.25 g of PVDF was dissolved in 5 ml of DMSO at 60°C under rigorous stirring until a transparent solution was obtained. Then, CuS nanoparticles (1-10% by mass) were added to the clear PVDF solution, and the mixture was stirred vigorously for 12 hours at 60°C to ensure homogeneity. The resulting mixture was transferred to a clean Petri dish and placed in a dust-free electric oven at 80°C for 4-5 hours, allowing the formation of a nanocomposite thin film (50-60 micrometer thickness). For comparison, a pure PVDF thin film was cast following the same procedure without nanoparticles. All fabricated thin films were carefully preserved in a vacuum desiccator for further characterization. The sample designations for the different concentration thin films are tabulated in Table 3.1.

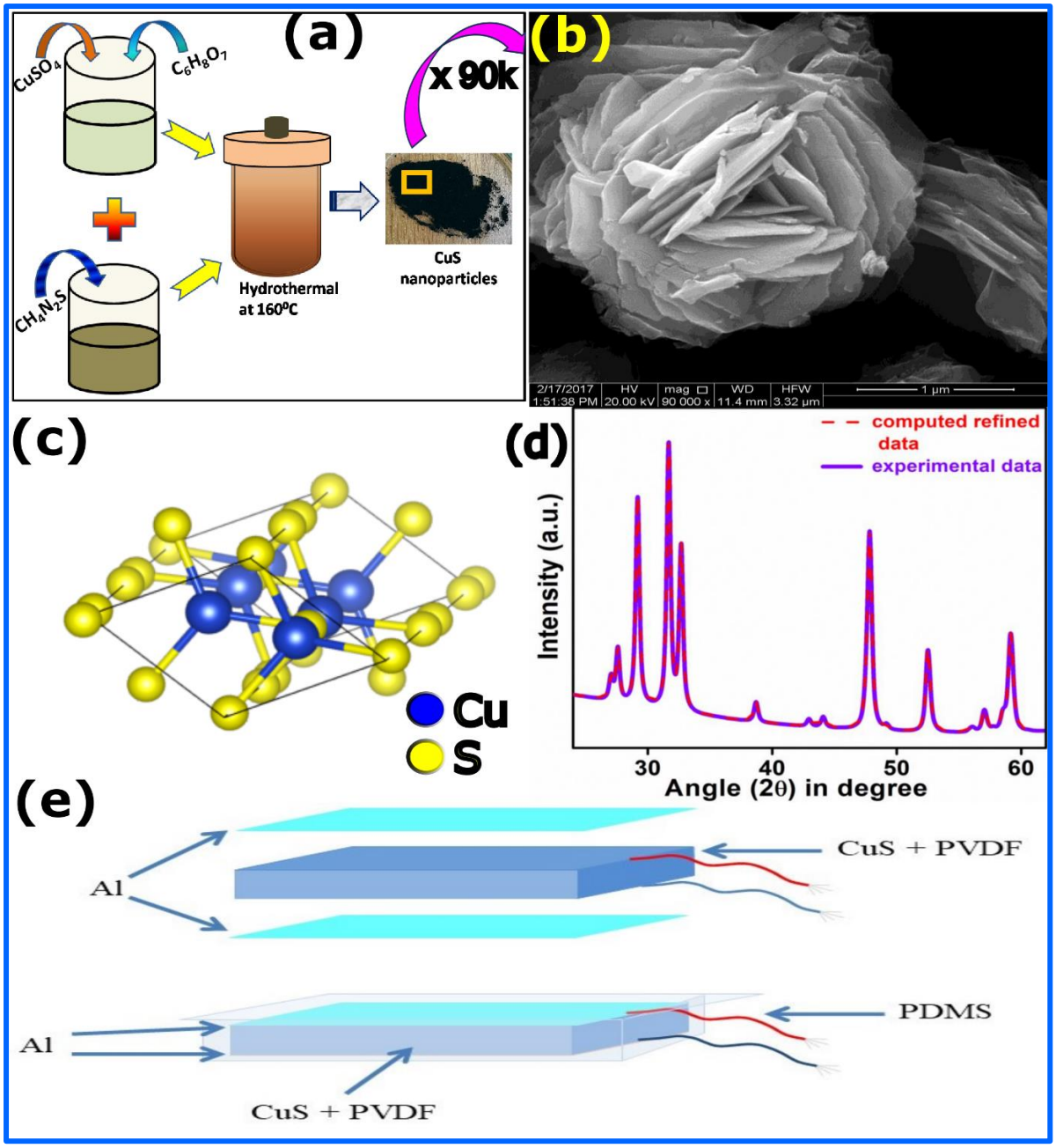

Figure 3.1: Schematic diagram of CuS nanoroses synthesis method (a), FESEM image of CuS nanoroses (b), the hexagonal structure of CuS nanoparticles (c) and (d) XRD data of CuS, the computed and experimental data.

Table 3.1: Designation of the sample with different amount of CuS nanorose concentrations:

Sample Designation	Amount of CuS NPs (g)	Amount of PVDF (g)	Percentage of CuS NPs (mass %)
CS0 (neat PVDF)	0.0000	0.2500	00
CS1	0.0005	0.2500	01
CS5	0.0125	0.2500	05
CS10	0.0250	0.2500	10

3.2.4. Fabrication of CPENG

A simple fabrication approach was employed to create a CuS nanoroses-based piezoelectric nanogenerator (CPENG). A PVDF-CuS nanorose nanocomposite thin film (CS5) was selected for this purpose. The CS5 sample had dimensions of 4 cm x 2 cm x 40 µm. Aluminium electrodes were affixed to both surfaces of the film, with wire leads attached for output connections. The device was then encapsulated with polydimethyl siloxane (PDMS) and dried in a dust-free electric oven at 60°C for 45 minutes {figure 3.1. (e)}.

3.3.Characterizations

The morphological microstructure of the surface of neat PVDF and CuS nanorose composite PVDF thin films was examined using field emission scanning electron microscopy (FESEM). The crystallographic structure was analyzed using Fourier transform infrared spectroscopy (FTIR) and X-ray diffractometry (XRD). The fraction of β-phase (F(β)) in the neat PVDF and CuS nanorose composite PVDF thin films was measured using Lambert-Beer law, which is given below

$$\mathbf{F(\beta)} = \frac{\mathbf{A_\beta}}{\left(\frac{\mathbf{K_\beta}}{\mathbf{K_\alpha}}\right)\mathbf{A_\alpha + A_\beta}} \times \mathbf{100\%} \qquad \mathbf{(3.1)}$$

where, A_α is the absorbance at 764 cm^{-1}; A_β is the absorbance at 840 cm^{-1}; K_β is the absorption coefficients at 840 cm^{-1} and K_α is the absorption coefficients at 764 cm^{-1} respectively. The values of the K_α and K_β are 6.1 x 10^4 cm^2 mol^{-1} and 7.7 x 10^4 cm^2 mol^{-1} respectively [31]

Thermal behaviour and phase crystallization were studied using differential scanning calorimetry (DSC). The melting enthalpies of fusion (ΔHm) and degree of crystallinity (χ_C) were evaluated from DSC thermographs:

$$\chi_C = \frac{\Delta H_m}{\Delta H_{100\%}} \times 100\% \quad \textbf{(3.2)}$$

where (ΔH_m) is the melting enthalpy of fusion and $\Delta H_{100\%}$ is the melting enthalpy of 100% crystalline PVDF with value 104.6 J/g [32].

Capacitance (C), tangent loss (tan δ), dielectric constant (ε), and ac conductivity (σac) were measured using a digital LCR meter and calculated using equations (3) and (4):

$$\varepsilon = Cd / \varepsilon_0 A \quad \textbf{(3.3)}$$

$$\sigma_{ac} = 2\pi f \varepsilon_0 \varepsilon \tan\delta \quad \textbf{(3.4)}$$

where, C, d, A and tan δ are the capacitance, thickness, area and tangent loss of the samples respectively; ε_0 is the permittivity of free space with the value of 8.854 x 10^{-12} F/m and f is the applied frequency in Hz [32].

3.4. Results and Discussions

3.4.1. FESEM analysis

Figure 3.1: (b) presents the Field Emission Scanning Electron Microscopy (FESEM) image of CuS nanoroses synthesized via a controlled hydrothermal process, showcasing their distinct rose-like nano-architecture. Figure 3.2: (a)-(d) displays the surface micrographs of pure PVDF and its composites (CS1, CS5, and CS10) integrated with CuS nanoroses. The images reveal a pronounced coarse texture in unadulterated PVDF {Figure 3.2: (a)}, while the subsequent images {{Figure 3.2:(b)-(d)} illustrate the spatial arrangement and affinity of CuS nanoroses within the PVDF matrix. The petal-like surface of the nanoroses, rich in positive charges, interact with the negatively charged regions of PVDF, inducing polarization. This polarization was confirmed through Fourier Transform Infrared (FTIR) spectroscopy, X-Ray Diffraction (XRD) patterns, and Differential Scanning Calorimetry (DSC) thermographs, providing comprehensive evidence of the polarization phenomenon.

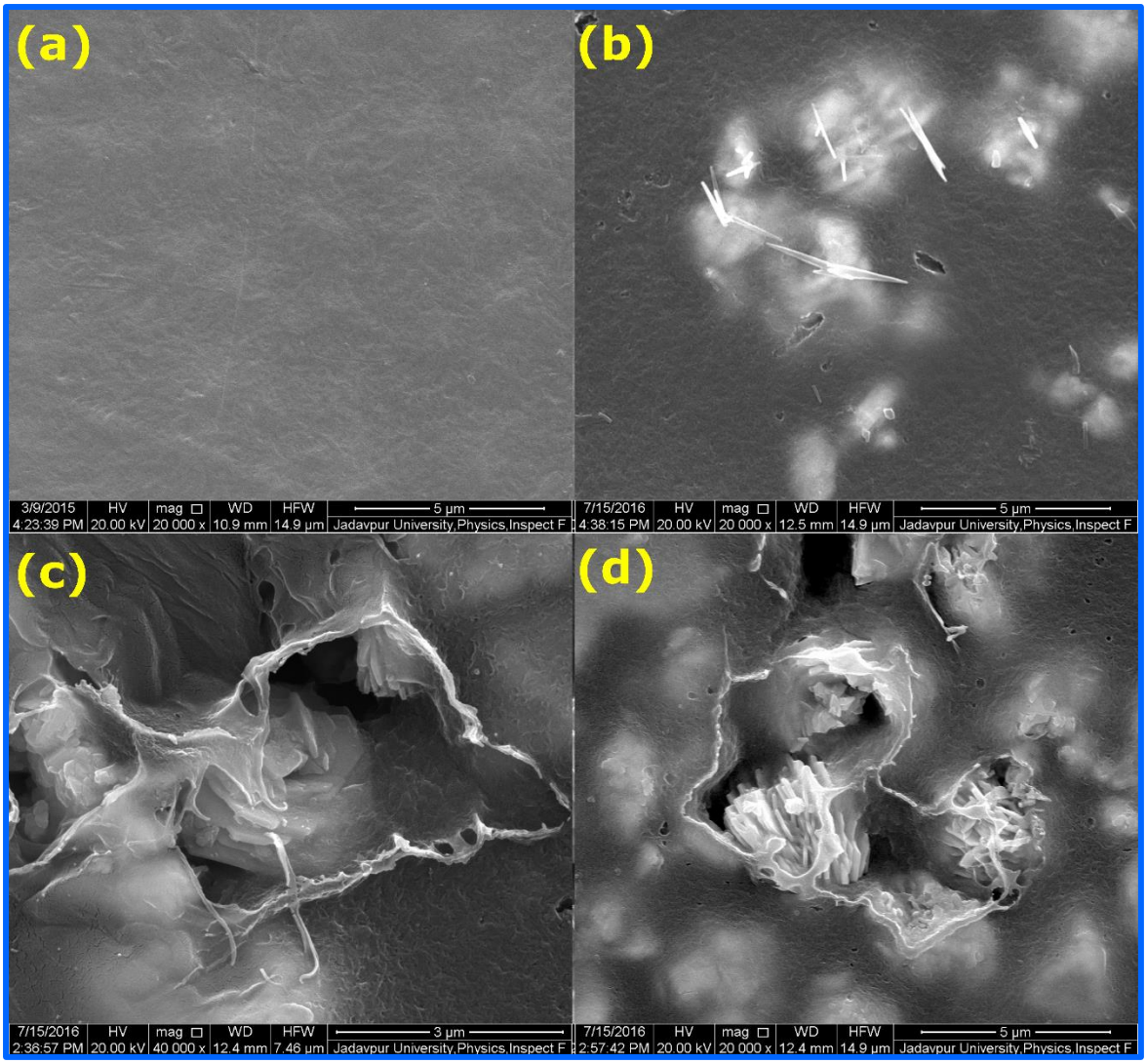

Figure: 3.2: FESEM image of (a) Neat PVDF (CS0), (b) CS1, (c) CS5 and (d) CS10.

3.4.2. FTIR Analysis

Figure 3.3:(a) displays the FTIR absorption spectra of neat PVDF and CuS nanorose loaded PVDF composite films, revealing characteristic peaks associated with the non-polar α-phase (532 cm^{-1}, 613 cm^{-1}, 763 cm^{-1}, 796 cm^{-1}, 854 cm^{-1}, 976 cm^{-1}, 1152 cm^{-1}, and 1212 cm^{-1}). The presence of α-phase in pure PVDF is shown in figure 3.3:(b). The peak at 840 cm-1 indicates crystallinity in the polymer matrix, attributed to a combination of β and γ-phases. The absence of the characteristic peak at 1234 cm-1 for γ-phase suggests that loading CuS nanorose into PVDF induces electroactive β-phases, reducing α-phase content [51]. This enhancement of β-phases is attributed to interfacial interactions between PVDF dipoles and CuS nanorose surface charges.

The fraction of β-phase (F(β)) was quantified using Lambert-Beer law {Equation (3.1)}[52] . Among the characterized samples, CS5 exhibited the highest F(β) value of 81%, while neat

PVDF, CS1, and CS10 showed F(β) values of 37%, 68%, and 76%, respectively. A comparative representation of F(β) across samples is shown in figure 3.3:(d).

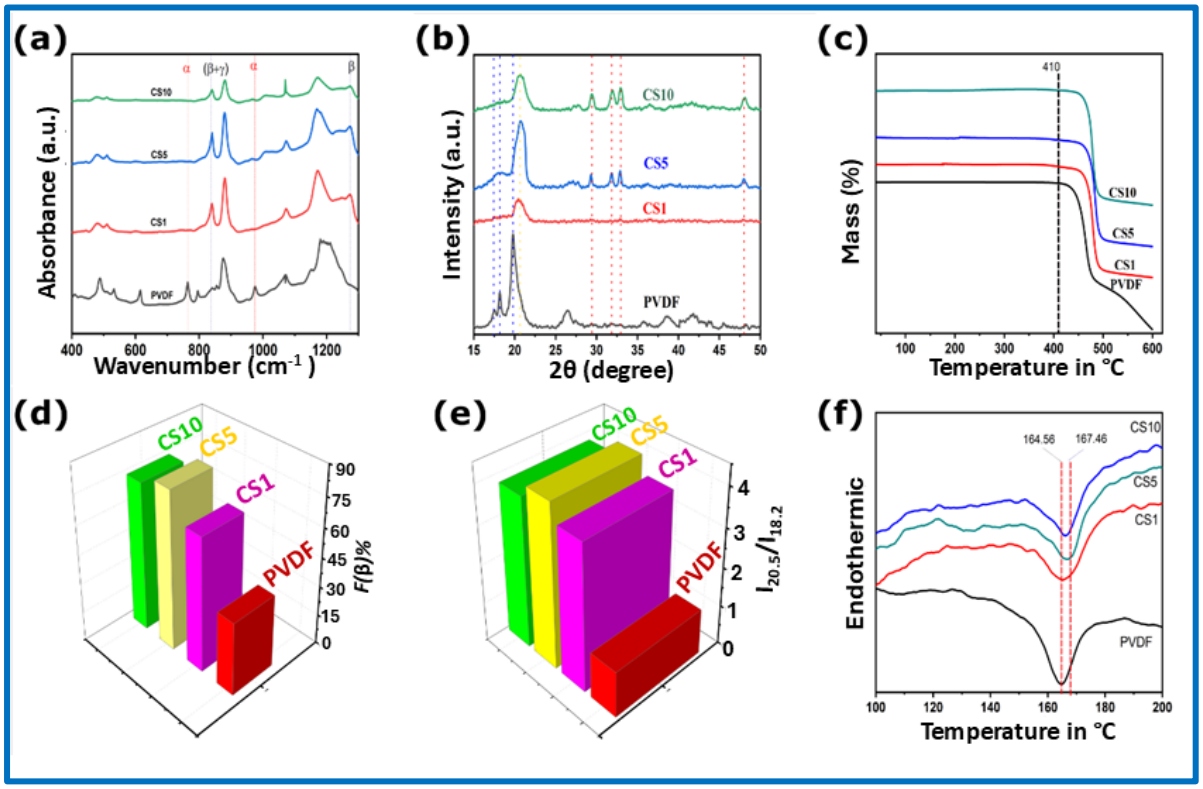

Figure 3. 3: (a) FTIR spectra of neat PVDF and CuS nanorose composite thin films (CS1, CS5, CS10); (b) XRD Pattern of neat PVDF and CuS nanorose composite thin films (CS1, CS5, CS10). (c) TGA thermograph of pure and nanocomposite thin films. (d) F(β)% of pure PVDF and nanocomposite thin films. (e) Ratio of $I_{20.6}$ and $I_{18.3}$ of the samples measured from XRD spectra. (f) DSC thermographs of unblended PVDF and CuS nanorose composite thin films

3.4.3 XRD Analysis

Figure 3.3:(b) displays the X-Ray diffraction (XRD) patterns of neat PVDF film and CuS nanorose incorporated PVDF thin films. The diffraction peaks at 2θ = 17.6°, 18.3°, 19.9°, and 26.6° correspond to the reflection planes of (100), (020), (021), and (201), (310), respectively, indicating the formation of nonpolar α-phase in neat PVDF. However, the incorporation of CuS nanorose leads to a decrease in α-phase peaks and an increase in β-phase peaks. The maximum intensity at 2θ = 20.5°, corresponding to the highest β-phase presence, is observed in CS10. The relative amount of β-phase is measured by the ratio $I_{20.5}/I_{18.3}$, with the maximum value found for CS5 {Figure 3.3:(e)}. This indicates that CS5 exhibits the maximum electroactive β-phase crystallization.

The synthesis procedure of CuS is schematically represented in figure 3.1:(a). XRD peaks confirm the formation of copper sulphide (CuS), matching JCPDS file No. 06-0464. The

morphological structure of synthesized nanoparticles is observed from the FESEM image, exhibiting a rose-like structure {Figure 3.1:(a)}. Rietveld refinement using Maud v2.94 software provides microstructure and crystal parameters, with computed and experimental data plotted in figure 3.1:(d) and refined parameters listed in Table 3.2. The hexagonal structure of CuS nanoparticles is visualized using VESTA 3.5.7 {Figure 3.1:(c)}. The average crystalline size of CuS nanoroses is estimated to be approximately 15.06 nm, revealing important structural properties. The obtained crystalline parameters of CuS are listed in Table 3.3.

Table 3.2: Refined parameters of the CuS nanoroses:

Parameters	**Value for CuS nanoroses**
a (Å)	**3.80**
b(Å)	**3.80**
c(Å)	**16.41**
α (º)	**90.00**
β(º)	**90.00**
γ (º)	**120.00**
V (Å^3)	**205.35**
Crystallite size (nm)	**15.060407**
R_p (%)	**6.47**
R_{wp} (%)	**8.07**
χ^2	**1.24**
Microstrain	**0.0010234112**

Table 3.3: Crystallographic parameters from XRD data of rose like CuS nanoparticles:

2Θ (in degree)	**FWHM (β)**	**Crystalline size (D) of CuS (in nm)**	**Dislocation density (ρ) (in nm^{-2})**	**Microstrain**
27.64739	0.75066	10.8987485	0.008419	0.01331116
29.31756	0.3278	25.05056521	0.001594	0.005467993
31.80952	0.52404	15.7631354	0.004025	0.008024486
32.80593	0.38006	21.78957279	0.002106	0.005633427
47.95441	0.40813	21.30342673	0.002203	0.004004036
52.6052	2.18908	4.048176343	0.061021	0.019324115
59.28373	0.42259	21.62963488	0.002137	0.00324033

3.4.4 DSC Analysis

Differential scanning calorimetry (DSC) was employed to investigate the crystallinity and melting enthalpy of the samples, complementing XRD and FTIR analyses. Figure 3.3:(a) displays the DSC thermographs for pure PVDF and its composites with integrated CuS nanoroses. The nonpolar α-phase of standard PVDF is characterized by an endothermic peak at 147.86°C [51]. With the inclusion of CuS nanorose, the melting point of PVDF increases at 5% concentration, decreases at 10% concentration, and then reduces further at higher concentrations {Figure 3.3:(f) and 3.3:(c)}. This trend indicates the transition to the electroactive β-phase within the PVDF matrix, consistent with XRD and FTIR findings.

The melting enthalpies (ΔH_m) were derived from the DSC thermographs, and the crystallinity degree (χ_C) was calculated using Equation 3.2. Figure 3.4 shows the relationship between CuS nanorose loading concentration and ΔH_m and χ_C. Notably, the CS5 specimen exhibited peak values of 58% for ΔH_m and 56.6% for χ_C, compared to 33% crystallinity in pure PVDF {Figure 3.4(a) and (b)}.

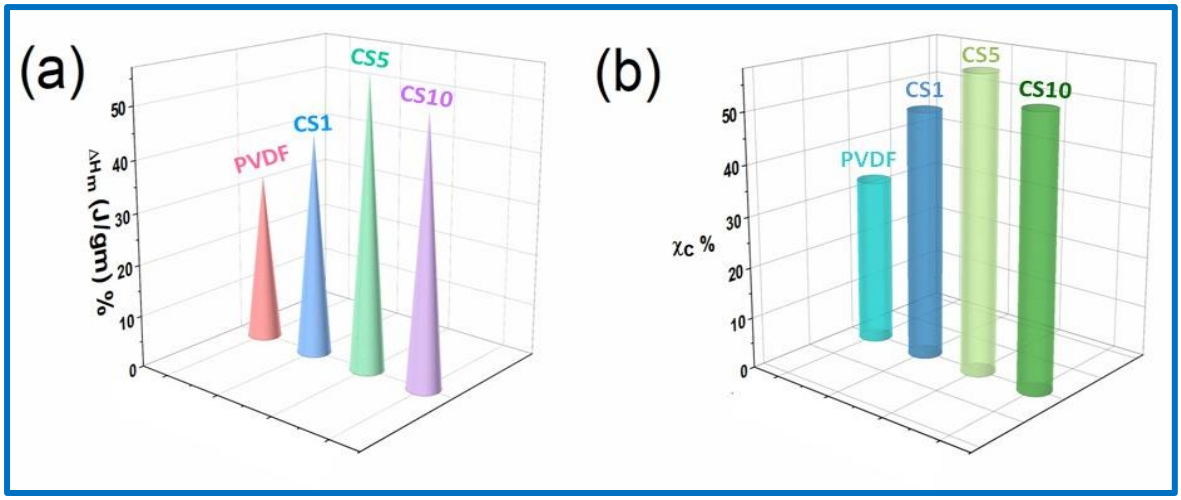

Figure 3.4: Enthalpy (a) and crystallinity (b) calculation of PVDF and composite thin films.

3.4.5 Dielectric Property Analysis

The dielectric behavior of CuS nanorose composite PVDF thin films exhibits a notable increase in the dielectric constant with the loading concentration of CuS nanorose, up to 5 masses%, which is attributed to the enhancement of the electroactive β-phase in the PVDF matrix, as confirmed by XRD and FTIR analyses. The frequency-dependent dielectric constants demonstrate a decrease in the dielectric constant with increasing frequency, a phenomenon explained by the Maxwell-Wagner-Sillars (MWS) interfacial polarization, whereby the electric dipoles in the composite PVDF freely move to the electrodes at lower frequencies but lag behind the applied field at higher frequencies. The highest dielectric constant ($\varepsilon \sim 44$) is achieved for CS5, attributed to its highest β-phase content, which facilitates the polarization of the PVDF matrix. Moreover, the frequency-dependent curve of ac conductivity (σ_{ac}) shows an increase in conductivity with frequency, arising from the interaction between CuS nanoroses and the PVDF polymer matrix, which enhances the charge transport and polarization properties of the composite. This comprehensive analysis highlights the potential of CuS nanorose composite PVDF thin films for advanced dielectric and electrical applications.

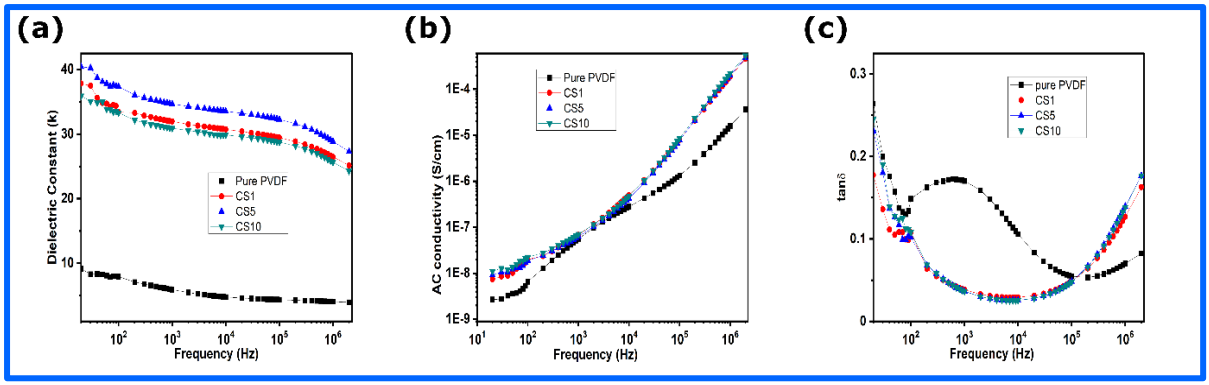

Figure 3.5: (a) Dielectric behaviour neat PVDF and CuS nanorose composite thin films (CS1, CS5, CS10), (b) AC conductivity of PVDF and CuS nanorose composite thin films and (c) tan δ for PVDF and CS1, CS5, CS10 samples.

3.5.Performance of the CPENG

Figure 3.1:(e) schematically illustrates the device, fabricated using the CS5 composite film selected for its pronounced β-phase and enhanced dielectric constant. The device's flexibility is demonstrated in Figure 5(g), showing it bent around a finger. The output voltage response to constant forces was recorded using a DSO, displaying an open-circuit voltage response to periodic finger pressure in figure 3.6:(a), with a magnified section in figure 3.6:(b) highlighting two distinct peaks. The output current response under consistent force application was documented using an electrometer, showcasing the short-circuit output current in figure 3.6:(d). Notably, the device outputs approximately 130 V open-circuit voltage (V_{oc}) and 1.25 µA short-circuit current (I_{sc}) under periodic finger pressures at 4 Hz. Figure 3.6:(e) shows the voltage drop across various external load resistances, achieving a maximum instantaneous power density of approximately 2640.6 µW/cm3 at 50 MΩ. Two CPENG sensors attached to the neck demonstrate robust responses to neck movements in figure 3.6:(f). The device sensitively captures minute mechanical pressures, including finger flexes {Figure 3.6:(g)} and wrist bends {Figure 3.6:(h)}.

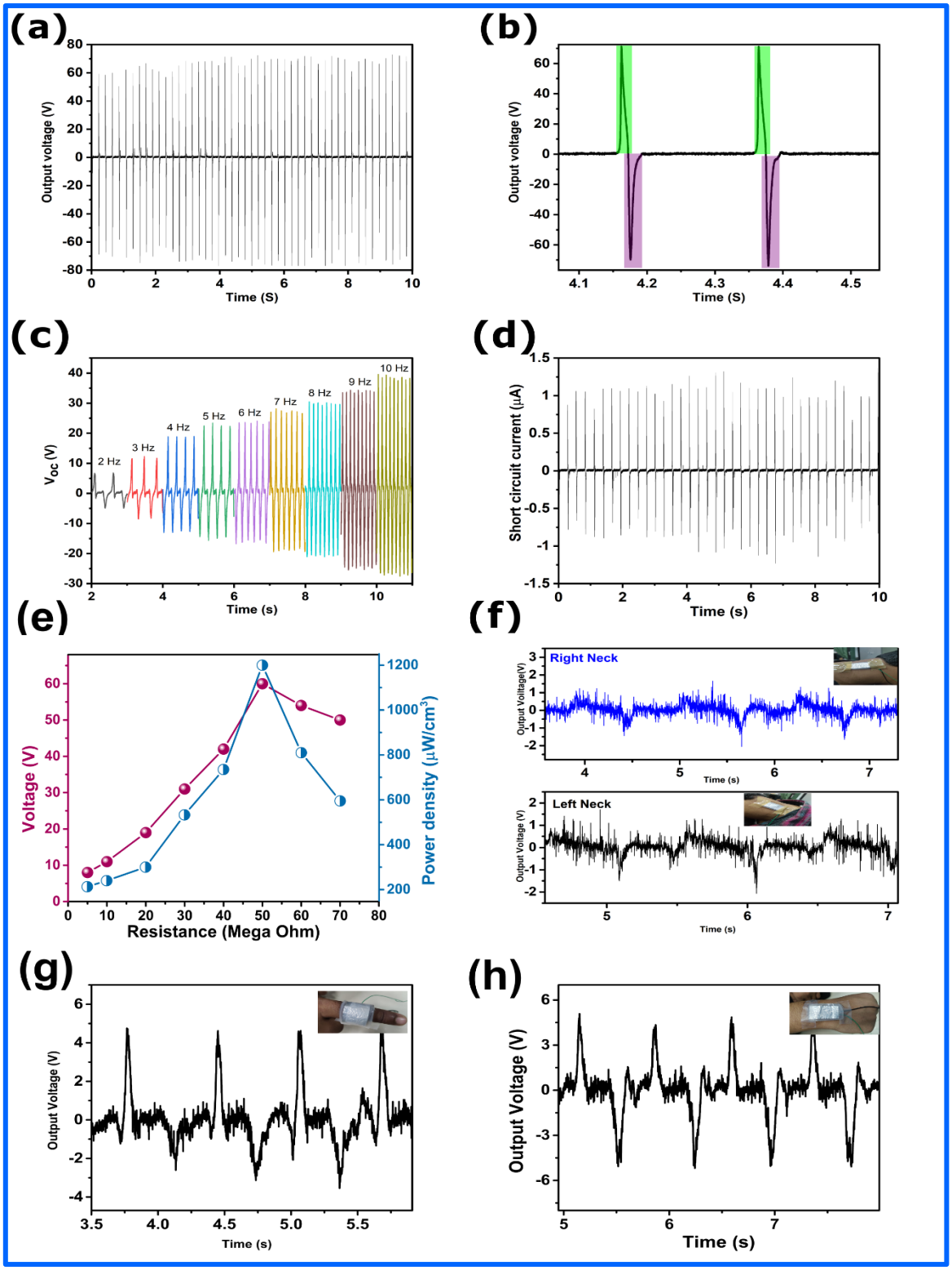

Figure 3.6: Output performance of CPENG (a) open circuit voltage by hand imparting, (b) magnification view of voltage output, (c) frequency variation (2 to 10 Hz) open circuit voltage of CPENG by vibrator with control force of 5 N, (d) short circuit current by finger imparting, (e) Voltage drop and instantaneous power density of CPENG across different external load resistances (f) Neck movement signal identified by CPENG. (g) finger movement signal detection by CPENG, and (h) wrist movement signal obtained by CPENG.

3.6.Working Mechanism

The four fundamental Maxwell's equations in Electrodynamics are given below

$\nabla.\vec{D} = \rho_f$ (Gauss's Law of electrostatics) **(3.5)**

$\nabla.\vec{H} = 0$ (Gauss's law magnetostatics) **(3.6)**

$\nabla x\vec{E} = -\frac{\partial\vec{B}}{\partial t}$ (Faraday's law) **(3.7)**

$\nabla x\vec{H} = \vec{J}_f + \frac{\partial\vec{D}}{\partial t}$ (Ampere's circuital law with Maxwell's addition) **(3.8)**

where, $\vec{E}$ is the electric field;$\vec{D}$ is the displacement electric field; $\vec{B}$ is the magnetic induction; $\vec{H}$ **is the** magnetic field; ρ_f is the volume charge density of free electron and $\vec{J}_f$ is the current density due to free electron flow.

Now the relation between the electric field ($\vec{E}$) and the displacement vector ($\vec{D}$) is given by

$$\vec{D} = \epsilon_0\vec{E} + \vec{P} \quad \textbf{(3.9)}$$

where, $\vec{P}$ is the dielectric polarization and ϵ_0 is the permittivity of free space.

For an isotropic media,

$$\vec{D} = \epsilon\vec{E} \quad \textbf{(3.10)}$$

where, ϵ is the permittivity of the dielectric.

In Maxwell's fourth equation, the second term is the displacement current and it is defined as

$$\vec{J}_D = \frac{\partial\vec{D}}{\partial t} = \epsilon_0\frac{\partial\vec{E}}{\partial t} + \frac{\partial\vec{P}}{\partial t} \quad \textbf{(3.11)}$$

From the above equation (3.8), we see that the displacement current is the time varying displacement vector and not an electric current of free electrons flow. It consists of two terms, one term is the time-varying electric field in vacuum or media and another term is the rate of changes of dielectric polarization in materials i.e., slight motion of charges bound in atoms.

In the Eq. (3.11), the first term $\epsilon_0\frac{\partial E}{\partial t}$ in the displacement current is responsible for the generation of electromagnetic wave. This mechanism is applied in wireless communication system like TV, cell phone, radio, radar and data transfer etc. The second term of the equation (3.11) gives birth to piezoelectric nanogenerators and sensors. Under a small uniform mechanical strain for an anisotropic piezoelectric material, the piezoelectric equations are given by [52-55].

$$\vec{P}_i = (e)_{ijk}\left(\vec{S}\right)_{jk} \quad \textbf{(3.12)}$$

$$\vec{T} = C_E\vec{S} - e^T\vec{E} \quad \textbf{(3.13)}$$

$$\vec{D} = e\vec{S} - k\vec{E} \quad (3.14)$$

where $\vec{S}$ is the mechanical strain; $(e)_{ijk}$ is the piezoelectric tensor of rank 3; $\vec{T}$ is the stress tensor and C_E is the elasticity tensor and k is the dielectric tensor.

The displacement current for the polarizing media is given by

$$\vec{J}_{Di} = \frac{\partial \vec{P}_i}{\partial t} = (e)_{ijk}\left(\frac{\partial \vec{S}}{\partial t}\right)_{jk} \quad (3.15)$$

Equation (3.15) implies that the output current density of the CPENG is directly proportional to the rate of change of the applied strain.

In the absence of any external applied electric field, the displacement field is the polarization vector. If the direction of polarization is along z-axis, then we have

$$D_z = P_z = \sigma_P(z) \quad (3.16)$$

where $\sigma_P(z)$ is piezoelectric polarization surface charges density.

Then the displacement current is

$$J_{DZ} = \frac{\partial P_z}{\partial t} = \frac{\partial \sigma_p(z)}{\partial t} \quad (3.17)$$

where $\sigma_P(z)$ is piezoelectric polarization surface charges density.

Equation (3.17) shows that the output current of a CPENG is directly proportional to the rate of change of surface polarization charges. The output voltage of the open circuit CPENG is given by

$$V_{OC} = \frac{Z\sigma_P(Z)}{\epsilon} \quad (3.18)$$

where Z (thickness of piezoelectric thin film) is a function of time.

In the presence of external load resistance R, the output of the CPENG is given by

$$RA\frac{d\sigma}{dt} = z\left[\sigma_p(z) - \sigma(z)\right]/\epsilon \quad (3.19)$$

where A is the area of the electrode, $\sigma_p(z)$ is the piezoelectric polarization surface charge density on the film surface and $\sigma(z)$ is the free electrons surface charge density on the electrode surface.

The equations (3.17, 3.18, and 3.19) reveal the direct proportional relationships between electric polarization and strain, rate of change of piezoelectric polarization and surface charge density, output voltage and rate of change of thickness, and output voltage and device area, respectively. Figure 3.7:(a) illustrates the device's response to applied force and subsequent force release, showcasing the conversation mechanism of energy harvesting by the CPENG. This mechanism leverages the synergistic effect of molecular dipoles in PVDF, enhanced by the addition of CuS nanoroses, which amplifies the electroactive β phase and piezo response.

The strong electrostatic interaction between CuS nanoroses and PVDF dipoles induces self-polarization in the composite film under applied force, leading to a secondary potential in CuS nanoroses. This secondary potential orients the PVDF dipoles in the direction of the applied force, resulting in self-polarization due to the interplay between mechanical stress and interfacial surface charge, as described by equation (3.12). The resulting piezo potential, given by equation (3.14), generates a current through an external load resistor (R), as expressed by equation (3.15). When compressional stress is applied, a positive piezo potential appears at the top electrode, and upon relaxation, a negative piezo potential arises at the bottom electrode, demonstrating the CPENG's dynamic response to mechanical stress.

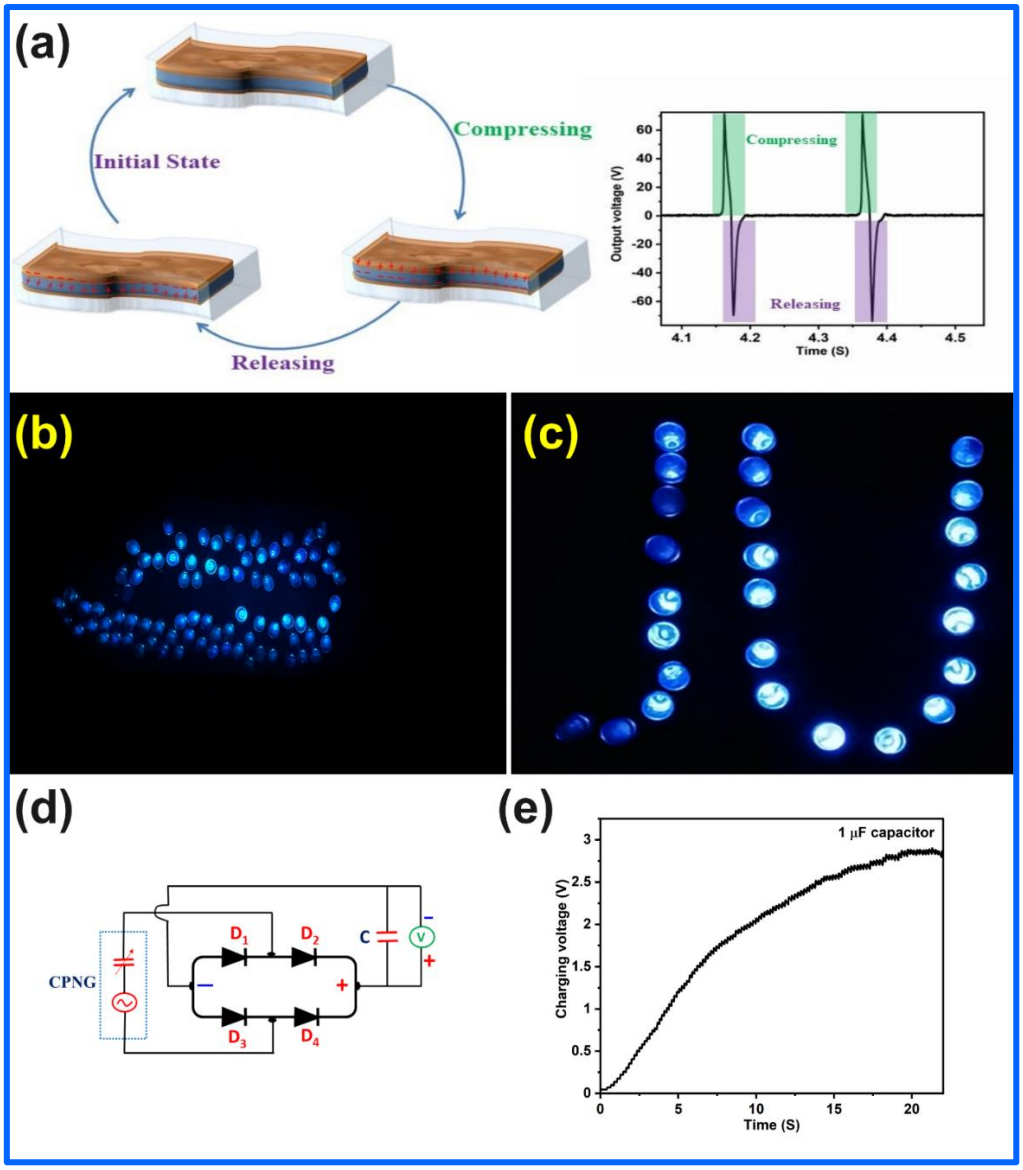

Figure 3.7: (a) Mechanism of CPENG and the output voltage generated by the CPENG, (b) Digital image of 85 numbers of LEDs in glowing condition (c) JU pattern with glowing LEDs (d) Circuit diagram for the charging capacitor and LEDs light up and (e) Charging performance of the 1µF capacitor.

3.7. Smart Insole-Based Gait Analysis

To improve the practical utility of the smart insole for sensing applications, a sophisticated real-time wireless gait assessment system was developed. This system features a pair of advanced insoles equipped with piezoelectric detection units, a comprehensive multichannel data collection framework, and specialized gait monitoring and analysis software for Android platforms. Each intelligent insole is fitted with multiple detection units that simultaneously capture and generate log signals from various sensors. These signals are transmitted via a direct wired interface to an Arduino system.

As shown in Figure 3.8:(a), when the forefoot makes contact with the ground, an initial positive peak is detected from the anterior piezoelectric nanogenerator sensor located at the insole's front. This is followed by a negative peak when the forefoot lifts off. The time interval (t) between these peaks is a key metric for detailed gait assessment. Additionally, placing a piezoelectric nanogenerator sensor at the posterior region of the insole allows for the analysis of the temporal differences between the anterior and posterior sensors, providing valuable insights into gait patterns.

Data from the strategically placed CPENGs, which display distinct positive and negative peaks, helps differentiate various locomotion behaviors such as stepping, walking, and running, as illustrated in Figures 3.8:(b) and 3.8:(c). For instance, during stepping {Figure 3.8:(b)}, the sequential lift of the right heel and forefoot corresponds with the positive peaks in zone (I). The right foot then descends, as seen in zone (II), with the forefoot contacting the ground before the heel. This pattern is similarly mirrored by the left foot in zones (III) and (IV), representing the complete signal generation mechanism for stepping.

Walking patterns are also clearly identified. As depicted in Figure 7(c), when the right heel contacts the ground, the left heel and forefoot lift successively, while the right forefoot settles. Running patterns, as shown in figure 3.8:(d), resemble walking but exhibit higher voltage peaks and shorter contact times due to increased force on the CPENGs. The greater rate of change in stress during running results in higher output voltage compared to walking, allowing for clear differentiation between the two activities based on the CPENGs output patterns.

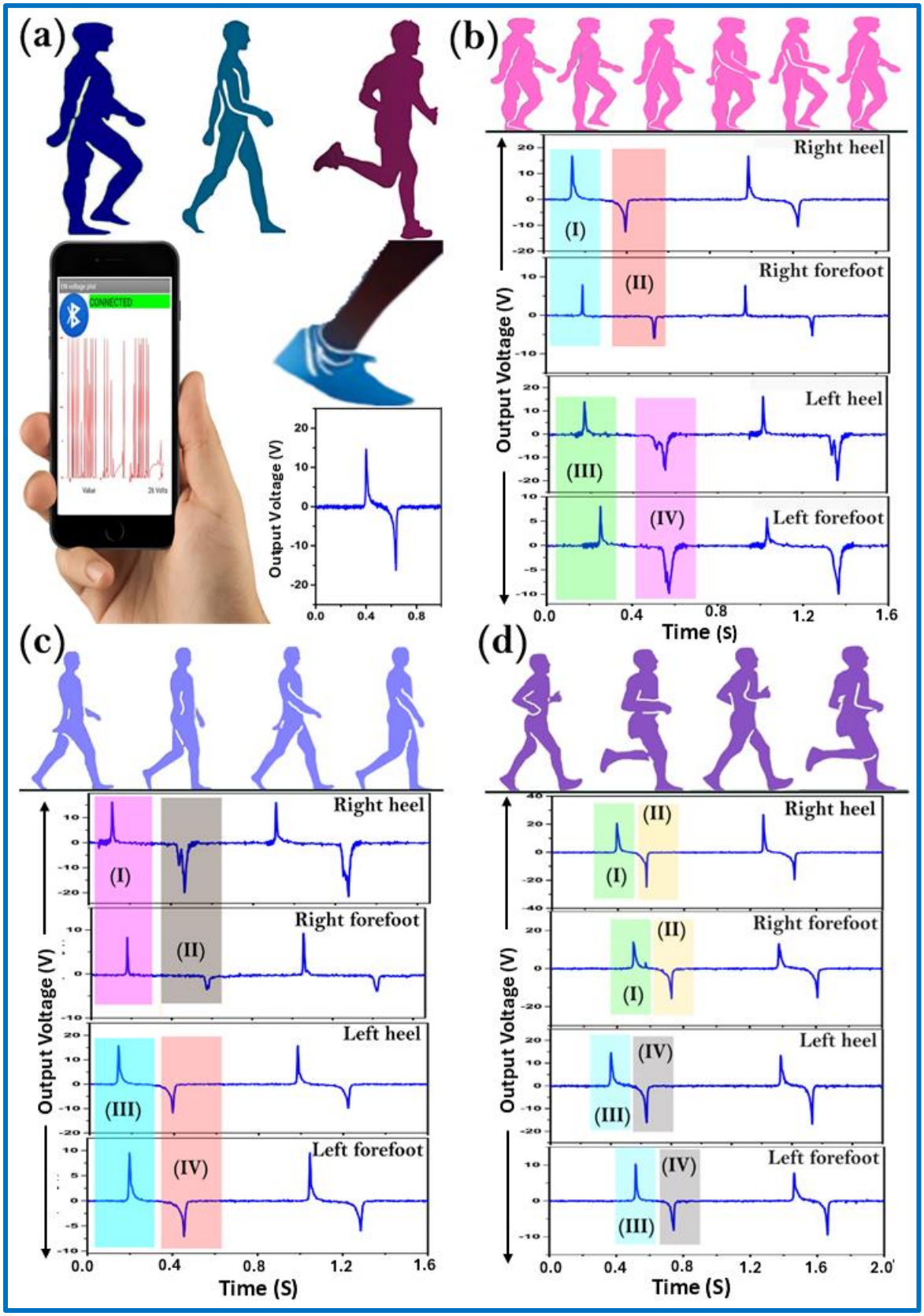

Figure 3.8: Gait detection by CPENGs (a) illustration of wireless gait detection, signal pattern for stepping and lift. Both leg's heel and forefoot gait signal for (b) stepping, (c) walking and (d) running.

3.8. Conclusions

This groundbreaking study revolutionizes the field by introducing a hydrophobic waterproofed CuS nanoparticle-embedded PVDF composite piezoelectric nanogenerator (CPENG) with a rose-like nanostructure, boasting unprecedented sensitivity. The synergistic interaction between CuS nanoroses and PVDF dipoles amplifies the electroactive β-phase formation, resulting in extraordinary piezoelectric properties and interfacial polarization. This innovative design yields a remarkable output performance, with an open-circuit voltage of 130 V and short-circuit current of 1.25 μA, translating to a power density of 2640.6 μWcm-3. This CPENG can power an impressive 26 blue LEDs in series or 85 LEDs in parallel, with output performance correlating with imparting frequency. Beyond energy harvesting, this versatile device generates unique waveforms, making it an invaluable tool for gait analysis, movement monitoring, and surveillance applications. Its hydrophobic design enables detection of subtle movements, such as finger, wrist, and neck movements, making it ideal for monitoring vulnerable populations and athletes. This CPENG is a game-changer in the field, offering immense potential for enhancing sports performance, gait analysis, and real-time movement monitoring.

*****

References:

[1] Zhu, M., Shi, Q., He, T., Yi, Z., Ma, Y., Yang, B., Chen, T. and Lee, C., 2019. Self-powered and self-functional cotton sock using piezoelectric and triboelectric hybrid mechanism for healthcare and sports monitoring. *ACS nano*, 13(2), pp.1940-1952.

[2] Zhang, W., Zhang, Y., Yang, G., Hao, X., Lv, X., Wu, F., Liu, J. and Zhang, Y., 2021. Wearable and self-powered sensors made by triboelectric nanogenerators assembled from antibacterial bromobutyl rubber. Nano Energy, 82, p.105769.

[3] Chen, J., Yu, Q., Cui, X., Dong, M., Zhang, J., Wang, C., Fan, J., Zhu, Y. and Guo, Z., 2019. An overview of stretchable strain sensors from conductive polymer nanocomposites. *Journal of materials Chemistry C*, *7*(38), pp.11710-11730.

[4] Lin, Z., Wu, Z., Zhang, B., Wang, Y.C., Guo, H., Liu, G., Chen, C., Chen, Y., Yang, J. and Wang, Z.L., 2019. A triboelectric nanogenerator-based smart insole for multifunctional gait monitoring. *Advanced Materials Technologies*, 4(2), p.1800360.

[5] Gao, W., Ota, H., Kiriya, D., Takei, K. and Javey, A., 2019. Flexible electronics toward wearable sensing. *Accounts of chemical research*, 52(3), pp.523-533.

[6] Kim, J., Campbell, A.S., de Ávila, B.E.F. and Wang, J., 2019. Wearable biosensors for healthcare monitoring. *Nature biotechnology*, 37(4), pp.389-406.

[7] Ray, T.R., Choi, J., Bandodkar, A.J., Krishnan, S., Gutruf, P., Tian, L., Ghaffari, R. and Rogers, J.A., 2019. Bio-integrated wearable systems: a comprehensive review. *Chemical reviews*, 119(8), pp.5461-5533.

[8] Zhao, T., Han, Y., Qin, L., Guan, H., Xing, L., Li, X., Xue, X., Li, G. and Zhan, Y., 2021. Bidirectional modulation of neural plasticity by self-powered neural stimulation. *Nano Energy*, 85, p.106006.
[9] Lou, Z., Wang, L., Jiang, K., Wei, Z. and Shen, G., 2020. Reviews of wearable healthcare systems: Materials, devices and system integration. *Materials Science and Engineering: R: Reports*, 140, p.100523.
[10] Su, C., Huang, X., Zhang, L., Zhang, Y., Yu, Z., Chen, C., Ye, Y. and Guo, S., 2023. Robust superhydrophobic wearable piezoelectric nanogenerators for self-powered body motion sensors. *Nano Energy*, 107, p.108095.
[11] Beigh, N.T., Beigh, F.T. and Mallick, D., 2023. Machine learning assisted hybrid transduction nanocomposite based flexible pressure sensor matrix for human gait analysis. *Nano Energy*, 116, p.108824.
[12] Shi, K., Chai, B., Zou, H., Shen, P., Sun, B., Jiang, P., Shi, Z. and Huang, X., 2021. Interface induced performance enhancement in flexible $BaTiO_3$/PVDF-TrFE based piezoelectric nanogenerators. *Nano Energy*, 80, p.105515.
[13] Deng, W., Zhou, Y., Libanori, A., Chen, G., Yang, W. and Chen, J., 2022. Piezoelectric nanogenerators for personalized healthcare. *Chemical Society Reviews*, 51(9), pp.3380-3435.
[14] Chen, G., Xiao, X., Zhao, X., Tat, T., Bick, M. and Chen, J., 2021. Electronic textiles for wearable point-of-care systems. *Chemical Reviews*, 122(3), pp.3259-3291.
[15] Mahapatra, S.D., Mohapatra, P.C., Aria, A.I., Christie, G., Mishra, Y.K., Hofmann, S. and Thakur, V.K., 2021. Piezoelectric materials for energy harvesting and sensing applications: roadmap for future smart materials. *Advanced Science*, 8(17), p.2100864.
[16] Feng, Z., Zhao, Z., Liu, Y., Liu, Y., Cao, X., Yu, D.G. and Wang, K., 2023. Piezoelectric effect polyvinylidene fluoride (PVDF): from energy harvester to smart skin and electronic textiles. *Advanced Materials Technologies*, 8(14), p.2300021.
[17] Rathinasamy, S.K., Maheswar, R. and Lorincz, J., 2023. Silk Fibroin-Based Piezoelectric Sensor with Carbon Nanofibers for Wearable Health Monitoring Applications. *Sensors*, 23(3), p.1373.
[18] Hu, Y., Xu, C., Zhang, Y., Lin, L., Snyder, R.L. and Wang, Z.L., 2011. A nanogenerator for energy harvesting from a rotating tire and its application as a self-powered pressure/speed sensor. *Advanced Materials*, 23(35), p.4068.
[19] Wu, W., Bai, S., Yuan, M., Qin, Y., Wang, Z.L. and Jing, T., 2012. Lead zirconate titanate nanowire textile nanogenerator for wearable energy-harvesting and self-powered devices. *ACS nano*, 6(7), pp.6231-6235.
[20] Das, K.K., Basu, B., Maiti, P. and Dubey, A.K., 2023. Piezoelectric nanogenerators for self-powered wearable and implantable bioelectronic devices. Acta Biomaterialia.
[21] Deng, W., Zhou, Y., Libanori, A., Chen, G., Yang, W. and Chen, J., 2022. Piezoelectric nanogenerators for personalized healthcare. *Chemical Society Reviews*, 51(9), pp.3380-3435.
[22] Riskowski, J.L., 2010. Gait and neuromuscular adaptations after using a feedback-based gait monitoring knee brace. *Gait & posture*, 32(2), pp.242-247.
[23] Wang, L., Hu, W. and Tan, T., 2003. Recent developments in human motion analysis. *Pattern recognition*, 36(3), pp.585-601.

[24] Jia, C., Zhu, Y., Sun, F., Zhao, T., Xing, R., Mao, Y. and Zhao, C., 2021. A flexible and stretchable self-powered nanogenerator in basketball passing technology monitoring. *Electronics*, 10(21), p.2584.
[25] Zhou, X., Parida, K., Halevi, O., Liu, Y., Xiong, J., Magdassi, S. and Lee, P.S., 2020. All 3D-printed stretchable piezoelectric nanogenerator with non-protruding kirigami structure. *Nano Energy*, 72, p.104676.
[26] Huang, C., Tan, T., Wang, Z., Zhang, S., Yang, F., Lin, Z. and Yan, Z., 2022. Origami dynamics based soft piezoelectric energy harvester for machine learning assisted self-powered gait biometric identification. *Energy Conversion and Management*, 263, p.115720.
[27] Beigh, N.T., Beigh, F.T. and Mallick, D., 2023. Machine learning assisted hybrid transduction nanocomposite based flexible pressure sensor matrix for human gait analysis. *Nano Energy*, 116, p.108824.
[28] Stone, E. and Skubic, M., 2011. Evaluation of an inexpensive depth camera for in-home gait assessment. *Journal of Ambient Intelligence and Smart Environments*, 3(4), pp.349-361.
[29] Greene, B.R., McGrath, D., O'Neill, R., O'Donovan, K.J., Burns, A. and Caulfield, B., 2010. An adaptive gyroscope-based algorithm for temporal gait analysis. *Medical & biological engineering & computing*, 48, pp.1251-1260.
[30] Sarkar, D., Das, N., Saikh, M.M., Biswas, P., Roy, S., Paul, S., Hoque, N.A., Basu, R. and Das, S., 2023. High β-crystallinity comprising nitrogenous carbon dot/PVDF nanocomposite decorated self-powered and flexible piezoelectric nanogenerator for harvesting human movement mediated energy and sensing weights. *Ceramics International*, 49(3), pp.5466-5478.
[31] Hoque, N.A., Thakur, P., Biswas, P., Saikh, M.M., Roy, S., Bagchi, B., Das, S. and Ray, P.P., 2018. Biowaste crab shell-extracted chitin nanofiber-based superior piezoelectric nanogenerator. *Journal of Materials Chemistry A*, 6(28), pp.13848-13858.
[32] Hoque, N.A., Thakur, P., Roy, S., Kool, A., Bagchi, B., Biswas, P., Saikh, M.M., Khatun, F., Das, S. and Ray, P.P., 2017. Er^{3+}/Fe^{3+} stimulated electroactive, visible light emitting, and high dielectric flexible PVDF film based piezoelectric nanogenerators: a simple and superior self-powered energy harvester with remarkable power density. *ACS applied materials & interfaces*, 9(27), pp.23048-23059.
[33] Lin, L., Choi, Y., Chen, T., Kim, H., Lee, K.S., Kang, J., Lyu, L., Gao, J. and Piao, Y., 2021. Superhydrophobic and wearable TPU based nanofiber strain sensor with outstanding sensitivity for high-quality body motion monitoring. *Chemical Engineering Journal*, 419, p.129513.
[34] Das, N., Sarkar, D., Saikh, M.M., Biswas, P., Das, S., Hoque, N.A. and Ray, P.P., 2022. Piezoelectric activity assessment of size-dependent naturally acquired mud volcano clay nanoparticles assisted highly pressure sensitive nanogenerator for green mechanical energy harvesting and body motion sensing. *Nano Energy*, 102, p.107628.
[35] Yang, Y., Pan, H., Xie, G., Jiang, Y., Chen, C., Su, Y., Wang, Y. and Tai, H., 2020. Flexible piezoelectric pressure sensor based on polydopamine-modified $BaTiO_3$/PVDF composite film for human motion monitoring. Sensors and Actuators A: Physical, 301, p.111789.

[36] Bagchi, B., Hoque, N.A., Janowicz, N., Das, S. and Tiwari, M.K., 2020. Re-usable self-poled piezoelectric/piezocatalytic films with exceptional energy harvesting and water remediation capability. *Nano Energy*, 78, p.105339.
[37] Saikh, M.M., Hoque, N.A., Biswas, P., Rahman, W., Das, N., Das, S. and Thakur, P., 2021. Self-Polarized ZrO_2/Poly (vinylidene fluoride-co-hexafluoropropylene) nanocomposite-based piezoelectric nanogenerator and single-electrode triboelectric nanogenerator for sustainable energy harvesting from human movements. *physica status solidi (a)*, 218(9), p.2000695.
[38] Jin, C., Hao, N., Xu, Z., Trase, I., Nie, Y., Dong, L., Closson, A., Chen, Z. and Zhang, J.X., 2020. Flexible piezoelectric nanogenerators using metal-doped ZnO-PVDF films. *Sensors and Actuators A: Physical*, 305, p.111912.
[39] Kumar, R.S., Sarathi, T., Venkataraman, K.K. and Bhattacharyya, A., 2019. Enhanced piezoelectric properties of polyvinylidene fluoride nanofibers using carbon nanofiber and electrical poling. *Materials Letters*, 255, p.126515.
[40] Mishra, S., Sahoo, R., Unnikrishnan, L., Ramadoss, A., Mohanty, S. and Nayak, S.K., 2020. Investigation of the electroactive phase content and dielectric behaviour of mechanically stretched PVDF-GO and PVDF-rGO composites. Materials Research Bulletin, 124, p.110732.
[41] Mondal, A., Faraz, M. and Khare, N., 2022. Magnetically tunable enhanced performance of CoFe2O4–PVDF nanocomposite film-based piezoelectric nanogenerator. *Applied Physics Letters*, 121(10).
[42] Sarkar, D., Das, N., Saikh, M.M., Biswas, P., Das, S., Das, S., Hoque, N.A. and Basu, R., 2021. Development of a sustainable and biodegradable sonchus asper cotton pappus based piezoelectric nanogenerator for instrument vibration and human body motion sensing with mechanical energy harvesting applications. *ACS omega*, 6(43), pp.28710-28717.
[43] Das, N., Sarkar, D., Yadav, N., Ali, A., Das, S., Ray, P.P. and Hoque, N.A., 2023. Development of a lead-free, high-frequency ultrasound transducer with broad bandwidth and enhanced pulse-echo response, employing β-$Ni(OH)_2$/PVDF-TrFE piezoelectric composite. Chemical Engineering Journal, 475, p.146322.
[44] Biswas, P., Hoque, N.A., Thakur, P., Saikh, M.M., Roy, S., Khatun, F., Bagchi, B. and Das, S., 2019. Portable self-powered piezoelectric nanogenerator and self-charging photo-power pack using in situ formed multifunctional calcium phosphate nanorod-doped PVDF films. *Langmuir*, 35(52), pp.17016-17026.
[45] Mondal, B., Mishra, H.K., Sengupta, D., Kumar, A., Babu, A., Saini, D., Gupta, V. and Mandal, D., 2022. Lead-free perovskite $Cs_3Bi_2I_9$-derived electroactive PVDF composite-based piezoelectric nanogenerators for physiological signal monitoring and piezo-phototronic-aided strain modulated photodetectors. *Langmuir*, 38(40), pp.12157-12172.
[46] Mishra, H.K., Sengupta, D., Babu, A., Pirzada, B.M., Sarkar, R., Naidu, B.S., Kundu, T.K. and Mandal, D., 2022. PVDF/Ag_2CO_3 nanocomposites for efficient dye degradation and flexible piezoelectric mechanical energy harvester. *Sustainable Energy & Fuels*, 6(6), pp.1625-1640.
[47] Maity, K., Garain, S., Henkel, K., Schmeißer, D. and Mandal, D., 2020. Self-powered human-health monitoring through aligned PVDF nanofibers interfaced skin-interactive piezoelectric sensor. *ACS Applied Polymer Materials*, 2(2), pp.862-878.

[48] Gebrekrstos, A., Muzata, T.S. and Ray, S.S., 2022. Nanoparticle-enhanced β-phase formation in electroactive PVDF composites: a review of systems for applications in energy harvesting, EMI shielding, and membrane technology. *ACS Applied Nano Materials*, 5(6), pp.7632-7651.
[49] Abdolmaleki, H. and Agarwala, S., 2020. PVDF-$BaTiO_3$ nanocomposite inkjet inks with enhanced β-phase crystallinity for printed electronics. *Polymers*, 12(10), p.2430.
[50] Wu, L., Yuan, W., Hu, N., Wang, Z., Chen, C., Qiu, J., Ying, J. and Li, Y., 2014. Improved piezoelectricity of PVDF-HFP/carbon black composite films. *Journal of Physics D: Applied Physics*, 47(13), p.135302.
[51] Meng, N., Ren, X., Santagiuliana, G., Ventura, L., Zhang, H., Wu, J., Yan, H., Reece, M.J. and Bilotti, E., 2019. Ultrahigh β-phase content poly (vinylidene fluoride) with relaxor-like ferroelectricity for high energy density capacitors. *Nature communications*, 10(1), p.4535.
[52] Wang, X., Yang, B., Liu, J., Zhu, Y., Yang, C. and He, Q., 2016. A flexible triboelectric-piezoelectric hybrid nanogenerator based on P(VDF-TrFE) nanofibers and PDMS/MWCNT for wearable devices. *Scientific reports*, 6(1), p.36409.
[53] Ikeda, T., 1996. Fundamentals of piezoelectricity. *Oxford university press*.
[54] Maugin, G.A., 2013. Continuum mechanics of electromagnetic solids. Elsevier.
[55] Wang, Z.L., 2017. On Maxwell's displacement current for energy and sensors: the origin of nanogenerators. *Materials today*, 20(2), pp.74-82.

Chapter 4

Advancements in Energy Harvesting Technologies: Comprehensive Analysis of Er-ZrO_2-Doped PVDF Nanocomposites for Piezoelectric Nanogenerators

4.1. Introduction:

The increasing focus on sustainable and efficient energy sources is growing significant interest in the development of nanogenerators that exhibit the ability to harvest mechanical energy from ambient environment sources [1-8]. These resources include seawater waves, solar energy, geothermal heat, rainfall and various forms of mechanical energy from human activities such as walking, talking, breathing, and other movements [9-16].

Piezoelectric nanogenerators (PENGs) and triboelectric nanogenerators (TENGs) are the emerging devices capable of harvesting energy from a wider range of mechanical vibrations effectively [6, 17-19]. These devices have promising potential to supply power to low powered electronics such as sensors and wearable gadgets. [6, 17-19].

In this context, PENGs offer a promising alternative for creating highly sensitive, durable, and low-power-consuming self-powered systems with high energy conversion efficiency [20-21]. These nanogenerators use piezoelectric materials or ceramics—such as ZnO [22, 23], $BaTiO_3$ [24-26], PMN-PT [22, 27-28], PZT [29-32], and (Na, K)NbO_3 [33]—to convert mechanical energy into electrical energy. This approach represents a significant advancement in green energy harvesting technology.

In recent times, erbium-zirconium oxide (Er-ZrO_2), a widely recognized piezoelectric ceramic is drawing significant attention due to its exceptional dielectric and piezoelectric characteristics. In this study a new emerging material has been introduced by incorporating flexible polymers like PVDF into Er-ZrO_2 which gives rise to a composite material that has effective applications in the field of piezoelectric and triboelectric nanogenerators.

Poly(vinylidene fluoride) (PVDF) and its related copolymers are potentially the prime examples of high performing polymers considered for its exceptional piezoelectric, pyroelectric, ferroelectric and dielectric properties, this makes them an exciting frontier for developing cutting edge PENGs[34-40]. The above choice can be attributed to the advantageous piezoelectric characteristics, low weight, plasticity, and compatibility with the environment. This polymer appears in five distinctive crystalline polymorphs, namely α, β, γ, δ, and ε [38, 41-42]. The most prevailing and environmentally stable form is the nonpolar α-phase, which is distinguished by a monoclinic unit cell exhibiting a TGTG′ (T-trans, G-gauche+, G′-gauche) dihedral conformation. Conversely, the polar β-phase and γ-phase exhibit orthorhombic unit cells characterized by all-trans (TTTT) and TTTGTTG′ conformations, respectively. Among the several phases, the β-phase exhibits the highest polarization and stands out due to its exceptional piezoelectric characteristics [43-44]. Furthermore, it exhibits

a significantly elevated melting point and enhanced stability in comparison to the γ-phase. Hence, the electroactive β- and γ-phases play a crucial role in the progress of PVDF-based nanogenerators (PENGs) [45-46].

The excellent flexibility of PVDF, combined with the exceptional piezoelectric response exhibited by Er-ZrO_2 offers this composite a highly suitable option for energy harvesting applications, specifically in the fields of wearable and portable electronics, where mechanical deformations arise with frequency.

Due to the presence of erbium ions, Er-ZrO_2 inherently exhibits excellent piezoelectric properties making it suitable for its effective energy conversion in PENGs and the high dielectric constant of Er-ZrO_2 enhances the piezoelectric responsiveness and efficiency. Also, improves the piezoelectric properties when combined with PVDF as composite.

The main objective of this work is to gain insight into the fundamental mechanisms that lead to its remarkable energy harvesting capabilities through structural, electrical and thermal characterizations of this composite material,. PVDF and Er-ZrO_2 nanocomposite offer significant contributions to the development and enhancement of forthcoming energy harvesting systems.

In light of the increasing demand for sustainable energy sources future energy needs will be met in large by the development of nanogenerators with efficiency, adaptability, and durability. This study signifies an advancement in this specific trajectory, presenting an imminent methodology for utilizing mechanical energy by Er-ZrO_2 nanocomposite piezoelectric nanogenerators (EPENG).

The Er-ZrO_2 PVDF-HFP Nanocomposite based EPEPNG exhibits an impressive output performance by generating an output voltage of about 133 V, a short circuit current (I_{sc}) of around 2.77 μA, an instantaneous power density of approximately 1.7 μW/cm². This EPENG can easily power 80 green LEDs under repeated compressive stress of approximately 27N and a frequency of about 4.0 Hz.

4.2. Experimental

4.2.1. Materials:

- Erbium chloride ($ErCl_3$,$6H_2O$).
- Zirconium oxychlorideoctahydrate($ZrOCl_2$,$8H_2O$).
- Hydrazine hydrate (>99% pure) (H_6N_2O) (Merck, India).

- Poly(vinylidene fluoride-co-hexafluoropropylene) [PVDF-HFP)] pellets (Aldrich, Germany. Mw: 455 000 GPC, Mn: 110 000).
- Dimethyl sulfoxide (DMSO) (Merck, India).
- Polydimethyl siloxane (PDMS, $[Si(CH_3)_2O]_n$) (Sylgard 184, Dow Curring, ratio of 1:10).

4.2.2. Preparation of Er-ZrO2nanoparticle:

Er-ZrO_2 nanoparticles were synthesis via hydrothermal route. At first 4.834 g of solid $ZrOCl_2$, $8H_2O$ salt and 0.5725g of $ErCl_3$, $6H_2O$ were dissolved in 150 ml of deionized water. After two hours of vigorous magnetic stirring at room temperature uniform aqueous solutions are obtained. 6ml hydrazine hydrate (N_2H_2) was added drop by drop in this aqueous solution. After adding hydrazine hydrate (N_2H_2) it was kept in the same magnetic stirrer with same speed and temperature for another four hours. Again 2 ml hydrazine hydrate (N_2H_2) was added for complete reaction. Then the solution were put into the autoclave and kept in 160^oC temperature for 24 hours. Er-ZrO2NPs precipitate were collected from auto clave and allowed to cool in room temperature followed by centrifugation and repeated washing with deionized water and alcohol. After washing it was dried at 80^oC in a dust free electric oven.

4. 2.3. Synthesis of PVDF-HFP Er-ZrO_2 nanocomposite films:

Initially 0.25 g of PVDF-HFP were added in 5ml DMSO and stirred at 60^o C to get a uniform solution. Then the desire amount of Er-ZrO_2 (1–15 mass %) were mixed with this uniform solution and stirred at 60 ^{o} C for 12 hours to obtained a homogeneous solution. Next the particular amount of this homogeneous solution was taken on clean glass petri dishes. Then these glass petri dishes were kept in a dust free electric oven at temperature 80^oC for evaporation. After near about 12 hours all the DMF were evaporated and Er-ZrO_2 nanoparticle composite thin film were obtained. Virgin PVDF-HFP thin films were also synthesized by following the similar route. All these nanocomposite films were kept in vacuum desiccator for further work. Names of the synthesized samples were assigned in the Table 1.

Table 4.1: Names of the synthesized samples and the amounts of Er-ZrO2NPs loading in PVDF-HFP matrix.

Sample Designation	Amount of Er-ZrO_2NPs (g)	Amount of PVDF-HFP (g)	Percentage of Er-ZrO_2NPs (mass %)
EZ0 (Pure PVDF-HFP)	0.0000	0.2500	00
EZ1	0.0005	0.2500	01
EZ5	0.0125	0.2500	05
EZ10	0.0250	0.2500	10
EZ15	0.0375	0.2500	15

4.2.4. Fabrication of EPNG:

For fabrication of EPNGs the sample EZ5 were taken. The dimensions of length, breadth and height of the taken sample EZ5 are 2.4 cm, 2.5 cm and 60 µm respectively. Then, aluminum electrodes of appropriate dimensions were attached to both surfaces of the EZ5 film.After that two wires are connected with these electrodes. Then the entire system were covered by Polydimethyl siloxane (PDMS, $[Si(CH_3)_2O]_n$) (Sylgard 184, Dow Curring, ratio of 1:10). Finally, the developed ENPG measures 5 cm in length, 3 cm in width, and 0.3 cm in height.

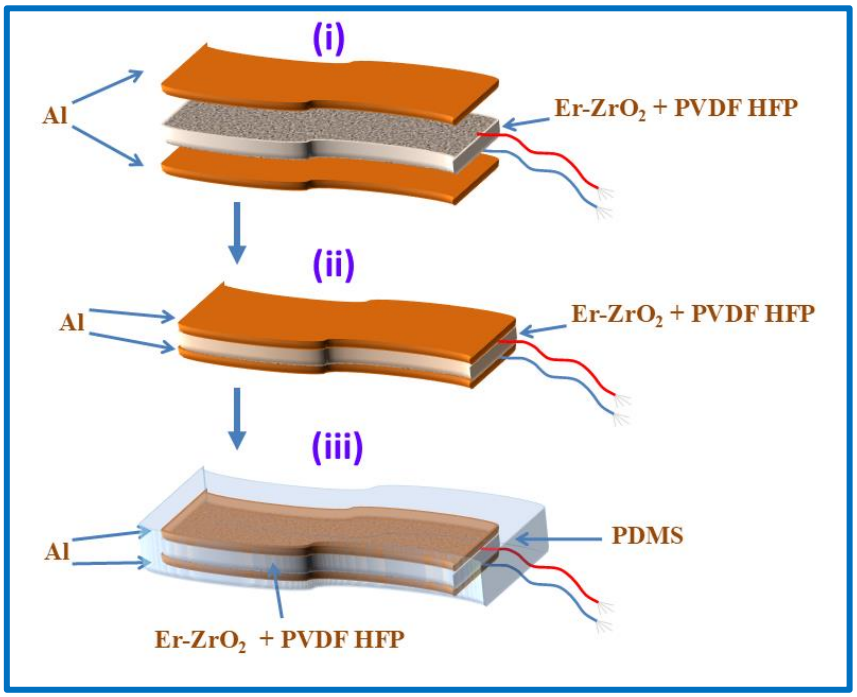

Figure 4.1: Fabrication of EPENG.

4.3. Characterizations

The surface microscopic structure of the Er-ZrO_2 NPs, pure PVDF-HFP thin film and Er- ZrO_2 NPs loaded PVDF-HFP thin films were observed in field emission scanning electron microscope (FESEM) (INSPECT F50, Netherland and JSM6700F, JEOL Ltd., Japan). The crystal structure nature of the Er-ZrO_2 NPs, pure PVDF-HFP thin film and Er-ZrO_2 NPs loaded PVDF-HFP thin films were examined by X-ray diffractometer (Model-D8, Bruker AXS Inc., Madison, WI). The crystallographic information and the amount of β-phase were investigated by Fourier transform infrared spectroscopy (FTIR-8400S, Shimadzu). The thermal behaviour and crystallinity were recorded by differential scanning calorimetry (DSC-60, Shimadzu, Singapore) and thermal gravimetric analysis (TGA) (TGA/SDTA851e, Mettler Toledo AG). The measurements of capacitance (*C*) and tangent loss (*tan δ*) of the samples were performed on a digital LCR meter (Agilent, E4980A).

4.4. Results and discussion:

4.1. Field Emission Electron Microscopy (FESEM) Morphology:

FESEM micrograph of Er-ZrO_2 NPs, pure PVDF-HFP film (EZ0) and EZ1, EZ5, EZ10 and EZ15 films are displayed in figure 4.2. The microstructure nature of Er-ZrO_2 NPs is shown in figure 4.2: (a). This figure confirms that the Er-ZrO_2 NPs formation is uniform with diameter ~ 50-60 nm. Figure 4.2: (b) is the FESEM of Pure PVDF-HFP which has a larger spherulites with diameter of about ~ 40 μm. It is showing that the Pure PVDF-HFP has nonpolar α phase [47]. The uniform distributions of Er-ZrO_2 NPs in PVDF-HFP matrix are shown in figure 4.2:(c-f). The size of the spherulites in Er-ZrO_2 NPs loaded PVDF-HFP matrix are decreases. The diameters of all the smaller spherulites are about ~ 50-60 nm due to β phage induced [48]. This confirms the formation electroactive β phase PVDF-HFP matrix due to Er-ZrO_2 NPs. The information and measurement of the electroactive β phase were investigated with XRD pattern, FTIR spectra; and DSC results.

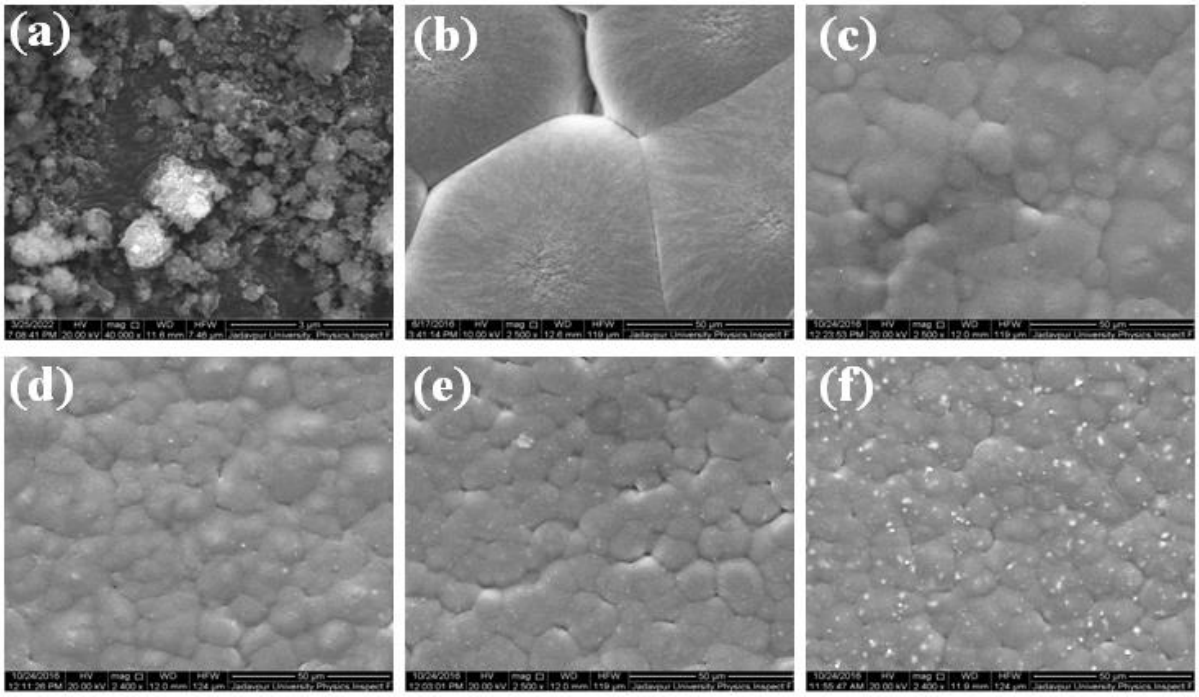

Figure 4.2: FE-SEM images of (a) Pure Er-ZrO2NPs; (b) Pure PVDF-HFP thin film; (c) EZ1; (d) EZ5;(e) EZ10 and (f) EZ15.

4.4.2. X-ray diffraction (XRD) analysis:

Figure 4.3 display the X-ray diffraction (XRD) crystallographic pattern of Er-ZrO_2NPs, pure PVDF-HFP and Er-ZrO_2NPs doped PVDF-HFP nanocomposite film. In previously reported literature, it has been shown that PVDF-HFP, like PVDF, exhibits at least five crystalline phases such as α, β, γ, δ and ε. The standard X-ray diffraction peaks at 2θ =17.7º, 18.4º, 19.9º, and 26.4º in virgin PVDF-HFP thin film correspond to the (100), (020), (110), and (021) reflections plane for nonpolar α-crystalline phase [49]. The X-ray diffraction peak at 2θ =20.4º represents the superposition of the crystalline planes (110) and (200) for electroactive β-phase. Another diffraction peak at 2θ =38.9^O corresponds to the crystalline plane (211) for polar γ phase. The intensity of the diffraction peaks at 2θ = 20.4° (110) and (200) and 38.9° (211) is very low, confirming that pure PVDF-HFP primarily forms the α-phase [50]. The addition of Er-ZrO_2 nanoparticles to the PVDF-HFP matrix demonstrates that the characteristic peaks for the α- and γ-phases vanishes. . Then only the diffraction peaks at 2θ =20.4º corresponds to polar β-phase strongly appeared. This diffraction pattern indicates that the addition of ZrO_2 nanoparticles to the PVDF-HFP matrix transforms the crystalline phase from the nonpolar α-phase to the polar β-phase.. The intensity of the characteristics peak for β-phase is maximum for the sample EZ5 shown in figure 2. The formation of β-phase in PVD-HFP matrix was quantitatively measured by the ratio of the intensity $I_{20.5}$ at 2θ =20.4º to the intensity$I_{18.2}$ at 2θ

=18.2^{o} (020). The value of this ratio is 0.499 for the pure PVDF-HFP calculated from the figure 4.3. Maximum value of this ratio is 5.4 found from figure 4.3 for the sample EZ5.

.

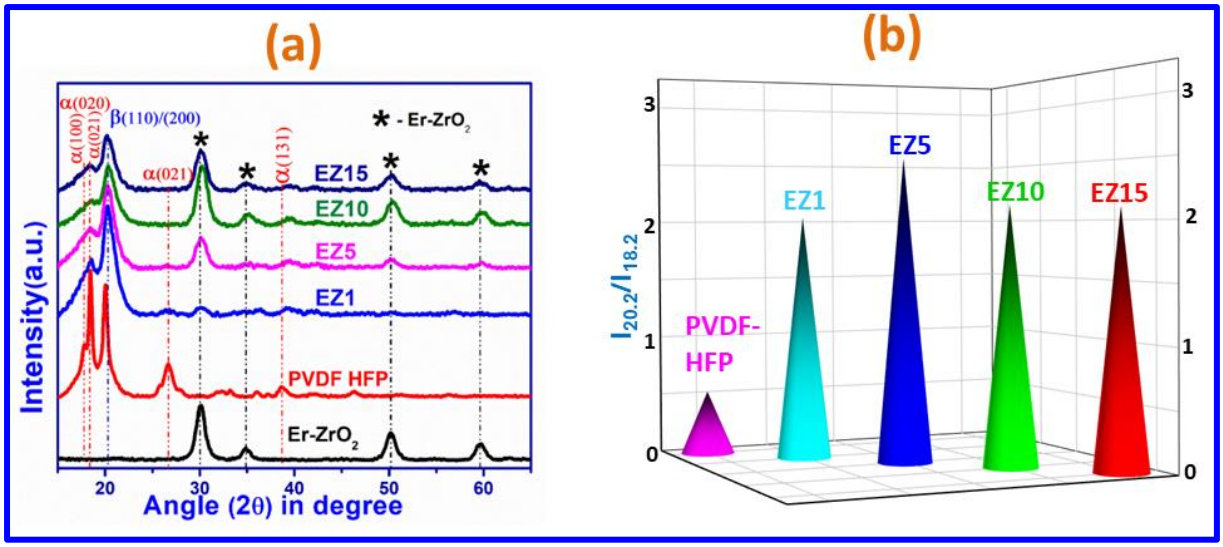

Figure 4.3: (a) XRD pattern of Er- ZrO_2 Nanoparticles, pure PVDF-HFP and Er-ZrO_2 NPs doped PVDF-HFP thin films (EZ1, EZ5, EZ5, EZ10 and E15). (b) Ratio of $I_{20.5}$ and $I_{18.2}$ of the samples.

4.4.3. FTIR analysis:

The crystallization behaviour of PVDF-HFP and Er-ZrO_2 NPs-doped PVDF-HFP thin films were further investigated using Fourier Transform Infrared (FTIR) spectroscopy. FTIR spectroscopy gives the more accurate information about the different phases of PVDF-HFP matrix. The FTIR spectra of the virgin PVDF-HFP and Er-ZrO_2 NPs doped PVDF-HFP thin films are shows in figure 4.4: (a). The characteristics absorbance bands at 488 cm^{-1} (CF_2 waging), 532 cm^{-1} (CF_2 bending), 615 and 764 cm^{-1} (CF2 bending and skeletal bending), 796 and 976 cm^{-1} (CH2 rocking) are all present in virgin PVDF-HFP thin film spectra for α-phase [51]. The characteristic absorbance bands corresponding to the electroactive β and γ phases appeared at 840 cm^{-1} (CH_2 rocking, CF_2 stretching and skeletal C-C stretching) and 813 cm^{-1} (CF_2 asymmetric stretching) respectively.[52] Figure 4.4: (a) shows that all the characteristics absorbance bands are present in the pure PVDF-HFP matrix. This confirms that the pure PVDF-HFP matrix consists of polar β phase. The FTIR spectra of the Er-ZrO_2 NPs doped PVDF-HFP thin films are showing that the characteristic absorbance bands at 445 cm^{-1} (CF_2 rocking and CH_2 rocking), 479 cm^{-1} (CF_2 deformation) 510 cm^{-1} (CF_2 stretching), 600 cm^{-1} (CF_2 wagging) and 840 cm^{-1} (CH_2 rocking, CF_2 stretching and skeletal C-C stretching) [53-55]

appeared strongly. This suggests the confirmation of the β-phase induced in Er-ZrO_2 nanoparticle-doped PVDF-HFP thin films.. All the characteristics absorbance bands correspond to non-polar α-phase vanish for Er-ZrO_2 NPs doped PVDF-HFP thin films FTIR spectra. Thus, the Er-ZrO_2 nanoparticles significantly enhance the β-phase in the PVDF-HFP matrix. This improvements of β phase appears due to the strong interaction between Er-ZrO_2 NPs and PVDF-HFP. Sample EZ5 shows the maximum enhancement of the β-phase, as illustrated in Figure 4.4(a). These results are consistent with the previous XRD findings.

The enhancement of the polar β-phase was quantitatively measured by the relative fraction of the α and β phases.The relative fraction of β-phase (F(β)) were determined by the Lambert-Beer law, and it's given in below [56].

$$\mathbf{F(\beta)} = \frac{\mathbf{A_\beta}}{\left(\frac{\mathbf{K_\beta}}{\mathbf{K_\alpha}}\right)\mathbf{A_\alpha + A_\beta}} \times \mathbf{100\%} \qquad \textbf{(4.1)}$$

where A_α and A_β are the absorbance at 764 cm^{-1} and 840 cm^{-1}, and K_β(= 7.7 × 104 cm^2 mol^{-1}) and K_α(= 6.1 × 104 cm^2 mol^{-1}) are the absorption coefficients at 840 and 764 cm^{-1}respectively. The changes of (F(β)) with the Er-ZrO_2 NPs content (vol%) are shown in figure 4.4 (b). The fraction of β-phase (F(β)) for the pure PVDF-HFP composite matrix is 38.062% and maximum value is 83.35437% for the EZ5 sample. These results are also consistent with the XRD findings.

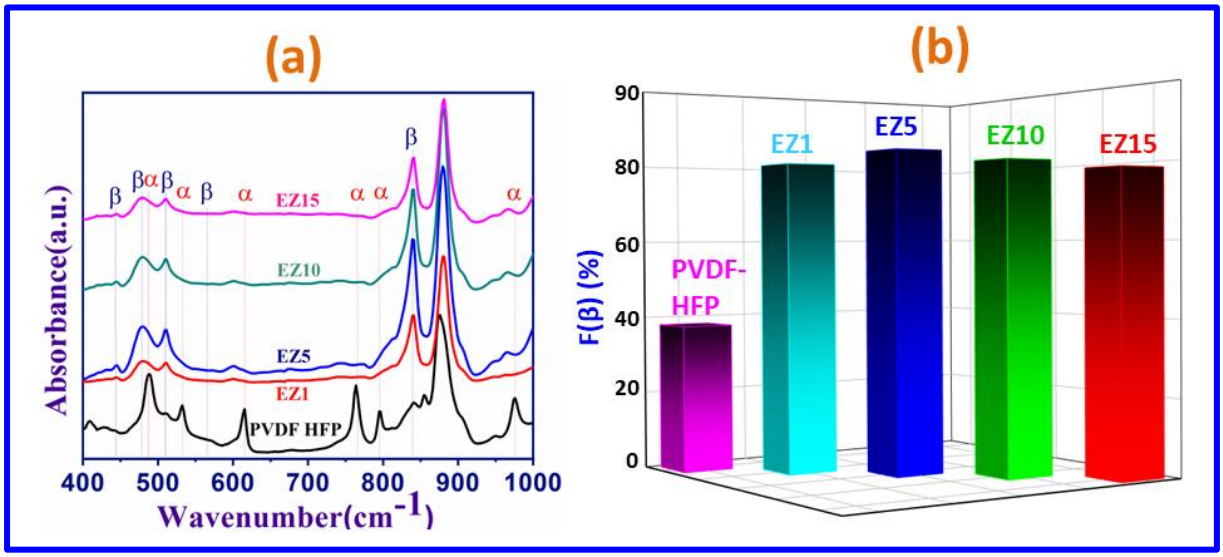

Figure 4.4: (a) Pure PVDF-HFP and Er-ZrO/PVDF-HFP composite thin films (EZ1, EZ5, EZ5, EZ10 and EP15). (d)Evaluation β-phase content of the samples.

4.4.4. DSC Analysis:

The thermal behaviour of Er-ZrO_2 dopped PVDF-HFP was characterised by Differential scanning calorimetry (DSC) analysis. Figure 4.5(a) displays the DSC curves of pure PVDF-HFP and Er-ZrO_2 nanoparticle-loaded PVDF-HFP nanocomposite thin films. In Figure 4.5:(a) it is shown that the melting peak for pure PVDF-HFP is at 151.5 °C due to non-polar α crystalline phase. Due to the addition of Er-ZrO_2 NPs in PVDF-HFP matrix, the melting peak changes to a higher temperature. This melting temperature confirms the formation of polar β crystal polymorph. Highest Melting peak observed for EZ5 sample. As the mass percentage of Er-ZrO_2 nanoparticles increases beyond EZ5, the temperature decreases due to theagglomeration of Er-ZrO_2 NPs in PVDF-HFP matrix. This result alsomatches with the

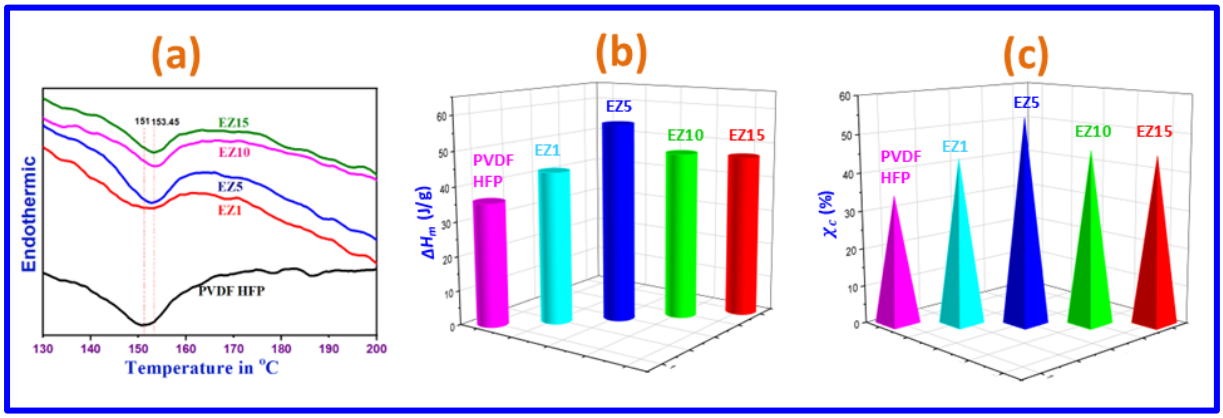

Figure 4.5:(a) DSC thermographs of pure PVDF-HFP and NPs doped PVDF-HFP thin films. (b) Evaluation of enthalpy of fusion and (c) Degree of crystallinity of pure PVDF-HFP and Er- ZrO_2 NPs loaded PVDF-HFP thin films.

previous XRD data. Here melting temperature of EZ5 sample is 153.45°C which is greater than the melting temperature of pure PVDF-HFP and Er-ZrO_2 NPs loaded PVDF-HFP nanocomposite which were measured from DSC curve. The melting enthalpies (ΔH_m), the degree of crystallinity (χ_c) of pure PVDF-HFP and the sample were calculated from the DSC thermographs. The relation between the melting enthalpy (ΔH_m) and the degree of crystallinity (χ_c) of the samples is given below [57].

$$\chi_c = \frac{\Delta H_m}{\Delta H_{100\%}} \times 100\% \qquad (4.2)$$

Where, $\Delta H_{100\%}$ (=104.6 J/g) is the melting enthalpy for 100% crystalline PVDF-HFP. The variation of enthalpy of fusion (ΔHm) with mass percentage of NPs is shown in figure 4.5:(b). This figure shows that the maximum enthalpy of fusion (ΔHm) is found for EZ5 sample.

Similarly figure 4.5: (b) gives the variation of degree of crystallinity (χ_c) with mass percentage of NPs. This figure also shows that the highest degree of crystallinity (χ_c) is observed for EZ5.

4.4.5. Dielectric behaviour:

The dielectric constant (ε_r) and a.c. conductivity(σ_{ac}) of the samples were given by the following relations.

$$\varepsilon_r = \frac{C \times d}{\varepsilon_0 A} \quad \textbf{(4.3)}$$

$$\sigma_{ac} = 2\pi f \varepsilon_r \varepsilon_0 \tan\delta \quad \textbf{(4.4)}$$

Where C is the capacitance, d is the thickness of the film, ε_0 is the permittivity of free space (8.854×10^{-10} F·m^{-1}), 'A' is the area of the film, $tan\delta$ is the tangent loss, and f (in Hz) is the applied frequency [58].

Figure 4.6 illustrate the dielectric nature of pure PVDF-HFP and Er-ZrO2NPs loaded PVDF-HFP nanocomposite. The dielectric constant (ε_r) of the sample varies with frequency and mass percentage, displayed in figure 4.6:(a). Maximum value of dielectric constant (ε_r) is found to be 13.5 for EZ5. This variation occurs due to Maxwell-Wagner-Sillars (MWS) surface interfacial polarization effect. If the electric field is applied in the lower frequency range, then the electric dipole present in the samples follows the electric field. In this frequency range the electric dipole has sufficient time to move from one electrode to another while the electric dipoles do not follow the same applied electric field at higher frequency range. In the higher frequency range, the applied electric field changes rapidly but the electric dipole cannot move so fast. As a result, they are lag behind the electric field. For this reason, the dielectric constant of the sample decreases at the higher frequency range. Tangent loss ($tan\delta$) and ac conductivity (σ_{ac}) of sample changes with the frequency for this same reason. As the mass percentage of Er-ZrO_2 nanoparticles in PVDF-HFP increases, the dielectric constant of the samples rises up to EZ5 and then decreases. This enhancement of dielectric constant confirms the transformation of polar β phase of PVDF-HFP from nonpolar α phase.

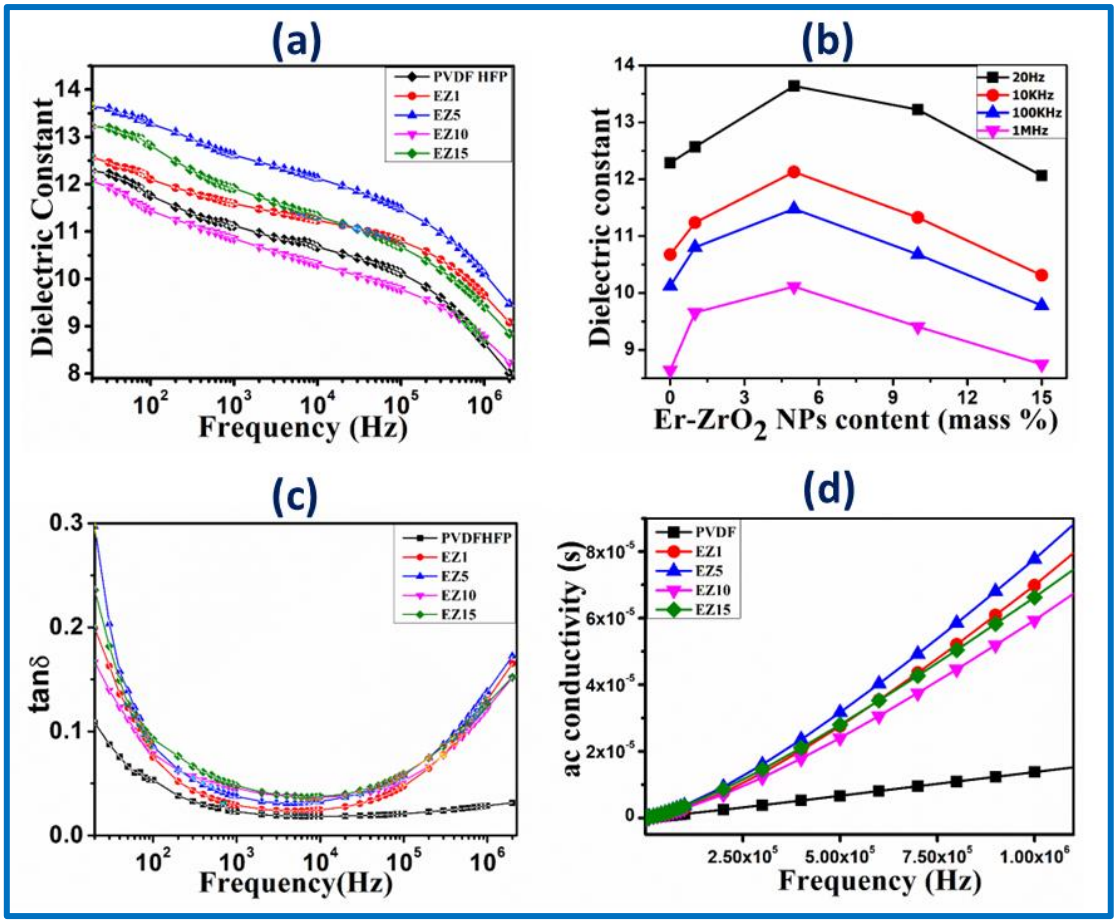

Figure 4.6: Frequency dependence of dielectric properties of pure PVDF-HFP and Er-ZrO_2/PVDF-HFP thin films; (a) dielectric constant, (b) tangent loss and (c) ac conductivity.

4.5. Performance of the PENG:

For the fabrication of the device EZ5 was selected due to its comparatively high dielectric constant and superior electroactive β-phase content.The piezoelectric properties of EZ5 are also very good with piezoelectric constant (d_{33}) ~ 74.5 pC/N at 50 Hz under the applied force about 0.5 N (Piezotest, PM300).

Figure 4.7:(a) and (b) shows the schematic diagram and digital photograph of the fabricated EPENG. Output response of the device is shown in figure 4.7: (c). Open circuit output response of the device is collected by digital storage oscilloscope (Keysight, Oscilloscope DSO-X 3012A). Enlargement view of open circuit output response is shown in figure 4.7: (d). Short circuit current output characteristics of the device were measured by Keysight Electrometer B2985. Figure 4.7: (f) and g gives the short circuit current output response nature and its wave nature. This device produces an open-circuit output voltage (Voc) of approximately 133 V and a short-circuit output current (Isc) of 2.77 μA when subjected to finger imparting .Maximum

power density of the EPNG is 8771 μWcm^{-3} which is greater than the previous reported literature. [56]. Frequency response of output voltage of the EPENGs is shown in figure 4.7: (e). By finger imparting (imparting force 27.5 N), frequency dependent output voltage performance of the manufactured PENGs was also observed from 1 Hz to 6 Hz as illustrated in figure 4.7: (e).

The output response of the EPENG as a function of frequency is shown in Figure 4.7(f).

The frequency-dependent output voltage performance of the fabricated EPENGs, measured from 1 Hz to 6 Hz, is also observed under finger tapping. (imparting force ~ 27.5 N) shown in figure 5f. Maximum output voltage have obtained at 6 Hz frequency. Possible mechanism and explanation of frequency dependent output performance are described at energy harvesting mechanism section. Stability of fabricated devices also tested over 1.5 years. Output voltage results demonstrate the high stability of fabricated devices giving almost same output voltage (V_{os}~ 133 V).

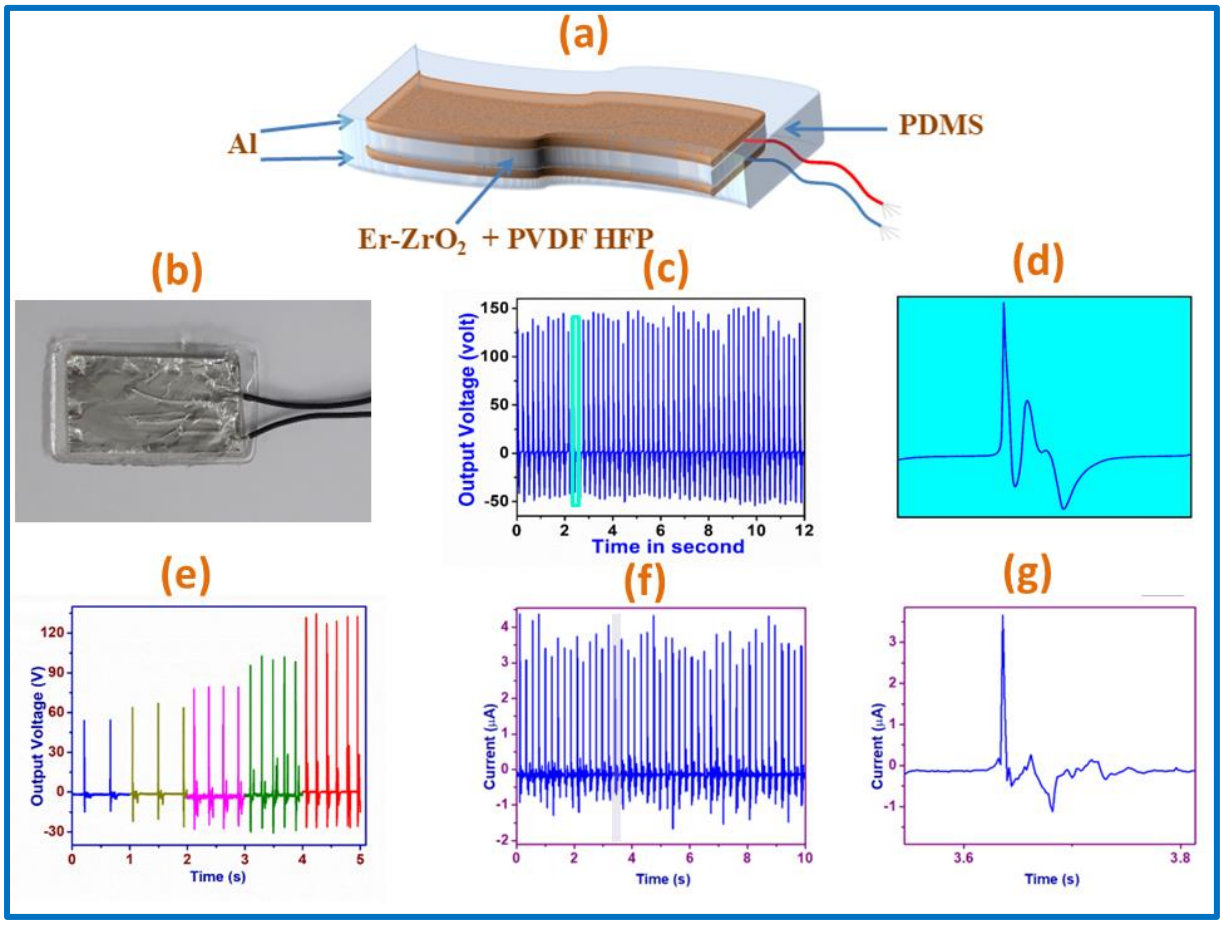

Figure 4.7: (a) Schematic diagram of the fabricated EPENG; (b) Photograph of fabricated EPENG; (c) Open circuit output voltage (V_{oc}); (d) Magnified view of open circuit output voltage (V_{oc}); (e) Frequency-dependent output voltage (V_{oc}); (f) Short circuit output current (I_{sc}) of PENG under the finger impetrating and (g) Magnified view of short circuit output current (I_{sc}).

4.6. Working Mechanism:

The well-known four fundamental Maxwell's equations for electromagnetic theory are given below,

$$\nabla.\vec{D} = \rho_f \quad \textbf{(Gauss's Law for electrostatics)} \quad \textbf{(4.5)}$$

$$\nabla.\vec{H} = 0 \quad \textbf{(Gauss's law for magnetostatics)} \quad \textbf{(4.6)}$$

$$\nabla x\vec{E} = -\frac{\partial \vec{B}}{\partial t} \quad \textbf{(Faraday's law for magnetic induction)} \quad \textbf{(4.7)}$$

$$\nabla x\vec{H} = \vec{J}_f + \frac{\partial \vec{D}}{\partial t} = \vec{J}_f + \vec{J}_D \quad \textbf{(Ampere's circuital law with Maxwell's addition)} \quad \textbf{(4.8)}$$

where $\vec{J}_f$ is the current density resulting from free electron flow and ρ_f is the volume charge density of free electron; $\vec{E}, \vec{D}, \vec{B}$ and $\vec{H}$ are the electric field, displacement electric field, magnetic induction and magnetic field respectively; and $\vec{J}_D = \frac{\partial \vec{D}}{\partial t}$ is the displacement current.

We know the displacement vector ($\vec{D}$) is known to be given by

$$\vec{D} = \epsilon_0\vec{E} + \vec{P} \quad \textbf{(4.9)}$$

Where $\vec{P}$ is the polarization vector and ϵ_0 is the permittivity of the vacuum.

For an isotropic medium, the displacement vector ($\vec{D}$) can be obtained given by

$$\vec{D} = \epsilon\vec{E} \quad \textbf{(4.10)}$$

Where ϵ is the dielectric permittivity.

Presently, displacement current is provided by

$$\vec{J}_D = \frac{\partial \vec{D}}{\partial t} = \frac{\partial(\epsilon\vec{E}+\vec{P})}{\partial t} = \epsilon\frac{\partial \vec{E}}{\partial t} + \frac{\partial \vec{P}}{\partial t} \quad \textbf{(4.11)}$$

This implies that the displacement current depends on both the rate of change of the electric field and the rate of change of polarization. It also indicates that the displacement vector is not associated with current flow due to free electrons.

The equations governing piezoelectric effects are as follows, specifically addressing the application of a small mechanical force to an anisotropic piezoelectric material. In displacement current equation, the term involving the rate of change of electric field ($\epsilon\frac{\partial \vec{E}}{\partial t}$) is crucial for generating Electromagnetic waves. This principle is used in wireless communicating system like television, mobile phones, radios, wi-fi, and radar. On the other hand, the second term in displacement current equation, which represent the rate of change of polarization, is responsible for phenomenon like the piezoelectricity and triboelectricity. These effects are

harnessed in technologies such as piezoelectric nanogenerators, triboelectric nanogenerators, and various sensors.

The equations governing piezoelectric effects are as follows, specifically addressing the application of a small mechanical force to an anisotropic piezoelectric material [59-61].

$$\vec{P}_i = (e)_{ijk}\left(\vec{S}\right)_{jk} \quad \textbf{(4.12)}$$

$$\vec{T} = C_E\vec{S} - e^T\vec{E} \quad \textbf{(4.13)}$$

$$\vec{D} = e\vec{S} - k\vec{E} \quad \textbf{(4.14)}$$

where $\vec{P}_i$ represent the polarization, $(e)_{ijk}$ denotes the piezoelectric tensor of rank 3; $\vec{S}$ represent the mechanical strain; $\vec{T}$ represent the stress tensor and C_E represent the elasticity tensor and k represent the dielectric tensor.

Further, the displacement current that emerges as a result of polarization can be expressed as

$$\vec{J}_{Di} = \frac{\partial \vec{P}_i}{\partial t} = (e)_{ijk}\left(\frac{\partial \vec{S}}{\partial t}\right)_{jk} \quad \textbf{(4.15)}$$

Equation (12) shows the linear relationship between the output current density and the rate of change of the applied strain. Here, the output current of EPNG is directly proportional to the rate at which the applied strain changes.

In the absence external applied electric field ($\vec{E} = 0$) the displacement vector is to be obtained by

$$\vec{D} = \epsilon_0 \times 0 + \vec{P} = \vec{P} \quad \textbf{(4.16)}$$

If the z-axis represents the direction of polarization, then we can define it as follows:

$$D_z = P_z = \sigma_P(z) \quad \textbf{(4.17)}$$

The parameter D_z is the z-component of the displacement vector, P_z represent the z-component of polarization and $\sigma_P(z)$ denotes the surface charge density resulting from piezoelectric polarization.

Hence, the displacement current in the z-direction can be expressed as

$$J_{DZ} = \frac{\partial P_z}{\partial t} = \frac{\partial \sigma_p(z)}{\partial t} \quad \textbf{(4.18)}$$

The above Equation (8) suggests that the output current of EPNG is directly proportional with the rate of change of surface charge polarization.

The equation representing the output voltage of the open-circuit EPNG is as follows:

$$V_{OC} = \frac{Z\sigma_P(Z)}{\epsilon} \quad \textbf{(4.19)}$$

Where Z represents the thickness of the EPNG and it is a function of time.

When an external load resistance R is introduced, the resulting output of EPNG can be expressed as follows:

$$RA\frac{d\sigma}{dt} = Z\left[\sigma_p(z) - \sigma(z)\right]/\epsilon \quad \textbf{(4.20)}$$

where A represent the area of the electrode.

Equation (11a) shows a direct proportionality between the electric polarization and the strain generated within the device. Furthermore, it can be derived from equation (14) that the displacement current density exhibits a direct proportionality to both the rate of change of polarization and the rate of change of surface charge density induced in the electrodes. Therefore, it can be observed that the displacement current exhibits a direct proportionality to the frequency of the applied force. The value of the output voltage of the EPNG is contingent upon the thickness of the device, as indicated by equation (4.19). Figure 4.9:(a) and figure 4.9:(b) represent the condition of the device when force is applied and released. Figure 4.9:(a) and figure 4.9:(b) illustrates the design of the energy harvesting mechanism of EPNG. The conversion of mechanical vibration energy into an electrical signal can be explained through the synergistic effect of molecular dipole motion.

The schematic figure in figure 4.9:(a) illustrates the energy conversion mechanism employed in the EPNG. The technique uses the potential synergistic effect of molecular dipoles that are inherent in PVDF. The incorporation of Er-ZrO_2 nanoparticle into PVDF results in a notable enhancement of the electroactive β phase and piezoelectric properties. The observed improvement can be attributed to the significant electrostatic interaction between the Er-ZrO_2 nanoparticle and the PVDF dipoles (Figure 4.8).

When an external force is exerted on the composite film, it results in the generation of a secondary potential within the Er-ZrO_2 nanoparticle. The secondary potential induces alignment of the PVDF HFP dipoles in the respective direction of the applied force. The occurrence of self-polarization in the Er-ZrO_2 nanoparticle-PVDF HFP composite can be attributed to the coupling between mechanical stress and interfacial surface charges. When subjected to compressional stress, the Er-ZrO_2 nanoparticle-PVDF HFP composite attains a positive piezoelectric potential at the top electrode and a negative piezoelectric potential at the bottom electrode {Figure 4.9:(b)}. After releasing the stress, potential of the electrodes decreases to zero and immediately gets the opposite potential due to elastic nature of the crystalline structure. Small voltage peaks arise due to the relaxations of the dipoles in crystalline structure {Figure 4.9:(b)}. Thus, under continuous application of compressive and release stress, the EPENG generates an alternating current (AC) voltage.The phenomenon of

self-polarization is mathematically represented by equation (4.12) and gives rise to a piezoelectric potential, as denoted by equation (4.19).

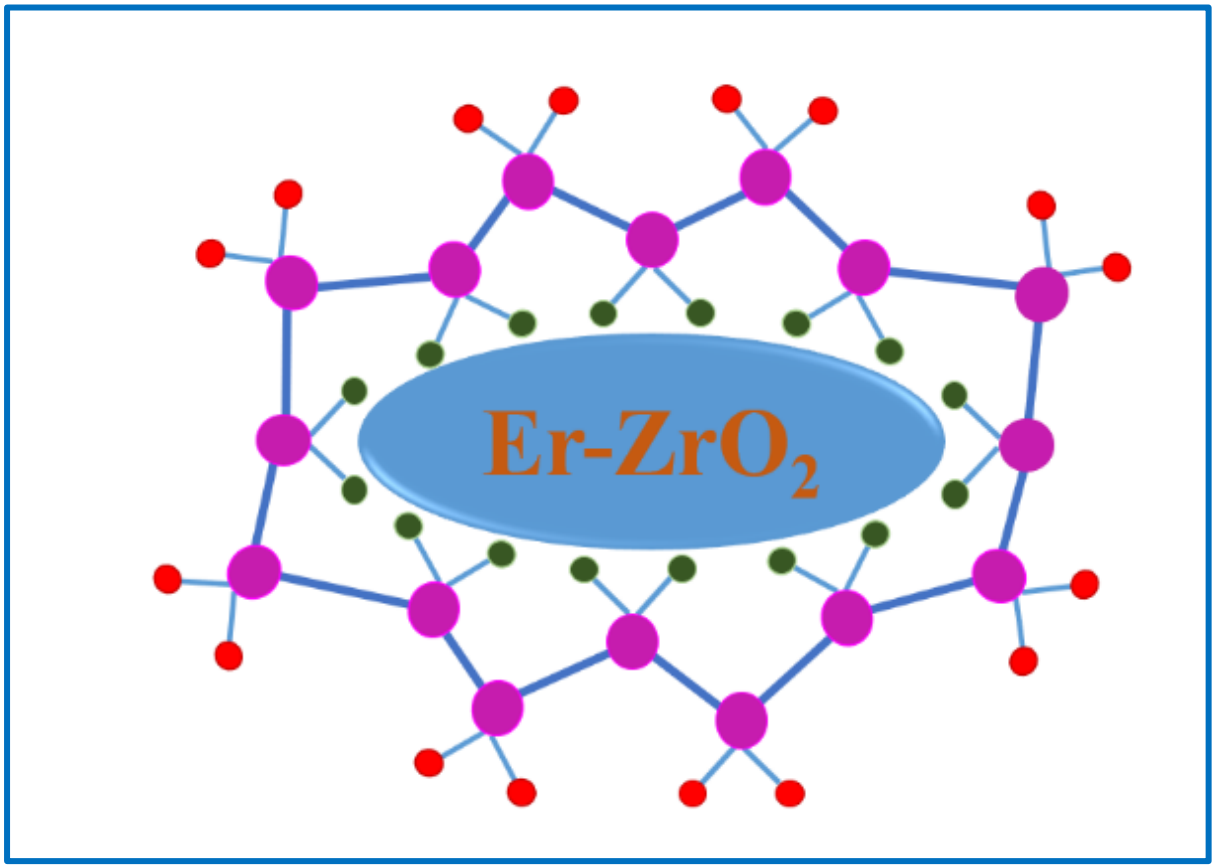

Figure 4.8: Schematic presentation of self-polarization and interaction between Er-ZrO_2 NPs and PVDF-HFP

As explained in Equation (4.20), when the two electrodes are linked through an external load resistor (R), an electric current passes through the resistor.

In practical applications, the EPENG can be used for charging capacitors and lighting LEDs. Figure 4.9:(e) demonstrates that a 1 μF capacitor can be charged to 2 V in just 16 seconds. Figure 4.9:(d) shows a digital image of 80 commercially available blue LEDs connected in series, which light up when powered by the EPENG.

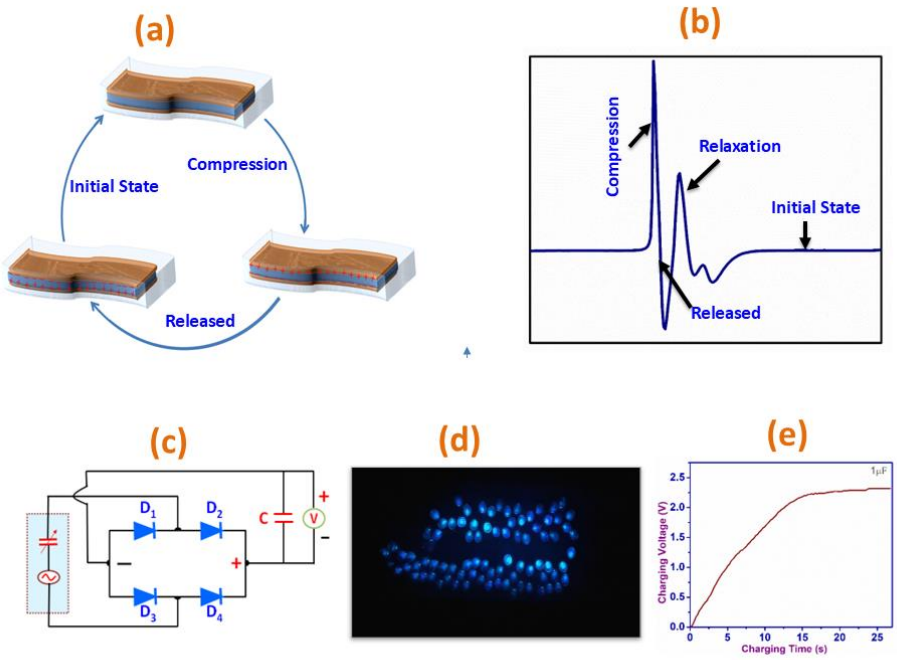

Figure 4.9: (a) and (b) Working mechanism of EPENG; (c) Circuit diagram of the charging capacitor; (d) Photograph of glowing LEDs by EPENG and (c) Capacitor charging (voltage vs. time) graph by PENG.

4.7. Conclusions:

In summary, we have developed a high-performance EPENG with Er-ZrO_2 NPs doped PVDF-HFP film for harvesting mechanical energy from the ambient environment. Addition of Er-ZrO_2 NPs, in the PVDF-HFP matrix, enhances the electroactive β-phase as well as output signals of PENG. Due to nucleation of electroactive β phase and large interfacial polarization, the developed PENG exhibits a large value of open circuit voltage (Voc=133 Volt) and short circuit current (Isc= 2.77 µA) with power density ~ 8771 μWcm^{-3} under a periodic finger imparting. Using a bridge rectifier, this developed PENG is capable of illuminating a large number of LEDs and charging a capacitor instantly. This EPENG can convert any kind of movement into electrical energy such as touching, drinking, talking, coughing, swallowing and also pulse of blood pressure. It also can be used in speech recognition and sensor applications. In future work, an Er-ZrO_2/PVDF-HFP composite-based TENG will be developed. This promising approach aims to provide a large-scale power supply, converting the small mechanical energy from human activities into electrical energy to realize a self-powered system.

*****

References:

[1]. Sripadmanabhan Indira, S., Aravind Vaithilingam, C., Oruganti, K.S.P., Mohd, F. and Rahman, S., 2019. Nanogenerators as a sustainable power source: state of art, applications, and challenges. *Nanomaterials*, *9*(5), p.773.

[2]. Hu, Y. and Wang, Z.L., 2015. Recent progress in piezoelectric nanogenerators as a sustainable power source in self-powered systems and active sensors. *Nano Energy*, *14*, pp.3-14.

[3]. Wang, X., 2012. Piezoelectric nanogenerators—Harvesting ambient mechanical energy at the nanometer scale. *Nano Energy*, *1*(1), pp.13-24.

[4]. Jie, Y., Jia, X., Zou, J., Chen, Y., Wang, N., Wang, Z.L. and Cao, X., 2018. Natural leaf made triboelectric nanogenerator for harvesting environmental mechanical energy. *Advanced Energy Materials*, *8*(12), p.1703133.

[5]. Pang, Y., Cao, Y., Derakhshani, M., Fang, Y., Wang, Z.L. and Cao, C., 2021. Hybrid energy-harvesting systems based on triboelectric nanogenerators. *Matter*, *4*(1), pp.116-143.

[6]. Fan, F.R., Tang, W. and Wang, Z.L., 2016. Flexible nanogenerators for energy harvesting and self-powered electronics. *Advanced Materials*, *28*(22), pp.4283-4305.

[7]. Nguyen, V., Zhu, R. and Yang, R., 2015. Environmental effects on nanogenerators. *Nano Energy*, *14*, pp.49-61.

[8]. Maiti, Sandip, Sumanta Kumar Karan, Jin Kon Kim, and Bhanu Bhusan Khatua. "Nature driven bio-piezoelectric/triboelectric nanogenerator as next-generation green energy harvester for smart and pollution free society." *Advanced Energy Materials* 9, no. 9 (2019): 1803027.

[9]. Rodrigues, C., Nunes, D., Clemente, D., Mathias, N., Correia, J.M., Rosa-Santos, P., Taveira-Pinto, F., Morais, T., Pereira, A. and Ventura, J., 2020. Emerging triboelectric nanogenerators for ocean wave energy harvesting: state of the art and future perspectives. *Energy & Environmental Science*, *13*(9), pp.2657-2683.

[10]. Xu, M., Zhao, T., Wang, C., Zhang, S.L., Li, Z., Pan, X. and Wang, Z.L., 2019. High power density tower-like triboelectric nanogenerator for harvesting arbitrary directional water wave energy. *ACS nano*, *13*(2), pp.1932-1939.

[11]. Zhu, J., Zhu, M., Shi, Q., Wen, F., Liu, L., Dong, B., Haroun, A., Yang, Y., Vachon, P., Guo, X. and He, T., 2020. Progress in TENG technology—A journey from energy harvesting to nanoenergy and nanosystem. *EcoMat*, *2*(4), p.e12058.

[12]. Jiang, D., Su, Y., Wang, K., Wang, Y., Xu, M., Dong, M. and Chen, G., 2020. A triboelectric and pyroelectric hybrid energy harvester for recovering energy from low-grade waste fluids. *Nano Energy*, *70*, p.104459.

[13]. Zhao, L., Duan, J., Liu, L., Wang, J., Duan, Y., Vaillant-Roca, L., Yang, X. and Tang, Q., 2021. Boosting power conversion efficiency by hybrid triboelectric nanogenerator/silicon tandem solar cell toward rain energy harvesting. *Nano Energy*, *82*, p.105773.

[14]. Zheng, Q., Shi, B., Li, Z. and Wang, Z.L., 2017. Recent progress on piezoelectric and triboelectric energy harvesters in biomedical systems. *Advanced Science*, *4*(7), p.1700029.

[15]. Zhu, M., Yi, Z., Yang, B. and Lee, C., 2021. Making use of nanoenergy from human–Nanogenerator and self-powered sensor enabled sustainable wireless IoT sensory systems. *Nano Today*, *36*, p.101016.

[16]. Zou, Y., Bo, L. and Li, Z., 2021. Recent progress in human body energy harvesting for smart bioelectronic system. *Fundamental Research*, *1*(3), pp.364-382.

[17]. Song, Y., Shi, Z., Hu, G.H., Xiong, C., Isogai, A. and Yang, Q., 2021. Recent advances in cellulose-based piezoelectric and triboelectric nanogenerators for energy harvesting: a review. *Journal of Materials Chemistry A*, *9*(4), pp.1910-1937.

[18]. Chandrasekaran, S., Bowen, C., Roscow, J., Zhang, Y., Dang, D.K., Kim, E.J., Misra, R.D.K., Deng, L., Chung, J.S. and Hur, S.H., 2019. Micro-scale to nano-scale generators for energy harvesting: Self powered piezoelectric, triboelectric and hybrid devices. *Physics Reports*, *792*, pp.1-33.

[19]. Zhao, C., Zhang, Q., Zhang, W., Du, X., Zhang, Y., Gong, S., Ren, K., Sun, Q. and Wang, Z.L., 2019. Hybrid piezo/triboelectric nanogenerator for highly efficient and stable rotation energy harvesting. *Nano Energy*, *57*, pp.440-449.

[20]. Peng, L., Hu, L. and Fang, X., 2014. Energy harvesting for nanostructured self-powered photodetectors. *Advanced Functional Materials*, *24*(18), pp.2591-2610.

[21]. Tang, W., Sun, Q. and Wang, Z.L., 2023. Self-powered sensing in wearable electronics─a paradigm shift technology. *Chemical Reviews*, *123*(21), pp.12105-12134.

[22]. Zhao, Z., Dai, Y., Dou, S.X. and Liang, J., 2021. Flexible nanogenerators for wearable electronic applications based on piezoelectric materials. *Materials Today Energy*, *20*, p.100690.

[23]. Briscoe, J. and Dunn, S., 2015. Piezoelectric nanogenerators–a review of nanostructured piezoelectric energy harvesters. *Nano Energy*, *14*, pp.15-29.

[24]. Zhou, P., Zheng, Z., Wang, B. and Guo, Y., 2022. Self-powered flexible piezoelectric sensors based on self-assembled 10 nm $BaTiO_3$ nanocubes on glass fiber fabric. *Nano Energy*, *99*, p.107400.

[25]. Qudus, A., 2024. Multifunctional Sensing Capabilities of $BaTiO_3$/PDMS/MWCNT Nanogenerators in Smart Wearable Technologies.

[26]. Yaseen, H.M.A. and Park, S., 2023. P (VDF-TrFE)/BaTiO3 nanocomposite Langmuir-Schaefer thin film for piezoelectric nanogenerator. *Journal of Alloys and Compounds*, *952*, p.169940.

[27]. Xu, S., Yeh, Y.W., Poirier, G., McAlpine, M.C., Register, R.A. and Yao, N., 2013. Flexible piezoelectric PMN–PT nanowire-based nanocomposite and device. *Nano letters*, *13*(6), pp.2393-2398.

[28]. Xu, S., Poirier, G. and Yao, N., 2012. PMN-PT nanowires with a very high piezoelectric constant. *Nano letters*, *12*(5), pp.2238-2242.

[29]. Park, K.I., Son, J.H., Hwang, G.T., Jeong, C.K., Ryu, J., Koo, M., Choi, I., Lee, S.H., Byun, M., Wang, Z.L. and Lee, K.J., 2014. Highly-efficient, flexible piezoelectric PZT thin film nanogenerator on plastic substrates. *Adv. Mater*, *26*(16), pp.2514-2520.

[30]. Liu, H., Lin, X., Zhang, S., Huan, Y., Huang, S. and Cheng, X., 2020. Enhanced performance of piezoelectric composite nanogenerator based on gradient porous PZT ceramic structure for energy harvesting. *Journal of Materials Chemistry A*, *8*(37), pp.19631-19640.

[31]. Chen, X., Xu, S., Yao, N. and Shi, Y., 2010. 1.6 V nanogenerator for mechanical energy harvesting using PZT nanofibers. *Nano letters*, *10*(6), pp.2133-2137.

[32]. Kang, M.G., Jung, W.S., Kang, C.Y. and Yoon, S.J., 2016, February. Recent progress on PZT based piezoelectric energy harvesting technologies. In *Actuators* (Vol. 5, No. 1, p. 5). MDPI.

[33]. Sumang, R., Charoonsuk, T., Vittayakorn, N. and Panpho, P., 2024. High-performance flexible lead-free piezo-antiferroelectric based on NaNbO3/PDMS composites for energy harvesting application. *Ceramics International*.

[34]. Zhang, Q.M., Bharti, V. and Kavarnos, G., 2002. Poly (vinylidene fluoride)(PVDF) and its copolymers. *Encyclopedia of smart materials*.

[35]. Lu, L., Ding, W., Liu, J. and Yang, B., 2020. Flexible PVDF based piezoelectric nanogenerators. *Nano Energy*, *78*, p.105251.

[36]. Sukumaran, S., Chatbouri, S., Rouxel, D., Tisserand, E., Thiebaud, F. and Ben Zineb, T., 2021. Recent advances in flexible PVDF based piezoelectric polymer devices for energy harvesting applications. *Journal of Intelligent Material Systems and Structures*, *32*(7), pp.746-780.

[37]. Mohammadpourfazeli, S., Arash, S., Ansari, A., Yang, S., Mallick, K. and Bagherzadeh, R., 2023. Future prospects and recent developments of polyvinylidene fluoride (PVDF) piezoelectric polymer; fabrication methods, structure, and electro-mechanical properties. *RSC advances*, *13*(1), pp.370-387.

[38]. Saxena, P. and Shukla, P., 2021. A comprehensive review on fundamental properties and applications of poly (vinylidene fluoride)(PVDF). *Advanced Composites and Hybrid Materials*, *4*, pp.8-26.

[39]. Abbasipour, M., Khajavi, R. and Akbarzadeh, A.H., 2022. A comprehensive review on piezoelectric polymeric and ceramic nanogenerators. *Advanced Engineering Materials*, *24*(6), p.2101312.

[40]. Kim, T.Y., Kim, S.K. and Kim, S.W., 2018. Application of ferroelectric materials for improving output power of energy harvesters. *Nano convergence*, *5*(1), p.30.

[41]. Ruan, L., Yao, X., Chang, Y., Zhou, L., Qin, G. and Zhang, X., 2018. Properties and applications of the β phase poly (vinylidene fluoride). *Polymers*, *10*(3), p.228.

[42]. Martins, P., Lopes, A.C. and Lanceros-Mendez, S., 2014. Electroactive phases of poly (vinylidene fluoride): Determination, processing and applications. *Progress in polymer science*, *39*(4), pp.683-706.

[43]. Thakur, P., Kool, A., Hoque, N.A., Bagchi, B., Roy, S., Sepay, N., Das, S. and Nandy, P., 2016. Improving the thermal stability, electroactive β phase crystallization and dielectric constant of NiO nanoparticle/C–NiO nanocomposite embedded flexible poly (vinylidene fluoride) thin films. *RSC advances*, *6*(31), pp.26288-26299.

[44]. Thakur, P., Kool, A., Bagchi, B., Hoque, N.A., Das, S. and Nandy, P., 2015. Improvement of electroactive β phase nucleation and dielectric properties of WO 3· H 2 O nanoparticle loaded poly (vinylidene fluoride) thin films. *RSC advances*, *5*(77), pp.62819-62827.

[45]. Purushothaman, S.M., Tronco, M.F., Kottathodi, B., Royaud, I., Ponçot, M., Kalarikkal, N., Thomas, S. and Rouxel, D., 2023. A review on electrospun PVDF-based nanocomposites: Recent trends and developments in energy harvesting and sensing applications. *Polymer*, p.126179.

[46]. Si, S.K., Karan, S.K., Paria, S., Maitra, A., Das, A.K., Bera, R., Bera, A., Halder, L. and Khatua, B.B., 2018. A strategy to develop an efficient piezoelectric nanogenerator through ZTO assisted γ-phase nucleation of PVDF in ZTO/PVDF nanocomposite for harvesting bio-mechanical energy and energy storage application. *Materials Chemistry and Physics*, *213*, pp.525-537.

[47]. Thakur, P., Kool, A., Bagchi, B., Hoque, N.A., Das, S. and Nandy, P., 2015. The role of cerium (iii)/yttrium (iii) nitrate hexahydrate salts on electroactive β phase nucleation and dielectric properties of poly (vinylidene fluoride) thin films. *Rsc Advances*, *5*(36), pp.28487-28496.

[48]. Martins, P.M., Miranda, R., Marques, J., Tavares, C.J., Botelho, G. and Lanceros-Mendez, S., 2016. Comparative efficiency of TiO 2 nanoparticles in suspension vs.

immobilization into P (VDF–TrFE) porous membranes. *RSC advances*, *6*(15), pp.12708-12716.

[49]. Pal, K., Kang, D.J., Zhang, Z.X. and Kim, J.K., 2010. Synergistic effects of zirconia-coated carbon nanotube on crystalline structure of polyvinylidene fluoride nanocomposites: electrical properties and flame-retardant behavior. *Langmuir*, *26*(5), pp.3609-3614.

[50]. Gleiter, H., 2000. Nanostructured materials: basic concepts and microstructure. *Acta materialia*, *48*(1), pp.1-29.

[51]. Biswas, P., Hoque, N.A., Thakur, P., Saikh, M.M., Roy, S., Khatun, F., Bagchi, B. and Das, S., 2019. Highly efficient and durable piezoelectric nanogenerator and photo-power cell based on CTAB modified montmorillonite incorporated PVDF film. *ACS Sustainable Chemistry & Engineering*, *7*(5), pp.4801-4813.

[52]. Zhu, D., Tudor, M.J. and Beeby, S.P., 2009. Strategies for increasing the operating frequency range of vibration energy harvesters: a review. *Measurement Science and Technology*, *21*(2), p.022001.

[53]. Hoque, N.A., Thakur, P., Biswas, P., Saikh, M.M., Roy, S., Bagchi, B., Das, S. and Ray, P.P., 2018. Biowaste crab shell-extracted chitin nanofiber-based superior piezoelectric nanogenerator. *Journal of Materials Chemistry A*, *6*(28), pp.13848-13858.

[54]. Wang, Y., Furlan, R., Ramos, I. and Santiago-Avilés, J.J., 2004. Synthesis and characterization of micro/nanoscopic Pb (Zr 0.52 Ti 0.48) O 3 fibers by electrospinning. *Applied Physics A*, *78*, pp.1043-1047.

[55]. Karan, S.K., Bera, R., Paria, S., Das, A.K., Maiti, S., Maitra, A. and Khatua, B.B., 2016. An approach to design highly durable piezoelectric nanogenerator based on self-poled PVDF/AlO-rGO flexible nanocomposite with high power density and energy conversion efficiency. *Advanced Energy Materials*, *6*(20), p.1601016. [56] J. Sun, A. Yang, C. Zhao, F. Liu, Z. Li, Sci. Bull. 2019, 64, 1336.

[56]. Singh, H.H. and Khare, N., 2019. Improved performance of ferroelectric nanocomposite flexible film based triboelectric nanogenerator by controlling surface morphology, polarizability, and hydrophobicity. *Energy*, *178*, pp.765-771.

[57]. Thakur, P., Kool, A., Bagchi, B., Hoque, N.A., Das, S. and Nandy, P., 2015. In situ synthesis of Ni (OH) 2 nanobelt modified electroactive poly (vinylidene fluoride) thin films: remarkable improvement in dielectric properties. *Physical Chemistry Chemical Physics*, *17*(19), pp.13082-13091.

[58]. Martins, P., Lopes, A.C. and Lanceros-Mendez, S., 2014. Electroactive phases of poly (vinylidene fluoride): Determination, processing and applications. *Progress in polymer science*, *39*(4), pp.683-706.

[59] W. Deng, Y. Zhou, A. Libanori, G. Chen, W. Yang, J. Chen, Piezoelectric nanogenerators for personalized healthcare, Chem. Soc. Rev. 51 (2022) 3380–3435.
[60] G. Chen, X. Xiao, X. Zhao, T. Tat, M. Bick, J. Chen, Electronic textiles for wearable point-of-care systems, Chem. Rev. 122 (2022) 3259–3291.
[61] S.D. Mahapatra, P.C. Mohapatra, A.I. Aria, G. Christie, Y.K. Mishra, S. Hofmann, V. K. Thakur, Piezoelectric materials for energy harvesting and sensing applications: Road map for future smart materials, Adv. Sci. (Weinh.) 8 (2021) 2100864.

Chapter 5

Synthesis of In-situ ZnO within PVDF-ZnCl2 Composite: Simultaneous Improvement of Optical and Piezoelectric Properties

5.1 Introduction

Nowadays, harvesting mechanical energy from the environment is a promising method for powering small electronics and eventually creating self-powered electronic gadgets [1-5]. Recent advancements in nanotechnology have shown a potential method for creating a self-sufficient, environmentally friendly, and sustainable power source [6-7]. It has been shown that several types of nanogenerators (NGs) based on different mechanisms, such as piezo-, pyro-, ferro-, and triboelectric effects, can power a variety of electronic devices [8-9]. One of these, the piezoelectric nanogenerators (PENGs), which transform mechanical energy into electrical energy, has been regarded as a significant energy harvester due to their simple structure, exceptional flexibility, and reliable mechanical characteristics [1,10]. Historically, fabrication of PENGs has utilized piezoelectric materials such as piezoelectric inorganic semiconductors (ZnO) [11-12], piezoelectric ceramics ($BaTiO_3$, $ZnSnO_3$) [13-16], and piezoelectric polymers Poly(vinylidene fluoride (PVDF), PVDF-HFP and PVDF-TrFE. Among previously reported piezoelectric materials, piezoelectric polymers are extensively utilized due to their lightweight nature, ease of production, and suitability for wearable technology. Poly(vinylidene fluoride)(PVDF), is one of the fascinating piezoelectric polymers for the fabrication of nanocomposites. [17-21] PVDF exhibits mainly four different crystalline phase, namely, α, β, γ, etc. Due to the difference in the polymer chain conformations in each phase, all of the phases do not show piezoelectric character. Thermodynamically, the α-phase is the most stable phase at room temperature and pressure. It is non-polar because it has a centrosymmetric "trans-gauche-trans-gauche" ($TGT\bar{G}$) structure. The β-phase of PVDF, which exhibits an all-trans conformation, is the most electrically active phase and more attractive because of its spontaneous polarization giving rise to piezoelectric property. There are several techniques to achieve and stabilize this phase of PVDF. Electrospinning methods result in in situ poling of the polymer chains, resulting in enhanced piezoelectric activity. The addition of external assisting agents like organic and inorganic fillers leads to local self-orientation of $–CH_2/–CF_2$ dipoles of the PVDF chain within the crystalline lamella. It is noted that PVDF nanocomposite is a key factor for formation of electroactive β-phase as well as piezoelectric performance [20-23].

This study focus an innovative approach for enhancing optical property as well as piezoelectric properties of Poly(vinylidene fluoride) (PVDF) by in situ formation of ZnO within a $ZnCl_2$/PVDF composite. Notably this work reveals the composite's dual increase of optical and piezoelectric capabilities. Synergistic interaction with the PVDF matrix, the ZnO nanoparticles

produced within the PVDF matrix enhance optical features and significantly enhance piezoelectric performance of the NGs by improving β-phase which can be used as a sensor, and energy harvesting devices.

5.2 Experimental Section

5.2.1 Materials

- Poly(vinylidene fluoride) (PVDF) pellets (Mw ≈275 000, Sigma-Aldrich, USA);
- N, N-dimethylformamide (DMF),(Merck Chemicals, India);
- $ZnCl_2$ (Sigma-Aldrich, USA);
- Poly(dimethylsiloxane) (PDMS) (sylgard, 184 silicone elastomer).

5.2.2. Synthesis of PVDF $ZnCl_2$ Nanocomposite Thin Films

To prepare the PVZn films, different wt (w/v) % (i.e., 0.5, 1, 1.5 and 2) of $ZnCl_2$, were added separately into the 6 wt% of PVDF−DMF solutions (10 ml). The films were prepared by solvent casting techniques from PVDF and DMF solution containing $ZnCl_2$. The solutions were vigorously stirred for 48 h and sonicated for about 10 min to uniformly disperse the $ZnCl_2$ into PVDF solutions. The solutions were casted on clean glass substrates and dried at 120°C for 6 h under vacuum condition. Finally, the films (PVZn) were shed from the substrates for characterizations, named as PVZn0.5, PVZn1, PVZn1.5, PVZn2. The prepared films are of average thickness 20 μm.

5.2.3. Fabrication of PVZNG

To make the composite nanogenerators Ni−Cu−Ni plated polyester fabric was attached on both sides of that films. Two copper wires were attached on the electrodes. Finally, the complete structure was encapsulated by soft poly(dimethylsiloxane) (PDMS) for prevention from external mechanical damage prepared by a 10:1 curing agent and procured in an oven at 60ºC for 30 min. The fabricated device is named as PVZNG.

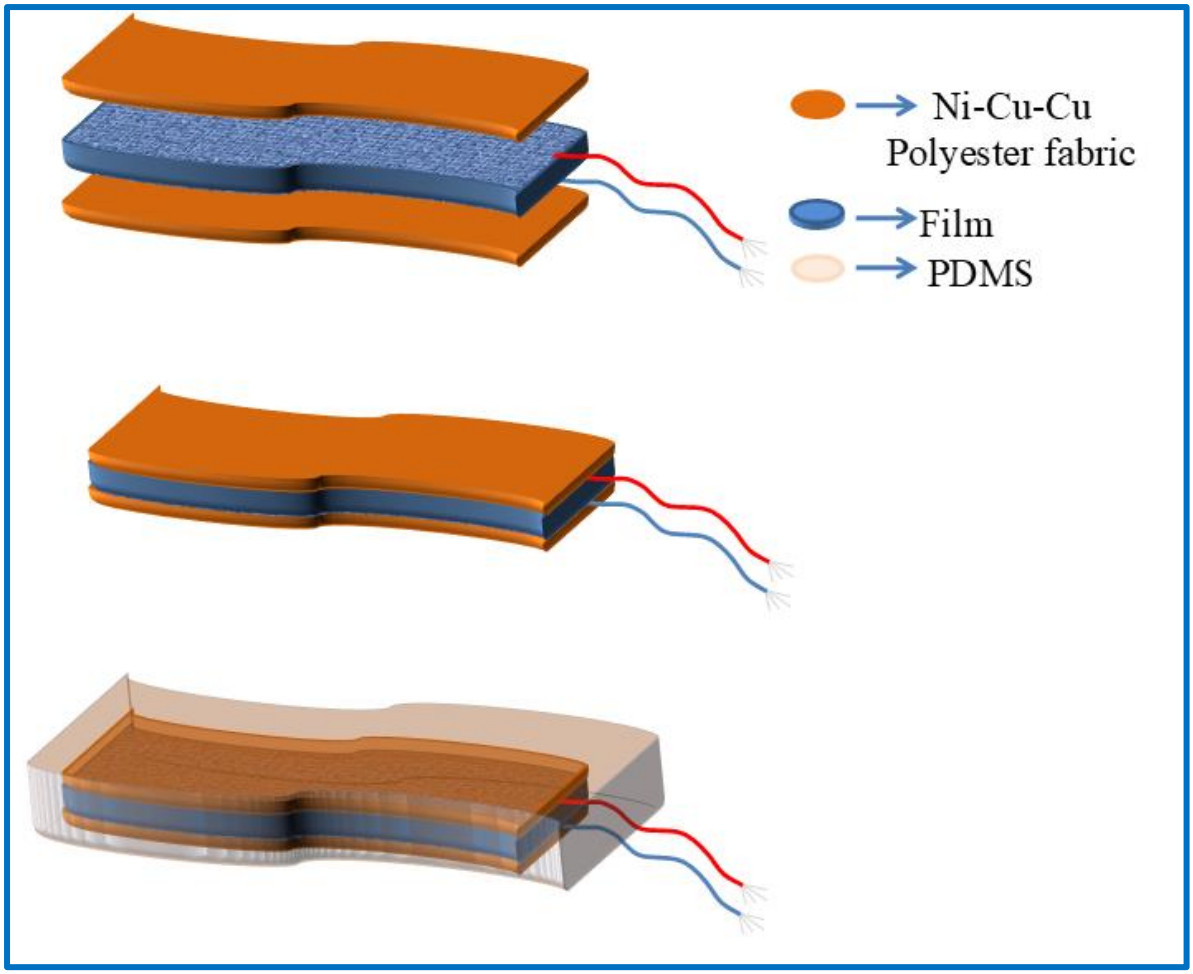

Figure5.1: Device Fabrication.

5.3. Characterizations

The classification of the composite thin films into different crystalline phases was verified using Fourier transform infrared spectroscopy (FT-IR) (TENSOR II, Bruker) and X-ray diffraction (XRD, Bruker, D 8 Advance) with a Cu Kα (λinc. ~1.54 Å) radiation under an operating voltage and current of 40 kV and 40 mA, respectively. The morphologies of the as-prepared composite films were observed by a field emission scanning electron microscopy (FE-SEM, INSPECT F50) operated at an acceleration voltage of 20 kV. The open circuit voltage under repeating finger impact from the nanogenerator (NG) was recorded using a digital storage oscilloscope (Agilent, DSO3102A).

5.4. Results and Discussions

5.4.1. FESEM analysis

The FE-SEM image of PVZn films is depicted in Figure 5.2. It is found that uniform distribution of in situ ZnO within the PVDF matrix is indicative of robust interfacial interactions. Uniform nano rod presents in PVZn1.5 composite films within the PVDF matrix, indicative of robust interfacial interactions. The presence of nanorods has a significant impact on the electrical properties of the PVZn nanocomposite, thus influencing its piezoelectric properties.

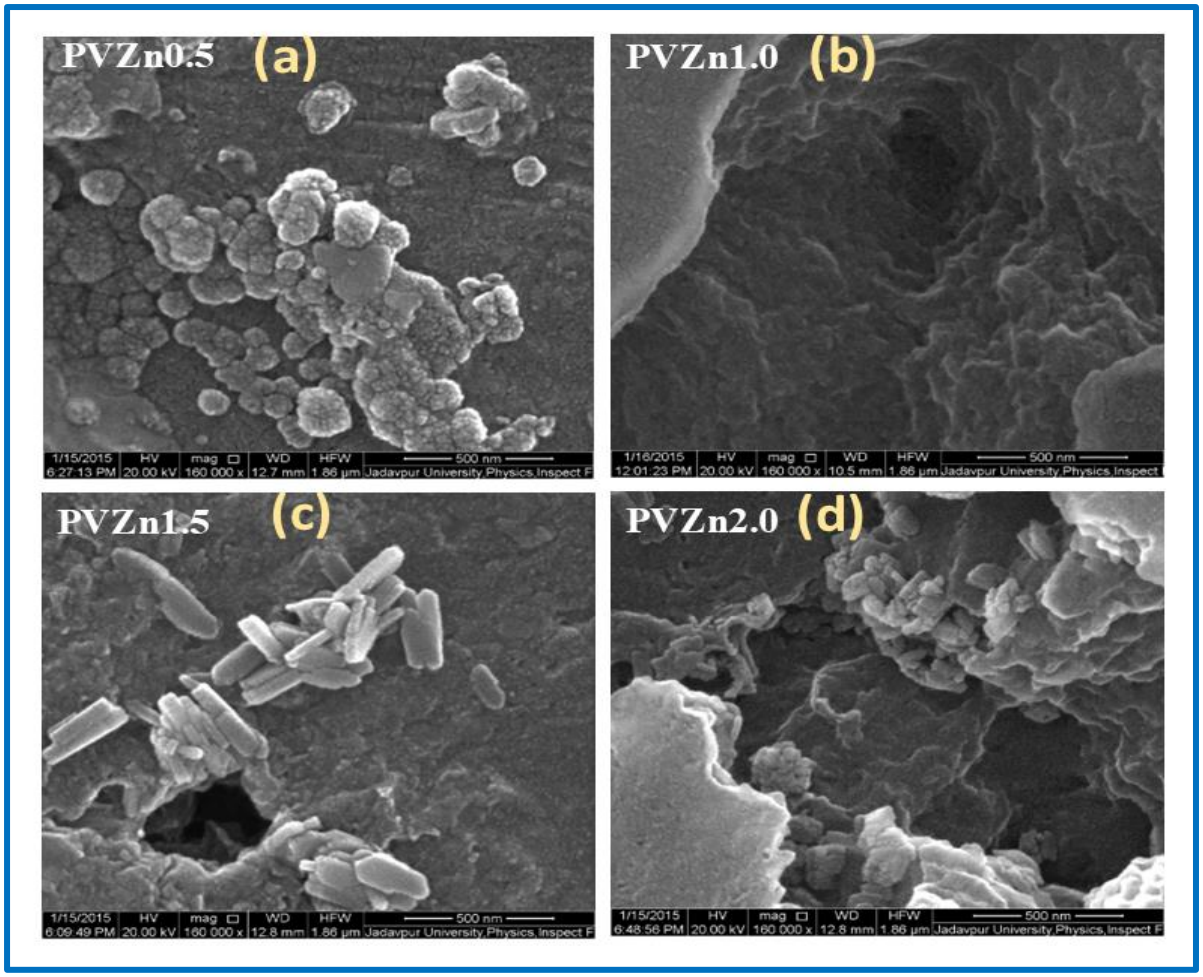

Figure 5.2: FE-SEM images of (a) PVZn0.5, (b) PVZn1.0, (c) PVZn1.5 and (d)PVZn2.0.

5.4.2. XRD analysis

X-ray diffraction (XRD) analysis confirmed the formation of in situ crystalline ZnO within the composite films as shown in Figure 5.3 (a). The diffraction peak at 2θ = 20.8 indicates the nucleation of the β-phase of the PVZn composites films. But small peaks at 17.7 (100), 18.4

(020), 19.9 (110) and 24.6 (021) are also present in the XRD pattern which indicates the existence of a small percentage of α-phase along with β-phase in PVZn film [17,20,23]. After increasing the wt% of $ZnCl_2$ within PVDF decreases the α-phase formation and consequently increases β-phase formation. A characteristic diffraction peak of PVZn1.5 at $2\theta = 32.61^{o}$ corresponding to the (001) plane ZnO which peak are left shift due to incorporation with PVDF.

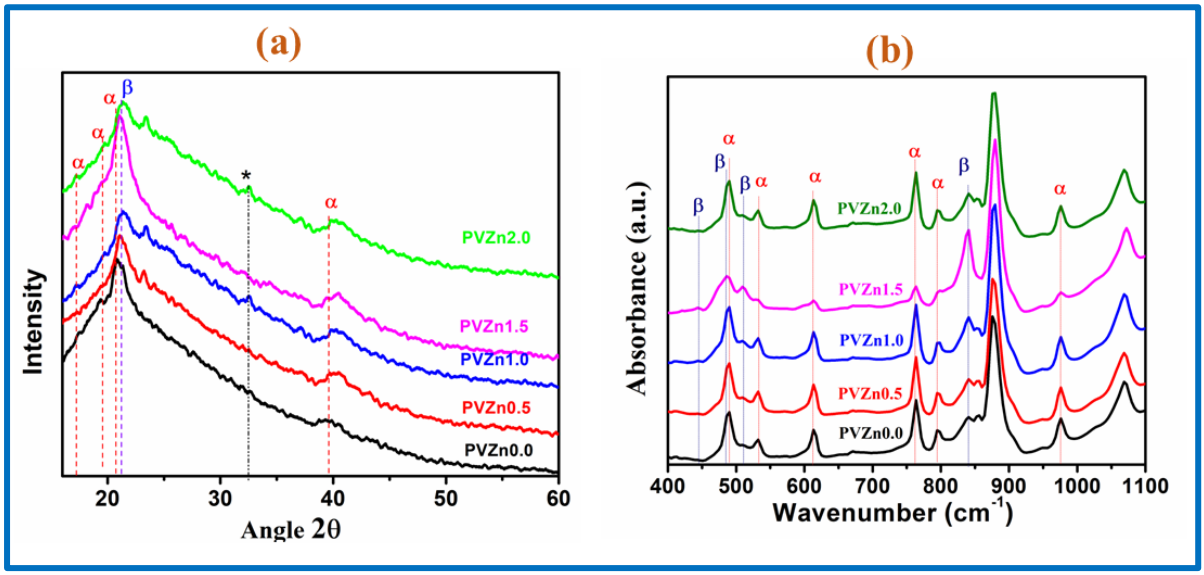

Figure 5.3:(a) XRD of PVDF and PVZn's film and (b) FT-IR spectra PVDF and PVZn's film within the frequency range of 400-1100 cm^{-1}.

5.4.3. FTIR Analysis

Fourier Transform Infrared Spectroscopy (FTIR) of the *in-situ* synthesis of ZnO within a PVDF-$ZnCl_2$ composites as shown in Figure 5.3(b) shows the successive formation of β-phase. The uniform intercalation of PVDF chains into $ZnCl_2$ induces β-phase in addition of α-phase. The strong vibrational bands arise of the PVZn films at 813 and 840 suggest successful nucleation of the in situ ZnO as well as of electroactive β-phase [17,18]. The sharp peak of PVZn1.5 reveals the maximum formation of β-phase.

5.4.4. Optical Properties

The optical characteristics of PVZn nanocomposites were obtained by means of Photoluminescence (PL) spectra and measurements (Figure 5.4). From PL spectra observed absorption peaks range about 380nm corresponding to the successful nucleation of in situ ZnO nanorod of the composite films which can be attributed to the annihilation of free excitons [24-26]. Additionally, the emission intensity of green light at a range 480 nm was found to be a result of the formation of oxygen vacancies [27-28]. It is commonly accepted that UV emission

can be ascribed to the radiative annihilation of excitons. The photoluminescence spectrum is primarily characterized by a prominent and intense UV emission. These optical properties of the nanocomposite films can be used as an optical sensor and optoelectronic devices.

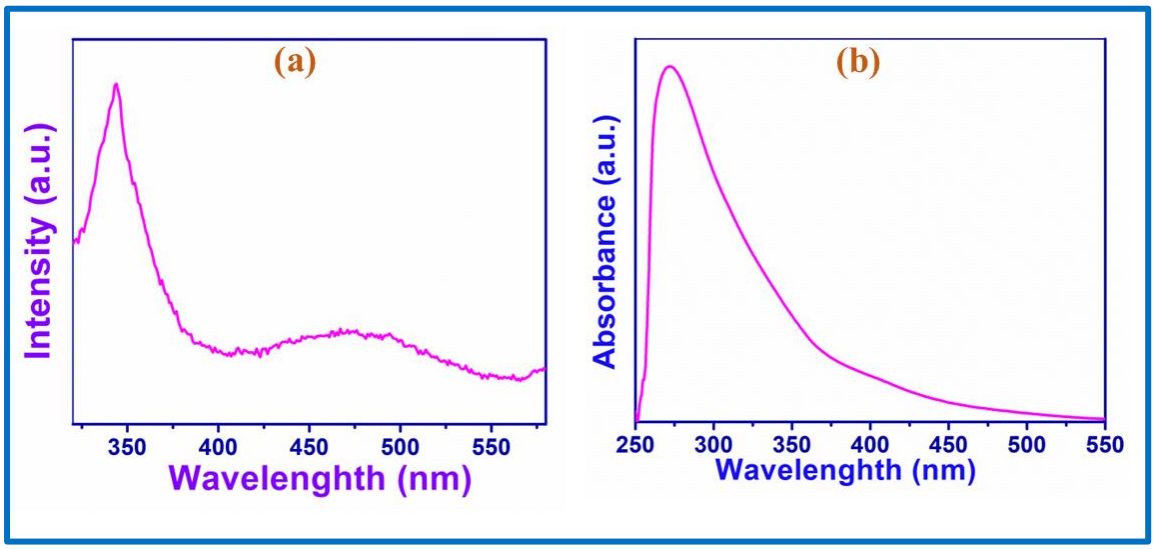

Figure 5.4. (a) UV-visible spectra (b)PL- spectra of PVZn films.

5.5 Performance of the PVZNG

The piezoelectric output performance of PVZNG and magnified view are shown in Figure 5.5 (a) and Figure 5.5(b). It is observed that the PVZn film-based nanogenerator, designated as PVZn1.5 shows the highest amplitude of output voltages among the PVZn films. The open circuit output voltage due to the repeated finger-tapping process is average 50V. Asymmetry of the positive and negative peaks arises due to the type of mechanical impacts, i.e., under fast pressing and slow releasing. These enhancements of output response were attributed due to the synergistic effects between the in situ-formed ZnO nanoparticles and the PVDF matrix [29]. In order to convert AC output voltage into DC output from PVZNG a typical bridge rectifier circuit is employed are shown in Figure 5.5 (c). To test the feasibility of practical implementation of the PVZNG, the piezoelectric energy generated by finger impact is directly utilized to successfully light up several commercial LEDs.

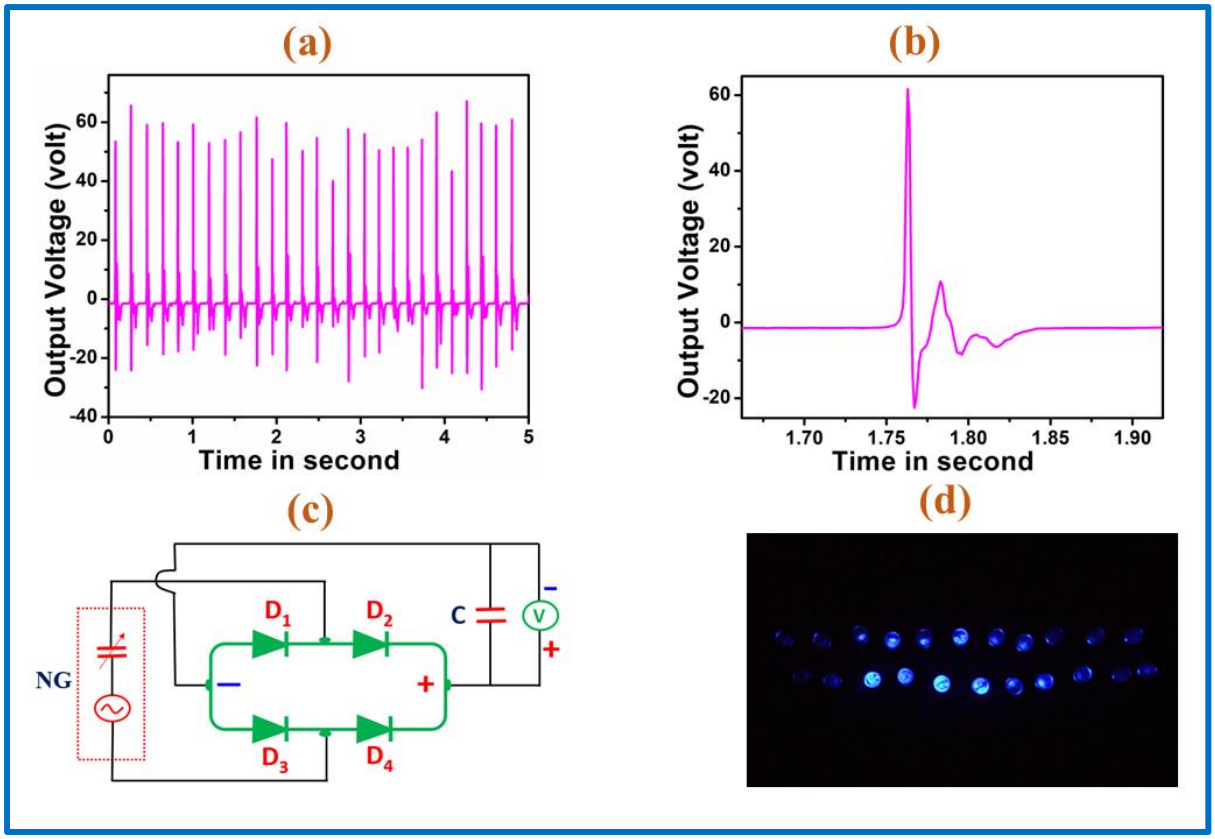

Figure 5.5 (a) Piezoelectric output performance of PVZNG and (b) Magnified View of Piezoelectric output performance of PVZNG (c) The schematic of circuit diagram for capacitor charging. (d)The photograph of glowing LED.

5.6 Conclusion

In summary, we synthesized the *in-situ* formation of ZnO within the PVDF-$ZnCl_2$ composite via the solution casting method. The successful fabrication and characterization of this composite present a highly promising avenue for enhancing optical properties as well as the piezoelectric properties of PVDF. Under a simple repeating finger imparting process, the open circuit output voltage generated from the composite-based nano-generator is 126pprox.. 50V.The output power generated from PVZNG is instantly lights up several blue LEDs. The synergistic interaction between ZnO and the PVDF matrix resulting in a material with multiple uses that has the potential to be useful for energy harvesting, sensors, and optoelectronic devices.

*****

References:

[1]. Fan, F.R., Tang, W. and Wang, Z.L., 2016. Flexible nanogenerators for energy harvesting and self-powered electronics. *Advanced Materials*, *28*(22), pp.4283-4305.

[2]. Tang, X., Wang, X., Cattley, R., Gu, F. and Ball, A.D., 2018. Energy harvesting technologies for achieving self-powered wireless sensor networks in machine condition monitoring: A review. *Sensors*, *18*(12), p.4113.

[3]. Zhu, M., Yi, Z., Yang, B. and Lee, C., 2021. Making use of nanoenergy from human–Nanogenerator and self-powered sensor enabled sustainable wireless IoT sensory systems. *Nano Today*, *36*, p.101016.

[4]. Zheng, Q., Tang, Q., Wang, Z.L. and Li, Z., 2021. Self-powered cardiovascular electronic devices and systems. *Nature Reviews Cardiology*, *18*(1), pp.7-21.

[5]. Wu, M., Yao, K., Li, D., Huang, X., Liu, Y., Wang, L., Song, E., Yu, J. and Yu, X., 2021. Self-powered skin electronics for energy harvesting and healthcare monitoring. *Materials Today* [6]. Liu, C.J., Burghaus, U., Besenbacher, F. and Wang, Z.L., 2010. Preparation and characterization of nanomaterials for sustainable energy production.

[7]. Yun, S., Zhang, Y., Xu, Q., Liu, J. and Qin, Y., 2019. Recent advance in new-generation integrated devices for energy harvesting and storage. *Nano Energy*, *60*, pp.600-619.

[8]. Chandrasekaran, S., Bowen, C., Roscow, J., Zhang, Y., Dang, D.K., Kim, E.J., Misra, R.D.K., Deng, L., Chung, J.S. and Hur, S.H., 2019. Micro-scale to nano-scale generators for energy harvesting: Self powered piezoelectric, triboelectric and hybrid devices. *Physics Reports*, *792*, pp.1-33.

[9]. Zhang, Y., Xie, M., Adamaki, V., Khanbareh, H. and Bowen, C.R., 2017. Control of electro-chemical processes using energy harvesting materials and devices. *Chemical Society Reviews*, *46*(24), pp.7757-7786.

[10]. *Dong, K., Peng, X. and Wang, Z.L., 2020. Fiber/fabric-based piezoelectric and triboelectric nanogenerators for flexible/stretchable and wearable electronics and artificial intelligence. Advanced Materials, 32(5), p.1902549.*

[11]. Rong, P., Ren, S. and Yu, Q., 2019. Fabrications and applications of ZnO nanomaterials in flexible functional devices-a review. *Critical reviews in analytical chemistry*, *49*(4), pp.336-349.

[12]. Wang, Z.L., 2007. Novel nanostructures of ZnO for nanoscale photonics, optoelectronics, piezoelectricity, and sensing. *Applied Physics A*, *88*, pp.7-15.

[13]. Yaqoob, U., Uddin, A.I. and Chung, G.S., 2017. A novel tri-layer flexible piezoelectric nanogenerator based on surface-modified graphene and PVDF-BaTiO3 nanocomposites. *Applied Surface Science*, *405*, pp.420-426.

[14]. Yan, J. and Jeong, Y.G., 2017. Roles of carbon nanotube and BaTiO3 nanofiber in the electrical, dielectric and piezoelectric properties of flexible nanocomposite generators. *Composites Science and Technology*, *144*, pp.1-10.

[15]. Rovisco, A., Dos Santos, A., Cramer, T., Martins, J., Branquinho, R., Águas, H., Fraboni, B., Fortunato, E., Martins, R., Igreja, R. and Barquinha, P., 2020. Piezoelectricity enhancement of nanogenerators based on PDMS and ZnSnO3 nanowires through microstructuration. *ACS applied materials & interfaces*, *12*(16), pp.18421-18430.

[16]. Placke, A., Kumar, A. and Priya, S., 2016. Synthesis and behavior of cetyltrimethyl ammonium bromide stabilized Zn1+ xSnO3+ x (0≤ x≤ 1) nano-crystallites. *Plos one*, *11*(5), p.e0156246.

[17]. Hoque, N.A., Thakur, P., Roy, S., Kool, A., Bagchi, B., Biswas, P., Saikh, M.M., Khatun, F., Das, S. and Ray, P.P., 2017. Er3+/Fe3+ stimulated electroactive, visible light emitting, and high dielectric flexible PVDF film based piezoelectric nanogenerators: a simple and superior self-powered energy harvester with remarkable power density. *ACS applied materials & interfaces*, *9*(27), pp.23048-23059.

[18]. Biswas, P., Hoque, N.A., Thakur, P., Saikh, M.M., Roy, S., Khatun, F., Bagchi, B. and Das, S., 2019. Portable self-powered piezoelectric nanogenerator and self-charging photo-power pack using in situ formed multifunctional calcium phosphate nanorod-doped PVDF films. *Langmuir*, *35*(52), pp.17016-17026.

[19]. Biswas, R., Das, S.K., Bhaduri, S.N., Bhaumik, A. and Biswas, P., 2020. AgNPs immobilized over functionalized 2D Hexagonal SBA-15 for Catalytic C–H oxidation of hydrocarbons with molecular oxygen under solvent-free conditions. *ACS Sustainable Chemistry & Engineering*, *8*(15), pp.5856-5867.

[20]. Saikh, M.M., Hoque, N.A., Biswas, P., Rahman, W., Das, N., Das, S. and Thakur, P., 2021. Self-Polarized ZrO2/Poly (vinylidene fluoride-co-hexafluoropropylene) nanocomposite-based piezoelectric nanogenerator and single-electrode triboelectric nanogenerator for

sustainable energy harvesting from human movements. *physica status solidi (a)*, *218*(9), p.2000695.

[21]. Das, N., Sarkar, D., Saikh, M.M., Biswas, P., Das, S., Hoque, N.A. and Ray, P.P., 2022. Piezoelectric activity assessment of size-dependent naturally acquired mud volcano clay nanoparticles assisted highly pressure sensitive nanogenerator for green mechanical energy harvesting and body motion sensing. *Nano Energy*, *102*, p.107628.

[22]. Sarkar, D., Das, N., Saikh, M.M., Biswas, P., Das, S., Das, S., Hoque, N.A. and Basu, R., 2021. Development of a sustainable and biodegradable sonchus asper cotton pappus based piezoelectric nanogenerator for instrument vibration and human body motion sensing with mechanical energy harvesting applications. *ACS omega*, *6*(43), pp.28710-28717.

[23]. Hoque, N.A., Thakur, P., Biswas, P., Saikh, M.M., Roy, S., Bagchi, B., Das, S. and Ray, P.P., 2018. Biowaste crab shell-extracted chitin nanofiber-based superior piezoelectric nanogenerator. *Journal of Materials Chemistry A*, *6*(28), pp.13848-13858.

[24]. Bahariqushchi, R., Cosentino, S., Scuderi, M., Dumons, E., Tran-Huu-Hue, L.P., Strano, V., Grandjean, D., Lievens, P., Poulin-Vittrant, G., Spinella, C. and Terrasi, A., 2020. Free carrier enhanced depletion in ZnO nanorods decorated with bimetallic AuPt nanoclusters. *Nanoscale*, *12*(37), pp.19213-19222.

[25]. Wang, L.Y., Shi, B.Y., Yao, C.B., Wang, Z.M., Wang, X., Jiang, C.H., Feng, L.F. and Song, Y.L., 2023. Size and morphology modulation in ZnO nanostructures for nonlinear optical applications: a review. *ACS Applied Nano Materials*, *6*(12), pp.9975-10014.

[26]. Buryi, M., Babin, V., Neykova, N., Wang, Y.M., Remeš, Z., Ridzoňová, K., Dominec, F., Davydova, M., Drahokoupil, J., Chertopalov, S. and Landová, L., 2023. Changes to Material Phase and Morphology Due to High-Level Molybdenum Doping of ZnO Nanorods: Influence on Luminescence and Defects. *Materials*, *16*(9), p.3294.

[27]. Shen, H., Shi, X., Wang, Z., Hou, Z., Xu, C., Duan, L., Zhao, X. and Wu, H., 2022. Defects control and origins of blue and green emissions in sol-gel ZnO thin films. *Vacuum*, *202*, p.111201.

[28]. Ansari, S.A., Khan, M.M., Kalathil, S., Nisar, A., Lee, J. and Cho, M.H., 2013. Oxygen vacancy induced band gap narrowing of ZnO nanostructures by an electrochemically active biofilm. *Nanoscale*, *5*(19), pp.9238-9246.

[29]. Sukumaran, S., Chatbouri, S., Rouxel, D., Tisserand, E., Thiebaud, F. and Ben Zineb, T., 2021. Recent advances in flexible PVDF based piezoelectric polymer devices for energy harvesting applications. *Journal of Intelligent Material Systems and Structures*, *32*(7), pp.746-780.

Chapter 6

Conclusion & Future work

6.1 Conclusion:

Modern civilization faces several urgent problems, such as energy shortages and climate change, which have spurred scientists to work on developing sustainable solutions. Biomechanical energy harvesting is a potentially effective method that entails transforming biological sources and human movement into electrical energy. Implantable gadgets, artificial limbs, and wearable sensors might all be powered by this technology. The need to provide sustainable and alternative energy solutions is more important than ever as the world's energy crisis worsens and fossil fuel supplies are quickly depleted. According to recent studies, the finite supplies of fossil fuels may run out within the next 150 years, making the conventional dependence on them more unsustainable. Examining and funding latest technologies that provide renewable and sustainable energy sources is essential in light of this impending crisis situation.

Piezoelectric nanogenerators (PENGs) and triboelectric nanogenerators (TENGs) have proven to be extremely effective in integrating in with wearable low-power devices. As a consequence, they are ideal for powering portable electronics and enabling continuous health monitoring. Even minimal mechanical movements, like walking, running, or the regular pulses of blood flow, may be converted into useful electrical energy using nanogenerators. Not only does the previously stated feature lessen reliance on traditional power sources, but it also opens up possibilities for autonomous health monitoring devices. In order to develop energy harvesting systems with increased efficiency, robustness and flexibility, this research aims to investigate the development and enhancement of piezoelectric nanogenerators (PENGs) and triboelectric nanogenerators (TENGs). By utilizing these technologies, we want to improve wearable health monitoring devices' dependability and performance while also making a major contribution to the overall goal of sustainable energy solutions.

The development and performance of advanced energy harvesting devices were the subject of a novel study that we presented in chapter 2. Specifically, we focused on two nanogenerators: a piezoelectric nanogenerator and a single-electrode triboelectric nanogenerator based on self-polarized ZrO_2-PVDF-HFP nanocomposite, that are intended to capture and transform human mechanical energy into useful electrical power. Using a ZrO_2-PVDF-HFP nanocomposite, the piezoelectric nanogenerator exhibited remarkable performance under periodic mechanical stress, achieving an amazing open-circuit voltage (Voc) of around 120 V and a short-circuit current (Isc) of about 1.95 µA. This device's computed power density of 7091 $\mu W/cm^3$ demonstrated how well it could transform mechanical strain into electrical energy. Due to its high power density, the gadget may find use in applications that call for small, effective energy

sources. This PENG can instantaneously turn on 55 blue light-emitting diodes that are commercially available in the market and connected in parallel using a bridge rectifier. Excellent capacitor charging performance is also noted; for example, a 2.2 μF capacitor may be charged to 3.5 V in under 17 seconds. Simultaneously, the single-electrode triboelectric nanogenerator demonstrated remarkable efficacy, achieving a peak output voltage of around 7 V with simple finger contact. Because of this, it is ideally suited for incorporation into wearable electronics and independently powered sensors, utilizing the triboelectric effect to generate energy from routine motions.

Thorough testing, including biomechanical energy harvesting from dynamic human actions like walking, running, and hand gestures, is used to verify both piezoelectric and triboelecric systems. These nanogenerators have a wide range of practical uses. They have the potential to integrate smart fabrics, wearable technology, and self-powered sensors to provide methods for collecting energy from regular physical activity. Their proven robustness and consistent performance over long durations further increase their viability for practical uses.

In chapter 3, with a focus on wireless gait monitoring applications, the study effectively produced a new piezoelectric energy nanogenerator (PENG) by embedding a nanorose-like copper sulfide (CuS) structure within a polyvinylidene fluoride (PVDF) composite thin film. In addition to improving the material's piezoelectric qualities, the CuS-PVDF composite's innovative design offers a reliable and adaptable platform for energy harvesting from biomechanical motions. By presenting a hydrophobic waterproofed CuS nanoparticle-embedded PVDF composite piezoelectric nanogenerator (CPENG) with a rose-like nanostructure and previously unheard-of sensitivity, this ground-breaking work transforms the field. CuS nanoroses and PVDF dipoles work in concert to enhance the electroactive β-phase production, which gives rise to remarkable interfacial polarization and piezoelectric characteristics. With an open-circuit voltage of 130 V and a short-circuit current of 1.25 μA, this creative design produces an impressive output performance that translates to a power density of 2640.6 μWcm^{-3}. 26 number of blue LEDs in series and 85 LEDs in parallel may be powered by this CPENG, and the output performance increased with the imparted frequency. In addition to its energy collecting capabilities, this adaptable gadget produces distinct waveforms, which makes it a priceless tool for surveillance, gait analysis, and movement tracking applications. Its hydrophobic construction makes it perfect for monitoring athletes and sensitive groups since it can detect little movements like those of the fingers, wrists, and neck. With its enormous potential to improve sports performance, gait analysis, and real-time movement tracking, this CPENG is a game-changer in the area.

In chapter 4, we have created a high-performance EPENG for mechanical energy harvesting in the surrounding environment using PVDF-HFP film doped with Er-ZrO_2 NPs. Er-ZrO_2 NPs are added to the PVDF-HFP matrix to improve the electroactive β-phase and PENG output signals. The generated PENG shows a high value of open circuit voltage (Voc=133 Volt) and short circuit current (Isc= 2.77 μA) with power density ~ 8771 μWcm^{-3} under a periodic finger imparting because of the nucleation of electroactive β phase and substantial interfacial polarization. This designed PENG can charge a capacitor and illuminate a huge number of LEDs quickly using a bridge rectifier. Any activity, including touching, drinking, talking, coughing, swallowing, and blood pressure pulse, may be converted into electrical energy with this EPENG. It may also be applied to sensor applications and voice recognition. The next effort will focus on developing a hybrid TENG based on Er-ZrO_2/PVDF-HFP composite. This intriguing technique offers a large-scale power source that can convert modest mechanical energy from human activities into electrical energy, enabling the realization of a self-powered system.

In chapter 5, we produced ZnO in situ using the solution casting technique for developing a PVDF-$ZnCl_2$ composite. A very promising path for improving PVDF's optical and piezoelectric capabilities has been opened up by the successful production and characterization of this combination. The open circuit output voltage produced by the composite based nano-generator is around 50V when subjected to a basic repetitive finger imparting operation. Several blue LEDs were instantaneously lit up with the output power produced by PVZNG. The material having numerous applications, including energy harvesting, sensors, and optoelectronic devices, is a consequence of the synergistic interaction between ZnO and the PVDF matrix. The study mainly demonstrates how the in-situ synthesis of ZnO inside the PVDF matrix significantly improves the material's piezoelectric characteristics. This enhancement is caused by the synergistic interaction between PVDF and ZnO, which improves dipole alignment and increases the crystallinity of the piezoelectric phase. Furthermore, the composite has improved optical characteristics because to the ZnO nanoparticles. Because of this, it may be applied in situations where piezoelectric responsiveness and light absorption are crucial. The piezoelectric nanogenerator (PENG), which is made of ZnO and PVDF, is a high-performance device that can quickly light up 20 light-emitting diodes and has an amazing open-circuit voltage (Voc) of around 50 V.

6.2. Future work plan:

The primary goal of my future research strategy is to enhance health monitoring technologies by developing triboelectric nanogenerators (TENGs) that integrate innovative 2D energy materials. The main goal is to improve the dielectric characteristics and overall performance of Tensor Electron Generators (TENGs) by optimizing lead-free materials like Siloxane, MXene, and other two-dimensional structures. This optimization will entail customizing the composition and structure of these materials to enhance electron transport, thereby optimising the energy conversion efficiency in TENGs. The research will concentrate on the fabrication of two distinct categories of triboelectric nanogenerators (TENGs): hybrid mode TENGs (HTENGs) and single electrode TENGs (STENGs). High-temperature electrochemical nanogenerators (HTENGs) will integrate vertical contact-separation and lateral sliding modes, whilst solid-state electrogenerators (STENGs) will employ 2D lead-free material nanoparticles to attain enhanced flexibility and sensitivity.

The manufactured triboelectric nanogenerators (TENGs) will be included into wearable health monitoring devices, where their capacity to quantify several physiological characteristics will be evaluated. The proposed systems aim to monitor various activities including joint movements, body rotations, and extensions. These systems have the potential to be applied in gesture recognition and facilitate sign language support for persons who have communication impairments. By integrating stretchable and malleable polymers such as PDMS and Ecoflex, these triboelectric nanogenerators (TENGs) would provide improved comfort and flexibility when used on human skin, ensure their practical usefulness in continuous health monitoring.

Moreover, the study will investigate the creation of a complete real-time health monitoring system that integrates self-powered TENG-based devices with wireless communication, signal capture technologies, and data processing based on machine learning. The purpose of this system is to facilitate immediate notifications for possible health crises, therefore making a valuable contribution to preventative healthcare. The primary objective is to introduce these health monitoring technologies based on TENG (Triboelectric Nanogenerators) to the market. These technologies provide sustainable, environmentally friendly, and economically viable solutions that can be extensively used in clinical and consumer health applications. Consequently, this will significantly progress the field of sustainable healthcare and enhance patient outcomes.

Publication

physica status solidi a
www.pss-a.com

Self-Polarized ZrO_2/Poly(vinylidene fluoride-*co*-hexafluoropropylene) Nanocomposite-Based Piezoelectric Nanogenerator and Single-Electrode Triboelectric Nanogenerator for Sustainable Energy Harvesting from Human Movements

Md. Minarul Saikh, Nur Amin Hoque, Prosenjit Biswas, Wahida Rahman, Namrata Das, Sukhen Das,* and Pradip Thakur**

Piezoelectric nanogenerators (PENGs) have been emerged as one of the most promising approach for harvesting energy from the movement of living system for low-power electronic devices. Herein, a simple PENG and single-electrode triboelectric nanogenerator (STENG) are reported that execute tremendous output performance. In zirconium oxide (ZrO_2)/poly(vinylidene fluoride-*co*-hexafluoropropylene) (PVDF-HFP) nanocomposite polymer, ZrO_2 acts as the nucleating agents for electroactive polymorph nucleation and also enhances the dielectric constant (≈23). Compared with previously reported PVDF-HFP-assisted prototype nanogenerators, this developed PENG exhibits excellent piezoelectric energy-harvesting performance with very high power density, high energy conversion efficiency and high durability. The PENG exhibits a large value of open-circuit voltage ≈120 V and short-circuit current ≈1.95 μA under periodic finger imparting with high power density ≈7091 μW cm^{-3}. Fabricated flexible PENG is capable to instantaneously light up commercially available 55 number of blue light emitting diode connected in parallel connection through bridge rectifier. High capacitor charging performance is also observed, such as 2.2 μF capacitor charged up to 3.5 V, in just 17 s time interval. Single-electrode-based TENG fabricated by this composite film also shows remarkable output voltage ≈7 V under finger touch.

1. Introduction

The aspiration for wearable, portable, flexible, sustainable self-powered nanodevices such as sensors, mobile phones, rollup displays, wearable electronic products, calculators, actuators, wristwatches, implantable medical goods, and speakers have prompted wide investigation of the pollution-free green energy sources.[1–5] For sustainable development of modern human civilizations, alternative energy resources have become more and more important rather than fossil fuels (stored solar energy, e.g., coal, petroleum, gas, etc.) as they are "limited resources" and cause pollution when they are used.[6–8] Harvesting energy from the ambient environment by the piezoelectric nanogenerators (PENGs) becomes a viable solution for the quick development of low-power electronic devices.[6] The most recent progress in the study of the development of environment friendly, biocompatible, light weight, durable, flexible, thin self-powered nanogenerators are capable of harvesting energy from the easily available resources in nature and our living environment system.[9–11] These resources are sea-water

M. M. Saikh, Dr. N. A. Hoque, P. Biswas, Dr. W. Rahman, N. Das, Prof. S. Das
Department of Physics
Jadavpur University
Kolkata 700032, India
E-mail: nuramin03@gmail.com; sdasphysics@gmail.com

M. M. Saikh
Department of Physics
Government General Degree College at Pedong
Kalimpong 734311, India

The ORCID identification number(s) for the author(s) of this article can be found under https://doi.org/10.1002/pssa.202000695.

DOI: 10.1002/pssa.202000695

Dr. N. A. Hoque
Department of Marine Information Technology
Ocean College
Zhejiang University
Zhoushan 316021, P. R. China

P. Biswas
Department of Physics
Kalimpong College
Kalimpong 734301, India

Dr. P. Thakur
Department of Physics
Netaji Nagar College for Women
Kolkata 700092, India
E-mail: pradipthakurju@gmail.com

wave, solar energy, geothermal energy, rain fall, biomass energies, nuclear energy, thermal energy, transportation, and mechanical resources in terms of human body movement (touching, walking, talking, breathing, finger imparting, pushing, pumping, jogging, stretching, bending, twisting, etc.).[11–13] Thus, the modern trends enter into the development of green energy-harvesting device. There is a variety of energy-harvesting nanogenerators, which have been developed using triboelectric,[3,6,8–13] piezoelectric,[1,3–5,7] and pyroelectric effects.[14–16] Among these, nanogenerators, triboelectric nanogenerators (TENGs) and PENGs are suitable for harvesting energy from mechanical and biomechanical motions. There may be some possibilities of the hybridization of piezoelectric and triboelectric effect in same unit and these types of studies are recently done by many scientists. TENGs are showing large output with excellent conversion efficiency but TENGs have a number of drawbacks like low durability, shelling problem for working in open environment, and humidity affects them easily.[17,18] Most of the TENGs are developed by the two layers of differently polarized triboelectric materials for electric induction to form a close circuit for electron flow.[19] Single-electrode TENGs (STENGs) are suitably chosen for wearable electronics because they can be easily developed on flexible substrates via low-cost simple integration methods with high efficiency for the moving bodies.[19–22] Thus, to attain highly sensitive, long lasting, low power consuming, self-powered system, and device with high energy conversion coefficient, PENGs have come to light as a promising green technique for harvesting electrical energy from mechanical energy resources via piezoelectric effect.[23–25] The use of common piezoelectric materials or ceramics (such as ZnO,[1] $BaTiO_3$,[26] PMN-PT,[27,28] PZT,[29] and (Na,K)NbO[5]) has been studied for the construction of prototype flexible self-powered PENGs.

Recently, poly(vinylidene fluoride) (PVDF) and its copolymers poly(vinylidene fluoride-*co*-hexafluoropropene) (PVDF-HFP), poly(vinylidene fluoride-trifluoroethylene) (PVDF-TrFE), poly (vinylidene fluoride-chloride trifluoride ethylene) (PVDF-CTFE), poly(vinylidene fluoride-trifluoro ethylene-chlorofluoroethylene) (PVDF-TrFECFE), and poly(vinylidene fluoride-trifluoroethylene-chloride trifluoride ethylene) (PVDF-TrFE-CTFE)[30–36] have emerged as the most favorable prospect for designing sophisticated PENGs because of their piezoelectric properties such as light weight, flexible, and environmental compatible.[37]

Semicrystalline PVDF has mainly five different types of crystalline polymorphs like α, β, γ, δ, and ε. Among these crystalline polymorphs, nonpolar α phase is the most common and stable polymorph of PVDF which has a monoclinic unit cell with TGTG′ (T-trans, G-gauche+, G′-gauche) dihedral conformation. The polar polymorph β phase and γ phase have an orthorhombic unit cell with all-trans (TTTT) conformation and TTTGTTG′ conformation, respectively.[38–42] Among all the crystalline polymorphs of PVDF, β phase shows attractive piezoelectric properties due to its highest polarization per unit cell (8×10^{-30} cm). The β phase is an excellent piezoelectric coeffcient with lowest melting point than the γ–phase.[39,42] So, the electroactive β and γ phases are important for the development of PVDF-based PENGs.

Recently, nanofillers have been the main focus for improving the functionalities of PVDF by stabilizing the β-polymorph, which is a very essential part for improving the piezoelectric energy-harvesting properties of PVDF-based nanocomposites.[40–42] Several researchers have attempted to improve the piezoelectric energy-harvesting performance by stabilizing electroactive phases of PVDF by adding nano- or microfillers, stretching, melt quenching, and blending with polymers which consist of carbonyl groups, application of high pressure, solution growth, electrospinning, addition of metal salts, and polarization via an applied field.[38–43] In this work, we use zirconium oxide (ZrO_2) nanoparticles (NPs) as nanofiller, to improve polar and electroactive β phase nucleation in PVDF-HFP polymer.[43] ZrO_2 is an industrial ceramic material. It has novel properties such as high oxygen ion conductivity, low thermal conductivity, high strength, high fracture toughness, high coefficient of thermal expansion, high thermal stability, and high thermal shock resistance.[44–46] Due to these properties, it is used for engineering purposes such as cutting tools, thermal barrier coating, automobile engine parts, refractory material, wire-drawing dies, and automobile engine parts.[40–42] Its additional uses are in jewelry, abrasion resistant materials, sands, and refractory ceramics for its high refractive index, toughness, and good wear resistance.[47–50] ZrO_2 NPs are also used in optically transparent devices, oxygen sensors, and fuel cells for their high refractive index and high oxygen-ion conductivity.[51–54] ZrO_2 nanoparticle is also a component of PZT which is known as good piezoelectric material.[27] Here, ZrO_2 NPs act as a nucleating agent.[43]

In this article, electroactive β polymorph ZrO_2 NPs/PVDF-HFP composite thin film has been synthesized via solution-casting method. Addition of ZrO_2 NPs in PVDF-HFP enhances the electroactive β polymorph. With the increment of electroactive β polymorph, dielectric constant also increases. Then, highly flexible ZrO_2 NPs/PVDF-HFP composite thin film-based PENG is designed to harvest electrical energy from mechanical energy. The fabricated PENG shows high output performance as well as long durability. Also, STENG has been fabricated by same composite film casted on ITO-coated PET surface. Only one triboelectric layer is used because epidermis layer can serve as another triboelectric layer. The flexible, light weight, and simple fabricated STENG shows the high output voltage by just touching on it with a finger. Thus, the designed ZrO_2 NPs/PVDF-HFP composite-based STENG can be used as energy collector and supplier as well as pressure sensor.

2. Experimental Section

2.1. Materials

Zirconium(IV) oxychloride octahydrate ($ZrOCl_2.8H_2O$); PVDF-HFP pellets (Aldrich, Germany. M_w: 455 000 GPC, M_n: 110 000); hydrazine hydrate (>99% pure) (N_2H_4) (Merck, India), and dimethyl sulfoxide (DMSO) (Merck, India).

2.2. Preparation of ZrO_2 Nanoparticles:

To synthesize ZrO_2 nanoparticles, at first 4.834 g of solid $ZrOCl_2.8H_2O$ salt was dissolved in 150 mL of deionized water to obtain 0.1 M aqueous solution under constant magnetic stirring at room temperature. After 2 h 6 mL hydrazine hydrate

(N_2H_4) was added drop wise to this aqueous solution. Then the solution was stirred at the same speed and same temperature for 4 h. Additional 6 mL hydrazine hydrate was added to this solution to complete the reaction. After that, the solution was put into an autoclave and kept in an electric oven at 160 °C for 24 h to carry out hydrothermal reaction. From this autoclave, we obtained the white ZrO_2 NPs precipitate. The precipitate was collected by repeated centrifugation and washing with deionized water to remove the unreacted part. Finally, the ZrO_2 NPs were dried at 80 °C in a hot air oven.

2.3. Synthesis of PVDF-HFP ZrO_2 Nanocomposite Films

First, 0.25 g of PVDF-HFP was dissolved in 5 mL DMSO and stirred at 60 °C to obtain a clear solution. Then the desired amount of ZrO_2 NPs (1–15 mass%) was added to the obtained clear PVDF-HFP solution and stirred for 12 h at 60 °C to form a homogeneous mixture. Then the homogeneous mixture was casted on clean petri dishes and was kept in a hot air oven at 80 °C for 12 h to obtain a nanocomposite thin film. Thicknesses of the PVDF/ZrO_2 nanocomposite thin films were measured by field emission scanning electron microscope (FESEM) micrograph image. FESEM micrograph showed the film thickness ≈50–60 μm which are shown in Figure S1, Supporting Information. In the similar way, a pure PVDF-HFP film was also drop casted in a petri dish. All the synthesized thin films were stored in a vacuum desiccator for further characterizations. Sample designations are shown **Table 1**.

2.4. Fabrication of PENG

At first, standardized PVDF-HFP/ZrO_2 film (PZ10) was taken with the dimension of (2.5 cm × 2.6 cm × 54 μm). Then, the two aluminum electrodes with slightly small area (2.4 × 2.5 cm^2) were attached to both sides of the film and two wires were connected to the electrodes. After that, the film and electrodes were shielded with the polydimethyl siloxane (PDMS) ($[Si(CH_3)_2O]_n$) (Sylgard 184, Dow Corning, ratio of 1:10) and dried at 60 °C for 45 min in a dust-free hot air oven. Finally, we obtained the PENG with dimension of 5 × 3 × 0.3 cm^3.

2.5. STENG Device Fabrication

For the fabrication of STENG, 750 μL PZ10 sample was solution-casted on an ITO-coated pet substrate (1.5 × 2 cm^2) and cured at 80 °C till it completely dried. A copper wire was attached on to ITO-coated PET surfaces for further output characterizations.

Table 1. Designation of the sample and different amounts of ZrO_2 NPs added in PVDF-HFP matrix.

Sample designation	Amount of PVDF-HFP [g]	Percentage of ZrO_2 NPs [mass%]	Amount of ZrO_2 NPs [g]
PZ0 (Pure PVDF-HFP)	0.2500	00	0.0000
PZ1	0.2500	01	0.0005
PZ5	0.2500	05	0.0125
PZ10	0.2500	10	0.0250
PZ15	0.2500	15	0.0375

3. Characterizations

The surface morphological microstructure of the pure PVDF-HFP and PVDF-HFP/ZrO_2 nanocomposite thin films were studied by FESEM (INSPECT F50, the Netherlands). The Crystallographic structure patterns of the samples were collected by X-ray diffraction (XRD) (Model-D8, Bruker AXS Inc., Madison, WI) and Fourier transform infrared spectroscopy (FTIR) (FTIR-8400S, Shimadzu). The total crystallinity and thermal stability of the PVDF-HFP/ZrO_2 composite thin films were measured using a differential scanning calorimetry (DSC) (DSC-60, Shimadzu, Singapore). The degree of crystallinity (X_c) was calculated by the ratio of the enthalpy of fusion (ΔH_m) to the melting enthalpy $\Delta H100\%$ of 100% crystalline PVDF with the value 104.6 J g^{-1}. The dielectric constant, tangent loss, and AC conductivity of the samples were measured using digital LCR meter (Agilent, E4980A).

4. Results and Discussions

4.1. FESEM Morphology

Figure 1 shows the FESEM micrograph of ZrO_2 NPs, pure PVDF-HFP film (PZ0), PZ1, PZ5, PZ10, and PZ15 films. FESEM image of ZrO_2 shows the formation of uniform and smaller ZrO_2 NPs with diameter ≈50–60 nm. In pure PVDF-HFP film, the diameter of the spherulites are about ≈40 μm which correspond to the presence of nonpolar α phase.[38] Figure 1c–f shows the dispersion and the distribution properties of NPs in the PVDF-HFP matrix. Formation of spherulites with lower diameter ≈4–6 μm and uniform distribution of the NPs have been noticed in composite films confirming nucleation of electroactive β phase.[31,35] Further detailed structure and β phase formation were confirmed by FTIR spectra, XRD pattern, and DSC results.

4.2. XRD Analysis

XRD patterns of pure PVDF-HFP and ZrO_2 NPs/PVDF-HFP nanocomposite films are shown in **Figure 2**a. The diffraction peaks at $2\theta = 17.7$, 18.4, 19.9, and 26.4° in pure PVDF-HFP composite films correspond to the (100), (020), (110), and (021) reflections crystalline plane of α-crystalline phase.[42] All the diffraction peaks of pure PVDF-HFP are similar to the standard diffraction peaks of α-PVDF.[49] The intensity of all the diffraction peaks correspond to α and γ phases which decrease after the addition of ZrO_2 NPs in the PVDF-HFP matrix. But the intensity of the diffraction peak at $2\theta = 20.4°$ corresponds to the superposition of the (110) and (200). Crystalline plane (200) is appeared strongly, suggesting the conformation of the polar β phase in the nanocomposite. PZ10, i.e., 10% ZrO_2 NP-loaded nanocomposite film shows a maximum intensity of main β-crystalline diffraction peak.

The nucleation of β phase is quantitatively measured by the ratio ($I_{20.5}/I_{18.2}$), where $I_{20.5}$ and $I_{18.2}$ are the intensities of the peak at 20.5° (200) and 18.2° (020), respectively. This ratio is about 0.499, as shown in Figure 2b, for pure PVDF-HFP. Figure 2b shows that the value of this ratio depends upon the loading wt% of ZrO_2 NPs. Highest value of this ratio is 2.92 found for the sample PZ10.

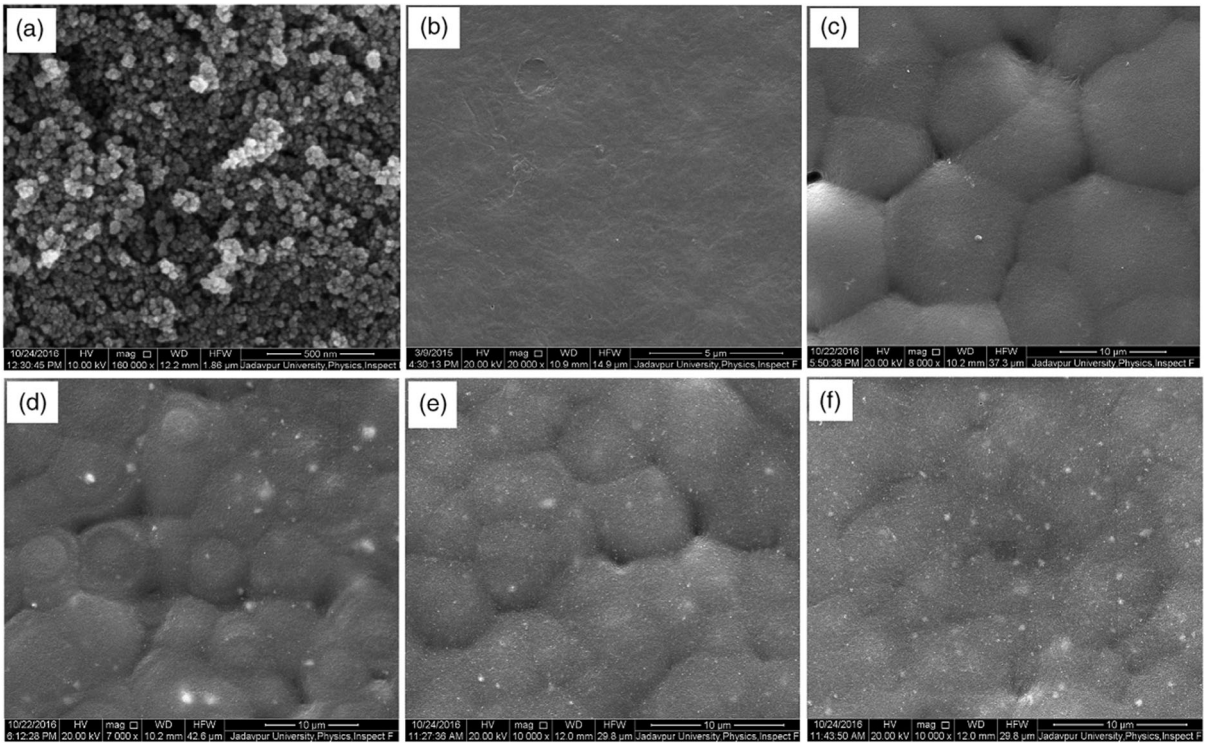

Figure 1. FESEM images of a) Pure ZrO_2 NPs; b) Pure PVDF-HFP thin film; c) PZ1; d) PZ5; e) PZ10; and f) PZ15.

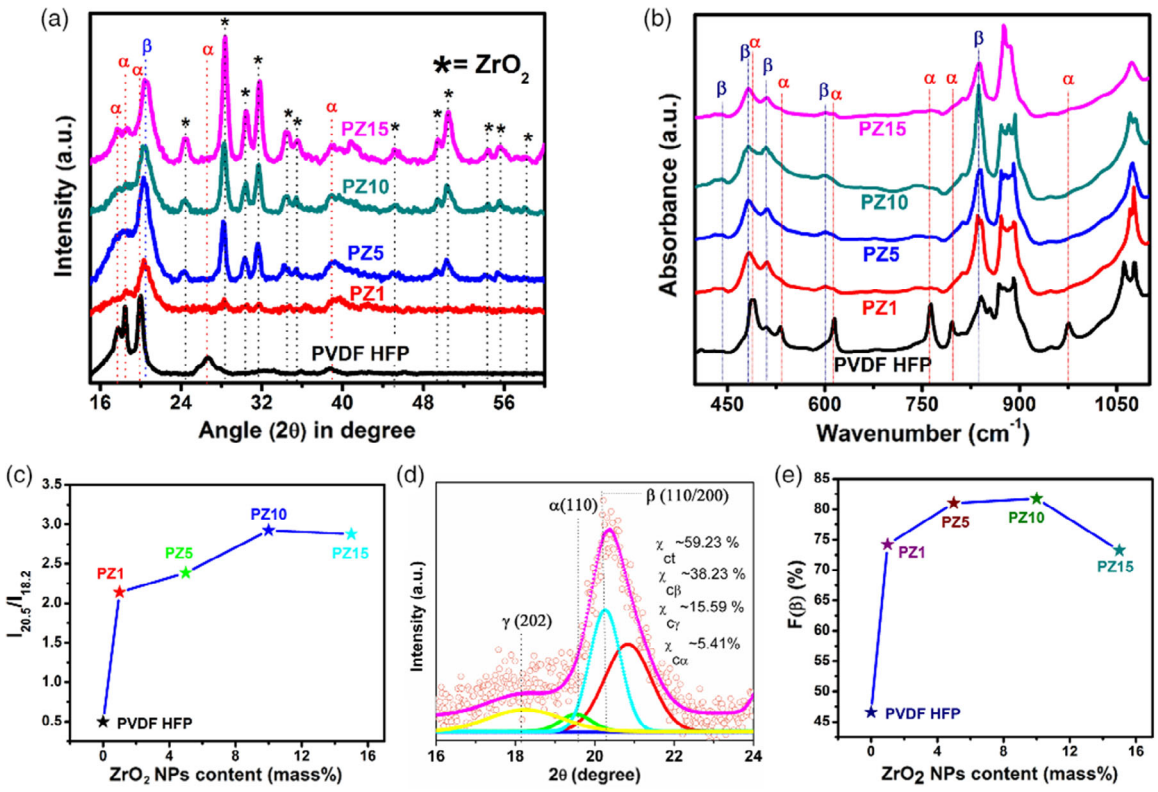

Figure 2. a) XRD pattern of pure PVDF-HFP and ZrO_2 NPs-doped PVDF-HFP thin films (PZ1, PZ5, PZ5, PZ10, and P15). b) Ratio of I20.5 and I18.2 of the samples. c) FTIR spectra of pure PVDF-HFP and ZrO_2/PVDF-HFP composite thin films (PZ1, PZ5, PZ5, PZ10, and P15). d) Evaluation of β-phase content of the samples.

4.3. FTIR Analysis

Figure 2c shows the FTIR spectra of the pure PVDF-HFP and ZrO_2 NPs/PVDF-HFP composite thin films. The absorbance bands for nonpolar α phase of pure PVDF-HFP thin film are at 488 cm^{-1} (CF_2 waging), 532 cm^{-1} (CF_2 bending), 615 and 764 cm^{-1} (CF_2 bending and skeletal bending), 796 and 976 cm^{-1} (CH_2 rocking).[34] The characteristic absorbance bands at 840 cm^{-1} (CH_2 rocking, CF_2 stretching, and skeletal C═C stretching) and 813 cm^{-1} (CF_2 asymmetric stretching)[10] correspond to the electroactive (or polar) phase of β and γ configurations, respectively. All the characteristic absorbance bands indicate that the pure PVDF-HFP is composed of the maximum amount nonpolar α-phase and a very small amount of polar β and γ phases. The characteristic absorbance bands of electroactive β phase of the ZrO_2 NPs/PVDF-HFP composite thin films have appeared prominently at 445 cm^{-1} (CF_2 rocking and CH_2 rocking), 479 cm^{-1} (CF_2 deformation), 510 cm^{-1} (CF_2 stretching), 600 cm^{-1} (CF_2 wag), and 840 cm^{-1} (CH_2 rocking, CF_2 stretching, and skeletal C═C stretching).[27,28,51] The maximum intensity of the main characteristic band at 840 cm^{-1} of β phase confirms the improvement of the β phase. In contrast, the characteristic absorbance bands at 532 cm^{-1} (CF_2 bending), 615 and 764 cm^{-1} (CF_2 bending and skeletal bending), 796 and 976 cm^{-1} (CH_2 rocking) are absent in the ZrO_2 NP-loaded PVDF-HFP composite thin films. Thus, the absence of all the characteristic absorbance bands corresponding to the α phase and the appearance of the characteristic absorbance bands corresponding to the β phase suggest that the improvement of the polar β-phase crystallization in PVDF-HFP matrix is due to the nucleating effect of the ZrO_2 NPs.[43] Figure 2c shows that the maximum intensity of the main characteristic band for β-phase is found for PZ10 sample. This result supports the XRD outcome.

The improvement of electroactive β phase may be quantified by the fraction β phase ($F(\beta)$). The fraction β phase ($F(\beta)$) was evaluated from FTIR spectra using Lambert–Beer law, given in Equation (1)[32]

$$F(\beta) = \frac{A_\beta}{\left(\frac{K_\beta}{K_\alpha}\right)A_\alpha + A_\beta} \times 100\% \quad (1)$$

where A_α is the absorbance at 764 cm^{-1}, A_β is the absorbance at 840 cm^{-1}, and K_β equals 7.7×104 $cm^2\,mol^{-1}$, and K_α equals 6.1×104 $cm^2\,mol^{-1}$ as the absorption coefficients at 840 and 764 cm^{-1}, respectively.

Figure 2d shows the variation of β phase fraction ($F(\beta)$) with the ZrO_2 NPs content (vol%). The value of $F(\beta)$ is found to be 46.58% for the pure PVDF-HFP composite matrix. This $F(\beta)$ value increases with the loading of NPs up to 10 mass% of ZrO_2 NPs content and then decreases. Maximum value of $F(\beta)$ is 82%, found for PZ10 sample. This result is also well matched with the XRD results. Strong electrostatic interaction between the polymer chains and the negatively charged leads to the alignment of TTTT conformation, i.e., nucleation of electroactive β phase in composite samples. The possible interaction and self-polarization of the polymer matrix in presence of ZrO_2 NPs are schematically shown in Figure S2, Supporting Information.

4.4. DSC Analysis

Figure 3a shows the DSC thermograph of pure PVDF-HFP and ZrO_2 NP-loaded PVDF-HFP composite films. The melting peak at 164.5 °C in the pure PVDF-HFP thermograph corresponds to nonpolar α polymorph of PVDF-HFP.[28] With the addition of ZrO_2 NPs in polymer matrix, the melting peak is shifted to the higher temperature. This phenomenon suggests that the morphological change occurs in the crystallinity of PVDF-HFP, i.e., the change of nonpolar α crystal morph (TGTG conformation) into β crystal morph (TTTT conformation). This is in good conformity with XRD results. Thus, with the loading of ZrO_2 NPs, the melting temperature (T_c) changes from 150.8 to 153.5 °C. This result suggests that the ZrO_2 NPs play an important role as nucleating agent for PVDF-HFP. The degree of crystallinity (X_c) was quantitatively measured by Equation (2)[40]

$$\chi_c = \frac{\Delta H_m}{\Delta H_{100\%}} \times 100\% \quad (2)$$

where ΔH_m is the melting enthalpy or enthalpy of fusion and $\Delta H_{100\%}$ is the melting enthalpy of 100% crystalline PVDF with the value of 104.6 J g^{-1}. Figure 3b,c shows the enthalpy of fusion (ΔH_m) and the degree of crystallinity (χ_c) of the pure and

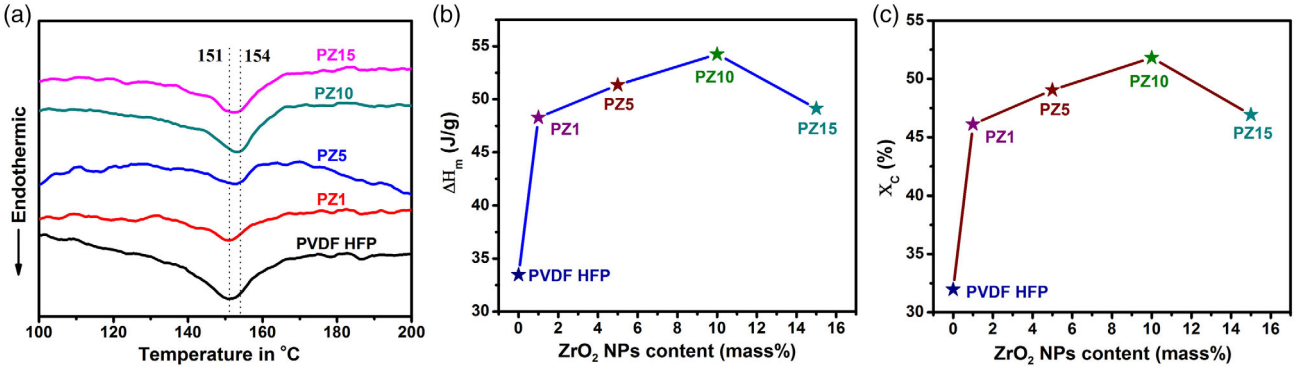

Figure 3. a) DSC thermographs of pure PVDF-HFP and ZrO_2 NPs/PVDF-HFP composite thin films. b) Evaluation of enthalpy of fusion and c) degree of crystallinity of pure PVDF-HFP and ZrO_2 NP-loaded PVDF-HFP thin films.

composite PVDF-HFP film. Figure 3c shows that the enthalpy of fusion and the degree of crystallinity (χ_c) increase up to 10 mass% loading of ZrO_2 NPs in PVDF-HFP matrix and then decrease for further loading of the ZrO_2 NPs. The maximum degree of crystallinity (χ_c) was obtained 67% for PZ10.

4.5. Dielectric Behavior

Using a digital LCR meter (Agilent, E4980A), capacitance (C) and tangent loss ($\tan\delta$) were obtained in the frequency range of 20–2 MHz at 1 V of AC voltage around the two electrodes. The dielectric constant (ε_r) and AC conductivity (σ_{ac}) were determined by Equation (3) and (4), respectively

$$\varepsilon_r = \frac{C \times d}{\varepsilon_0 A} \tag{3}$$

$$\sigma_{ac} = 2\pi f \varepsilon_r \varepsilon_0 \tan\delta \tag{4}$$

where A and d are the area and thickness of the film, respectively; f (in Hz) is the applied frequency; and ε_0 is the permittivity of free space (8.854×10^{-10} F m^{-1}).[41]

The dielectric constant of the ZrO_2 NPs/PVDF-HFP nanocomposite film increases with the increase in ZrO_2 NPs doping concentration for 10 mass% ZrO_2 NPs loading in PVDF-HFP matrix and then reduces for higher doping (**Figure 4**a). With the increase in frequency, the dielectric constant of the sample decreases (Figure 4a). The increase in dielectric constant with doping concentration and the reduction of it with increase in frequency can be explained by Maxwell–Wagner–Sillars (MWS) interfacial polarization. In the low-frequency range, the electric dipoles follow the applied AC electric field and move effortlessly for a large period of time toward the electrode. In contrast, at the higher-frequency range, the electric dipoles are unable to follow the AC electric field frequency and lag behind the electric field. As a result, there is a decrease in dielectric constant. The increment of dielectric constant occurs for up to 10 mass% of ZrO_2 NP-loaded PVDF-HFP matrix which is probably due to the formation of maximum electroactive β phase of PVDF-HFP (Figure 4b). For the same reason, tan δ of the samples decrease with increasing frequency which is represented in Figure 4c. Highest dielectric constant has been developed $\varepsilon \approx 23$ for PZ10 at 20 Hz. Figure 4d shows the frequency response of AC conductivity (σ_{ac}) of the pure PVDF-HFP and ZrO_2 NP-modified PVDF-HFP samples. Due to MWS effect between the interface of the ZrO_2 NPs and the PVDF-HFP polymer chain AC conductivity (σ_{ac}) increases with the frequency.[26]

4.5.1. Performance of the PENG

The device fabrication procedures are discussed in the Experimental Section. Transparencies of different concentrations of ZrO_2/PVDF-HFP composite thin films are shown in **Figure 5**a,b, which shows the schematic illustration of the fabricated device. Among all the composites films, PZ10 shows the highest electroactive β phase and enhanced value of dielectric constant. Also, PZ10 sample shows good piezoelectric coefficient (d_{33}) ≈72.5 pC/N at 50 Hz under constant applied force 0.5 N (Piezotest, PM300). According to the aforementioned results,

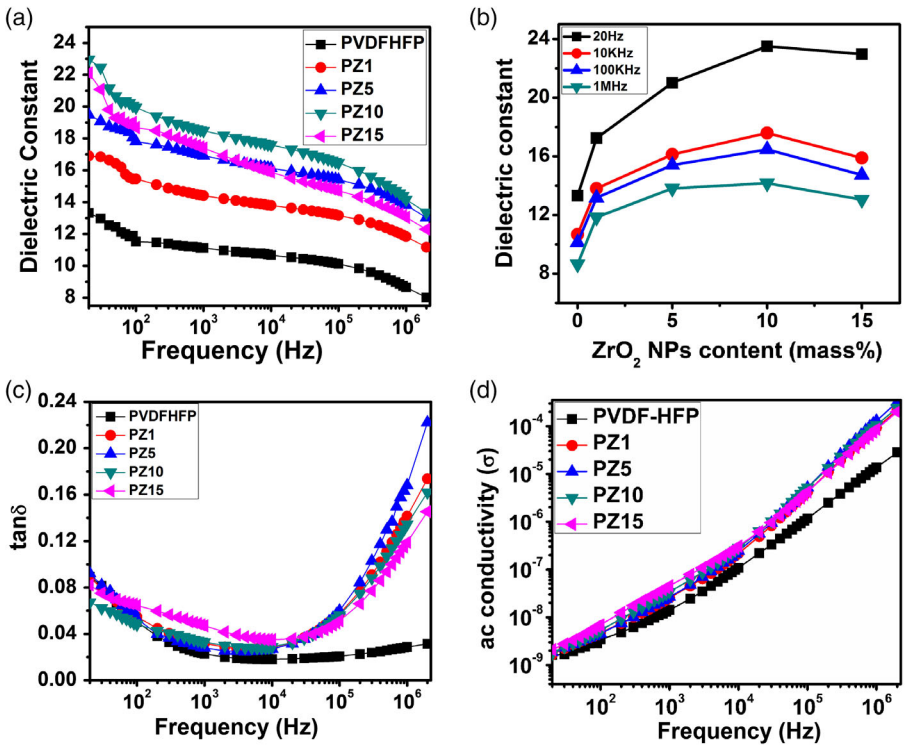

Figure 4. Frequency dependence of dielectric properties of pure PVDF-HFP and ZrO_2/PVDF-HFP nanocomposite thin films; a) dielectric constant, b) tangent loss, and c) AC conductivity.

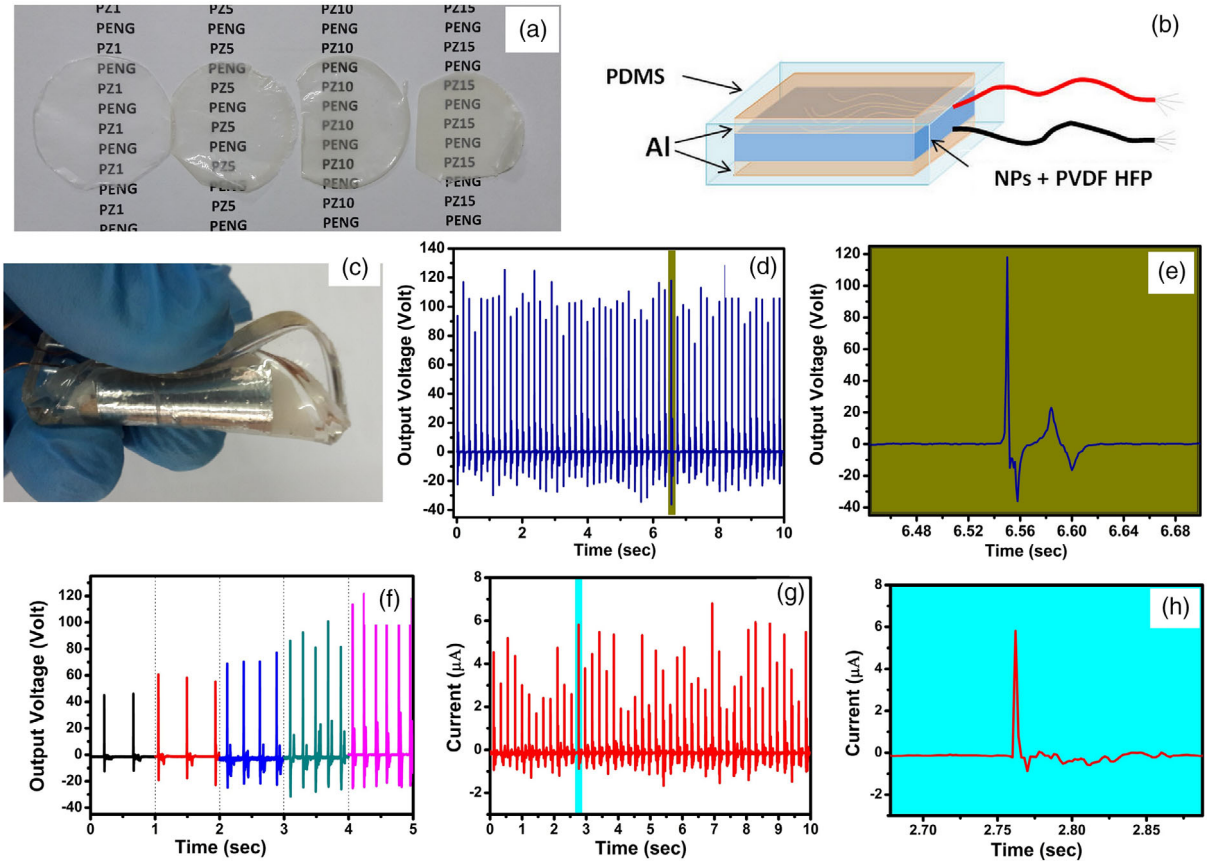

Figure 5. a) Transparency nature of ZrO_2/PVDF-HFP nanocomposite thin films; b) schematic diagram of the fabricated; c) Photograph of fabricated PENG. d) Open-circuit output voltage (V_{oc}). e) Magnified view of open-circuit output voltage (V_{oc}). f) Frequency-dependent output voltage (V_{oc}). g) Short-circuit output current (I_{sc}) of PENG under the finger impetrating. h) Magnified view of short-circuit output current (I_{sc}).

PZ10 film has been chosen to fabricate PENG and characterized for piezoelectric response and piezosensitivity. In Figure 5c, the flexibility of the fabricated PENG is shown. Figure 5d shows the open-circuit output voltage response of fabricated PENG under the continuous finger imparting (frequency ≈6 Hz) and is detected by digital storage oscilloscope (DSO) (Keysight, Oscilloscope DSO-X 3012 A). Magnifying open-circuit voltage is shown in Figure 5e. In magnifying voltage=time, a tiny second peak of voltage generation has been observed which may be due to the damping force present in the PENG after releasing the finger and the vibration present in the free device. Short-circuit current output performance and magnifying view of PENG are also measured (recorded by Keysight, Electrometer B2985) and graphically shown in Figure 5g,h, respectively. Under the periodic finger imparting, the fabricated PENG generates a positive open-circuit voltage (V_{oc}) ≈120 V and short-circuit current (I_{sc})–1.95 μA (imparting frequency ≈6 Hz), corresponding to the instantaneous power density ≈7091 μW cm^{-3}. The maximum instantaneous power density obtained by fabricated PENG is larger than the previously reported PVDF/AlO-rGO composite PENG by Karan et al. and many others and the comparative tabulated forms are shown in Supporting Information T1.[55–60] Frequency-dependent output voltage performance is also observed from 1 to 6 Hz of the fabricated PENGs by finger imparting (imparting force ≈28 N), as shown in Figure 5f. Maximum output voltage has been obtained at 6 Hz frequency. Possible mechanism and explanation of frequency-dependent output performance is described in the energy-harvesting mechanism section. Stability of fabricated devices is also tested over 18 months. The output voltage results show the high stability of fabricated devices giving almost same output voltage (V_{oc} ≈ 120 V). Further, we have checked the piezoelectric output data in bending mode as well as connecting in reverse mode to clarify the triboelectric effect. The output data in bending mode are found to be very small ≈70 mV (peak-to-peak voltage), proving the negligible contribution to the obtained output data by triboelectric effect. Thus, the triboelectric contribution to piezoelectric output data is very negligible in our study.

Energy-harvesting mechanism from mechanical energy to electrical signal by the PENGs is shown in **Figure 6**a. This mechanism explains the synergistic effect of the molecular dipoles present in PVDF-HFP. The ZrO_2 NPs improve the electroactive β phase as well as piezoelectric properties in the PVDF-HFP by the strong electrostatic interaction between the ZrO_2 NPs and the dipoles of PVDF-HFP. Under the action of the finger imparting a secondary potential is produced in the ZrO_2 molecules which aligned the PVDF-HFP dipoles along the action direction. Thus, the NP-loaded PVDF-HFP produces a self-polarization

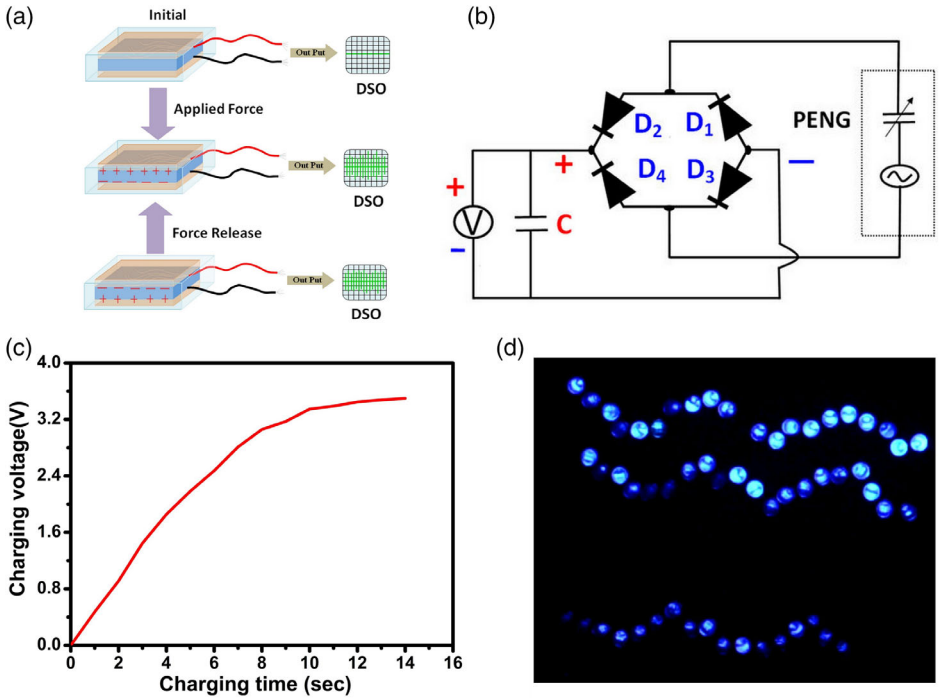

Figure 6. a) Working mechanism of the PENG. a) Circuit diagram of the charging capacitor. c) Capacitor charging (voltage vs time) graph by PENG. d) Photograph of glowing of LEDs by PENG.

due to the effect of mechanical stress and the interfacial surface charge on polarization. At the top electrode, a positive piezoelectric potential arises when a vertical compressional stress is applied on the PENGs, whereas at the bottom electrode, a negative piezoelectric potential appears after releasing the stress by the crystalline structure deformation of PVDF-HFP nanocomposite. Thus, a self-polarization is developed in the PVDF-HFP nanocomposite due to the action of mechanical stress and the interfacial surface charge polarization interaction. This piezoelectric potential-assisted to self-polarization causes the flow of electrons when two electrodes are connected through an external load resistor. With the releasing of compressive stress, the piezoelectric potential immediately diminishes and the electrons accumulated at the bottom electrode flow back to the other electrode via an external circuit, leading to an opposite electrical output.[55,61] Thus, under periodic compression and relaxation processes, the fabricated PENGs generate a periodic output voltage.

For realistic application of fabricated PENG, it is also checked by charging a 1 μF capacitor which was charged by 3.4 V in just 13 s, shown in Figure 6c. Fabricated PENG is also capable to light up 55 kinds of commercially available blue light emitting diodes (LEDs) which were connected in series connection, of which a digital photograph is shown in Figure 6d.

4.5.2. Performance of STENG

Digital photograph of single-electrode triboelectric nanogenerator (STENG) is shown in **Figure 7**b. Here, the upper surface of STENG and epidermis are used as two triboelectric layers. The epidermis has highest tendency to lose electric charge to PVDF/ZrO_2 thin film according to triboelectric series. So, the epidermis was a good selection for triboelectric layer to generate electric charge commonly available in human body. The output performance of fabricated STENG is measured by DSO (Keysight, Oscilloscope DSO–X 3012A). The fabricated STENG was attached in forearm, and data were collected for arm moving condition, and the maximum output voltage is obtained ≈7 V, as shown in Figure 7c. Possible electrical output generation mechanism is schematically shown in Figure 6a. Before the contact between PVDF/ZrO_2 thin film and epidermis (human finger), there is no charge transferred or any potential difference is produced. When the finger surface comes in contact with PVDF/ZrO_2 thin-film surface, charges are produced on the PVDF/ZrO_2 thin film and get transferred into human body and generate equivalent negative and positive electric charges on the two surfaces. When finger was removed from the composite film surface, the accumulated electron on the composites film surface was transferred into Al electrode from ground electrode due to their different potentials. This electron transfer stops when the electrostatic equilibrium happens, by increasing the distance between the two surfaces. As the finger moved toward the composite surface, electrons flowed from the Al electrode to the ground until the full contact between two surfaces and generated reversed output signal.

5. Conclusions

In summary, we have developed a high-performance PENG from ZrO_2/PVDF-HFP composite thin film for harvesting mechanical

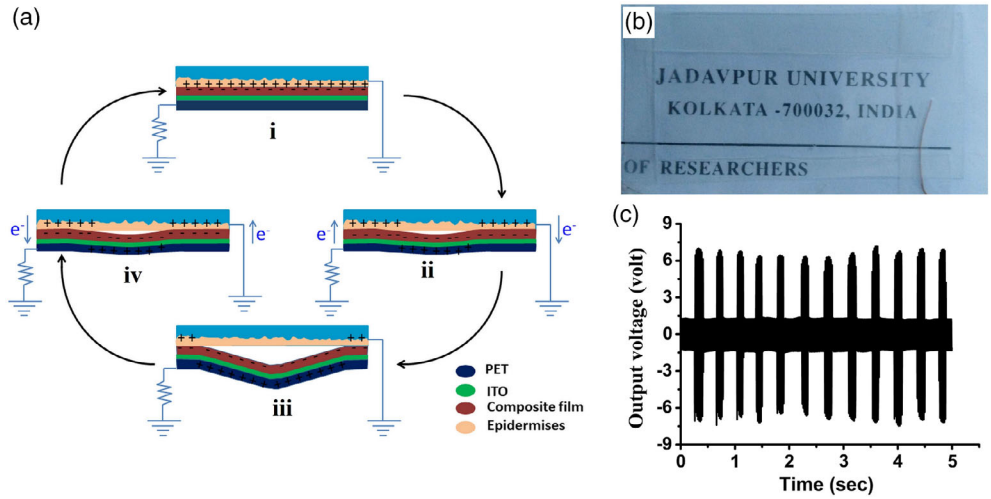

Figure 7. a) Working mechanism of STENG, b) digital photograph of transparent STENG and c) output voltage performance of STENG.

energy in the ambient environment. By adding ZrO_2 NPs in the PVDF-HFP matrix, enhancement of the β phase as well as output signals of PENG takes place. Due to the nucleation of electroactive β phase and large interfacial polarization, the developed PENG exhibits a large value of open-circuit voltage ($V_{oc} = 120$ V) and short-circuit current ($I_{sc} = 1.95$ μA) with power density ≈7091 μW cm^{-3}, under a periodic finger imparting. Using a bridge rectifier, this developed PENG is capable to glow instantly large number of LED and can charge a capacitor. ZrO_2/PVDF-HFP composite base STENG also shows remarkable output performance i.e., ≈7 V with just finger touch. This promising approach provides a large-scale power supply to realize a self-powered system from small mechanical energy of human activities into electrical energy. And STENG may be applicable in touch sensor field as well as powering low-energy-consuming portable gadgets.

Supporting Information

Supporting Information is available from the Wiley Online Library or from the author.

Acknowledgements

This work was financially supported by University Grants Commission (UGC) and Science & Engineering Research Board (SERB), Government of India.

Conflict of Interest

The authors declare no conflict of interest.

Data Availability Statement

Research data are not shared.

Keywords

piezoelectric nanogenerators, piezoelectricity, poly(vinylidene fluoride-*co*-hexafluoropropylene), triboelectrics, zirconium oxide, nanoparticles, β phases

Received: November 5, 2020
Revised: February 12, 2021
Published online: March 9, 2021

[1] Z. L. Wang, J. Song, *Science* **2006**, *312*, 242.
[2] P. Martins, C. M. Costa, M. Benelmekki, G. Botelho, S. Lanceros-Mendez, *Cryst. Eng. Comm.* **2012**, *14*, 2807.
[3] F. R. Fan, W. Tang, Z. L. Wang, *Adv. Mater* **2016**, *28*, 4283.
[4] S. H. Shin, Y. H. Kim, M. H. Lee, J. Y. Jung, J. H. Seol, J. Nah, *ACS Nano* **2014**, *8*, 10844.
[5] H. B. Kang, J. Chang, K. Koh, L. Lin, Y. S. Cho, *ACS Appl. Mater. Interfaces* **2014**, *6*, 10576.
[6] J. Chen, J. Yang, H. Guo, Z. Li, L. Zheng, Y. Su, Z. Wen, X. Fan, Z. L. Wang, *ACS Nano* **2015**, *9*, 12334.
[7] L. Gu, N. Cui, L. Cheng, Q. Xu, S. Bai, M. Yuan, W. Wu, J. Liu, Y. Zhao, F. Ma, Y. Qin, Z. L. Wang, *Nano Lett.* **2013**, *13*, 91.
[8] J. Liu, N. Cui, L. Gu, X. Chen, S. Bai, Y. Zheng, C. Hu, Y. Qin, *Nanoscale* **2016**, *8*, 4938.
[9] W. Yang, J. Chen, G. Zhu, J. Yang, P. Bai, Y. J. Su, Q. S. Jing, X. Cao, Z. L. Wang, *ACS Nano* **2013**, *7*, 11317.
[10] J. Yang, J. Chen, Y. Liu, W. Yang, Y. Su, Z. L. Wang, *ACS Nano* **2014**, *8*, 2649.
[11] D. Zhu, M. J. Tudor, S. P. Beeby, *Meas. Sci. Technol.* **2010**, *21*, 022001.
[12] J. Chen, G. Zhu, W. Yang, Q. Jing, P. Bai, Y. Yang, T. C. Hou, Z. L. Wang, *Adv. Mater.* **2013**, *25*, 6094.
[13] R. A. Surmenev, T. Orlova, R. V. Chernozem, A. A. Ivanova, A. Bartasyte, S. Mathur, M. A. Surmeneva, *Nano Energy* **2019**, *62*, 475.
[14] Y. Yang, W. Guo, K. C. Pradel, G. Zhu, Y. Zhou, Y. Zhang, Y. Hu, L. Lin, Z. L. Wang, *Nano Lett.* **2012**, *12*, 2833.
[15] X. Wang, Y. Dai, R. Liu, X. He, S. Li, Z. L. Wang, *ACS Nano* **2017**, *11*, 8339.
[16] A. Sultana, S. K. Ghosh, M. M. Alam, P. Sadhukhan, K. Roy, M. Xie, C. R. Bowen, S. Sarkar, S. Das, T. R. Middya, D. Mandal, *ACS Appl. Mater. Interfaces* **2019**, *11*, 27279.

[17] L. Lin, Y. Xie, S. Niu, S. Wang, P. K. Yang, Z. L. Wang, *ACS Nano* **2015**, *9*, 922.
[18] M. L. Seol, J. H. Woo, D. I. Lee, H. Im, J. Hur, Y. K. Choi, *Small* **2014**, *10*, 3887.
[19] H. Guo, T. Li, X. Cao, J. Xiong, Y. Jie, M. Willander, X. Xia Cao, N. Wang, Z. L. Wang, *ACS Nano* **2017**, *11*, 856.
[20] Y. Yang, H. Zhang, Z. H. Lin, Y. S. Zhou, Q. Jing, Y. Su, J. Yang, J. Chen, C. Hu, Z. L. Wang, *ACS Nano* **2013**, *7*, 9213.
[21] Y. Yang, H. Zhang, J. Chen, Q. Jing, Y. S. Zhou, X. Wen, Z. L. Wang, *ACS Nano* **2013**, *7*, 7342.
[22] Y. Yang, Y. S. Zhou, H. Zhang, Y. Liu, S. Lee, Z. L. Wang, *Adv. Mater.* **2013**, *25*, 6594.
[23] G. Zhu, J. Chen, T. Zhang, Q. Jing, Z. L. Wang, *Nat. Commun.* **2014**, *5*, 487.
[24] Y. Zi, L. Lin, J. Wang, S. Wang, J. Chen, X. Fan, P. K. Yang, F. Yi, Z. L. Wang, *Adv. Mater.* **2015**, *27*, 2340.
[25] W. Yang, J. Chen, Q. Jing, J. Yang, X. Wen, Y. Su, G. Zhu, P. Bai, Z. L. Wang, *Adv. Funct. Mater.* **2014**, *24*, 4090.
[26] Z. H. Lin, Y. Yang, J. M. Wu, Y. Liu, F. Zhang, Z. L. Wang, *J. Phys. Chem. Lett.* **2012**, *3*, 3599.
[27] C. Li, W. Luo, X. Liu, D. Xu, K. He, *Nanomaterials* **2016**, *6*, 67.
[28] N. A. Hoque, P. Thakur, P. Biswas, M. M. Saikh, S. Roy, B. Bagchi, S. Das, P. P. Ray, *J. Mater. Chem. A* **2018**, *6*, 13848.
[29] Y. Wang, R. Furlan, I. Ramos, J. J. Santiago-Aviles, *Appl. Phys. A: Mater. Sci. Process.* **2004**, *78*, 1043.
[30] P. Thakur, A. Kool, B. Bagchi, S. Das, P. Nandy, *Phys. Chem. Chem. Phys.* **2015**, *17*, 1368.
[31] P. Martins, A. C. Lopes, S. L. Mendez, *Prog. Polym. Sci.* **2013**, *39*, 683.
[32] P. Thakur, A. Kool, B. Bagchi, S. Das, P. Nandy, *Appl. Clay Sci.* **2014**, *99*, 149.
[33] H. H. Singh, N. Khare, *Energy* **2019**, *178*, 765.
[34] Y. Feng, W. L. Li, Y. F. Hou, Y. Yu, W. P. Cao, T. D. Zhang, W. D. Fei, *J. Mater. Chem. C* **2015**, *3*, 1250.
[35] P. Biswas, N. A. Hoque, P. Thakur, M. M. Saikh, S. Roy, F. Khatun, B. Bagchi, S. Das, *ACS Sustainable Chem. Eng.* **2019**, *7*, 4801.
[36] B. S. I. Gunduz, R. Alpern, D. Amare, J. Crawford, B. Dolan, S. Jones, R. Kobylarz, M. Reveley, P. Cebe, *Polymer* **2010**, *51*, 1485.
[37] C. E. Chang, V. H. Tran, J. B. Wang, Y. K. Fuh, L. W. Lin, *Nano Lett.* **2010**, *10*, 726.
[38] P. Thakur, A. Kool, B. Bagchi, N. A. Hoque, S. Das, P. Nandy, *RSC Adv.* **2015**, *5*, 28487.
[39] P. Adhikary, D. Mandal, *Phys. Chem. Chem. Phys.* **2017**, *19*, 17789.
[40] P. Thakur, A. Kool, N. A. Hoque, B. Bagchi, F. Khatun, P. Biswas, D. Brahma, S. Roy, S. Banerjee, S. Das, *Nano Energy* **2018**, *44*, 456.
[41] P. Thakur, A. Kool, B. Bagchi, N. A. Hoque, S. Das, P. Nandy, *Phys. Chem. Chem. Phys.* **2015**, *17*, 13082.
[42] P. Martins, A. C. Lopes, S. Lanceros-Mendez, *Prog. Polym. Sci.* **2014**, *39*, 683.
[43] K. Pal, D. J. Kang, Z. X. Zhang, J. K. Kim, *Langmuir* **2010**, *26*, 3609.
[44] S. Shukla, S. Seal, *Int. Mater. Rev.* **2005**, *50*, 45.
[45] J. Liang, X. Jiang, G. Liu, Z. Deng, J. Zhuang, F. Li, Y. Li, *Mater. Res. Bull.* **2003**, *38*, 161.
[46] N. Chandra, D. K. Singh, M. Sharma, R. K. Upadhyay, S. S. Amritphale, S. K. Sanghi, *J. Colloid Interface Sci.* **2010**, *342*, 327.
[47] M. J. Mayo, J. R. Seidensticker, D. C. Hague, A. H. Carim, *Nanostruct. Mater.* **1999**, *11*, 271.
[48] S. Y. Song, M. S. Park, D. Lee, J. W. Lee, J. S. Yun, *Mater. Design* **2019**, *180*, 107960.
[49] M. Gell, *Mater. Sci. Eng. A: Struct. Mater. Prop. Microstruct. Process* **1995**, *204*, 51.
[50] H. Gleiter, *Mater.* **1992**, *1*, 19.
[51] B. Zhu, C. R. Xia, X. G. Luo, *Thin Solid Films* **2001**, *385*, 209.
[52] N. G. Petrik, D. P. Taylor, T. M. Orlando, *J. Appl. Phys.* **1999**, *85*, 6770.
[53] A. Bastianini, G. A. Battiston, R. Gerbasi, M. Porchia, S. Daolio, *J. Phys. IV France* **1995**, *05*, C5-525.
[54] A. Corma, *Chem. Rev.* **1995**, *95*, 559.
[55] S. K. Karan, R. Bera, S. Paria, A. K. Das, S. Maiti, A. Maitra, B. B. Khatua, *Efficiency Adv. Energy Mater.* **2016**, *6*, 1601016.
[56] J. Sun, A. Yang, C. Zhao, F. Liu, Z. Li, *Sci. Bull.* **2019**, *64*, 1336.
[57] A. Gaur, S. Tiwari, C. Kumar, P. Maiti, *Nanoscale Adv.* **2019**, *1*, 3200.
[58] J. Sun, H. Guo, J. Ribera, C. Wu, K. Tu, M. Binelli, G. Panzarasa, F. W. Schwarze, Z. L. Wang, I. Burgert, *ACS Nano* **2020**, *14*, 14665.
[59] M. Koç, L. Paralı, O. Şan, *Polym. Testing* **2020**, *90*, 106695.
[60] Z. L. Wang, *Mater. Today* **2017**, *20*, 74.
[61] J. H. Lee, H. J. Yoon, T. Y. Kim, M. K. Gupta, J. H. Lee, W. Seung, H. Ryu, S. W. Kim, *Adv. Funct. Mater.* **2015**, *25*, 203.

Conferences Attended

American Chemical Society

ACS Publications
Most Trusted. Most Cited. Most Read.

nano tech

Printed Electronics Association

CERTIFICATE OF PARTICIPATION

VERIFYING THAT

Md. Minarul Saikh

Attended the **ACS Publications Summit** at
nano tech 2024 International Nanotechnology Exhibition & Conference
on February 02, 2024.

James Milne, Ph.D.
President, ACS Publications

Faculty of Engineering and Technology, JADAVPUR UNIVERSITY

TEQIP-II SPONSORED ONE-DAY NATIONAL WORKSHOP

ON

REVISITING INTELLECTUAL PROPERTY RIGHTS IN THE CONTEXT OF RECENT DEVELOPMENTS

IN

SCIENCE & TECHNOLOGY

CERTIFICATE OF PARTICIPATION

This is to certify that Prof./ Dr./ Mr./ Mrs./ Ms. Md Minarul Saikh
of Jadavpur University *attended the* ~~two day~~ *National Workshop organized by the Faculty of Engineering and Technology, Jadavpur University on October 20, 2016.*

Coordinator TEQIP-II	*Nodal Officer, TEQIP-II R&D Committee*	*Workshop Coordinators*

National Seminar on

New Directions in Physical Sciences 2020 (NDPS 2020)

Organised by

Department of Physics, Jadavpur University

In association with

Indian Photobiology Society

Certificate of Participation

This is to certify that Prof./Dr./Mr./Ms. Md. Minarul Saikh of Jadavpur University has participated/ presented a poster entitled Piezoelectric Nanogenerator Mediated Energy Harvesting at the seminar on 'New Directions in Physical Sciences 2020' at Jadavpur University, Kolkata on February 25, 2020.

25/2/2020

Dr. Soumen Mondal
Convener, NDPS 2020

Prof. Mitali Mondal
Convener, NDPS 2020

25/02/2020

Prof. Sukhen Das
Head, Dept. of Physics

TWO DAYS SEMINAR

on

Twists and Turns in Physics Research : Special Emphasis on Condensed Matter and Biophysics (TTPR-2017)

Organised by

Department of Physics, Jadavpur University, Kolkata

Supported by UGC-DSA-I Programme

CERTIFICATE OF PARTICIPATION

This is to certify that Mr./ Mrs/ Dr./ Prof. Md. Minarul Saikh

has participated/ presented (oral/ poster) a paper entitled .....

..... *In the two days seminar on "Twists and Turns in Physics Research: Special Emphasis on Condensed Matter and Biophysics (TTPR-2017)" on 21-22 February, 2017 held at Department of Physics, Jadavpur University, Kolkata – 700032.*

Conveners

Dr. Dipankar Mandal
Dr. Subrata Sarkar
Dr. Sk Saiyad Ali
Dr. Saikat Kr. Seth

Prof. Argha Deb
Head, Department of Physics
Jadavpur University

Recent Trend in Composite Material 2016

Technical Education Quality Improvement Programme - II (TEQIP - II)
Sponsored One Day Seminar - August 18, 2016
Mechanical Engineering Department, Jadavpur University, Kolkata

This is to certify that MD. MINARUL SAIKH

Participated / ~~Presented Paper~~ / ~~Delivered Invited Talk~~ in the Seminar of **RECENT TREND IN COMPOSITE MATEIRAL** on **18th August, 2016** in the Machanical Engineering Department under TEQIP - JU program.

Co-ordinator	Nodal Officer, R&D TEQIP II - JU	Co-ordinator, TEQIP II - JU

Jadavpur University, Kolkata

Certificate of Participation

This is to certify that MD MINARUL SAIKH *has participated in the workshop on Awareness in Fire Safety and Recent Technologies, held at Dr. Triguna Sen Auditorium on 21st October, 2016, organized by Jadavpur University, funded by TEQIP Phase II .*

Prof. Somnath Ghosh
Co-ordinator ,TEQIP-II
Jadavpur University

Saswati Mazumdar
Prof. Saswati Mazumdar
Convener of the workshop
Jadavpur University

RAITH
NANOFABRICATION

CENTRE FOR
S. N. BOSE NATIONAL
BASIC SCIENCES 1986
1894-1974
विज्ञानेन परिपश्यन्ति धीराः

INDIA NANO 2019

S. N. Bose National Centre for Basic Sciences, Kolkata

Certificate of Participation

This is to certify that Ms/Mr/Dr ..... Md. Minarul Saikh .....

from ..... Govt. Degree College, Pedong ....., has participated in the Workshop on Nanolithography and Nanofabricationon July 9,2019organised by Raith India in Cooperation withS. N. Bose National Centre for Basic Sciences, Kolkata.

The topics covered were electron and ion beam nano-patterning technologies,as well related process technologies.

Mr. Masum Khan
CEO, Raith India

Prof. S.K. Ray
Director, SNBNCBS

DST-SERB Sponsored

One Day Workshop on Material Synthesis & Characterization Techniques

Organized by: Department of Physics, Jadavpur University, Kolkata-700032

Certificate of Presentation

This Certificate is awarded to

Mr/ Ms. Md. Minarul Saikh *for successfully presenting a paper entitled* Piezoelectric Nanogenerator *in the Workshop organized by Department of Physics, Jadavpur University, Kolkata on 29th February 2020.*

29/02/2020

Head, Department of Physics, Jadavpur University

Jadavpur University

ज्ञान-विज्ञान विमुक्तये
UGC
University Grants Commission

NTNU
Norwegian University of Science and Technology

INTERNATIONAL WORKSHOP ON

"Advanced Hybrid Separation Techniques in Industrial Wastewater Management"

Sponsored by

UGC, under Indo-Norwegian Collaboration program (INCP – 2014)

Certificate of Participation

This is to certify that ..... Minarul Saikh ..... *has participated in the International Workshop on "Advanced Hybrid Separation Techniques in Industrial Wastewater Management", held on December 8 – 9, 2017*

Organized by

Chemical Engineering Department, Jadavpur University
in association with CHEMBridge

Gisle Øye	Kajari Kargupta	Bhattacharjee
Prof. Gisle Øye	**Prof. Kajari Kargupta**	**Prof. Chiranjib Bhattacharjee**
Professor	Head	Dean, Faculty of Engineering & Technology
Dept. of Chemical Engineering	Chemical Engineering Department	Professor & Former Head
NTNU, Norway	Jadavpur University, Kolkata, India	Chemical Engineering Department
		Jadavpur University, Kolkata, India

CIRE

CENTRE FOR INTERDISCIPLINARY RESEARCH AND EDUCATION

404B, Jodhpur Park, Kolkata – 700068

25th March, 2017

CERTIFICATE OF PARTICIPATION

This is to certify that

Md. Minarul Saikh

has contributed through Lecture / Oral Presentation / Poster Presentation / Participation to the success of the One Day National Symposium on Nanotechnology: From Materials to Medicine and their Social Impact held on 25th March, 2017 at Birla Industrial and Technological Museum, Kolkata.

Prof Sanjib Sarkar
President, CIRE

ONE DAY SEMINAR-CUM-WORKSHOP ON

Python Computing : Some Applications in Mathematical Physics.

[Paper PHSA CC8 (practical)]

Basanti Devi College &
Nabagram Hiralal Paul College

in Collaboration with Undergraduate Board of Studies in Physics, University of Calcutta

Certificate Of Participation

This is to certify that Dr. /Prof. /Sri/Smt. Md. MINARUL SAIKH (Govt. General Degree College at Pedong) *has participated in the One-day Seminar-cum-Workshop on Python Computing: Some Applications in Mathematical Physics [Paper PHSA CC-8 (Practical)] held at Basanti Devi College, Kolkata on February 28, 2020, organized jointly by the Department of Physics, Basanti Devi College & Nabagram Hiralal Paul College in Collaboration with Undergraduate Board of Studies in Physics, University of Calcutta.*

Dr. Indrila Guha
Principal
Basanti Devi College

Dr. Srikanta Samanta
Principal
Nabagram Hiralal Paul College

Prof. Salil Kumar Biswas
Chairman, UG BOS in Physics
University of Calcutta

KHARAGPUR COLLEGE

INDA, KHARAGPUR, PASCHIM MEDINIPUR, WEST BENGAL, INDIA, 721305

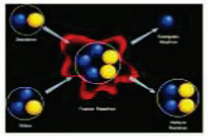

No. : ZM17LC-CE000421

CERTIFICATE OF PARTICIPATION

ADVANCEMENT OF PLASMA PHYSICS AND NANOSCIENCE

This is to certify that Dr/Mr/Mrs. Md. Minarul Saikh , Assistant Professor of Govt.General Degree College at Pedong has participated successfully in the one-day National Webinar on "Advancement of Plasma Physics and Nano-science " On 30th june, 2020 Organised by Department of Physics.

Dr. Jyotirmoy Pramanik Convener Organising Committee	Dr. Ritwik Saha Secretary Organising Committee	Dr. Bidyut Samanta Principal & Chairman Organising Committee

SMIT SIKKIM MANIPAL UNIVERSITY
SIKKIM MANIPAL INSTITUTE OF TECHNOLOGY

Webinar on
Advanced Nanotechnology, Versatile Molecule & Spectroscopy

Organised by
Dept. of Chemistry, Sikkim Manipal Institute of Technology
in Collaboration with
Association of Chemistry Teachers (ACT)
C/O Homi Bhabha Centre for Science Education, Mumbai

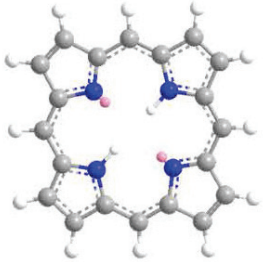

Certificate of Participation

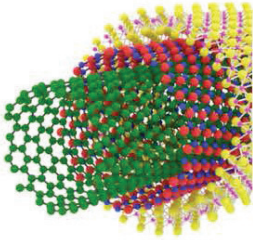

Md. Minarul Saikh

Govt. General Degree College at Pedong, Kalimpong

has participated in the Webinar held on 3rd & 4th July, 2020.

Prof. N. K. Bhattacharyya	**Prof. Brijesh Pare**	**Prof. Sanjay Dahal**
Webinar Coordinator	President, ACT	HOD Chemistry, SMIT

AMITY UNIVERSITY
KOLKATA

CERTIFICATE OF PARTICIPATION

This is to certify that Mr./Ms./Mrs./Dr./Prof. MD. MINARUL SAIKH

has attended the five days **Faculty Development Programme on "Recent Advances in Material Science"**

during 8th July to 12th July, 2020 organised by Amity Institute of Applied Sciences (Department of Chemistry),

Amity University Kolkata.

Dr. Saumya Dasgupta
Head of Institution, Amity Institute of Applied Sciences

Prof. (Dr.) Ankita Chakravarty Bhattacharya
Pro Vice Chancellor,
Amity University, Kolkata

IDHAYA COLLEGE FOR WOMEN, KUMBAKONAM-612 001

(Run by Immaculate Sisters)

Affiliated to Bharathidasan University, Tiruchirapalli.

G.O. NO.237/dt 22.06.2000

UGC Recognized 2(f) & 12(B) Institution

Certificate of Participation

This is to certify that

MD. MINARUL SAIKH

Assistant Professor, Govt. General Degree College at Pedong

has participated in the *International Webinar* on "*NANOMATERIALS & ITS TOOLS*" *on 22 July 2020* Organized *by PG & Research Department of Physics, Idhaya College for Women, Kumbakonam, Thanjavur (Dt)-612 001.*

Dr. N.S.K. Gowthaman
Post-Doctral Researcher,
Institute of Advanced Technology,
University Putra Malaysia.

Dr. S. Sudaramoorthi
Asst. Professor in Physics,
Agni College of Technology,
Chennai.

Dr. N. Mahendran
Organizing Secretary

Mrs.K. Kanimozhi
Convenor

Rev. Sr. Dr. Eugin Amala
Principal

SPIU
UTTAR PRADESH

RAJ KUMAR GOEL INSTITUTE OF TECHNOLOGY

(ISO 9001:2015 CERTIFIED INSTITUTE) www.rkgit.edu.in

DEPARTMENT OF ELECTRONICS & COMMUNICATION ENGINEERING

Jointly Organized by

State Project Implementation Unit-Uttar Pradesh

TECHNICAL EDUCATION QUALITY IMPROVEMENT PROGRAMME-III

(A WORLD BANK ASSISTED PROJECT UNDER MINISTRY OF HRD, GOVT. OF INDIA)

CERTIFICATE OF PARTICIPATION

This is to certify that **Md. Minarul Saikh** from **Govt. General Degree College at Pedong, Kalimpong** Participated in the International Webinar on the topic "New Ideas and Innovations in the Technology and Use of IoT in Telecommunications" delivered by "Mr. Abhishek Srivastava, MD & CEO, Telenoetica Ltd., Lagos, Nigeria" on July 23, 2020 organized by Raj Kumar Goel Institute of Technology, Ghaziabad, Uttar Pradesh, India. (College Code: 033)

(Dr. Pavan Kumar Shukla)	(Dr. R.K. Yadav)	(Dr. Anil Kumar)	(Dr. D.R. Somashekar)
Convenor	HOD, ECE	Administrator SPIU - UP	Director

POWERED BY: elenoetica ...where intellect drives excellence

DLS PG COLLEGE

BILASPUR (CHHATTISGARH)

NAAC B+

Affiliated to

ATAL BIHARI VAJPAYEE VISHWAVIDYALAYA, BILASPUR (CHHATTISGARH)

INTERNATIONAL E-CONFERENCE

RECENT TRENDS ON ADVANCED MATERIALS & ENVIRONMENT (RTAME) 2020

E-CERTIFICATE OF PARTICIPATION

This is to certify that Mr./Mrs./Ms./Dr. Md. Minarul Saikh,

of Govt. General Degree College at Pedong Participated in one day **International e-Conference** on **"RECENT TRENDS ON ADVANCED MATERIALS & ENVIRONMENT (RTAME) 2020"** organized by Department of Chemistry, IQAC and Research & Development Cell on **05 August 2020** and enriched its quality by his innovative and meaningful ideas.

Dr. Priti Mishra Convenor D.L.S. P.G. College, Bilaspur (C.G.)	Dr. Ranjana Chaturvedi Principal D.L.S. P.G. College, Bilaspur (C.G.)	Shri Basant Sharma Chairman D.L.S. P.G. College, Bilaspur (C.G.)

Raj Kumar Goel Institute of Technology, Ghaziabad

(ISO 9001:2015 Certified Institute) www.rkgit.edu.in

Department of Applied Sciences and Humanities

CERTIFICATE OF PARTICIPATION

This is to certify that Mr. Md. Minarul Saikh of Govt. General Degree College at Pedong, Kalimpong has Participated in the International Webinar on the topic **"Next-Generation High Power Laser Technology"** delivered by **"Dr. Rajeev Pattathil, Professor** at **"Rutherford Appleton Laboratory, United Kingdom"** on August 7, 2020 organized by Raj Kumar Goel Institute of Technology, Ghaziabad, Uttar Pradesh, India.

Dr. Sanjeev Goyal Coordinator	Dr. Poonam C Kumar Convener	Sh. H. G. Garg Dean (SW)	Dr. D. R. Somashekar Director, RKGIT

Certificate ID CDKW8C-CE000241

Date of Certificate Generation 8/7/2020

Shri. Shivaji Education Society, Amravati's

Shri. Shivaji Science and Arts College, Chikhli, Dist.Buldana.

National Level Webinar on

RECENT ADVANCES IN NANOTECHNOLOGY

CERTIFICATE

This is to certify that

Md. Minarul Saikh

has actively participated in national level webinar on Recent Advances in Nanotechnology organized by department of Chemistry, Shri.Shivaji Science and Arts College, Chikhli on 8th August 2020.

Dr. S. R. Patil	Prof. S. L. Kumbhare	Prof. Dr. V. U .Pochhi	Prof. Dr. A. M .Garode
Organizing Secretary	Convener & Head	IQAC Coordinator	Principal

SRI BHUVANENDRA COLLEGE

College with potential for excellence awarded by UGC
(Sponsored by the Academy of General Education, Manipal)
KARKALA, UDUPI DISTRICT-574104,
KARNATAKA, INDIA.

Certificate of Participation

This is to certify that

Mr.Md. Minarul Saikh

Govt. General Degree College at pedong, Kalimpong

has participated in the International Webinar on

"ADVANCED FUNCTIONAL MATERIALS VIA CHEMICAL VAPOR DEPOSITION: PROCESS DEVELOPMENT AND APPLICATION"

Organized by the department of PHYSICS

& Internal Quality Assurance Cell on 11th August 2020.

Mrs. Vijaya Kumari
HOD of Physics
Webinar Convener

Dr. Manjunatha A Kotian
Principal

Raj Kumar Goel Institute of Technology, Ghaziabad

(ISO 9001:2015 Certified Institute) www.rkgit.edu.in

Department of Applied Sciences and Humanities

CERTIFICATE OF PARTICIPATION

This is to certify that Mr. Md. Minarul Saikh of Govt. General Degree College at Pedong, Kalimpong has Participated in the International Webinar on the topic "Photonics Revolution" delivered by "Prof. Anurag Sharma, IIT Delhi" on August 12, 2020 organized by Raj Kumar Goel Institute of Technology, Ghaziabad, Uttar Pradesh, India.

Dr. Sanjeev Goyal
Coordinator

Dr. Poonam C Kumar
Convener

Sh. H. G. Garg
Dean (SW)

Dr. D. R. Somashekar
Director, RKGIT

Certificate ID 1UC03S-CE000046

Date of Certificate Generation 8/12/2020

Dr.M.G.R
EDUCATIONAL AND RESEARCH INSTITUTE

(Deemed to be University with Graded Autonomy Status)

Maduravoyal, Chennai - 600 095. Tamilnadu. India.
(An ISO 21001:2018 Certified Institution)

Certificate Number : MGRCMC-2009015

Certificate Issued Date: 15 September 2020

FACULTY OF HUMANITIES AND SCIENCE

ADAYALAMPATTU PHASE -II CAMPUS

DEPARTMENT OF CHEMISTRY

A TWO DAY NATIONAL LEVEL WEBINAR ON

EMERGING TRENDS IN MODERN CHEMISTRY

Certificate of Participation

This certificate is proudly presented to

Mr. MD. MINARUL SAIKH, ASSISTANT PROFESSOR *of*
PHYSCICS, GOVT. GENERAL DEGREE COLLEGE AT PEDONG

for his/her active participation in the Two Day National Level Webinar on **" Emerging Trends in Modern Chemistry "** *organized by the Department of Chemistry, Faculty of Humanities and Science, Adayalampattu Phase - II campus on 14th & 15th September 2020.*

Dr. S. VALLIAMMAI
HoD/Chemistry

Dr. S. Manivannan
Dean Phase - II

Dr. C.B. Palanivelu
Registrar

RAJIV GANDHI UNIVERSITY OF KNOWLEDGE TECHNOLOGIES, A.P.

Catering to the Educational Needs of Gifted Rural Youth of Andhra Pradesh

(Established by the Govt. of Andhra Pradesh in 2008 and recognized as per Section 2(f) of UGC Act, 1956)

Department of Physics, Rajiv Knowledge Valley, YSR Kadapa District, Pin- 516330, India

Date: 27-8-2020

Certificate ID : 6HJAMA-CE000119

Certificate of Participation

This is to Certify that **Mr. MD. MINARUL SAIKH** from **GOVT. GENERAL DEGREE COLLEGE AT PEDONG** has attended Three Day International Webinar Series on ***" Synthesis and Characterization of Nano-materials and their Novel Applications"*** organized by ***Department of Physics, R.K.Valley,*** **Rajiv Gandhi University Of Knowledge Technologies, A.P (RGUKT-AP)** from 17th to 19th August 2020.

Organizer
Mr M Bhaskaraiah

HOD. Physics
Dr. E.Bhawani

Convenor
Dr. G Ramesh

Director
Prof. B. Sudheer Prem Kumar

SREENIVASA INSTITUTE OF TECHNOLOGY AND MANAGEMENT STUDIES

Autonomous, Accredited by NBA, NAAC, Affiliated to JNTUA, Anantapuramu

Dr.D.K.Audikesavulu Marg (Bangalore-Tirupati Bye-Pass Road, Murukambattu, Chittoor-517127

Certificate of Appreciation

This is to certify that

Mr. Md. Minarul Saikh

Faculty: Assistant Professor, Govt. General Degree College at Pedong

has participated in a One Day Online **International Webinar** entitled "**MATERIAL SCIENCE AND IMPORTANCE OF DEVELOPING COMPOSITE MATERIALS**" on **21st August 2020** organized by the **Department of Science and Humanities,** Sreenivasa Institute of Technology and Management Studies , Chittoor, AP, India

H Umamahy

Dr.H.Umamahesvari
Professor & HOD , S&H, (Convenor)

Dr.P.Ramesh Kumar
Principal

Organized by

Department of Economics
Mazbat College,Mazbat
Udalguri.Assam,India

Department of Geography
Khoirabari College
Udalguri, Assam,India

In Association with
IQAC &
Department of Education
Mazbat College
And
IQAC, Khoirabari College

RSADA-389

One Day International Webinar
On
Remote Sensing and It's Application in Disaster Management

Date: 24-08-2020

CERTIFICATE OF PARTICIPATION

This is to certify that

Mr. Md. Minarul Saikh

of Govt. General Degree College at Pedong

has participated in the international Webinar on Remote Sensing and It's Application in Disaster Management organized jointly by the Dept. of Economics, Mazbat College, Mazbat and Dept. of Geography , Khoirabari College, Khoirabari, in Association with IQAC, Khoirabari College and IQAC & Dept. of Education, Mazbat College on 24th August, 2020

Dr Debabrata Sen	Dr Pradip Kr Sarma	Dr Uttam Kalita	Mr Manash Kalita	Mr Jayanta Kalita
Principal i/c	Principal	Coordinator	Coordinator	HOD,Education
Khoirabari College	Mazbat College	Khoirabari College	Mazbat College	Mazbat College

सत्यमेव जयते

P. R. Thakur Government College

Thakurnagar, Gaighata, North 24 Parganas, West Bengal - 743287

One Day International Webinar on "Physics & Life at Nano Scale of Length"

Organised by Department of Physics

Certificate of Participation

This is to certify that ..... *Mr. Md. Minarul Saikh* ..... *from* ..... *Govt. General Degree College At Pedong* ..... *has participated in the One day International Webinar on "Physics & Life at Nano Scale of Length", organised by Department of Physics, P. R. Thakur Govt. College held on August 28, 2020.*

Convenor	IQAC Representative	Officer-in-Charge

Dr.M.G.R
EDUCATIONAL AND RESEARCH INSTITUTE
(Deemed to be University)

Maduravoyal, Chennai - 600 095. Tamilnadu. India.
(An ISO 21001:2018 Certified Institution)
University with Special Autonomy Status

ACCREDITED WITH GRADE A NAAC

Certificate Number : MGRNSNT-20080454

Certificate Issued Date: 28 August 2020

FACULTY OF HUMANITIES AND SCIENCE

ADAYALAMPATTU PHASE -II CAMPUS

DEPARTMENT OF CHEMISTRY

A ONE DAY NATIONAL LEVEL WEBINAR ON

INTRODUCTION TO NANOSCIENCE AND NANOTECHNOLOGY

Certificate of Participation

This certificate is proudly presented to

Mr.MD. MINARUL SAIKH, ASSISTANT PROFESSOR *of*
PHYSICS, GOVT. GENERAL DEGREE COLLEGE AT PEDONG

for his/her active participation in the One Day National Level Webinar on **" Introduction to Nanoscience and Nanotechnology "** *organized by the Department of Chemistry, Faculty of Humanities and Science, Adayalampattu Phase - II campus on 28th August 2020.*

Dr. S. Valliammai
HoD/Chemistry

Dr. S. Manivannan
Dean Phase - II

Dr. C.B. Palanivelu
Registrar

Dr.M.G.R
EDUCATIONAL AND RESEARCH INSTITUTE
(Deemed to be University)

Maduravoyal, Chennai - 600 095. Tamilnadu. India.
(An ISO 21001:2018 Certified Institution)
University with Special Autonomy Status

Certificate Number : MGRPHM-2009113

Certificate Issued Date: 01 September 2020

FACULTY OF HUMANITIES AND SCIENCE

ADAYALAMPATTU PHASE -II CAMPUS

DEPARTMENT OF PHYSICS

A ONE DAY NATIONAL LEVEL WEBINAR ON

CERAMIC MATERIALS IN BIOMEDICAL FIELD: A PROSPECTIVE VIEW

Certificate of Participation

This certificate is proudly presented to

Mr.MD. MINARUL SAIKH, ASSISTANT PROFESSOR *of*
PHYSICS, GOVT. GENERAL DEGREE COLLEGE AT PEDONG

for his/her active participation in the One Day National Level Webinar on **" Ceramic Materials in Biomedical Field: A Prospective View "** *organized by the Department of Physics, Faculty of Humanities and Science, Adayalampattu Phase - II campus on 1st September 2020.*

Dr. S. Radhakrishnan
HoD/Physics

Dr. S. Manivannan
Dean Phase - II

Dr. C.B. Palanivelu
Registrar